



**HAL**  
open science

# Analyse des mécanismes primaires de pyrolyse de la biomasse

Yann Le Brech

► **To cite this version:**

Yann Le Brech. Analyse des mécanismes primaires de pyrolyse de la biomasse. Alimentation et Nutrition. Université de Lorraine, 2015. Français. NNT : 2015LORR0106 . tel-01751801

**HAL Id: tel-01751801**

**<https://hal.univ-lorraine.fr/tel-01751801>**

Submitted on 29 Mar 2018

**HAL** is a multi-disciplinary open access archive for the deposit and dissemination of scientific research documents, whether they are published or not. The documents may come from teaching and research institutions in France or abroad, or from public or private research centers.

L'archive ouverte pluridisciplinaire **HAL**, est destinée au dépôt et à la diffusion de documents scientifiques de niveau recherche, publiés ou non, émanant des établissements d'enseignement et de recherche français ou étrangers, des laboratoires publics ou privés.



## AVERTISSEMENT

Ce document est le fruit d'un long travail approuvé par le jury de soutenance et mis à disposition de l'ensemble de la communauté universitaire élargie.

Il est soumis à la propriété intellectuelle de l'auteur. Ceci implique une obligation de citation et de référencement lors de l'utilisation de ce document.

D'autre part, toute contrefaçon, plagiat, reproduction illicite encourt une poursuite pénale.

Contact : [ddoc-theses-contact@univ-lorraine.fr](mailto:ddoc-theses-contact@univ-lorraine.fr)

## LIENS

Code de la Propriété Intellectuelle. articles L 122. 4

Code de la Propriété Intellectuelle. articles L 335.2- L 335.10

[http://www.cfcopies.com/V2/leg/leg\\_droi.php](http://www.cfcopies.com/V2/leg/leg_droi.php)

<http://www.culture.gouv.fr/culture/infos-pratiques/droits/protection.htm>



# THÈSE

Présentée à l'Université de Lorraine  
Ecole Doctorale R.P.2E. : Ressources, Procédés, Produits, Environnement  
Laboratoire Réactions et Génie des Procédés (UMR 7274 CNRS)  
pour l'obtention du grade de

**Docteur de l'Université de Lorraine**  
**Spécialité : Génie des Procédés et des Produits**

Par

**Yann LE BRECH**

---

## **Analyse des mécanismes primaires de pyrolyse de la biomasse**

---

Soutenue le 10 Septembre 2015 devant la Commission d'Examen

Rapporteurs : Michel BARDET – Commissariat à l'Energie Atomique  
Olivier BOUTIN – Université Aix-Marseille

Examineurs : Nadège CHARON –IFP Energies Nouvelles  
Roger GADIOU – Université de Haute-Alsace (Président du jury)  
Nicolas BROSSÉ – Université de Lorraine (Directeur de thèse)  
Anthony DUFOUR – CNRS-Université de Lorraine (co-directeur de thèse)

Invités : Jésus RAYA – CNRS-Université de Strasbourg  
Luc DELMOTTE – CNRS-Université de Haute-Alsace



## **Le projet PYRAIM**

Le projet PYRAIM (Etude méthodologique de la PYRolyse de la biomasse avec Analyses In-situ et Modélisation détaillée) a été financé par l'ANR (Agence National de la Recherche). Ce projet a été/est coordonné par Anthony Dufour chercheur CNRS (Centre National de la Recherche Scientifique) au LRGP (Laboratoire des Réactions et du Génie des Procédés). De nombreux partenaires ont participé et/ou participent activement à ce projet :

- 1) l'Université de Lorraine avec le Professeur Nicolas Brosse membre du LERMAB (Laboratoire d'Etude et de Recherche sur le Matériau Bois), Sébastien Leclerc ingénieur au CRM<sup>2</sup> (Laboratoire de Cristallographie, Résonance Magnétique et Modélisations, UMR CNRS 7036) et au LEMTA (Laboratoire d'Energétique et de Mécanique Théorique et Appliquée, UMR 7563) ;
- 2) l'Institut de Science des Matériaux de Mulhouse (IS2M) avec le Professeur Roger Gadiou et Luc Delmotte (ingénieur de recherche CNRS) ;
- 3) l'Université de Strasbourg avec Jésus Raya (ingénieur de recherche CNRS).

J'exprime mes sincères remerciements à mon directeur de thèse, Professeur Nicolas BROSSE, pour son soutien et sa disponibilité. J'exprime également mes profonds remerciements à Monsieur Anthony DUFOUR (co-directeur de thèse) pour m'avoir confié un projet qu'il a construit et soutenu. J'exprime une grande gratitude vis-à-vis des personnes qui m'ont aidé à avancer dans mes recherches en contribuant à ce projet. Je pense particulièrement à Monsieur Luc DELMOTTE et à Monsieur Jésus RAYA qui m'ont initié aux joies et aux peines de la Résonance Magnétique Nucléaire. Je les remercie tout particulièrement pour avoir pris le temps de m'enseigner quelques notions de cette technique. Merci également au Professeur Roger GADIOU pour son implication dans ce projet. Merci également à Monsieur Sébastien LECLERC et toute l'équipe du laboratoire de Cristallographie, Résonance Magnétique et Modélisations de la faculté de Vandoeuvre pour leur encadrement lors des essais de pyrolyse « in situ ». Un grand merci à Monsieur Thierry GHISLAIN pour m'avoir enseigné une infime part de son savoir en spectrométrie de masse et techniques séparatives. Un grand merci à Monsieur Michel MERCY pour sa disponibilité et ses conseils avisés lors de mes expérimentations.

Je tiens également à remercier chaleureusement les membres de l'équipe GREENER au LRGP pour m'avoir supporté lors de ces quatre années. Merci à Francis, Guillaïn, George, Airy, Ludivine, Christophe, Roberto, Chloé, Riccardo, Jia, Benjamin, Binod, Felipe, Jenny, Libeth. Je tiens à remercier particulièrement Monsieur Sadio CISSE, stagiaire Master 2, que j'ai eu le plaisir d'encadrer et qui a fourni un excellent travail. Mes remerciements vont aussi aux membres du LERMAB avec qui j'ai eu le plaisir d'évoluer. Merci à François, Lyne, Nicolas et Dominique.

Je remercie les membres du LRGP avec qui j'ai eu l'occasion de travailler et qui m'ont aidé à réaliser ce projet. Merci aux membres de l'atelier de mécanique : Pascal, Christian, Alain, Yann et Laurent. Merci aux membres du service analytique : Steve, Emilien et Hélène. Merci aux membres de l'équipe du service électronique : Franck, Hakim et David. Je remercie toutes les autres personnes avec qui j'ai eu l'occasion d'interagir quotidiennement ou occasionnellement : Valérie, Olivier, Véronique, Nathalie, Gérard et Bruno. Merci aux membres de l'équipe d'enseignement de chimie minérale avec qui j'ai eu le plaisir de travailler pendant trois ans : Merci à Mohammed, Ludivine, Nathalie, Dominique et Melissa. Merci également à tous les copains de thèse : Jessica, Florent, Marie-Claire, Lubin, Darwin, Mathilde, Nicolas, Laurent, Ivana, Billy, Milena.



# Sommaire

<b>I.</b>	<b>Introduction générale .....</b>	<b>1</b>
<b>II.</b>	<b>Etude Bibliographique .....</b>	<b>9</b>
II.1	La biomasse lignocellulosique .....	11
II.2	La composition chimique de la matière lignocellulosique .....	11
II.3	La valorisation de la biomasse lignocellulosique .....	17
II.4	La pyrolyse de la biomasse lignocellulosique .....	18
II.4.1	Définitions et généralités .....	18
II.4.2	Pyrolyse de la cellulose .....	21
II.4.3	Pyrolyse des hémicelluloses .....	31
II.4.4	Pyrolyse de la lignine .....	34
II.4.5	Pyrolyse de la biomasse .....	37
II.4.6	Influence des minéraux sur les mécanismes de pyrolyse de la biomasse .....	38
II.5	Organisation de la démarche de la thèse .....	40
<b>III.</b>	<b>Etude des mécanismes de formation du biochar par RMN haute résolution .....</b>	<b>49</b>
III.1	Article 1: High resolution solid state 2D NMR analysis of biomass and biochar .....	51
III.1.1	Abstract .....	51
III.1.2	Main text .....	51
III.1.3	References .....	57
III.1.4	Supporting information .....	60
III.2	Article 2: Mechanism of biomass char formation investigated by advanced solid state NMR .....	68
III.2.1	Abstract .....	68
III.2.2	Introduction .....	68
III.2.3	Material and methods .....	70
III.2.4	Results and discussion .....	72
III.2.5	Conclusion .....	85
III.2.6	References .....	86
III.2.7	Supporting information .....	90
<b>IV.</b>	<b>Etude de l'influence du potassium sur les mécanismes de pyrolyse de la biomasse .....</b>	<b>99</b>
IV.1	Article 3: Effect of potassium on the mechanisms of biomass pyrolysis as studied by in-situ <sup>1</sup> H NMR, TG-DSC and LC/MS .....	101
IV.1.1	Abstract .....	101
IV.1.2	Introduction .....	102
IV.1.3	Material and methods .....	104
IV.1.4	Results and discussion .....	107
IV.1.5	Conclusion .....	119
IV.1.6	References .....	120
IV.1.7	Supporting information .....	124
<b>V.</b>	<b>Etude de la formation des composés volatils .....</b>	<b>129</b>
V.1	Article 4: Biomass slow pyrolysis in a fixed bed reactor: mass balance, gas composition and analysis of primary volatiles by on-line VUV photoionisation mass spectrometry and off-line GC*GC/MS-FID .....	131

V.1.1	Abstract.....	131
V.1.2	Introduction .....	131
V.1.3	Material and methods .....	133
V.1.4	Results .....	135
V.1.5	Conclusion.....	149
V.1.6	References .....	150
V.1.7	Supporting information.....	153
<b>VI.</b>	<b>Multianalyse de la pyrolyse du miscanthus.....</b>	<b>163</b>
	Article 5: Multianalytical analysis of miscanthus pyrolysis.....	165
	<b>Conclusion et perspectives.....</b>	<b>169</b>
	<b>Liste des communications écrites et orales .....</b>	<b>171</b>
	<b>Annexes : Techniques d'analyses et de caractérisations.....</b>	<b>172</b>
	Broyage de la biomasse.....	172
	Détermination du taux de lignine de Klason .....	172
	Analyses par chromatographie ionique (IC) HPAEC-PAD.....	172
	Analyses élémentaires.....	173
	Analyses Organique Carbone Total (TOC).....	173
	Analyses Chromatographie d'exclusion stérique .....	174
	Analyses par calorimétrie.....	176
	Calibration de la température pour les mesures en <sup>1</sup> H RMN Haute Température.....	177
	Analyse par chromatographie gazeuse et spectrométrie de masse et détecteur à ionisation de flamme avec « heartcutting » (GC*GC/FID*MS).....	178
	Analyse par µGC.....	178

# Liste des Figures

Figure I-1 : L'évolution de la production mondiale en énergie primaire <sup>1</sup> .....	3
Figure I-2 : Les différentes sources de la production d'énergie primaire mondiale en 2012 <sup>1</sup> .....	4
Figure I-3 : Le mix énergétique comme solution préventive .....	5
Figure II-1 : La photosynthèse au centre du cycle court du carbone.....	11
Figure II-2 : L'organisation des parois cellulaire <sup>11</sup> .....	12
Figure II-3 : La structure chimique de la cellulose.....	13
Figure II-4 : La structure moléculaire des principaux sucres constituant les hémicelluloses <sup>19</sup> .....	14
Figure II-5 : Les structures des trois monolignols de la lignine .....	15
Figure II-6 : Un exemple d'une structure chimique d'une lignine (résineux) <sup>20,24,25</sup> .....	15
Figure II-7 : Les différentes voies de transformation de la biomasse lignocellulosique .....	17
Figure II-8 : L'influence de la température et de la densité de flux de chaleur sur le rendement massique des produits de pyrolyse (adapté de X.Deglise, et A.Donnot, Techniques de l'ingénieur, 2004).....	19
Figure II-9 : L'influence du temps de séjour et de la température sur la nature chimique des goudrons de pyrolyse <sup>44</sup> .....	19
Figure II-10 : Les différentes étapes de la pyrolyse d'après Robert J. Evans et Thomas Milne <sup>40</sup> .....	20
Figure II-11 : Le schéma cinétique de Broido et Kilzer .....	21
Figure II-12 : Le schéma de Broido-Shafizadeh.....	22
Figure II-13 : Le schéma de Waterloo .....	23
Figure II-14 : Le schéma de Diebold .....	23
Figure II-15 : Le schéma de Banyasz .....	24
Figure II-16 : Le schéma de Wang et Garcia-Perez <sup>43</sup> .....	25
Figure II-17 : Mécanisme de déshydratation inter-moléculaire inspiré de Broido <sup>55</sup> et Scheirs <sup>92</sup> .....	28
Figure II-18 : Le mécanisme concerté de transglycosylation d'une chaîne de cellulose <sup>40</sup> .....	29
Figure II-19 : Le mécanisme de Richard <sup>60</sup> .....	30
Figure II-20 : Le bilan global de la dégradation thermique primaire de la cellulose.....	31
Figure II-21 : Mécanisme de formation du 1,4-anhydro-D-xylopyranose inspirée des travaux de Ponder <sup>116</sup> ...	32
Figure II-22 : Mécanisme de formation des pyranones d'après les travaux de Shafizadeh .....	33
Figure II-23 : Le bilan global de la dégradation thermique d'une structure partielle <sup>13</sup> de xylane .....	33
Figure II-24 : Le schéma de la dégradation du réseau ligneux par C $\gamma$ élimination et déshydratation.....	34
Figure II-25 : Le schéma de la dégradation des liaisons éthers du réseau ligneux .....	35
Figure II-26 : L'évolution de la structure chimique des volatils issus de la décomposition thermique de la lignine en fonction de la température.....	36
Figure III-1: Schematic representation of the main moieties of miscanthus giganteus <sup>2</sup> and notations for carbon atoms.....	53
Figure III-2: a) <sup>1</sup> H- <sup>13</sup> C 2D HETCOR spectra of miscanthus, b) zoom on 175-100ppm zone.....	54
Figure III-3: <sup>1</sup> H- <sup>13</sup> C 2D HETCOR spectra a) comparison between native miscanthus and biochar produced at 300°C, b) zoom on 165-100 ppm $\delta^{13}$ C zone of biochar, c) zoom on 70-50 ppm $\delta^{13}$ C comparison between native miscanthus and biochar highlighting the shielding of methoxyl group in lignin-based aromatic clusters .....	55
Figure III-4: Representation of some chemical moieties in char .....	56
Figure III-5: <sup>13</sup> C solid state NMR spectras for different char .....	64

Figure III-6: Effect of contact time on 1D <sup>13</sup> C CP/MAS analysis of miscanthus (green curve: 1ms, red: 2ms, black: 3ms, blue: 4ms).....	64
Figure III-7: Effect of contact time on 1D <sup>13</sup> C CP/MAS analysis of 350°C char.....	65
Figure III-8: <sup>1</sup> H- <sup>13</sup> C Hector spectrum for cellulose extracted from Miscanthus .....	65
Figure III-9: <sup>1</sup> H- <sup>13</sup> C Hector spectrum for 300°C Miscanthus char.....	66
Figure III-10 : Thermo-gravetric analysis of miscanthus.....	66
Figure III-11: Procedure for lignin, holocellulose and cellulose extractions from Miscanthus x Giganteus.....	70
Figure III-12: Fixed bed pyrolysis reactor.....	71
Figure III-13: Thermo-gravimetric analysis (lines) compared to char mass yield from fixed bed experiments (points) .....	73
Figure III-14: Comparison of NMR signal from CP/MAS APHH (in blue) and DP/MAS APHH (in red) ....	74
Figure III-15: Schematic representation of the main moieties in Miscanthus x Giganteus <sup>38</sup> and notations for carbon atoms.....	75
Figure III-16: <sup>13</sup> C NMR CP/MAS APHH spectra of native miscanthus (20°C) and chars produced after different final temperature (fixed bed, 5 K/min). Char yields are recalled at the right of each spectrum. See table III-4 for the assignment of the main bands.....	77
Figure III-17: Evolution of main moieties (%mol of original carbon) during pyrolysis of MxG as a function of temperature.....	78
Figure III-18: Solid-state NMR <sup>13</sup> C CPMAS spectra evolution for fractionated macromolecules as a function of temperature.....	79
Figure III-19: Evolution of main moieties (% Original Carbons) during pyrolysis for extracted macromolecules as a function of temperature .....	80
Figure III-20: <sup>1</sup> H- <sup>13</sup> C HETCOR spectra from holocellulose biochar produced at 300°C.....	82
Figure III-21: Quantitative evolution of aromatic carbons (mmolC/g biomass) into MxG char and fractionated biomass as a function of temperature.....	85
Figure III-22: Solid-state 1D <sup>13</sup> C CPMAS APHH spectrum of Miscanthus with spectral deconvolution.....	94
Figure III-23: Solid-state 1D <sup>13</sup> C CPMAS APHH spectrum of Miscanthus char 300°C with spectral deconvolution .....	94
Figure III-24: 2D <sup>1</sup> H- <sup>13</sup> C Hetcor spectrum of Holocellulose .....	96
Figure IV-1: Simplified scheme of a) U-shape quartz fixed bed, b) calorimeter fixed bed, c) 1H NMR High temperature probe equipped with flushing gas.....	105
Figure IV-2: Effect of carrier gas flow rate on fluidity development during Miscanthus pyrolysis.....	109
Figure IV-3: DSC, DTG , % Mobility and TOC evolution as function of temperature for Cellulose and Impregnated Cellulose.....	111
Figure IV-4: Effect of pyrolysis temperature on the composition of water soluble compounds extracted from char quenched at various pyrolysis temperatures for a) cellulose and b) K-impregnated cellulose.....	112
Figure IV-5: Quantification of the levoglucosan and cellobiosan in the water soluble fractions extracted from char quenched at various pyrolysis temperatures for pure cellulose.....	113
Figure IV-6: DSC, DTG, <sup>1</sup> H NMR and TOC for a) Miscanthus, b) Misc_Demin, c) Misc_Demin_1K .....	115
Figure IV-7: SEC-DEDL of water extracted Misc. a), water Misc_Demin b), water Mis_Demin_1K c) .....	116
Figure IV-8: Miscanthus, douglas, oak : a) DSC, b) <sup>1</sup> H NMR c) DTG.....	118
Figure IV-9: Evolution of the Mobile hydrogen fractions as function of temperature for a) miscanthus and b) demineralised miscanthus.....	125
Figure IV-10: ELSD a) and TIC b) from the water-soluble fraction of cellulose char 300°C .....	126
Figure IV-11: Anhydro-sugars MS spectra identified in water-soluble fractions.....	128

Figure V-1: Schematic of the fixed bed reactor.....	134
Figure V-2: Mass balances for miscanthus slow pyrolysis .....	135
Figure V-3: Mass balances for oak and douglas slow pyrolysis .....	136
Figure V-4: The gas release from the slow primary pyrolysis pyrolysis of miscanthus.....	137
Figure V-5: Chromatogram for the condensable sampled from the three biomasses at 500°C final temperature .....	138
Figure V-6: Effect of the final pyrolysis temperature on the yield of some key primary tar compounds from miscanthus. a) Low molecular weight molecules, b) furan derivatives, c) phenol derivatives .....	140
Figure V-7: Simplified mechanism of cellulose pyrolysis highlighting the main degradation pathways and key markers.....	141
Figure V-8: Total mass spectra accumulated on whole experimental time until 500°C .....	142
Figure V-9: On-line analysis of key markers by SPI-MS vs. temperature of pyrolysis for miscanthus, a) hemicelluloses and carbohydrate fragments, b) main cellulose markers, c) lignin markers at low temperature, d) lignin markers at high temperature. ....	143
Figure V-10: On-line analysis of key markers by SPI-MS vs. temperature of pyrolysis for oak, a) hemicelluloses and carbohydrate fragments, b) main cellulose markers, c) lignin markers at low temperature, d) lignin markers at high temperature. ....	145
Figure V-11: On-line analysis vs. time of pyrolysis for douglas slow pyrolysis, a) hemicelluloses and carbohydrate fragments b) main cellulose markers c) lignin markers low temperature d) lignin markers high temperature.....	147
Figure V-12: Simplified mechanism of lignin pyrolysis highlighting the formation of the different markers as a function of temperature .....	148
Figure V-13: DTG curves (5K/min of the TGA) .....	153
Figure V-14: Comparison between thermogravimetric analysis (line) and char yield obtained in the fixed bed reactor after char quenching (points) for miscanthus pyrolysis (5K/min) .....	153
Figure V-15: The gas release from pyrolysis of oak and douglas .....	156
Figure V-16: Plots for calibration of compounds on de Saint Laumer heart-cutting method.....	158
Figure V-17: Comparison between experimental response factors and predicted by de Saint Laumer method .....	158
Figure VI-1: Multi-analytical study of biomass pyrolysis .....	165
Figure VI-2: Evolution of main moieties (%mol of original carbon) during pyrolysis of Miscanthus .....	166
Figure VI-3: Formation of coniferaldehyde.....	167
Figure VI-4: On-line analysis vs. time of pyrolysis for Miscanthus slow, a) hemicelluloses and carbohydrate fragments, b) main cellulose markers c) lignin markers low temperature d) lignin markers high temperature .....	167
Figure VI-5: % Mobility determined by in-situ <sup>1</sup> H NMR as function of temperature during miscanthus pyrolysis.....	168
Figure A-1 : Calibration pour analyses Total Organique Carbone .....	173
Figure A-2 : Calibration pour la quantification des sucres solubles .....	175
Figure A-3 : Les droites de calibration en température pour les analyses en calorimétrie.....	176
Figure A-4 : La droite de calibration en température pour les analyses <sup>1</sup> H RMN.....	177

## Liste des tableaux

Tableau II-1 : Compositions élémentaires de différentes biomasses (*calculé par différence).....	12
Tableau II-2 : Composition en sucres pour différentes biomasses. *inclut le glucose venant de la cellulose .....	14
Tableau II-3 : Composition en éléments inorganiques de différentes biomasses .....	16
Tableau II-4 : Tableau récapitulatif de différents travaux sur la caractérisation de la cellulose active.....	27
Tableau II-5 : Rendements en charbons obtenus en thermogravimétrie pour les différents constituants de la biomasse (% Charbon) sur masse sèche).....	37
Tableau II-6 : Influence de la présence d'inorganiques sur la dégradation thermique des constituants de la biomasse (Ti = Température de début de perte de masse ; Tmax = Température de vitesse maximale de conversion ; % charbon sur masse sèche) .....	39
Table III-1: Elemental composition of miscanthus .....	60
Table III-2: Ash composition of miscanthus .....	60
Table III-3: Composition of miscanthus .....	60
Table III-4 : Assignments of <sup>13</sup> CP/MAS APHH bands on miscanthus and extracted macromolecules and chars (band numbers are reported in Figures III-16 and III-18 on the NMR spectra, see Figure III-15 for the nomenclature of carbon notations) <sup>31,32,51-53</sup> .....	76
Table III-5: Tentative assignment of 2D <sup>1</sup> H- <sup>13</sup> C correlations analysed in holocellulose char at 300°C .....	82
Table III-6: Composition of Miscanthus and extracted polymers .....	91
Table III-7: Inorganics content in the different samples .....	91
Table III-8: Molecular weight distribution analysis .....	92
Table III-9: Elemental analysis of miscanthus and extracted macromolecules .....	93
Table IV-1: Initial temperature decomposition (Ti), maximum degradation rate temperature (Tmax) and char weight yield (%char) for different biomass samples and various potassium contents .....	103
Table IV-2: Inorganic elemental contents in sample before and after mineralization/demineralization .....	108
Table IV-3: Compositions before and after demineralization .....	108
Table IV-4: Comparison of char yields for the different experimental techniques (*NMR at 420°C final temperature) .....	109
Table IV-5: Analysis of lignin and sugars composition in biomasses .....	124
Table IV-6: Identified compounds as function of samples .....	127
Table V-1: Main compounds quantified (mg/g dry biomass) by GC/MS-FID (* n.q means not quantified) .....	139
Table V-2: Elemental analysis for miscanthus, oak and douglas .....	154
Table V-3: Analysis of lignin and sugars composition in biomasses.....	155
Table V-4: Organics content of the different biomasses .....	155
Tableau A-1 : Résultats des analyses TOC des extraits de charbon .....	174
Tableau A-2 : Les standards utilisés pour la calibration de la température en calorimétrie.....	176

## **I. Introduction générale**



## Introduction générale

La croissance démographique mondiale, l'industrialisation et l'urbanisation de nos sociétés modernes se sont accompagnées d'une forte augmentation de la demande en énergie primaire. Selon l'Agence Internationale de l'Énergie (AIE), la production mondiale d'énergie primaire<sup>1</sup> a été estimée à 13,371 Gtep<sup>a</sup> ( $5,6 \times 10^{20}$  J) en 2012 (Figure I-1). D'après les données publiées par l'AIE, on observe une augmentation constante de la production en énergie primaire à l'échelle mondiale entre 1970 et 2012. La production d'énergie devrait continuer d'augmenter pour atteindre environ 18,5 Gtep en 2035 dans le cas du « *Current Policies Scenario* » qui considère les réformes politiques actuelles.

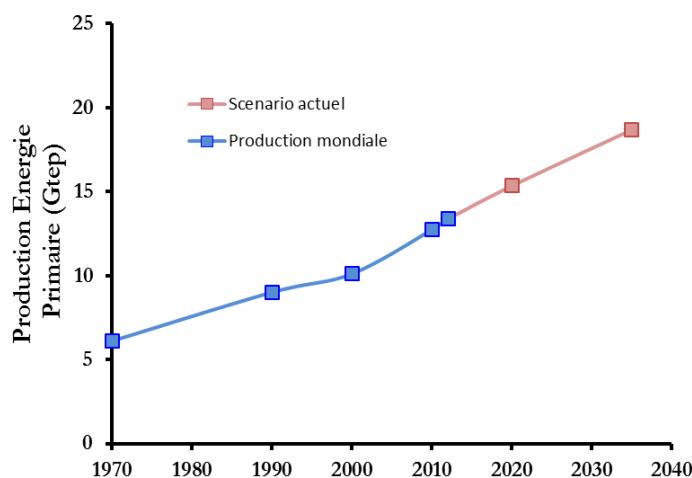


Figure I-1 : L'évolution de la production mondiale en énergie primaire<sup>1</sup>

D'après les chiffres de l'année 2012<sup>1</sup>, l'approvisionnement en énergie primaire est principalement basé sur les ressources géologiques : le pétrole (31,4%), le charbon (29%), le gaz naturel (21,3%) et le nucléaire (4,8%). Les énergies dites renouvelables<sup>2</sup> ne représentant « uniquement » 13,5% de l'énergie primaire produite en 2012 : 2,4% pour l'hydraulique, 10% pour la « biomasse et déchets » et seulement 1,1% pour l'ensemble géothermie, solaire, et éolien (Figure I-2).

La production énergétique mondiale est par conséquent dépendante des énergies dites épuisables puisqu'on estime à plusieurs milliers d'années voire des millions d'années pour que les réserves géologiques se reforment<sup>2</sup>. Avec un rythme d'exploitation inchangé, les réserves en pétrole correspondraient à environ une cinquantaine d'années. Le pic de production devrait d'après Rolland Vialy<sup>3</sup>, géologue à l'IFP Energies nouvelles, être atteint en 2035 pour les scénarios les plus optimistes. Cependant il ne faut pas négliger le fait que des découvertes de nouvelles réserves<sup>4</sup> (e.g. en Arctique) ou des avancées technologiques (notamment des techniques de forage) pourraient repousser davantage la fin de l'hégémonie de la ressource fossile.

<sup>a</sup> tep = tonnes équivalent pétrole (41,868 GJ)

## Introduction générale

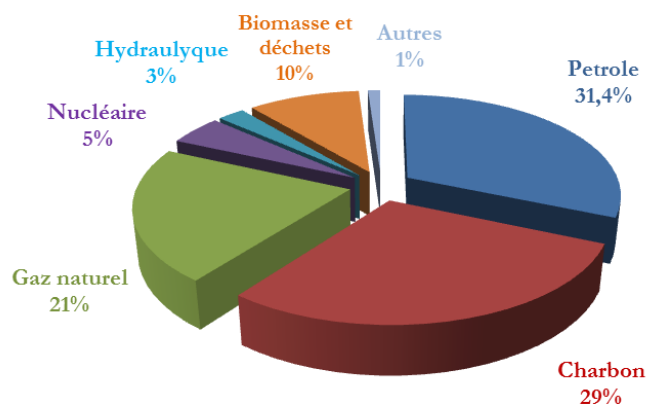


Figure I-2 : Les différentes sources de la production d'énergie primaire mondiale en 2012<sup>1</sup>

La problématique de l'approvisionnement de l'énergie mondiale ne se résume pas uniquement au problème de la disponibilité de la ressource fossile (96 millions de barils de pétrole consommés par jour !)<sup>3</sup> mais aussi aux perturbations climatiques, politiques et économiques engendrées. En effet, la surexploitation d'énergie carbonée à cycle long (de formation) entraîne sans équivoque une perturbation de la stabilité du climat<sup>5</sup> due notamment à l'émission de gaz à effet de serre (31 Gt de CO<sub>2</sub> en 2102 à 99,5% d'origine fossile)<sup>1</sup>. De plus, la raréfaction et la répartition inégale des ressources géologiques sur la planète ont pour conséquence de créer des conflits à travers la planète motivés par la volonté de contrôler des filières ou des zones d'approvisionnement par des états ou des organisations. L'accès à l'énergie pour les populations les plus défavorisées reste difficile. Il est donc nécessaire d'envisager et de préparer une transition énergétique qui devra déboucher sur un système énergétique largement basé sur des énergies renouvelables, à impact limité sur le climat et plus égalitaire.

La plupart des scénarios énergétiques envisagés montrent qu'une utilisation optimisée de l'énergie et l'augmentation de la part des énergies renouvelables permettraient de réduire les impacts néfastes provoqués. Un grand nombre de pays se sont engagés à travers différents sommets internationaux (Kyoto 1997, Copenhague 2009, Rio 2012) à prendre différentes mesures comme la diminution des émissions de gaz à effet de serre afin de lutter contre le réchauffement de la planète. L'Alliance nationale de coordination de la recherche pour l'énergie (Ancre) souligne que la décarbonisation du système énergétique ainsi que la promotion de l'efficacité énergétique à l'horizon 2050 se fera par des changements plus ou moins marqués dans les comportements des consommateurs et vers davantage d'énergies renouvelables dans le mix énergétique<sup>6</sup> (Figure I-3). C'est dans ce contexte que le développement des énergies dites bio-sourcées présente un très fort intérêt. La transformation de la ressource lignocellulosique<sup>7</sup> en énergies (combustibles ou électricité) apparaît à ce jour comme une alternative prometteuse car elle demeure rapidement applicable, réduit le conflit entre nourriture ou carburant (*Food or Fuel*) pour l'usage des sols et présente de faibles impacts sur l'environnement (cycle court du carbone).<sup>8</sup> Historiquement cette solution a déjà été envisagée, au début du 20<sup>ème</sup> siècle par plusieurs industries qui se sont intéressées au potentiel de la matière lignocellulosique dans la production de composés chimiques ou d'énergie produits actuellement principalement à partir de ressources fossiles.<sup>9</sup> La crise pétrolière des années 1970 a ravivé l'engouement pour cette ressource et de nombreuses recherches ont été effectuées afin de développer et d'optimiser la transformation de la biomasse en énergie.



Figure I-3 : Le mix énergétique comme solution préventive

Malgré ces innovations, la production et la consommation d'énergie provenant de ressources géologiques ont continué à dominer notre système énergétique amenant nos sociétés dans une totale dépendance. Cependant l'intérêt concernant la transformation de la matière lignocellulosique est à nouveau source de recherches et de développements<sup>10</sup>. Ces principaux avantages sont qu'elle est la principale ressource en carbone renouvelable et qu'elle n'est pas une source d'énergie produite de manière intermittente (comme le solaire ou l'éolien). En effet la matière lignocellulosique est principalement constituée de carbone, d'hydrogène et d'oxygène. Actuellement le bois est la forme la plus utilisée dans le monde pour le chauffage ou la cuisson<sup>11</sup>. Mais ses propriétés lui permettent également d'être utilisée dans des unités de production de chaleur et d'électricité de grandes tailles en substitution des énergies fossiles<sup>12</sup> ainsi que dans des bio-raffineries afin de produire des carburants liquides ou des biomatériaux<sup>10</sup>. Les filières de valorisations thermochimiques (combustion, gazéification, pyrolyse et liquéfaction) de cette ressource sont actuellement en plein essor et s'inscrivent pleinement dans l'objectif de 23% d'énergies renouvelables, à l'horizon 2020, dans la consommation énergétique française fixé par le Grenelle de l'environnement<sup>13</sup>. L'Union Européenne, pour sa part, vise l'objectif de 20% de la part d'énergies renouvelables dans le mix énergétique pour 2020<sup>13</sup>. Cependant, il est évident que ce nouvel essor présente également de nombreux verrous écologiques et technologiques. La mobilisation de quantités importantes de ressources lignocellulosiques risque à terme d'engendrer une surexploitation des forêts ou des sols<sup>12</sup>. La mobilisation et le transport de cette ressource solide et à faible densité énergétique causent également des limitations majeures quant à son utilisation. Les procédés de transformations thermochimiques demandent encore à être optimisés par des recherches fondamentales et technologiques.

Depuis le début de l'humanité la biomasse a été une des sources majeures d'énergie et actuellement elle demeure encore la source principale d'énergie pour la moitié de la population mondiale<sup>14</sup>. Cette dernière présente un fort potentiel dans le développement du mix énergétique. On estime que  $120 \times 10^{15}$  g de biomasse sèche sont produites chaque année sur la planète représentant environ  $2,2$  à  $4,5 \times 10^{21}$  joules (J) d'énergie solaire capturées par les plantes.<sup>14,15</sup> Le potentiel de production de bioénergies en 2050 est estimé de  $33$  à  $1135 \times 10^{18}$  J principalement à partir des cultures dédiées (*Energy Crops*) et de résidus agricoles.<sup>14,15</sup> Le potentiel

## Introduction générale

mobilisable en biomasse serait de 2230 Mtep/an<sup>16,17</sup> (sans risque de déforestation) et la biomasse pourrait correspondre à 30% de nos besoins énergétiques mondiaux en 2050<sup>15</sup> à condition que la production de biomasse soit optimisée à travers le développement et l'amélioration, par exemple, des techniques d'irrigation, de fertilisation et de gestion de cette ressource.<sup>14</sup> Le potentiel de la matière végétale en France est estimé à environ 30 millions de tep, ce qui correspond à 10% de la consommation en énergie primaire<sup>2</sup>. Les sources potentielles en biomasse englobent les forêts (6,2-10,2 Mtep/an), les déchets organiques (5,4 Mtep/an), les résidus agricoles (4,3 Mtep/an) et les cultures dédiées (1-5 Mtep/an).

Cette thèse porte principalement sur le *Miscanthus x Giganteus* (MxG). Le MxG est plus communément appelé le roseau de Chine ou herbe à éléphant. Il est issu d'une hybridation entre le *Miscanthus Sinensis* et le *Miscanthus Sacchariflorus*. Implanté pour la première fois au Danemark (1983), il n'a cessé de se développer en Europe de l'ouest, principalement en Allemagne et en Angleterre. Cette plante a suscité un intérêt croissant lors des 20 dernières années dans le domaine de la valorisation de la matière lignocellulosique. En effet, elle possède plusieurs caractéristiques qui lui confèrent un fort potentiel au sein du développement de la filière lignocellulosique. Le MxG est une espèce stérile, d'où un risque de propagation incontrôlée réduit. La production de biomasse provenant du MxG est estimée entre 15 et 25 tonnes de matière sèche par hectare après trois années de croissance. La tige du miscanthus est composée de 75 à 80% d'holocelluloses et de 25 à 30% de lignine, ce qui fait du MxG une ressource intéressante en polysaccharides (cellulose et hémicelluloses) et en lignine<sup>18</sup>.

**Références**

- (1) IEA. *Key World Energy Statistics 2014*; 2014.
- (2) Mosseri, R.; Jeandel, C. *L'énergie À Découvert*, CNRS EDITIONS.; 2013.
- (3) Vialy, R. Les Réserves de Pétrole-IFP Energies Nouvelles-[Http://www.ifpenergiesnouvelles.fr](http://www.ifpenergiesnouvelles.fr), 2013.
- (4) Hureau, G.; Vialy, R. *Nouvelles Découvertes de Pétrole et de Gaz Conventionnels-IFP Panorama*; 2014.
- (5) Ragauskas, A. J.; Beckham, G. T.; Bidy, M. J.; Chandra, R.; Chen, F.; Davis, M. F.; Davison, B. H.; Dixon, R. A.; Gilna, P.; Keller, M.; Langan, P.; Naskar, A. K.; Saddler, J. N.; Tschaplinski, T. J.; Tuskan, G. A.; Wyman, C. E. Lignin Valorization: Improving Lignin Processing in the Biorefinery. *Science* **2014**, *344* (6185).
- (6) Hache, E. *Les Scénarios Énergétiques de l'Ancre-IFP Panorama*; IFP energies nouvelles, 2014.
- (7) David, K.; Ragauskas, A. J. Switchgrass as an Energy Crop for Biofuel Production: A Review of Its Ligno-Cellulosic Chemical Properties. *Energy Environ. Sci.* **2010**, *3* (9), 1182–1190.
- (8) Dufour, A. Geological Sequestration of Biomass Char to Mitigate Climate Change. *Environ. Sci. Technol.* **2013**, *47* (18), 10106–10107.
- (9) Ragauskas, A. J.; Williams, C. K.; Davison, B. H.; Britovsek, G.; Cairney, J.; Eckert, C. A.; Frederick, W. J.; Hallett, J. P.; Leak, D. J.; Liotta, C. L.; Mielenz, J. R.; Murphy, R.; Templer, R.; Tschaplinski, T. The Path Forward for Biofuels and Biomaterials. *Science* **2006**, *311* (5760), 484–489.
- (10) Brosse, N.; Dufour, A.; Meng, X.; Sun, Q.; Ragauskas, A. Miscanthus: A Fast-Growing Crop for Biofuels and Chemicals Production. *Biofuels Bioprod. Biorefining-Biofpr* **2012**, *6* (5), 580–598.
- (11) Baumlin, S. Craquage Thermique Des Vapeurs de Pyrolyse-Gazéification de La Biomasse En Réacteur Parfaitement Auto-Agité Par Jets Gazeux, l'Institut National Polytechnique de Lorraine, 2006.
- (12) François, J. Modélisation et Évaluation Environnementale Des Filières de Cogénération Par Combustion et Gazéification Du Bois, Université de Lorraine: Institut Jean Lamour, 2014.
- (13) Dussud, F.-X.; Rabai, Y. *Objectifs Énergétiques Europe 2020 : La France doit poursuivre ses efforts pour les énergies renouvelables*; Commissariat général au développement durable, 2014.
- (14) Bhaskar, T.; Pandey, A. Chapter 1 - Advances in Thermochemical Conversion of Biomass—Introduction. In *Recent Advances in Thermo-Chemical Conversion of Biomass*; Sukumaran, A. P. B. S. K., Ed.; Elsevier: Boston, 2015; pp 3–30.
- (15) Guo, M.; Song, W.; Buhain, J. Bioenergy and Biofuels: History, Status, and Perspective. *Renew. Sustain. Energy Rev.* **2015**, *42*, 712–725.
- (16) Dufour, A. Optimisation de La Production D'hydrogène Par Conversion Du Méthane Dans Les Procédés de Pyrolyse/gazéification de La Biomasse, 2007.
- (17) Parikka, M. Global Biomass Fuel Resources. *Biomass Bioenergy* **2004**, *27* (6), 613–620.
- (18) El Hage, R. Prétraitement Du Miscanthus X Giganteus. Vers Une Valorisation Optimale de La Biomasse Lignocellulosique, Université de Nancy, 2010.



## II. Etude Bibliographique



## II.1 La biomasse lignocellulosique

Dans le domaine des bioénergies, la biomasse désigne l'ensemble des matières organiques d'origine végétale qui sont transformées en énergie. Les plantes transforment l'énergie solaire en matière organique par la transformation du  $\text{CO}_2$  en sucres (photosynthèse, Figure II-1) afin de constituer un stock de « combustible vert » qui se trouve localisé au sein des organismes végétaux sous la forme de molécules (saccharose, amidon, lipides). Ce stock de molécules convient essentiellement à un mode de transformation<sup>1</sup> dit enzymatique ou biologique intervenant naturellement au sein des plantes afin de fournir l'énergie et les matériaux nécessaires à leur survie et leur croissance. Les composants chimiques synthétisés par cette « manufacture biochimique » permettent de constituer les éléments structuraux des plantes (matière lignocellulosique) comme les polysaccharides et la lignine des parois végétales.

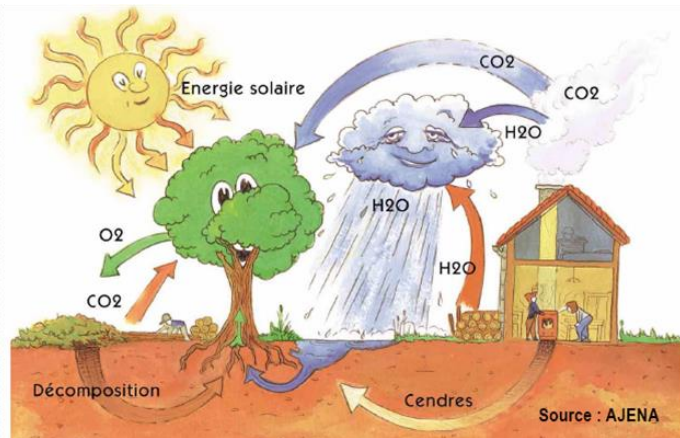


Figure II-1 : La photosynthèse au centre du cycle court du carbone

## II.2 La composition chimique de la matière lignocellulosique

La matière lignocellulosique est principalement constituée de carbone (C), d'hydrogène (H), d'oxygène (O), d'azote (N), de soufre (S) et de matière inorganiques (Si, K, Na, Ca, Mg,...). L'eau est le constituant le plus important dans la biomasse lignocellulosique. Elle est localisée dans la sève et les cellules végétales. La teneur en eau varie sensiblement d'une espèce à une autre<sup>2</sup>. Afin de valoriser la biomasse lignocellulosique par voie thermochimique (combustion, gazéification et pyrolyse), il est important de noter qu'une étape de séchage est nécessaire afin d'obtenir une biomasse dite sèche. Cette étape, bien que très étudiée<sup>3</sup>, ne sera pas présentée ici et les différentes données concernant les biomasses utilisées et les produits obtenus sont par conséquent toujours données en masse sèche (ou anhydre). L'étape de séchage peut être évitée lorsque par des procédés de conversion hydrothermaux (sous pression en milieu liquide, eau et/ou autres media).

Les concentrations en éléments C, H, O varient assez peu d'une biomasse lignocellulosique à une autre (Tableau II-1). Le carbone reste en général l'élément le plus abondant en masse (~50%) suivi par l'oxygène (~40%) et l'hydrogène (~6%). L'azote et le soufre ne représentent qu'une part très faible (~1,5%). La teneur en minéraux peut varier d'une espèce à l'autre (Tableau II-3). Les teneurs en éléments peuvent varier en fonction des conditions climatiques, de l'échantillonnage, de l'âge de la plante, du sol, du taux d'écorce, etc...

Tableau II-1 : Compositions élémentaires de différentes biomasses (\*calculé par différence)

	%masse sèche sans cendre				Références
	C	H	N	O*	
<b>Panic érigé</b> ( <i>Switchgrass</i> )	44,8	5,8	0,3	49,1	4
<b>Paille de blé</b> ( <i>Wheat straw</i> )	48,7	6,2	0,6	44,5	5
<b>Miscanthus</b>	49,1	6,0	0,3	44,5	5
<b>Saule</b> ( <i>Willow</i> )	47,9	5,9	0,3	46,0	4
<b>Hêtre</b> ( <i>Beech</i> )	46,1	6,2	0,1	47,6	6
<b>Peuplier</b> ( <i>Poplar wood</i> )	48,2	6,7	0,1	44,9	7
<b>Pinus teada</b> ( <i>Loblolly pine</i> )	50,8	6,3	0,1	42,8	8
<b>Pinus Armandii</b> ( <i>Chinese pine</i> )	47,6	6,1	0,1	46,2	9

Les parois végétales sont des structures multimoléculaires assurant l'imperméabilité et la rigidité de la plante. La composition, la structure, l'organisation de la paroi cellulaire dépendent à la fois de l'espèce étudiée, des conditions de croissance mais aussi de la couche de la paroi considérée<sup>10</sup>. Ces parois sont principalement constituées de cellulose (40-60%), d'hémicelluloses (10-30%) et de lignine (20-25%).

Les fibres de cellulose (polysaccharides) peuvent être qualifiées de squelette de la paroi cellulaire et le regroupement de ces fibres permet de former la paroi fibrillaire. Les hémicelluloses (polysaccharides) sont le plus souvent associées à la cellulose pour former l'holocellulose. Elles sont localisées à l'extérieur des fibrilles de cellulose et renforcent leur cohésion et leur structure. La lignine est considérée comme le ciment de la paroi végétale (Figure II-2), elle assure le lien entre les fibrilles de cellulose pour rigidifier la structure végétale.

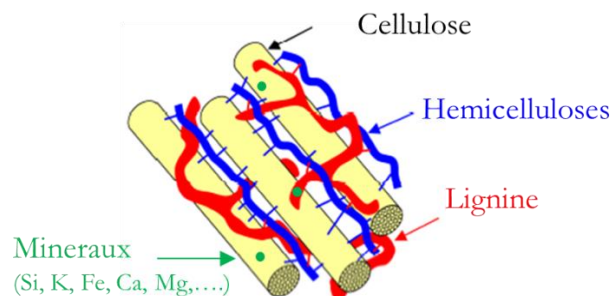


Figure II-2 : L'organisation des parois cellulaires<sup>11</sup>

**La cellulose** est le polymère terrestre le plus abondant (43 à 60% en masse de la biomasse végétale)<sup>12</sup>. Sa production annuelle par les plantes est estimée à plus de 50 milliards de tonnes<sup>13</sup> et la ressource totale en cellulose est estimée à 100 milliards de tonnes dont 80% localisées dans les forêts, ce qui fait du bois la principale source de cellulose. Elle est définie comme étant un homopolymère à haute masse moléculaire dont l'élément de base est le motif cellobiose<sup>14</sup>. Ce polymère est composé d'unités  $\beta$ -D-glucopyranose (anhydroglucopyranose) liées entre elles par des liaisons osidiques de type  $\beta(1,4)$  (Figure II-3) et dont la formule chimique est  $(C_6H_{10}O_5)_n$ <sup>15</sup> ( $n$ =nombre d'unités  $\beta$ -D-glucopyranose). Les chaînes de cellulose sont associées entre elles par des liaisons hydrogènes et van der Waals pour former des fibrilles.

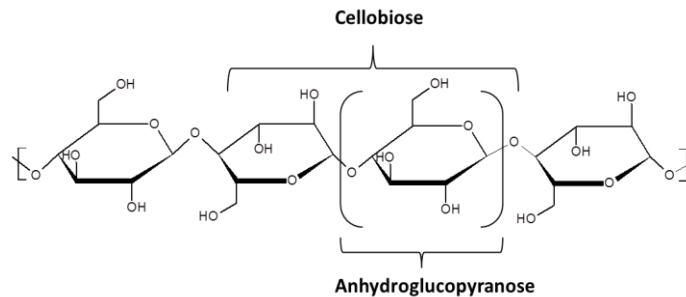


Figure II-3 : La structure chimique de la cellulose

Au sein de ces fibrilles, les chaînes sont ordonnées suivant différents degrés donnant naissance à des zones cristallines (organisation importante, liaisons hydrogènes importantes) et des zones amorphes (organisation faible, peu de liaisons hydrogènes entre les chaînes). Au sein d'une macromolécule de cellulose, les cycles pyranoses des molécules de glucose sont en conformation chaise et les groupements hydroxyles sont en équatorial du plan du cycle d'où une organisation des liaisons hydrogènes dans un même plan (*hydrogen bonded plan*)<sup>16</sup>. Les liaisons hydrogènes sont appelées intra-macromoléculaires si elles s'établissent au sein d'une même chaîne. Ces liaisons sont moins fortes que les liaisons covalentes cependant elles donnent une rigidité au brin de cellulose et diminuent leur flexibilité. Elles seraient aussi responsables de l'insolubilité de la cellulose dans l'eau ou dans la plupart des solvants organiques. Dans le cas où elles s'opèrent entre deux chaînes différentes, ces liaisons sont appelées inter-macromoléculaires, elles sont responsables de l'organisation des brins de cellulose en feuillets rigides et résistants. Les caractéristiques de ces liaisons hydrogènes ont été sources de nombreuses investigations, elles sont principalement étudiées par spectrométrie infrarouge<sup>16</sup>, diffraction des rayons-X<sup>17</sup> et Résonance Magnétique Nucléaire (RMN)<sup>18</sup>.

**Les hémicelluloses** sont la deuxième source la plus importante de polysaccharides de la biomasse végétale après la cellulose. Les hémicelluloses sont des macromolécules ramifiées à courtes chaînes (degré de polymérisation de 100 à 200) constituées de monosaccharides de natures variables (Tableau II-2). Du fait de la diversité des types de végétaux et de la grande variété de types cellulaires, il n'est pas possible de décrire les hémicelluloses de manière exhaustive. Les monosaccharides constituant les hémicelluloses sont principalement : des pentoses (xylose, arabinose,) et des hexoses (acide glucuronique, acide galacturonique, mannose, galactose et glucose) (Figure II-4). Ces glucides sont liés par plusieurs types de liaisons osidiques ( $\beta(1,4)$  ;  $\beta(1,3)$  ;  $\alpha(1,2)$  ; etc).

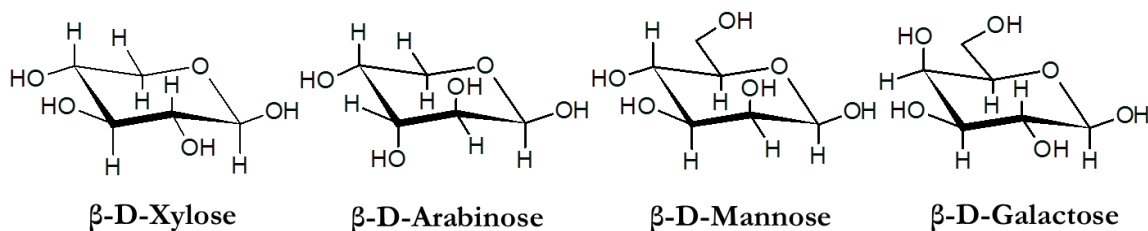


Figure II-4 : La structure moléculaire des principaux sucres constituant les hémicelluloses<sup>19</sup>

Les hémicelluloses sont des polyosides en étroite association avec la cellulose et la lignine. On trouve principalement quatre types d'hémicelluloses au sein des parois végétales : les glucanes, les xylanes, les mannanes et les galactanes. Du fait de leurs très grandes hétérogénéités concernant leurs constituants, les hémicelluloses présentent une structure amorphe au sein de la structure végétale.

Tableau II-2 : Composition en sucres pour différentes biomasses. \*inclut le glucose venant de la cellulose

	%masse sèche					Références
	Glucose*	Xylose	Mannanose	Galactose	Arabinose	
<b>Paille de blé</b> ( <i>Wheat straw</i> )	42,7	23,1	0	—	—	4
<b>Miscanthus</b>	48,5	18,1	0	—	—	5
<b>Chêne falcate</b> ( <i>red oak</i> )	41	19	2	1,2	0,4	2
<b>Epicéa</b> ( <i>Norway spruce</i> )	43	7,4	9,5	2,3	1,4	2
<b>Douglas</b> ( <i>Douglas fir</i> )	44	2,8	11	4,7	2,7	2

**La lignine** est un polymère de nature phénolique dont la structure exacte n'est pas établie avec précision. A la différence des carbohydrates (notamment cellulose) qui sont présents chez toutes les plantes. La lignine est caractéristique des plantes dites vasculaires ou trachéophytes. La présence de la lignine au sein de la structure d'une plante permet d'assurer : 1) la rigidité des parois cellulaires et ainsi permettre aux plantes de croître en hauteur sans support extérieur ; 2) l'imperméabilité des parois cellulaires afin de permettre la conduction de la sève dans un réseau de vaisseaux et de résister aux attaques biologiques extérieures.

Trois molécules peuvent être présentées comme les monomères de base de la lignine : l'alcool coumarylique (unité hydroxyphényle), l'alcool coniférylique (unité guaiacyle) et l'alcool sinapylique (unité syringyle). Ces unités sont plus couramment appelées les monolignols<sup>20</sup> (Figure II-5). Ces monomères sont liés entre eux par différents types de liaisons chimiques : des liaisons éthers ( $\beta$ -O-4,  $\alpha$ -O-4 et 4-O-5), des liaisons carbone-carbone ( $\beta$ -5,  $\beta$ - $\beta$ , 5-5' et  $\beta$ -1) (Figure II-6). La liaison  $\beta$ -O-4 est celle que l'on trouve le plus souvent entre les unités de base de la lignine. Parmi les liaisons carbone-carbones, les plus importantes sont les liaisons 5-5 et  $\beta$ - $\beta$  caractéristiques des structures pinorésinol ou syringarésinol<sup>13</sup>.

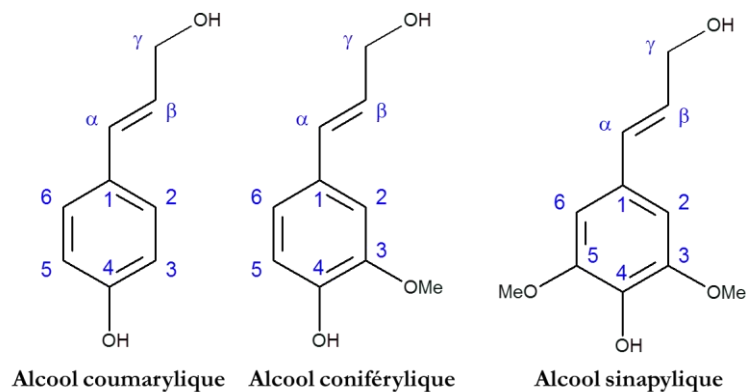


Figure II-5 : Les structures des trois monolignols de la lignine

Les chaînes aliphatiques oxygénées des monomères de la lignine peuvent également présenter des groupements acétyles<sup>21</sup> et carboxyliques<sup>13</sup>. L'acétylation des carbones des chaînes propyles avec de l'acide p-coumarique (Figure II-6) et/ou p-hydroxybenzoïque est observée chez certaines plantes<sup>22,23</sup>. L'acétylation du carbone  $\gamma$  des chaînes propyles semble importante chez certaines plantes comme notamment le *Miscanthus x Giganteus* et le kenaf. La définition de la structure chimique de la lignine est difficile car elle varie sensiblement d'une espèce à l'autre. Par exemple les unités guaiacyles dans les conifères représentent environ 90% des unités phénoliques tandis qu'elles sont moins présentes chez les feuillus. Les teneurs en lignine varient également en fonction des espèces. Les conifères sont décrits comme ayant des teneurs en lignine plus importantes que les feuillus et les plantes herbacées (*Miscanthus*)<sup>24</sup>.

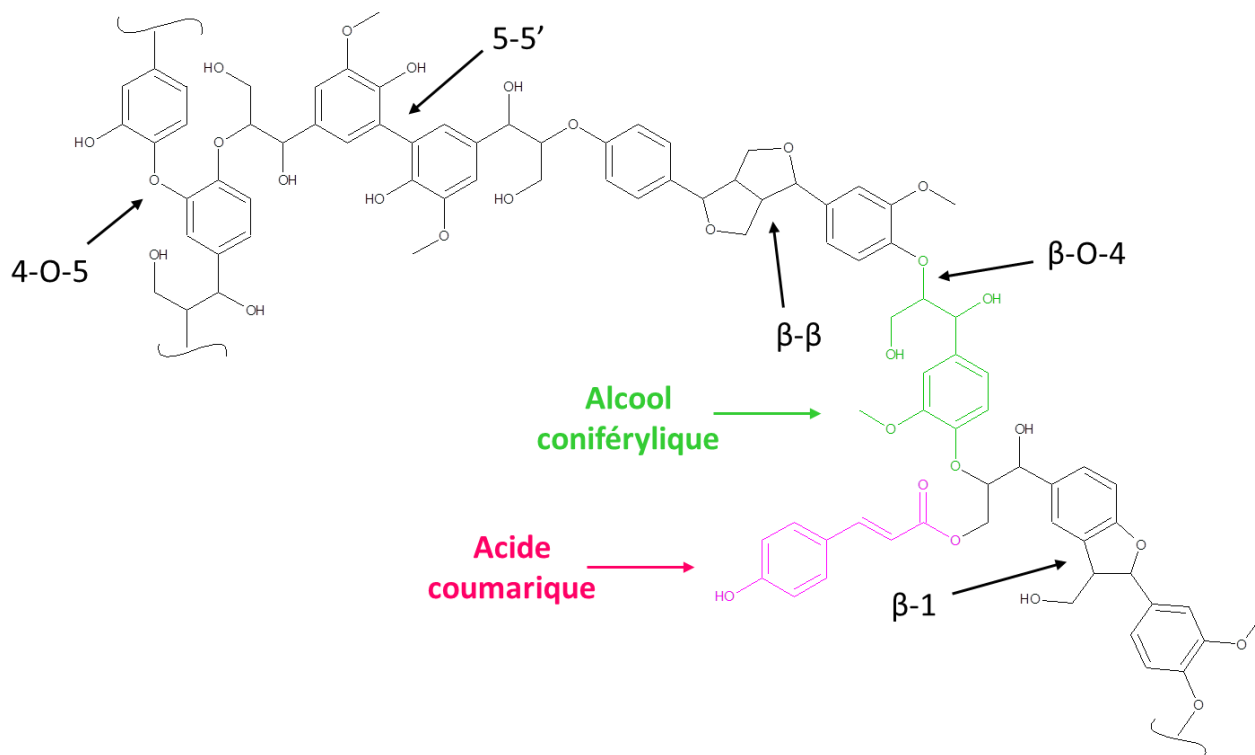


Figure II-6 : Un exemple d'une structure chimique d'une lignine (résineux)<sup>20,24,25</sup>

**Les extractibles :** Des composés définis par le terme extractible sont présents au sein de la biomasse lignocellulosique : 1 à 5% de la biomasse sèche (extraction éthanol-benzène)<sup>2</sup>. Ces extractibles sont le plus souvent composés de résines, tanins, pectines, etc.

**La composition en inorganiques** de la biomasse dépend principalement de l'espèce considérée (Tableau II-3) mais aussi d'autres facteurs comme la composition des sols. La composition et la concentration en inorganiques peuvent aussi varier en fonction de la partie de la plante considérée. Des analyses TEM-EDX<sup>26</sup> (*Transmission Electron Microscopy-Energy Dispersive X-Ray*) ont permis de mettre en évidence que les minéraux étaient répartis avec des concentrations différentes au sein des différentes lamelles des parois végétales. Les biomasses contiennent principalement du silicium (Si), du potassium (K), du calcium (Ca), du magnésium (Mg), du phosphore (P), du chlore (Cl), du fer (Fe) et du sodium (Na).<sup>27</sup> Certains de ces minéraux sont nécessaires à la vie de la plante d'autres non. Il est difficile de connaître avec exactitude la composition en minéraux d'une biomasse ainsi que la nature de leurs associations au sein de celle-ci<sup>28</sup>. Ces métaux seraient présents sous forme d'oxalates, de carbonates, de sulfates ou liés aux groupements acides des macromolécules (acides uroniques).

Tableau II-3 : *Composition en éléments inorganiques de différentes biomasses*

	%masse sèche					Références
	Si	K	Ca	Mg	Na	
<b>Panic erigé</b> ( <i>Switchgrass</i> )	–	0,07	0,62	0,054	0,016	4
<b>Paille de blé</b> ( <i>Wheat straw</i> )	1,4	0,9	0,43	0,08	0,01	5
<b>Miscanthus</b>	0,45	0,485	0,13	0,055	0	5
<b>Saule</b> ( <i>Willow</i> )	–	0,2	0,3	0,038	0,006	4
<b>Peuplier</b> ( <i>Poplar wood</i> )	0	0,07	0,08	0,03	0	7
<b>Pinus stobe</b> ( <i>US white pine</i> )	–	0,03	0,02	0,007	0	8

## II.3 La valorisation de la biomasse lignocellulosique

Les constituants lignocellulosiques demeurent un stock de matière carbonée pouvant être valorisé<sup>29,30</sup> par transformations biochimiques ou par transformations thermochimiques (Figure II-7) en énergie (chaleur, électricité), en carburants (ex : biohuiles, biogaz) ou en molécules chimiques à haute valeur ajoutée.

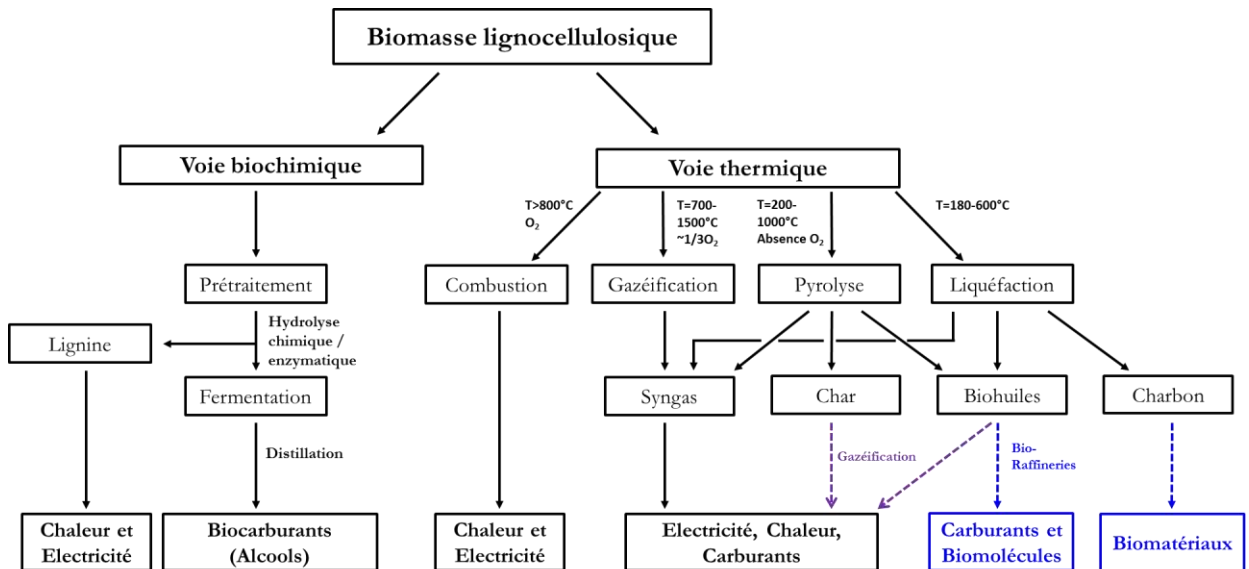


Figure II-7 : Les différentes voies de transformation de la biomasse lignocellulosique

Les transformations biochimiques nécessitent un prétraitement afin de rendre la matière « digérable » par les micro-organismes ou attaquant par des agents chimiques ou enzymatiques afin de transformer la matière lignocellulosique en carburant liquide (ex : éthanol) ou gazeux (ex : hydrogène). Cette voie de transformation peut également fournir des produits chimiques<sup>31</sup> dits bio-sourcés pouvant être utilisés dans des domaines variés (composites, plastiques, etc). Dans le cas des traitements thermochimiques, la biomasse peut être convertie en électricité, chaleur, carburants ou composés chimiques par quatre procédés principaux : pyrolyse, gazéification, liquéfaction et combustion.

En pyrolyse, la biomasse est chauffée sous atmosphère inerte non oxydante et produit trois phases : solide (charbon ou biochar), gaz ( $\text{CO}$ ,  $\text{CO}_2$ ,  $\text{H}_2$ ,  $\text{CH}_4$ ) et des vapeurs condensables (huiles de pyrolyse ou goudrons, eau)<sup>32</sup>. Les procédés de pyrolyse dite rapide consistent à soumettre la biomasse à de hauts flux de chaleur pour optimiser la production de gaz ou de vapeurs condensables. Ce procédé est l'un des plus étudiés dans le cadre de la valorisation de la biomasse lignocellulosique<sup>33,34</sup>. La pyrolyse lente (ou carbonisation) favorise la production de charbon.

La gazéification peut être opérée en présence d'air, d'oxygène ou de vapeur d'eau suivant différentes technologies : lits fixes, lits fluidisés et lits entraînés. Elle consiste principalement à produire un gaz de synthèse, le « *syngaz* » ( $\text{H}_2 + \text{CO}$ ). Ce gaz peut être utilisé en combustion afin de produire de l'électricité et de la chaleur mais aussi dans la production de carburants liquides (comme la synthèse Fischer Tropsch), de  $\text{CH}_4$  (par méthanation) ou d'hydrogène. Le procédé de gazéification produit également des vapeurs condensables (goudrons, principalement des composés aromatiques, eau) et d'autres gaz ( $\text{CH}_4$ ,  $\text{CO}_2$ ,  $\text{C}_2+$ ). La qualité du « *syngaz* » produit dépend de la technologie utilisée ainsi que des caractéristiques de la biomasse gazéifiée (teneur en eau, minéraux, composition chimique,...). De nombreux procédés de gazéification ont été

développés au cours des dernières décennies (*TNEE* en France ; *Lurgi* en Allemagne ; *Xylowatt* en Belgique ; *FICFB* en Autriche)<sup>35</sup>. Les recherches se focalisent notamment sur les moyens de purification et de traitement des goudrons dans le but d'optimiser la production de carburants (alcools, gazoles) et la combustion des gaz dans les moteurs thermiques<sup>36</sup>.

La combustion est le procédé le plus simple de transformation de la biomasse en chaleur et/ou en électricité. Ce procédé consiste à chauffer la biomasse sous atmosphère oxydante ( $O_2$ ) afin de produire de la chaleur. Les produits majoritairement formés sont des gaz ( $CO_2$ ,  $CO$ ) et du charbon. La combustion est actuellement le procédé le plus répandu commercialement grâce notamment à son faible coût d'investissement. Elle correspond à 97% de la production de bioénergie dans le monde<sup>37</sup>.

La liquéfaction qui se déroule sous pression (20-200 bars) en phase liquide transforme la biomasse en trois produits qui sont : une phase solide (charbon), une phase liquide (biohuiles) et une phase gaz. Le but final étant d'obtenir des bio-huiles faiblement oxygénées<sup>38</sup> qui après raffinage (hydrodésoxygénation) peuvent être utilisées comme carburants ou comme composés chimiques. L'avantage des procédés de liquéfaction est qu'ils sont directement applicables sur la biomasse lignocellulosique sans étape de séchage pour une large gamme de températures 180 à 600°C.

Il est important d'optimiser la pureté et la nature des produits formés (charbons, bio-huiles et gaz). Ces avancées permettront d'obtenir une meilleure efficacité énergétique pour la production d'énergies (électricité, chaleur) et une production de bioproduits (matériaux, additifs agro-alimentaires, etc.) plus compétitive et moins nocive pour l'environnement. La pyrolyse étant le premier mécanisme intervenant dans tous les procédés de conversion thermochimique, il est par conséquent primordial d'étudier les mécanismes chimiques intervenant pendant cette étape afin d'optimiser et de guider ces procédés de valorisation.

## II.4 La pyrolyse de la biomasse lignocellulosique

### II.4.1 Définitions et généralités

La pyrolyse est un processus de conversion de la biomasse par action de la chaleur sous atmosphère inerte. Il conduit à la formation de trois produits : charbon (biochar), gaz ( $CO$ ,  $CO_2$ ,  $H_2$ ,  $CH_4$ , ...) et un liquide (ou bio-huiles ou goudrons) composé d'un mélange d'eau et de plusieurs centaines de composés organiques oxygénés<sup>39,40</sup>. Selon les conditions opératoires utilisées (température, flux de chaleur, temps de séjour, granulométrie, humidité, pression, quantité de matière), différents rendements et des compositions variées peuvent être obtenus<sup>41</sup>. La température du réacteur, la densité de flux de chaleur apportée par le réacteur à la biomasse et le temps de séjour (des trois produits, notamment de la phase gaz) sont les principaux paramètres influençant les rendements et la composition des produits. Une densité de flux de chaleur importante, comme utilisée dans les procédés de pyrolyse rapide, favorise la formation de bio-huiles. Pour un flux de chaleur plus faible, la production de solide carboné est plus importante<sup>41</sup>. On distingue par conséquent deux types de pyrolyse : 1) la pyrolyse dite lente qui s'opère pour des températures comprises entre 300 et 500°C pour des densités de flux de chaleur faibles ( $<10\text{kW/m}^2$ ) ; 2) la pyrolyse rapide ou flash qui nécessite des densités de flux de chaleur importantes ( $>10\text{kW/m}^2$ ). Les frontières (seuil de densité de puissance, température, etc.) entre ces deux types de pyrolyse ne sont pas formellement établies et il existe un gradient progressif de régime de pyrolyse de lente à intermédiaire et à rapide (voire « flash »). La plupart des études caractérisent leur procédé de pyrolyse par une vitesse de montée en température. Le fait de parler de vitesse de montée en température peut être considéré comme un abus de langage puisque lors de la pyrolyse, la montée en température des particules de biomasse est très variable, en réalité difficilement maîtrisable et contrôlée par des compétitions entre cinétique chimique et transferts de chaleur<sup>42</sup>. Les transferts de chaleur dans la particule

dépendent de différents paramètres : taille de particule, humidité, conductivité thermique de la matière, etc.. La Figure II-8 décrit l'influence de la température et de la densité de flux de chaleur sur la répartition globale des produits de pyrolyse.

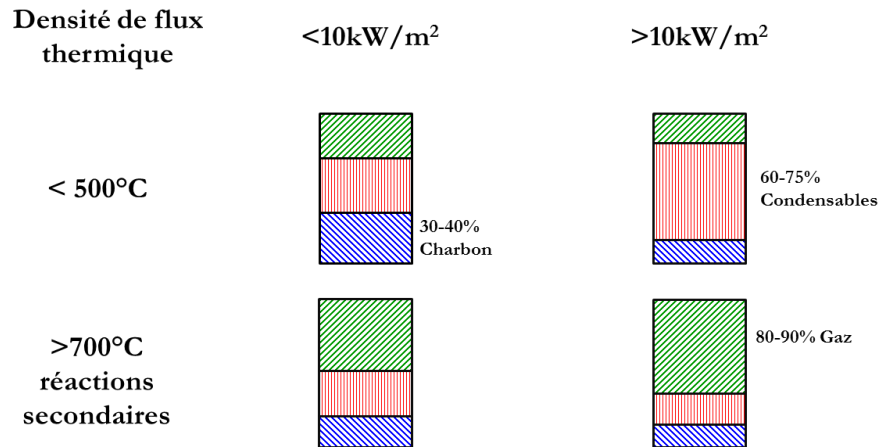


Figure II-8 : L'influence de la température et de la densité de flux de chaleur sur le rendement massique des produits de pyrolyse (adapté de X.Deglise, et A.Donnot, Techniques de l'ingénieur, 2004)

Sous l'effet de la chaleur, la biomasse se dégrade suivant différents mécanismes chimiques en produits dits « primaires » (Figure II-9). Ces composés peuvent par la suite subir des réactions dites secondaires (voire même tertiaires) si le temps de séjour des vapeurs (goudrons et gaz) à une température supérieure à environ  $500^\circ\text{C}$  au sein du réacteur est suffisamment long (supérieur à environ 1s). La géométrie des particules pyrolysées est un paramètre important car si la taille ou l'épaisseur sont trop élevées, le temps de séjour des goudrons au sein des particules augmente ce qui peut provoquer la dégradation de ces goudrons via des réactions secondaires<sup>43</sup> intra-particulaires. La Figure II-9 décrit l'influence du temps de séjour et de la température de la phase vapeur sur la nature des produits de pyrolyse.

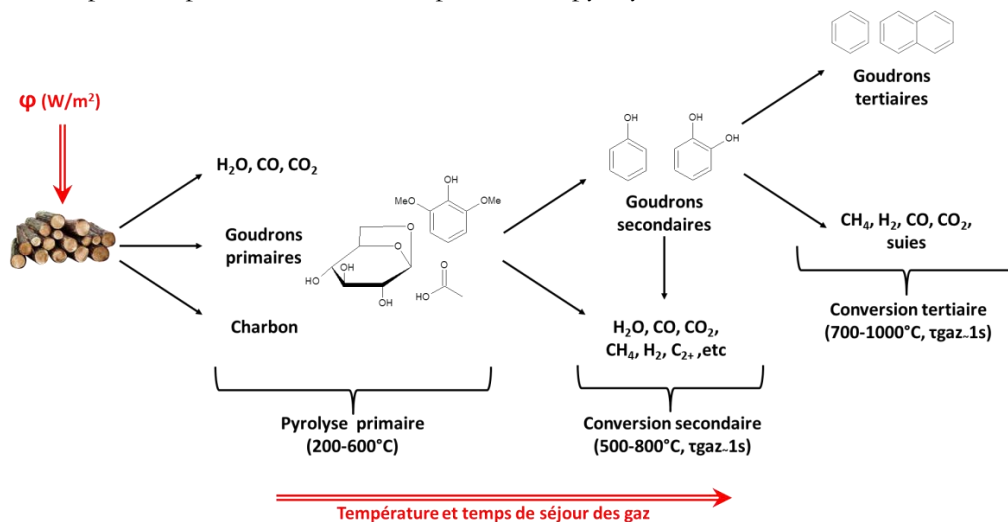


Figure II-9 : L'influence du temps de séjour et de la température sur la nature chimique des goudrons de pyrolyse<sup>44</sup>

Une caractérisation détaillée et une classification par étape (primaire, secondaire et tertiaire) des produits de pyrolyse sont très difficiles à réaliser car les mécanismes chimiques demeurent encore mal détaillés et les investigations présentent une trop grande hétérogénéité au niveau des conditions de pyrolyse. L'étude de Evans et Milne<sup>40</sup>, présente actuellement l'une des meilleures classifications des produits issues de la pyrolyse. Les produits sont classés en fonction de la « sévérité » du traitement thermique, du temps de séjour et de la pression (Figure II-10). Cette étude a été réalisée en couplant un spectromètre de masse à impact électronique (15-22.5 eV) directement relié à un réacteur de pyrolyse tubulaire<sup>40</sup> permettant ainsi d'obtenir une caractérisation « *in-situ* » des espèces volatiles formées en fonction des conditions de pyrolyse

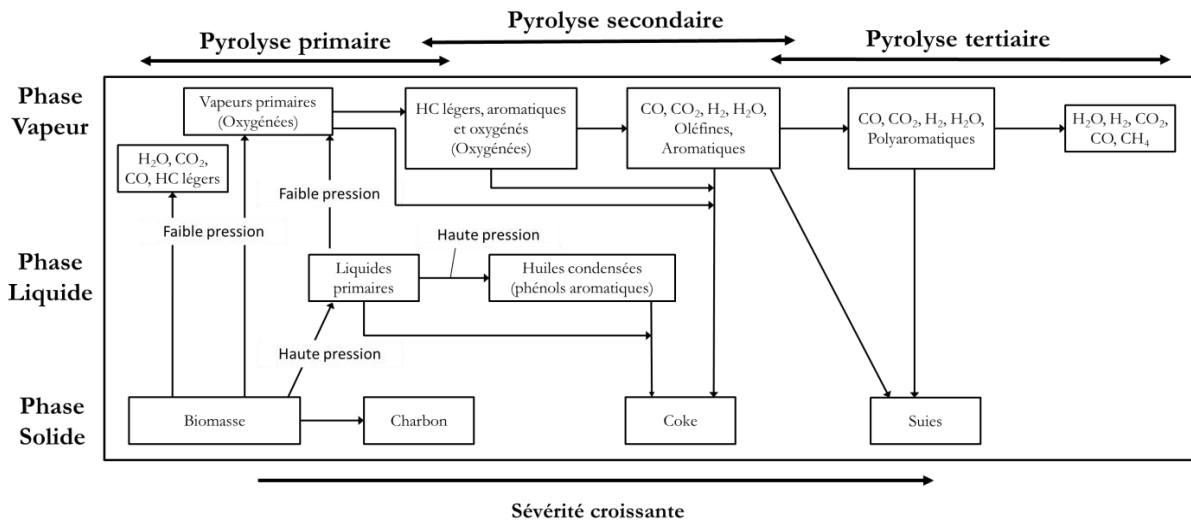


Figure II-10 : Les différentes étapes de la pyrolyse d'après Robert J. Evans et Thomas Milne<sup>40</sup>

On distingue alors les produits primaires qui sont des composés oxygénés provenant de la dégradation de la cellulose et des hémicelluloses (levoglucosane, furfural, furanes,...) et de la dégradation de la lignine (alkyl-methoxyphenols). Les produits secondaires sont des produits carbonés moins complexes résultant de la dégradation des vapeurs primaires en aromatiques faiblement oxygénés (phénol, crésols, etc.). Les produits tertiaires sont des composés majoritairement non oxygénés aromatiques (benzène, toluène) ou polyaromatiques (naphtalène, anthracène,...) précurseurs de la formation de suies.

Les mécanismes chimiques opérant lors de la pyrolyse de la biomasse lignocellulosique se trouvent étroitement corrélés avec les mécanismes propres à chacun de ses constituants (cellulose, hémicelluloses, lignine). Il est donc par conséquent important de présenter les mécanismes relatifs à chacun de ces composés.

## II.4.2 Pyrolyse de la cellulose

Comme nous l'avons mentionné, la cellulose est le principal composant de la matière lignocellulosique et ainsi la connaissance de ses mécanismes propres de dégradation est fondamentale. L'étude de la dégradation thermique de la cellulose a été et continue à être le sujet de nombreuses recherches scientifiques<sup>45</sup>. Il est difficile, voire impossible de connaître la date précise des premières études portant sur la pyrolyse de la cellulose. Au cours du 19<sup>ième</sup> siècle, avec l'avènement de la chimie organique et de l'industrialisation mondiale, la pyrolyse du bois fut l'objet de nombreuses investigations dont le but était principalement d'obtenir des produits chimiques comme le méthanol, l'acide acétique et du charbon de bois. Cependant devant l'avènement de l'industrie pétrolière, ces développements ont été abandonnés et la recherche sur la pyrolyse de la cellulose est restée purement académique. Historiquement, on observe, une production scientifique assez faible<sup>46</sup> jusque dans les années soixante malgré un regain d'intérêt pendant la seconde guerre mondiale. Ces recherches ont continué de susciter l'intérêt notamment dans les domaines du textile et des produits anti-feu<sup>47</sup>.

En 1918, Pictet et Sarasin<sup>48</sup>, lors de la distillation de la cellulose sous vide, isolèrent une substance au sein des goudrons. Cette substance, nommée lévoglucosane, a été identifiée comme composant majoritaire des goudrons<sup>49</sup> et son mécanisme de formation a été grandement étudié par la suite. Les recherches effectuées avant les années 1960, bien que très peu détaillées analytiquement, ont réussi à cerner les principales problématiques de la pyrolyse de la cellulose<sup>50-52</sup> (influence du degré de polymérisation, du taux de cristallinité, mécanismes chimiques de dégradation).

Les recherches sur la pyrolyse de la cellulose n'ont vraiment pris un envol conséquent qu'à partir de ces années 1960 avec l'avènement d'équipements plus fiables<sup>53</sup> pour la mesure continue de la masse d'un échantillon soumis à un traitement thermique. Ainsi, plusieurs éléments concernant les mécanismes chimiques de pyrolyse de la cellulose ont été étudiés comme le mécanisme de formation du lévoglucosane et la nature des produits issus de sa dégradation thermique<sup>54</sup>. Broido et Kilzer<sup>55</sup> ont mis en évidence la formation de cellulose deshydratée à basse température (200-280°C). Dans leur modèle cinétique (Figure II-11), cette réaction entre en compétition avec une deuxième réaction, la dépolymérisation des molécules de cellulose (280-340°C) qui a pour conséquence la formation de goudrons (majoritairement du lévoglucosan).

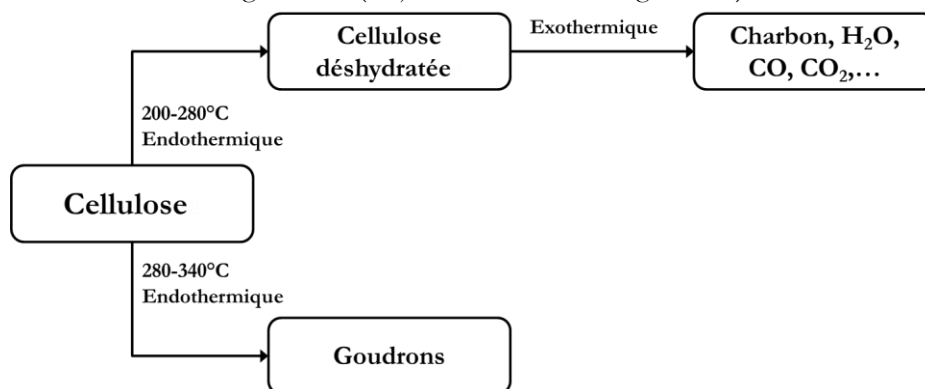


Figure II-11 : Le schéma cinétique de Broido et Kilzer

Ce schéma réactionnel est repris par Arseneau<sup>56</sup> en 1970, qui lors d'études par calorimétrie a montré qu'un léger endotherme à 180°C suivi d'un léger exotherme pouvait correspondre à la formation d'anhydrocellulose comme suggéré par Broido et Kilzer. Un endotherme plus important a été observé à partir de 280°C. Cet endotherme semble être dû à deux réactions différentes étant donné la rupture de la courbe observée à 350°C.

Les deux réactions contribuant à cet endotherme semblent être une dépolymérisation du résidu cellulosique suivi par une volatilisation des produits formés (majoritairement le lévoglucosane).

L'intérêt pour la recherche concernant les mécanismes de pyrolyse a été renforcé par les chocs pétroliers (1973 et 1979) qui a introduit une volonté de chercher d'autres sources d'énergies et de « molécules plateforme ». Le modèle de Broido-Shafizadeh, publié en 1979, est encore aujourd'hui considéré par la plupart des spécialistes comme le schéma simplifié de référence. Ce schéma est inspiré des travaux de Broido<sup>55</sup> et de Shafizadeh<sup>57</sup> (Figure II-12). Il propose la formation d'un composé intermédiaire (active cellulose) issu d'une réaction d'activation de la cellulose sans perte de masse.

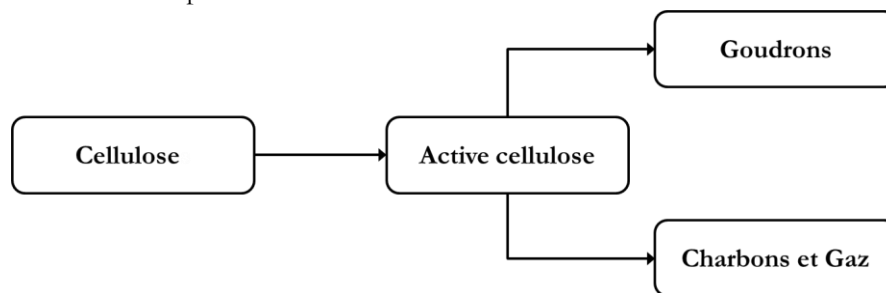


Figure II-12 : Le schéma de Broido-Shafizadeh

La plupart des modèles proposés jusqu'au schéma de Broido-Shafizadeh ne tiennent pas compte de la distribution en produits volatils. En effet, des modèles plus élaborés ont montré que suivant les conditions de chauffage ou de pureté de la cellulose analysée, la nature et les proportions en produits volatils pouvaient être différentes. D'après les travaux de Piskorz et Radlein<sup>58</sup>, la formation de composés volatils légers (exemple : hydroxyacétaldéhyde) pourrait être le résultat de la décomposition du lévoglucosane lors de la pyrolyse. En effet ce dernier est décrit comme un produit minoritaire de la pyrolyse du bois tandis que des molécules oxygénées de faibles masses sont les produits majoritaires<sup>59</sup>. Cette idée est écartée, par la suite, par Richards<sup>60</sup> et Piskorz<sup>59</sup>. Richards propose la formation de hydroxyacétaldéhyde directement à partir de la cellulose par une réaction de déshydratation suivie d'une réaction de fragmentation (*retro Diels Alder*). Cette idée est confirmée par des études statistiques analysant les rendements des produits en fonction de la température<sup>59</sup>. Une telle scission aurait une énergie d'activation importante et par conséquent serait favorisée par l'augmentation de la température. La présence de cations alcalins est décrit comme pouvant inhiber le mécanisme de formation du lévoglucosane tout en favorisant les réactions de fragmentation<sup>61</sup>.

D'après Radlein et Piskorz<sup>62</sup>, la dégradation de la cellulose passerait par la formation d'une cellulose dépolymérisée. Le schéma cinétique présenté par Piskorz et al<sup>63</sup> (Figure II-13) a été établi à l'Université de Waterloo. Les études ont été réalisées dans un réacteur lit fluidisé sous pression atmosphérique pour des températures variant de 400 à 650°C. Le temps de séjour des vapeurs est estimé à moins d'une seconde afin de minimiser les réactions secondaires. Néanmoins, à partir de 500°C, des réactions secondaires pourraient être présentes. Les expériences réalisées sur du bois (peuplier) semblent indiquées que ce dernier suit le même schéma que la cellulose.

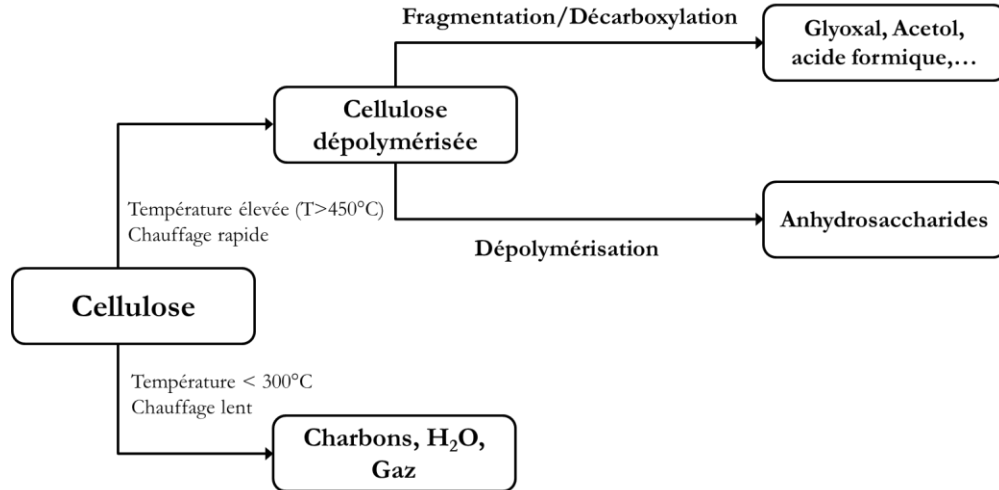


Figure II-13 : Le schéma de Waterloo

Un schéma plus complet, réalisé à partir de données cinétiques provenant de la littérature, est proposé par Diebold<sup>64</sup> (Figure II-14). Pour ce dernier, il est difficile d'établir un modèle permettant de prédire les produits de pyrolyse de la cellulose du fait des nombreuses réactions compétitives à considérer. Pour des températures et des vitesses faibles, la production de charbon est favorisée, tandis que pour une pyrolyse rapide avec des températures modérées, la production de goudrons est favorisée. En ce qui concerne la pyrolyse rapide avec des températures élevées, la production de gaz est favorisée. Des vapeurs primaires se forment directement à partir du composé intermédiaire et se décompose par la suite en gaz et en vapeurs secondaires.

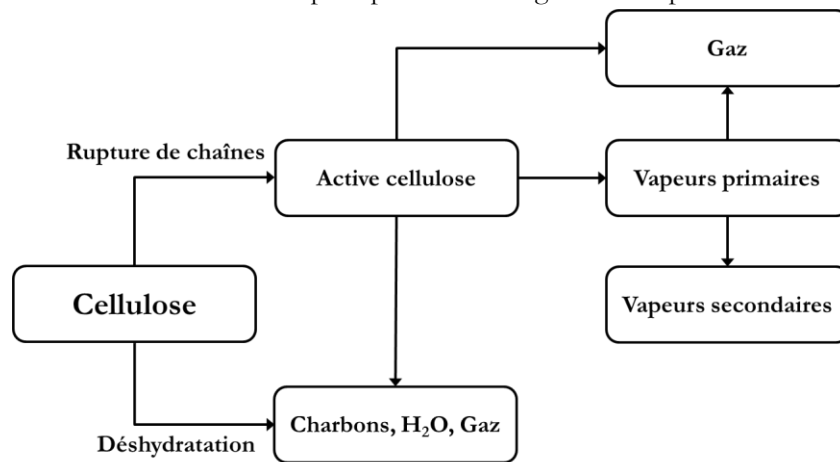


Figure II-14 : Le schéma de Diebold

La formation d'une dizaine de composés volatils a été étudiée par Banyasz et al<sup>65,66</sup> lors de la pyrolyse en chauffage rapide (400°C/min à 800°C/min) au sein d'un four tubulaire équipée d'un détecteur infra-rouge à transformée de Fourier EGA (*fast evolved gas-FTIR apparatus*). Premièrement, la cellulose est décrite comme se dégradant par deux réactions concurrentes (Figure II-15) : 1) la formation de la cellulose dépolymérisée ; 2) la formation de cellulose déshydratée (Anhydrocellulose) qui conduit à la formation de charbon. Pour des vitesses de montée en température importantes les proportions en hydroxyacétaldéhyde, formaldéhyde et monoxyde de carbone détectées augmentent au détriment de la formation de dioxyde de carbone. La décomposition de la cellulose dépolymérisée est par conséquent décrite comme s'effectuant via deux réactions concurrentes : 1) la formation de goudrons (principalement lévoglucosane) et de charbon ; 2) la formation de

molécules à faibles masses molaires (hydroxyacétaldéhyde, formaldéhyde,...). Cette seconde voie de dégradation peut être associée à la réaction de fragmentation décrite par Piskorz<sup>63</sup>. Cependant la formation de ces composés à faibles masses molaires ne semble pas être issue directement de la dégradation de la cellulose dépolymérisée mais d'un composé intermédiaire. L'augmentation du temps de séjour des gaz augmente le rendement en gaz (notamment en formaldéhyde). Ce produit semble par conséquent être un produit secondaire issu du craquage des vapeurs formées.

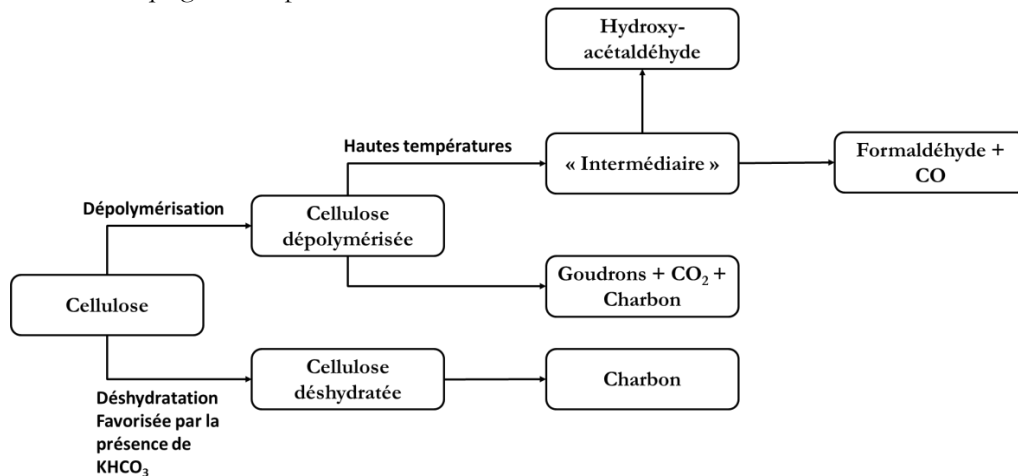


Figure II-15 : Le schéma de Banyasz

L'existence d'un intermédiaire lors de la dégradation de la cellulose (cellulose active<sup>67</sup>, cellulose dépolymérisée<sup>68</sup>,...) a été et demeure toujours source de débats. Certains auteurs ne le considèrent pas car ils estiment que dans certaines conditions de chauffage (pyrolyse rapide) sa formation et sa disparition sont trop rapides pour qu'il soit considéré<sup>69,70</sup>. Les expériences de pyrolyses ablatives<sup>71,72</sup> ont permis d'assimiler la formation de cet intermédiaire à une fusion. Des observations microscopiques des échantillons ont également permis de mettre en évidence la formation d'un intermédiaire liquide<sup>73</sup>. Olivier Boutin et Jacques Lédé ont montré la formation d'un intermédiaire liquide lors d'expériences de pyrolyses réalisées à l'aide d'un four à image à flux concentré ( $10^5$  à  $7 \cdot 10^6$  W/m<sup>2</sup>) sur des particules de cellulose (poudre compactée). Des observations microscopiques ainsi que des analyses HPLC-MS ont permis de caractériser ce liquide jaunâtre soluble dans l'eau. Cet intermédiaire a été nommé le composé intermédiaire liquide (ILC *Intermediate Liquide Compound*). Il est composé de lévoglucosane et d'oligosaccharides anhydres ayant des degrés de polymérisation compris entre 2 (cellobiosane) et 7.

La sélectivité en lévoglucosane et en cellobiosane n'est pas très importante pour ces expériences de four à image. En effet, les oligosaccharides ayant un degré de polymérisation plus élevés (3-7) sont formés en plus grande quantité montrant ainsi que le lévoglucosane n'est pas un produit issu directement de la cellulose mais qu'il résulte bien d'une dégradation aléatoire s'effectuant le long des chaînes cellulosiques. Ces ruptures aléatoires induisent la formation de chaînes plus ou moins courtes (degrés de polymérisation variés) de cellulose présentant une molécule de lévoglucosane en bout de chaîne. Pour des densités de flux supérieures à  $9 \cdot 10^5$  W/m<sup>2</sup>, la formation de charbon n'est pas observée montrant que dans le cas de densités de flux importantes les goudrons (vapeurs condensables) peuvent être formés directement à partir de l'intermédiaire liquide comme décrit dans le modèle de Broido-Shafizadeh. La formation d'oligosaccharides anhydres lors de pyrolyses rapides (four tubulaire) est également étudiée par Piskorz et al<sup>42</sup> à l'aide d'analyses HPLC (couplé à un détecteur à indice de réfraction) et Pyrolyse-CI-MS (*chemical ionization mass spectrometry*). La présence de matières inorganiques (lithium) semble inhiber la formation d'oligosaccharides anhydres. Une opération de prétraitement par chauffage (175°C/20h) de la cellulose permet d'obtenir dans ces conditions de pyrolyse un

rendement plus important en lévoglucosane et en cellobiosane. L'opération de prétraitement semble induire une pré-dépolymérisation de la cellulose pouvant correspondre à l'instar de l'étude de Broido<sup>74</sup> à la cellulose dépolymérisée (*active cellulose*).

La formation d'oligosaccharides anhydres a également été observée en pyrolyse lente à l'aide d'analyses de chromatographies à colonnes échangeuses d'anions (HPAEC) et détection ampérométrique pulsée (PAD)<sup>75,76</sup>. Ces composés sont extraits de charbons de cellulose obtenus par pyrolyse lente en lit fixe (10°C/min) et maintenus trente minutes à température constante. Pour différentes températures, une phase dite soluble est extraite de ces charbons avec de l'eau et analysée par HPAEC-PAD. Ces analyses permettent d'observer la présence oligosaccharides anhydres de tailles variées (degrés de polymérisation de 1 à 10) au sein des charbons confirmant que la production de lévoglucosane résulte d'une dégradation aléatoire des chaînes de cellulose. La formation d'oligosaccharides (polymères de glucose) est observée pour des températures plus faibles (100-250°C) tandis que la formation d'oligosaccharides anhydres est observée pour des températures plus élevées (200-300°C). La présence dans les charbons de composés hydrolysables mais non extractibles (par H<sub>2</sub>O) sont décrits comme des oligomères modifiés traduisant la présence de voies de dégradation autres que la dépolymérisation (Figure II-16). Les oligosaccharides anhydres sont décrits comme formés directement à partir de la cellulose tandis que la formation des oligosaccharides semble due à la dégradation des chaînes courtes présentes dans les zones amorphes de la cellulose. L'absence de liaisons hydrogènes au sein de ces zones amorphes augmente le rendement en oligosaccharides anhydres<sup>76</sup> ainsi que leur taille (DP de 1 à 16) lors de la pyrolyse de celluloses « amorphisées ». Les zones amorphes forment une phase dite liquide tandis que les zones cristallines forment une cellulose dite dépolymérisée<sup>77</sup>. La formation d'oligosaccharides anhydres est concurrencée par les réactions de déshydratation et de condensation<sup>77-79</sup>. Ces réactions semblent être plus importante pour la cellulose amorphe<sup>77</sup>. Le couplage d'analyses sur les charbons par Résonance Magnétique Nucléaire du carbone (RMN <sup>13</sup>C CPMAS *cross-polarization magic-angle spinning*) et dosage des sucres hydrolysables révèle que ce phénomène est accéléré dans les zones amorphes de la cellulose<sup>78</sup>.

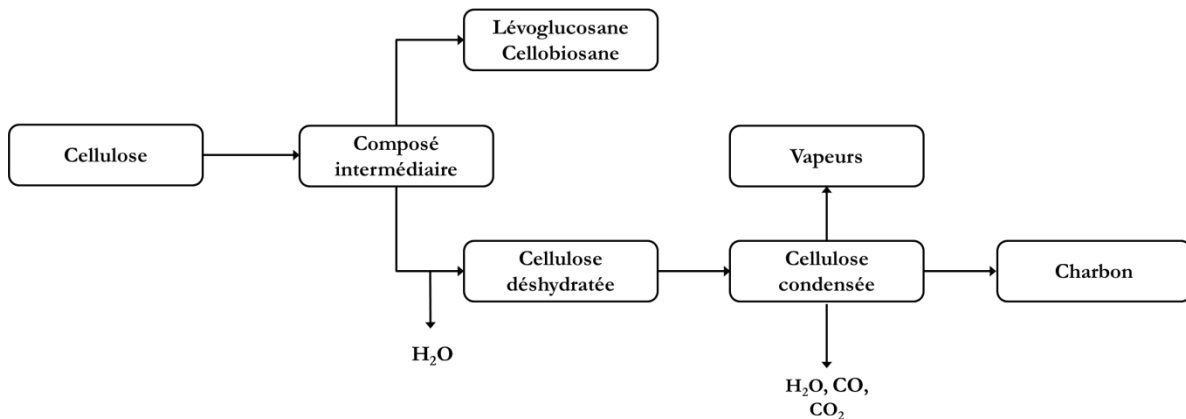


Figure II-16 : Le schéma de Wang et Garcia-Perez<sup>43</sup>

La formation de cette « active cellulose » a également été étudiée par RMN <sup>13</sup>C CPMAS<sup>80</sup>. Les échantillons de cellulose sont maintenus à 300°C dans un four pour différents temps de séjour (5 à 210 minutes). Après refroidissement rapide, le résidu est analysé par RMN <sup>13</sup>C CPMAS et la soustraction successive des spectres RMN obtenus pour différents temps de pyrolyse permet la mise en évidence de la formation d'un composé s'apparentant à la cellulose active nommé le composé intermédiaire (« *intermediate compound* »). Ce composé est défini comme étant une matrice complexe de chaînes de cellulose désordonnées à faibles degrés de polymérisation. La formation de cette matrice est associée à la formation de la cellulose active décrite par

Piskorz et Lédé montrant qu'elle peut également être observée pour des températures plus basses. La dégradation de cet intermédiaire pour des temps de pyrolyse plus importants conduit à la formation d'un charbon composé de structure aromatique et de résidu d'oligosaccharides (« *final carbohydrates* »). La présence de potassium induit une dégradation plus rapide de la cellulose vers une structure aromatique. L'analyse RMN a également été utilisée par Dufour et al<sup>11</sup> pour caractériser la formation de l'intermédiaire liquide. Ces analyses ont été réalisées par RMN haute température « *in-situ* » <sup>1</sup>H (*Proton magnetic resonance thermal analysis* PMRTA) permettant de caractériser l'état de la matière (liquide ou solide) pendant un chauffage lent (5 °C/min). L'intégration des spectres RMN obtenus au cours de la pyrolyse de cellulose extraite de paille de miscanthus permet de mettre en évidence la formation d'une phase liquide.

Les techniques de pyrolyse et les techniques d'analyses sont différentes d'une étude à l'autre (Tableau II-4), il est par conséquent difficile d'établir une caractérisation précise de cet intermédiaire. A basse température, l'intermédiaire semble correspondre à un polymère cellulosique composé de chaînes avec un degré de polymérisation situé autour de la valeur de 200<sup>40,74</sup>. La technique de refroidissement doit être assez rapide lors de ces expériences à basse température pour éviter d'hypothétiques réactions de repolymérisation<sup>45</sup>. A haute température, l'intermédiaire semble être constitué d'oligosaccharides anhydres (DP<7), cependant l'intermédiaire observé à basse température (DP=200) est peut être transformé trop rapidement pour être observé dans ces expériences de pyrolyse rapide. La formation de charbon par des réactions dites de déshydratations est pour certaines études décrites comme résultant d'une dégradation directe de la cellulose<sup>81,82</sup> tandis que pour d'autres études elle semble intervenir après la formation d'un composé intermédiaires<sup>83</sup>.

Tableau II-4 : Tableau récapitulatif de différents travaux sur la caractérisation de la cellulose active

Auteurs/Date	Procédé de pyrolyse	Températures /Flux	Temps de séjour	Echantillons	Observations	Analyses
Goring <sup>84</sup> 1963	Mesure du point de fusion	-	-	Cellulose, hémicelluloses, lignine	Utilisation d'un appareil à mesure de point de fusion ( <i>softening point apparatus</i> )	
Diebold <sup>85</sup> 1980	Fil chaud ( <i>Hot Wire</i> )	3-15 W/cm <sup>2</sup>	-	Particules de bois	Schéma global de la pyrolyse de la cellulose. La formation des produits de la pyrolyse montre le passage par un intermédiaire : <i>Intermediate active state</i> .	Observations microscopes (MEB)
Lédé 1985	Disque tournant	550°C	-	Particules de bois	Comportement du bois semblable à un phénomène de fusion pour une pyrolyse rapide (T= 739K)	
Vladars <sup>42</sup> 1993	<i>flow reactor transport</i>	850°C-1200°C	10 ms	Avicel cellulose	La dépolymérisation de la cellulose intervient par un état de fusion	
Boutin <sup>73</sup> 1998	Four à image ( <i>image furnace</i> )	2 MW/m <sup>2</sup>	0,2-1s	Whatman microgranular CC31 cellulose	Observations microscopiques des échantillons après réaction: mise en évidence d'un intermédiaire liquide jaunâtre, soluble dans l'eau.	Observations microscopes (MEB)
Piskorz <sup>42</sup> 2000	Reacteur tubulaire ( <i>Flash Tubular Reactor</i> )	850°C-1200°C	35-75 ms	Avicel Cellulose PH102	Obtention d'une fraction soluble contenant des anhydrosaccharides. Influence du Lithium.	Observations microscopiques/HPLC/PyCIMS
Boutin <sup>86</sup> 2002	Four à image	Flux concentré (10 <sup>5</sup> à 7,4 *10 <sup>6</sup> W/m <sup>2</sup> )	0-1s	Microgranular cellulose powder (Whatman CC 31)	Etude de la pyrolyse de pelletes de cellulose. Mise en évidence d'un intermédiaire liquide (ILC).	Observations microscopes (MEB)
Lédé 2002	Four à image	Flux concentré	0,05 - quelques secondes	Whatman CC31 cellulose	ILC et les vapeurs sont condensés et analysés. Seuls des oligosaccharides anhydres sont détectés. Pour le ILC : DP <7 avec 11% de cellobiosane et 5% de lévoglucosane.	HPLC/MS
Wooten <sup>80</sup> 2004	Four de pyrolyse	300°C	5-120 min	Avicel Cellulose PH102	Analyse de l'évolution de la structure du charbon en fonction du temps pour une pyrolyse à 300°C	RMN <sup>13</sup> C CPMAS
Luo <sup>87</sup> 2004	Four	300-1000°C	0,12 s	Papier filtre (Hangzhou Xinhua Paper Industry)	La déshydratation est favorisée à basse température (300°C). On obtient la formation de molécules à faibles masses molaires directement à partir de l'active cellulose	GC/MS
Liu <sup>88</sup> 2008	Flash radiatif	Flash radiatif (2-3,5*10 <sup>6</sup> W/m <sup>2</sup> )	0 à quelques secondes	Avicel PH 105 (Dp = 220)	Un intermédiaire jaune soluble dans l'eau a été identifié sous deux flux différents. La composition en composé dépend de l'intensité et du temps de "flash".	HPLC
Schoeter <sup>89</sup> 2011	Cisaillage mécanique, pression uniaxiale et chauffage laser	Intensité du laser 5-20W/m <sup>2</sup>	0,3-7 s	Coton	Etude de l'importance des liaisons hydrogènes dans la formation de l'active cellulose	Infrarouge et observations microscopes (MEB)
Dufour <sup>11</sup> 2012	Sonde RMN hautes températures	25°C-500°C	5 °C/min	Cellulose extraite de Miscanthus	Caractérisation « <i>in-situ</i> » de la formation d'une phase liquide	RMN <sup>1</sup> H « <i>in-situ</i> »
Hongwei Wu <sup>76,90</sup> 2012-2015	Réacteur lit fixe	25-400°C	10 °C/min + 30min à T const	Avicel cellulose PH102	Formation d'oligosaccharides anhydres	HPLC-PAD

D'après les études thermogravimétriques<sup>11,79</sup>, la cellulose se dégrade de façon significative à partir de 300°C suivant plusieurs mécanismes concurrentiels favorisés ou inhibés selon les conditions de pyrolyses ou la présence de catalyseurs (minéraux). La réaction de déshydratation de la cellulose intervient principalement à basse température (ou pour des vitesses de chauffes lentes), cette réaction qui conduit au dégagement de molécules d'eau induit la formation, au sein du réseau cellulosique, de liaisons carbonées insaturées. Ces dernières sont responsables de la « condensation » de la structure chimique de la cellulose<sup>79</sup>. Plusieurs mécanismes chimiques sont proposés afin de décrire la réaction de déshydratation : 1) les mécanismes intra-moléculaires<sup>79,91,92</sup> qui entraînent la formation d'insaturations au sein des cycles pyranoses, la formation de fonctions enols peut via un équilibre céto-enolique entraîner la formation de fonctions cétones<sup>92</sup> ; 2) les mécanismes inter-moléculaires qui conduisent à la condensation des différentes chaînes de cellulose<sup>55,92</sup> (Figure II-17). La combinaison de ces mécanismes de déshydratation avec les mécanismes d'ouverture/cyclisation permet d'établir un mécanisme chimique de formation de structures hydrofuranes.

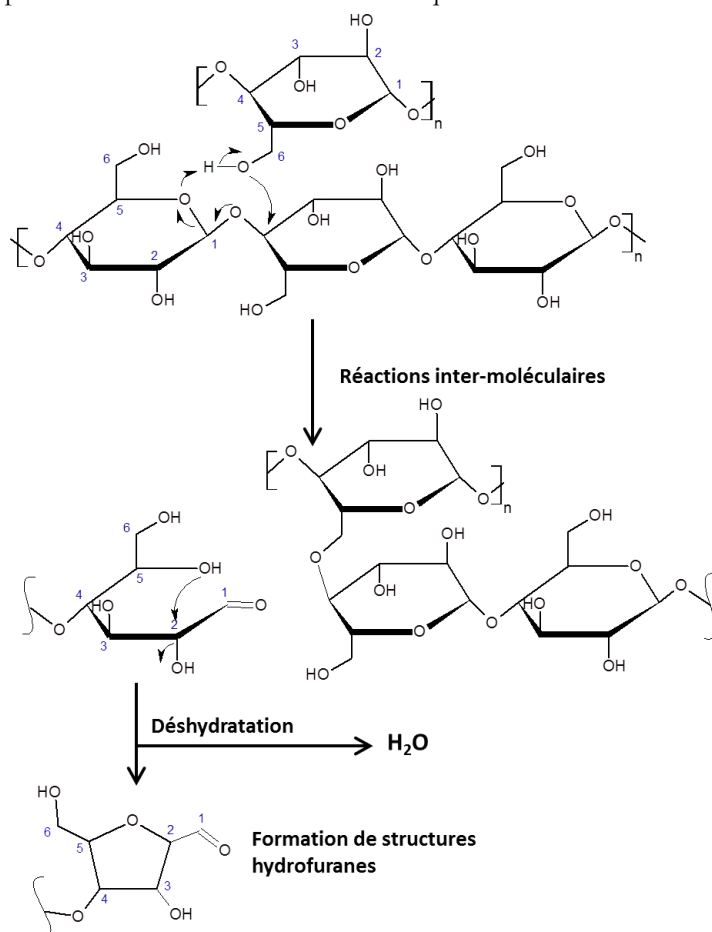


Figure II-17 : Mécanisme de déshydratation inter-moléculaire inspiré de Broido<sup>55</sup> et Scheirs<sup>92</sup>

La rupture des liaisons glycosidiques  $\beta(1,4)$  est une réaction prépondérante qui entre en compétition avec la réaction de déshydratation<sup>58,79,93</sup> (favorisée à basse température). La rupture des liaisons glycosidiques est une réaction très rapide qui a lieu sur une gamme de température très restreinte (300-350°C) entraînant la formation de composés volatils<sup>94</sup>. Cette réaction de dépolymérisation est favorisée pour des conditions de pyrolyse rapide<sup>61</sup>. Elle s'effectue par une réaction de transglycosylation<sup>40,95</sup> dont le mécanisme chimique est encore débattu. Plusieurs auteurs ont proposé des mécanismes de types ioniques (hétérolytiques)<sup>95</sup> ou

radicalaires (homolytiques)<sup>96,97</sup> transformant les chaînes cellulosiques en de courtes chaînes constituées d'une molécule de lévoglucosane à une extrémité et une molécule de glucose dite non réductrice à l'autre.

En ce qui concerne les mécanismes hétérolytiques plusieurs mécanismes sont décrits dans la littérature : 1) le mécanisme *un-zipping*<sup>98</sup> au sein duquel la réaction de transglycosylation intervient exclusivement à la fin des chaînes de cellulose ; 2) un mécanisme de transglycosylation qui se déroule aléatoirement le long des chaînes de cellulose<sup>42</sup>. La Figure II-18 présente le mécanisme concerté de transglycosylation<sup>95</sup>. Les groupements hydroxyles primaires (C<sub>6</sub>) sont, majoritairement dans le cas d'une matrice cellulose cristalline, inclus dans des liaisons hydrogènes intra ou inter-macromoléculaires. Lors du chauffage, ces liaisons sont rompues, le carbone hémiacétal (C<sub>1</sub>) du cycle glucopyranose est attaqué par l'oxygène du groupement hydroxyle primaire libre pour former un pont oxygène entre le carbone C<sub>6</sub> et le carbone hémiacétal C<sub>1</sub>. Il en résulte également la formation d'une fin de chaîne dite non réductrice.

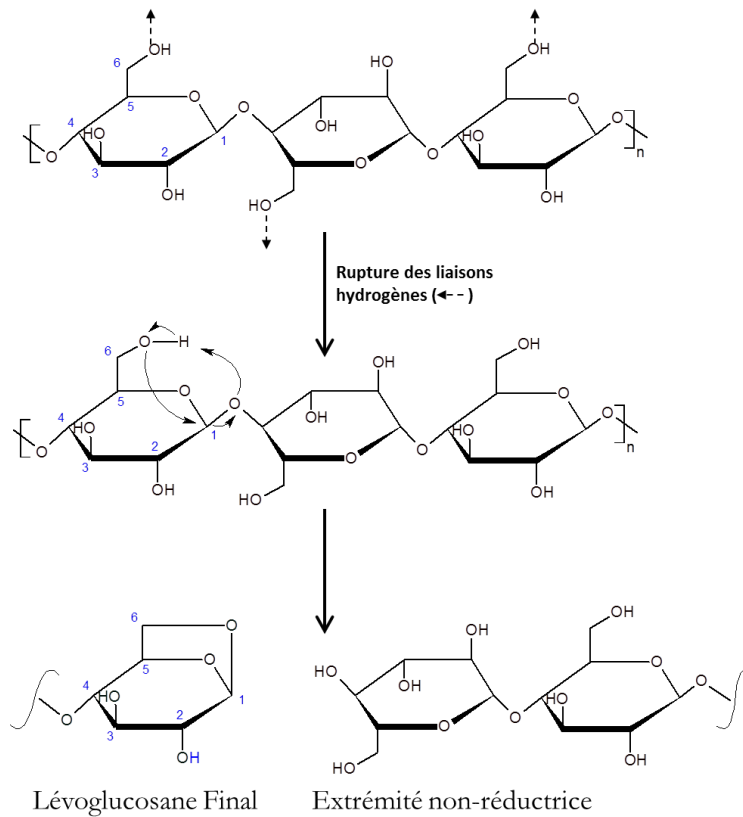


Figure II-18 : Le mécanisme concerté de transglycosylation d'une chaîne de cellulose<sup>40</sup>

Les réactions de dépolymérisation couplées aux réactions de déshydratation de la matrice cellulose entraînent la formation de composés furaniques<sup>77,92</sup> (furfural, furfuryl alcool) détectées au sein des vapeurs<sup>94</sup> et des charbons<sup>99,100</sup>. Des réactions de fragmentations/ouvertures de cycle concurrentes aux deux premières réactions conduisent à la formation de molécules de faibles masses molaires telles que l'hydroxyacétaldéhyde, le formaldéhyde ou des dérivés du furfural<sup>61</sup> et de gaz. Richards et al<sup>60</sup> ont proposé un mécanisme chimique (Figure II-19) illustrant la formation de l'hydroxyacétaldéhyde directement à partir de la cellulose via une réaction de déshydratation et de fragmentation (retro Diels Alder).

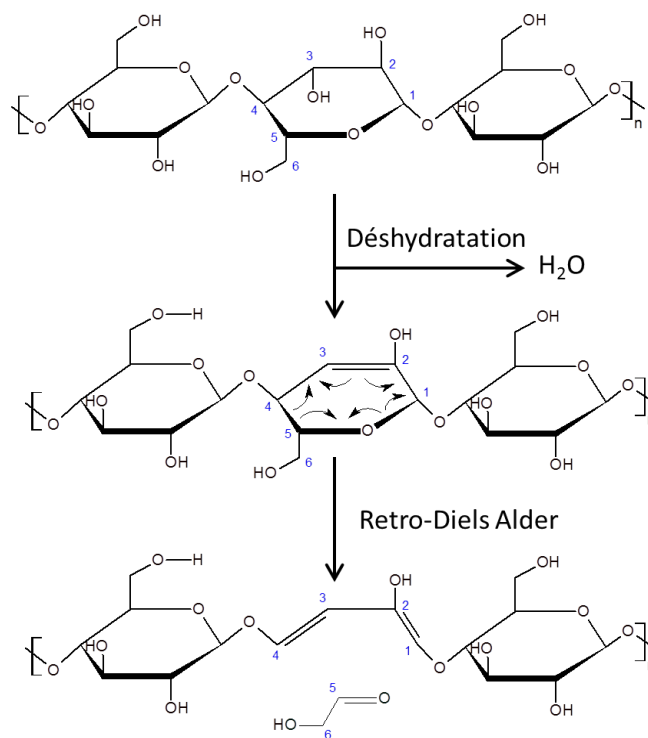


Figure II-19 : Le mécanisme de Richard<sup>60</sup>

La formation de ces composés à faibles masses molaires pourrait être issue également de la dégradation par un mécanisme d'élimination<sup>95</sup> ( $\beta$ -élimination). Cependant la formation de ces produits peut être confondue avec des produits de dégradation du lévoglucosane ou des oligosaccharides formés (réactions secondaires). Ces réactions de fragmentations sont susceptibles de se dérouler à haute température<sup>96</sup> mais la présence de composés inorganiques peut favoriser (catalyser) ce mécanisme de dégradation à de plus basses températures<sup>40,101,102</sup>.

L'étude des différents mécanismes chimiques montre que la formation des produits caractéristiques de la pyrolyse de la cellulose (levoglucosane, furanes, hydroxyacétaldéhyde) n'est pas issue d'un unique mécanisme chimique mais d'une combinaison de mécanismes. La formation de furanes nécessite des réactions d'ouvertures de cycles afin de former un cycle furanose à partir d'un cycle pyranose et des réactions de déshydratation pour former les insaturations du cycle furane. Les formations de composés furanones<sup>103-105</sup> et pyranones<sup>40,106</sup> ont été décrits dans la littérature. La formation de furanone semble être la combinaison de réactions d'ouvertures de cycles et des réactions de déshydratations. Dufour et al<sup>105</sup> ont mis en évidence la formation d'un composé de masse molaire 128 lors d'expériences en pyrolyse rapide couplée à un spectromètre à ionisation douce. La formation de structure pyranones pourrait être issue d'un mécanisme de double élimination<sup>106</sup>.

Cette analyse de la littérature nous amène à proposer le schéma global des mécanismes de pyrolyse de la cellulose présenté sur la Figure II-20. Les principales voies de dégradation de la cellulose sont résumées dans ce schéma global. La dégradation de la cellulose est décrite comme se faisant par un mécanisme unique amenant à la formation de la cellulose active. Cette dernière semble résulter de la dégradation primaire de la cellulose via dans un premier temps la rupture des liaisons hydrogènes et par une dépolymérisation des chaînes de cellulose. Le mécanisme exact de formation de cet intermédiaire reste cependant à définir.

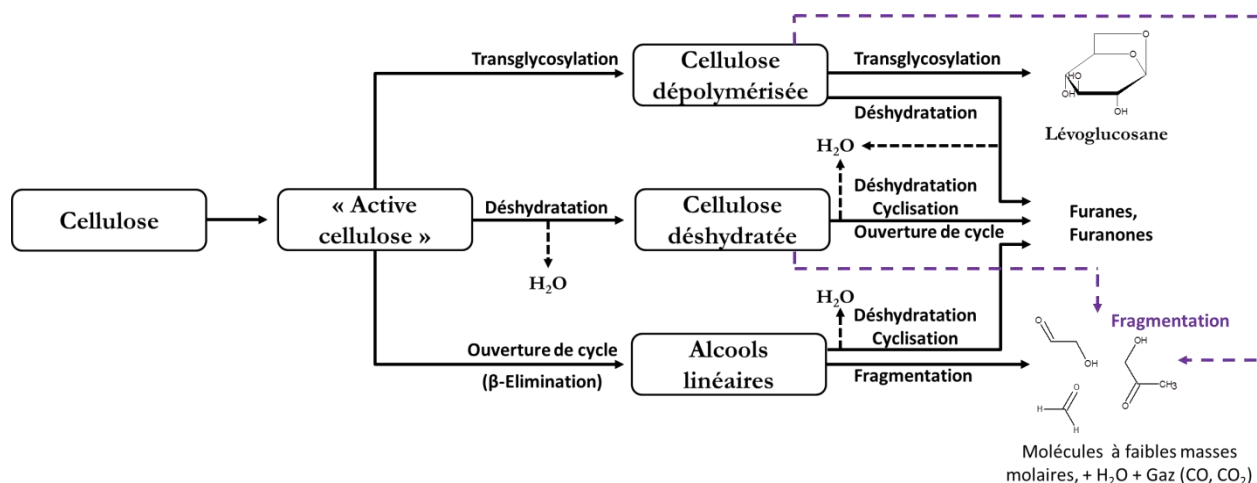


Figure II-20 : Le bilan global de la dégradation thermique primaire de la cellulose

### II.4.3 Pyrolyse des hémicelluloses

La grande diversité de structures des hémicelluloses rend leur étude très complexe car il est difficile d'établir des modèles précis<sup>102</sup>. De plus, les procédés d'extractions altèrent sensiblement la structure chimique des hémicelluloses. Par conséquent, l'étude de leurs mécanismes chimiques de dégradation thermique est plus complexe que pour la cellulose. Cependant, l'étude de ces mécanismes demeure un enjeu important pour l'optimisation des réacteurs de transformation thermochimique dans la mesure où les hémicelluloses peuvent représenter 25% en masse de la biomasse sèche. Les hémicelluloses se décomposent sur une gamme de températures plus importante (200-350°C) que la cellulose car les chaînes des hémicelluloses sont constituées de différentes unités liées entre elles par différentes liaisons chimiques ( $\beta(1,4)$ ,  $\beta(1,3)$ ,...) induisant par conséquent des stabilités thermiques différentes<sup>107</sup>. Le faible degré de polymérisation des chaînes d'hémicelluloses ainsi que leur caractère amorphe (non organisé) sont aussi responsables de leur « moins bonne » stabilité thermique. Le xylane (polymère de xylose) est la substance modèle la plus utilisée pour étudier le comportement thermique des hémicelluloses<sup>108,109</sup>.

A basse température (150-250°C), les hémicelluloses subissent principalement des réactions de déshydratation<sup>110</sup> et de fragmentation de certaines fonctions chimiques<sup>108</sup>. Il en résulte la dégradation des groupements acétyles<sup>111</sup>, carboxyliques et méthoxyles<sup>108</sup> (présents au sein des acides glucuroniques) entraînant la formation d'acide formique, d'acide acétique et de méthanol.

Pour des températures plus élevées (250-350°C), les composés volatils formés sont plus complexes. On observe la formation de composés furaniques (furfurals) et d'anhydro-saccharides (lévoglucofuranose, levogalactosane,...) par les ruptures des liaisons glycosidiques et carbone-carbone au sein de la structure des hémicelluloses<sup>112</sup>. Le furfural est l'un des composés majoritaires formés lors de la pyrolyse du xylane, cependant son mécanisme de formation n'est pas défini avec exactitude. Plusieurs réactions chimiques combinées semblent être responsables de la formation de furfural : 1) une dépolymérisation des chaînes saccharides par la rupture des liaisons glycosidiques ; 2) des réactions d'ouverture de cycle couplées à des réactions de déshydratation<sup>113</sup>.

Les hémicelluloses constituées de cycles pyranoses substitués d'un groupement hydroxyle<sup>112</sup> primaire (ex : les glucomannanes) entraînent la formation de composés anhydro-pyranose par l'établissement d'une liaison éther entre le C<sub>6</sub> et le C<sub>1</sub> via un mécanisme de transglycosylation. Les cycles pyranoses démunis de groupement hydroxyle primaire (ex : le xylose) ne peuvent former ces « 1,6 anhydro-pyranoses » (ex : lévoglucosane). Cependant la formation de composés anhydro-pyranoses de type 1,4-anhydro-D-xylopyranose, comme

produit de la pyrolyse de xylane, est décrite dans la littérature<sup>40,114,115</sup>. La dépolymérisation des liaisons glycosidiques entraînerait la formation de cations xylopyronosyles stabilisés par la formation d'une liaison éther entre le carbone C<sub>1</sub> et C<sub>4</sub>. Ce mécanisme présenté Figure II-21 est inspiré des travaux de Ponder et al<sup>116</sup>. La formation de cet intermédiaire cationique combiné à l'absence de groupement hydroxyle libre pourrait être une raison de la formation de taux de charbons plus importants lors de la pyrolyse de xylane. En effet, la liaison éther 1,4 ne semble pas aussi stable thermiquement qu'une liaison éther 1,6 issue du mécanisme de transglycosylation. Ainsi, ce cation xylopyronosyle est susceptible d'être stabilisé par des réactions intermoléculaires entraînant la condensation des macromolécules. Ce réseau condensé va par la suite être soumis à des réactions de déshydratation et entraîner la formation de charbon (structure aromatique). Les liaisons éthers intramoléculaires (1,4) sont décrites comme ne présentant pas une grande stabilité thermique, ce qui a pour conséquence de favoriser la dégradation thermique des molécules 1,4-anhydro-D-xylopyranose en phase vapeur<sup>108</sup>.

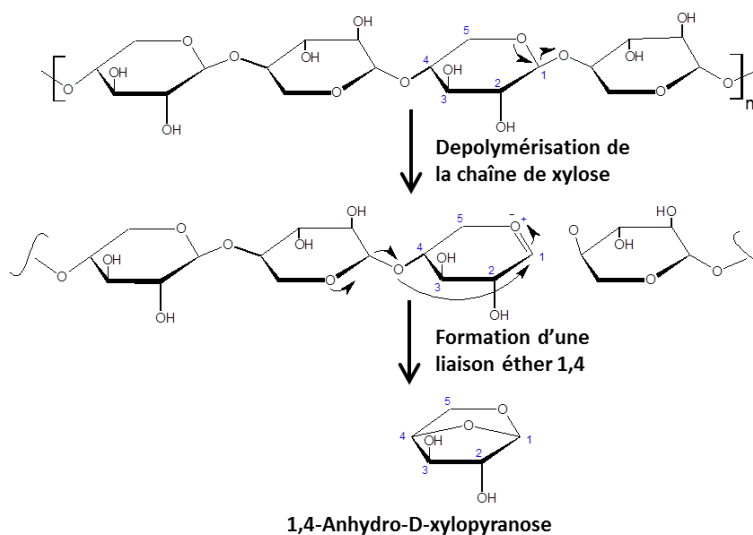


Figure II-21 : Mécanisme de formation du 1,4-anhydro-D-xylopyranose inspirée des travaux de Ponder<sup>116</sup>

Le mécanisme de formation du furfural le plus probable semble être la succession de réactions de dépolymérisation détruisant les liaisons glycosidiques couplées à des réactions d'ouverture de cycle entraînant la formation de molécules linéaires (aldoses et/ou kétooses) subissant simultanément des réactions de déshydratations/cyclisations et de fragmentations (Figure II-23). La formation de furanones est détectée au cours de la pyrolyse de xylane<sup>114</sup>. Des réactions d'ouvertures de cycle et de déshydratations<sup>117</sup> pourraient expliquer la formation de furanones, ces composés seraient par la suite susceptibles de subir des réactions de déshydratations supplémentaires entraînant la formation de furfural.

Des composés pyranones, principalement le 1,5-anhydro-4-deoxy-pent-1-en-3-ulose<sup>114</sup>, ont été identifiés comme produits issus de la dégradation du xylane<sup>40,118</sup>. Un mécanisme de double élimination proposé par Shafizadeh et al<sup>106</sup> pourrait expliquer la formation de ces composés (Figure II-22). La stabilité de ces composés à haute température n'est, à notre connaissance, pas déterminée. Il est probable qu'ils se décomposent via des réactions de fragmentations.

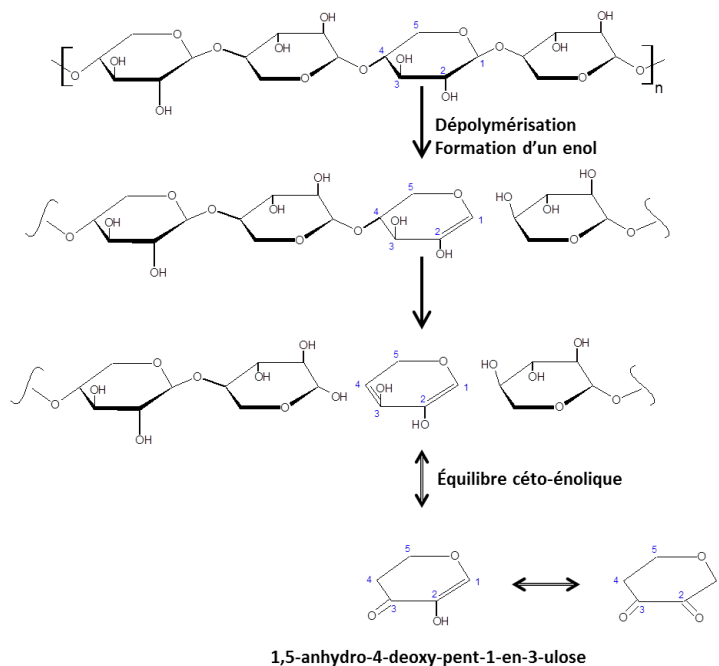


Figure II-22 : Mécanisme de formation des pyranones d'après les travaux de Shafizadeh

Pour des températures supérieures à 350°C, des molécules benzéniques oxygénées (méthylphénols) sont détectées au sein des volatils ainsi que du méthane<sup>113</sup> traduisant l'aromatisation du résidu solide (charbon). La Figure II-23 présente un bilan global de la dégradation du xylane.

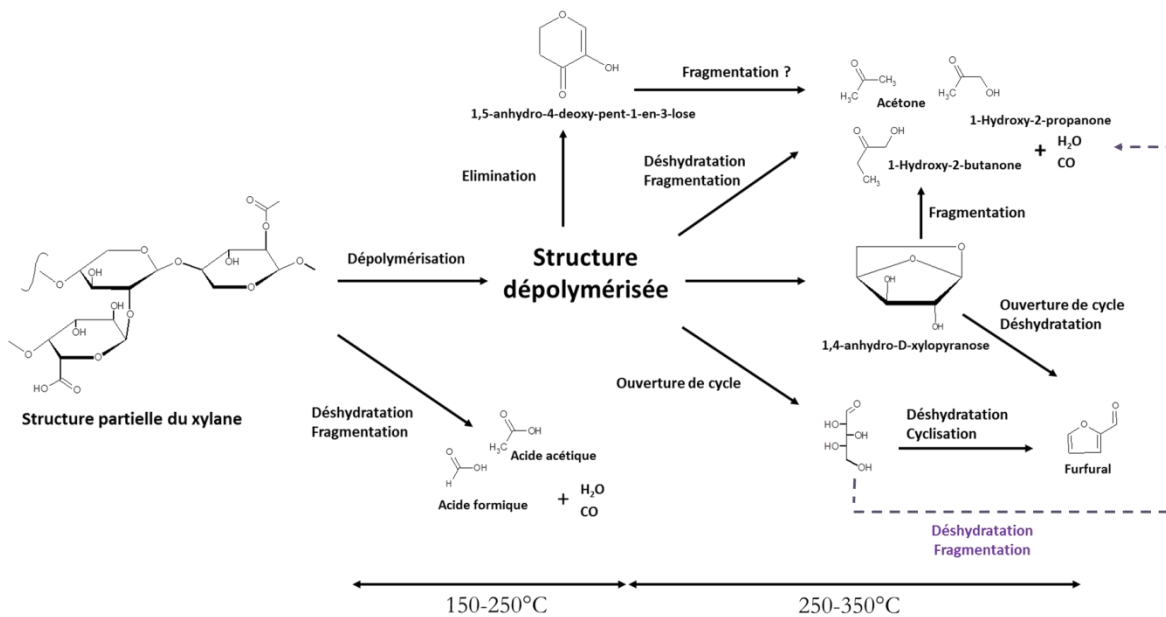


Figure II-23 : Le bilan global de la dégradation thermique d'une structure partielle<sup>13</sup> de xylane

## II.4.4 Pyrolyse de la lignine

Contrairement à la cellulose et aux hémicelluloses, la dégradation de la lignine s'effectue sur une gamme de températures<sup>119</sup> plus importante (150-500°C) due aux différentes stabilités thermiques attribuées aux nombreux types de liaisons chimiques entre les monomères. La mise au point de modèles cinétiques portant sur la dégradation thermique de la lignine est compliquée car sa structure chimique varie selon les types de biomasse<sup>20,120</sup>. Chaque procédé d'extraction engendre des modifications au sein de la structure chimique de la lignine<sup>121</sup> rendant ainsi encore plus complexe l'étude de la dégradation thermique de la lignine extraite de la biomasse lignocellulosique.

A basse température (150-300°C), les chaînes aliphatiques oxygénées du réseau polyphénolique de la lignine subissent des transformations. Les carbones substitués par des groupements hydroxyles libres sont éliminés et la formation de formaldéhyde et d'eau sont observées<sup>120,122,123</sup>. La formation d'eau est due principalement à des réactions de déshydratation des chaînes aliphatiques hydroxylées. Ces réactions entraînent la formation d'une structure présentant des chaînes aliphatiques insaturées (Figure II-24). La formation de dioxyde de carbone et d'acide formique résulte de la dégradation des fonctions carboxyliques et acétyles<sup>120</sup> présentes sur les chaînes aliphatiques oxygénées.

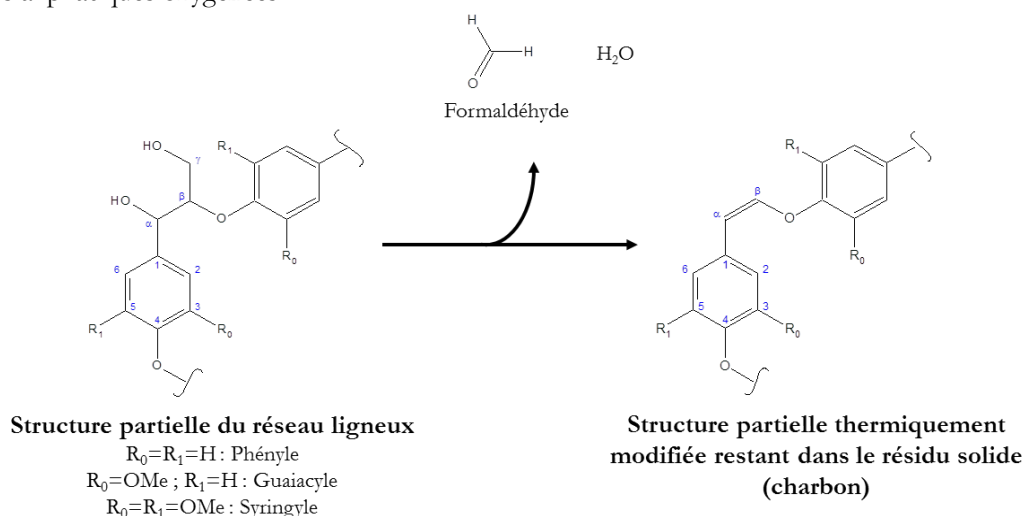


Figure II-24 : Le schéma de la dégradation du réseau ligneux par C $\gamma$  élimination et déshydratation

Les liaisons éthers ( $\beta$ -O-4 et  $\alpha$ -O-4)<sup>124</sup> sont également détruites entraînant une dépolymérisation du réseau polyphénolique (Figure II-25) tandis que les liaisons éthers présentes sur les carbones  $\gamma$  sont décrites comme thermiquement plus stables<sup>20</sup>. Cette dépolymérisation entraîne la volatilisation d'unités phénoliques présentant des chaînes aliphatiques insaturées composées de deux ou trois carbones<sup>40</sup> (vinyl-guaiacol, eugénol).

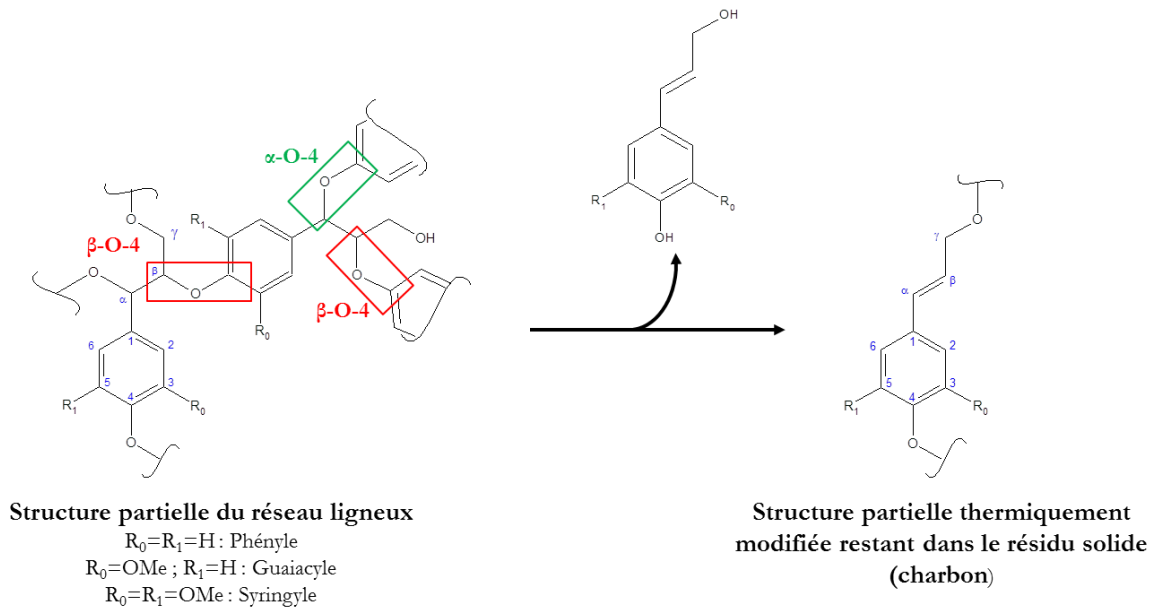


Figure II-25 : Le schéma de la dégradation des liaisons éthers du réseau ligneux

Ces ruptures s'accompagnent également de la formation de gaz ( $CO$ ,  $CO_2$  et  $H_2O$ ) provenant du réarrangement (par des réactions de condensation) s'établissant au sein du réseau ligneux modifié<sup>9,125</sup>. Pour des températures supérieures à  $300^\circ C$ , la conversion des chaînes aliphatiques est totale<sup>126</sup>. La volatilisation d'unités phénoliques sans chaîne aliphatique (guaiacol, syringol) ou à chaînes aliphatiques constituées d'un seul carbone (4-methylguaiacol) est observée<sup>40</sup> (Figure II-26). Cette étape se traduit par une volatilisation massive d'unités phénoliques et une condensation plus importante du résidu. Les groupements méthoxyles présents au sein de ce résidu deviennent réactifs vers  $370^\circ C$ <sup>120</sup>. Il en résulte la production de méthanol par déméthoxylation et de méthane<sup>40</sup> par déméthylation des groupements méthoxyles substitués aux cycles aromatiques du résidu. Des composés phénoliques déméthoxylés (phénol) ou déméthylés (dihydroxybenzène) sont alors volatilisés.

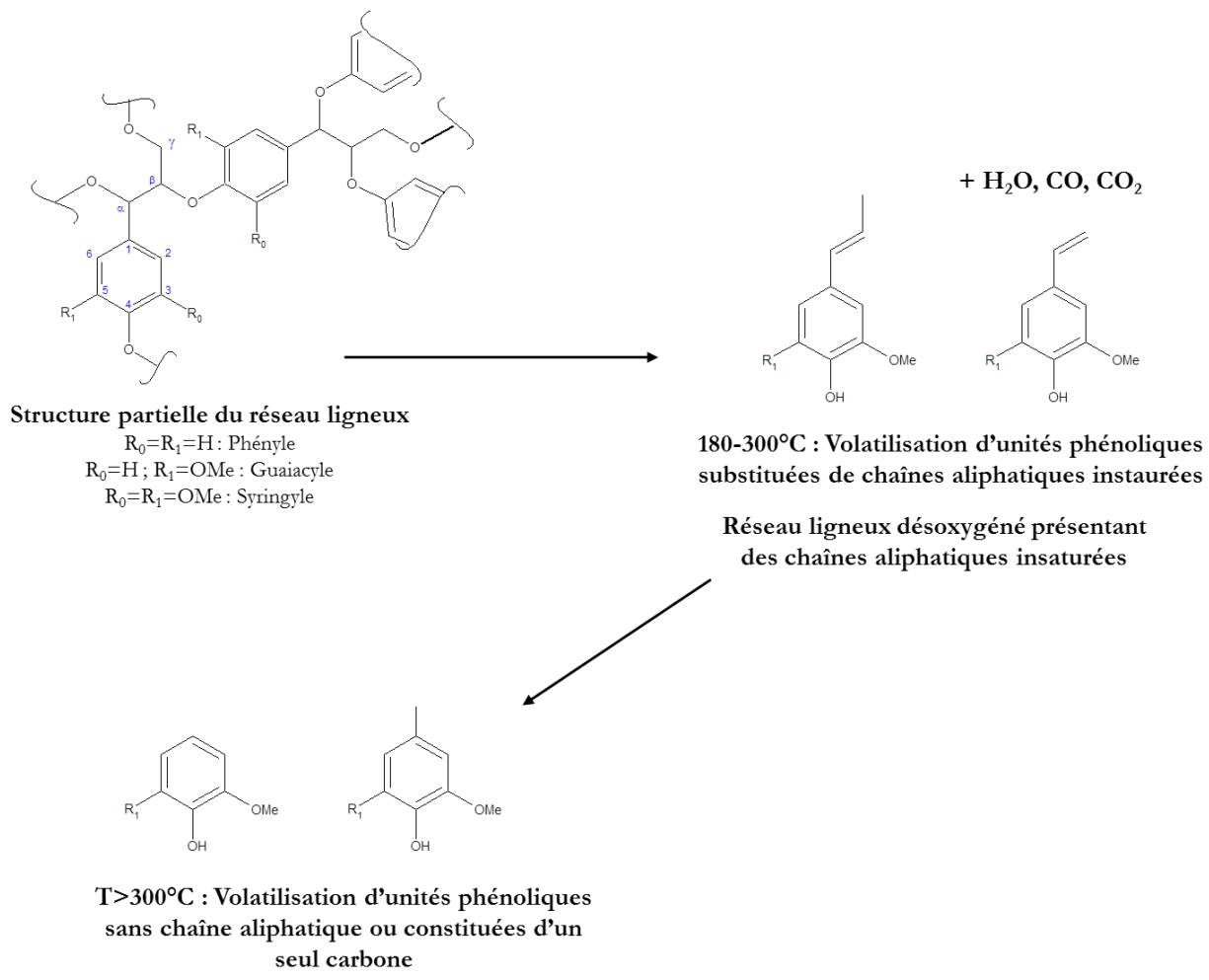


Figure II-26 : L'évolution de la structure chimique des volatils issus de la décomposition thermique de la lignine en fonction de la température

## II.4.5 Pyrolyse de la biomasse

La répartition en différents produits (char/condensables/gaz) ainsi que leurs compositions dépendent d'une part des conditions opératoires (pyrolyse lente, pyrolyse rapide) mais aussi des caractéristiques physico-chimiques des constituants de la biomasse : 1) la teneur en minéraux, 2) la teneur en différentes unités phénoliques<sup>127</sup> (hydroxyles, guaïcyles, syringyles) de la lignine ; 3) la composition des hémicelluloses<sup>108,128</sup> ; 4) le taux de cristallinité de la cellulose<sup>77</sup> et son degré de polymérisation<sup>129</sup>.

Le rendement en charbon de la lignine est plus élevé que pour les deux autres constituants (Tableau II-5) à cause de la présence de composés aromatiques au sein de sa structure native qui ont tendance à se condenser lors d'un traitement thermique<sup>110</sup>.

Tableau II-5 : Rendements en charbons obtenus en thermogravimétrie pour les différents constituants de la biomasse (% Charbon) sur masse sèche

Echantillons	Rampe	% Charbon (température finale)	Références
Cellulose Advantec	5°C/min	8% (500°C)	79
Cellulose Microcristalline	10°C/min	4% (500°C)	113
Cellulose (coton)	20°C/min	9,9% (600°C)	130
Cellulose Microcristalline	25°C/min	7,7% (900°C)	131
Hémicelluloses (extraits de paille de blé)	5°C/min	26,3 % (700°C)	111
Xylane (Bouleau)	10°C/min	25% (500°C)	113
Xylane (Hêtre)	10°C/min	35% (500°C)	108
Hémicelluloses ( <i>pinus sylvestris</i> )	20°C/min	31% (800°C)	132
Xylane (Épeautre)	25°C/min	21,7% (900°C)	131
Lignine (Dioxane)	5°C/min	37,2% (600°C)	133
Lignine (Organosolv, paille de blé)	10°C/min	37% (500°C)	113
Lignine (Organosolv)	20°C/min	35% (900°C)	120
Lignine (Organosolv)	25°C/min	36,8% (900°C)	131

L'étude de la pyrolyse de la biomasse native est plus complexe que la simple superposition de la décomposition de ces trois constituants. Les mécanismes de pyrolyse d'une biomasse native ne peuvent être résumés à la décomposition simultanée sans interaction de ces trois constituants<sup>134-136</sup>. Ces derniers sont liés entre eux par différentes liaisons au sein de la matrice lignocellulosique créant ainsi une proximité spatiale : 1) les hémicelluloses sont liées aux fibrilles de cellulose par des liaisons hydrogènes<sup>2</sup> ; 2) les hémicelluloses et la lignine sont liées par des liaisons covalentes<sup>137</sup>. Cette proximité est susceptible d'engendrer des interactions lors de la décomposition thermique des différents constituants et d'influer sur la structure chimique des produits de pyrolyse.

Plusieurs études sur des mélanges artificiels de constituants ont mis en évidence ce phénomène. La présence de la lignine, lors de la pyrolyse de la cellulose, semble changer la nature des volatils obtenus<sup>104</sup>. Elle semble également diminuer la quantité d'eau obtenue ainsi que celle de lévoglucosane au détriment du furfural<sup>138</sup>. Une loi d'additivité sur les rendements en gaz et leur composition semble également impossible à obtenir<sup>135</sup>. La structure chimique du charbon de la pyrolyse d'une biomasse native est également décrite comme pouvant résulter de réactions de polymérisation entre les différents produits formés lors de la dégradation thermique des constituants<sup>125</sup>.

Ces interactions au sein de la biomasse native n'ont pas uniquement un effet sur la répartition et la composition en produits mais également sur les propriétés physico-chimiques de la biomasse (transfert de matière et de chaleur)<sup>110</sup>. Par conséquent des expériences de pyrolyse sur des mélanges artificiels semblent inutiles pour représenter les mécanismes chimiques opérants lors de la pyrolyse de biomasse native. Des études de modélisation, basées sur les paramètres cinétiques propres à chacun des constituants ainsi que leurs compositions, ont néanmoins montré des résultats proches des résultats expérimentaux<sup>139,140</sup>. Le modèle de Ranzi<sup>139,141</sup> est l'un des modèles cinétiques les plus aboutis pour simuler la dégradation de la biomasse. Cependant, il reste limité dans la description des produits intermédiaires de pyrolyse et la prise en compte de l'influence des minéraux (effets catalytiques) au sein des mécanismes chimiques de pyrolyse.

#### **II.4.6 Influence des minéraux sur les mécanismes de pyrolyse de la biomasse**

La présence d'éléments inorganiques comme le potassium, le sodium, le calcium et le magnésium au sein de la biomasse est définie comme ayant une influence importante sur les mécanismes de pyrolyse modifiant ainsi la répartition et la composition des produits<sup>142-144</sup>. La présence de ces éléments entraîne également des problèmes dans les procédés de transformation thermo-chimique comme la diminution de la qualité des produits obtenus (bio-huiles, gaz de synthèse), l'augmentation des problèmes de corrosion et d'agglomération dans les procédés de combustion ou de gazéification.<sup>145,146</sup>

D'après les analyses thermogravimétriques (Tableau II-6), la conversion de la biomasse est initiée à plus basse température lorsque des éléments inorganiques sont présents au sein de la matrice lignocellulosique<sup>4,113</sup>. Dans le cas de la cellulose, le rendement en lévoglucosane est réduit considérablement<sup>94,147</sup> et les formations de charbon et de gaz<sup>113</sup> sont favorisées ainsi que la formation de composés furaniques<sup>40</sup>. Les métaux alcalins et alcalinoterreux sont décrits comme pouvant inhiber le mécanisme de transglycosylation et ainsi favoriser les réactions de déshydratation<sup>90</sup> et de fragmentation<sup>101,142</sup>. L'influence des inorganiques sur les hémicelluloses étudiées par des expériences de thermogravimétrie après imprégnations avec différents sels alcalins ne semble pas très marquée<sup>5</sup>. Cependant il est important de noter que les hémicelluloses commerciales peuvent contenir des inorganiques<sup>107</sup> car ces polysaccharides sont naturellement riches en minéraux<sup>110</sup> et les techniques de purification ne permettent pas d'enlever totalement ces éléments. Ce phénomène pourrait expliquer la raison pour laquelle les études menées sur des imprégnations d'hémicelluloses ne permettent pas de visualiser l'effet des minéraux. Cependant même après déminéralisation, la pyrolyse d'hémicelluloses commerciales (800°C,

30s)<sup>112</sup> semble donner des rendements en charbon très importants (20% pour le xylane, 30% pour le glucomannane).

Les investigations menées sur des échantillons de lignine imprégnés ne permettent pas de distinguer de variations significatives quant aux rendements en produits. Il est pourtant avéré que les inorganiques alcalins favorisent certains mécanismes chimiques de dégradation comme la déméthoxylation, la déméthylation, les réactions de condensation et les C $\gamma$ -éliminations<sup>147,148</sup>.

Tableau II-6 : Influence de la présence d'inorganiques sur la dégradation thermique des constituants de la biomasse (Ti = Température de début de perte de masse ; Tmax = Température de vitesse maximale de conversion ; % charbon sur masse sèche)

Echantillons	Purs			Imprégnés			Rampe °C/min	Références
	Ti	Tmax	%charbon	Ti	Tmax	%charbon		
Cellulose (Coton, 1%masseK, K <sub>2</sub> CO <sub>3</sub> )	263	372	9% (900°C)	185	357	21,6%	20	130
Cellulose (1%masseK, KC <sub>2</sub> H <sub>3</sub> O <sub>2</sub> )		368	7,7% (900°C)		325	27,7% (900°C)	25	131
Xylan (Bouleau, 2%masse KCl)	238	287	25% (700°C)	238	287	28,4 (700°C)	10	113
Xylan (Blé, 1%masseK, KC <sub>2</sub> H <sub>3</sub> O <sub>2</sub> )		315	21,7% (900°C)		317	21,6 (900°C)	20	131
Xylan (Bouleau 10%masseK, K <sub>2</sub> CO <sub>3</sub> )			42% (450°C)			43% (450°C)	10	5
Organosolv (2%masse KCl)	227		37% (700°C)	227		39,7% (700°C)	10	113
Organosolv (1%masseK, KC <sub>2</sub> H <sub>3</sub> O <sub>2</sub> )		397	36,8% (900°C)		330	50,7% (900°C)	25	131
Organosolv (10%masse, K <sub>2</sub> CO <sub>3</sub> )			50% (450°C)			48% (450°C)	10	5

La connaissance de l'influence des minéraux sur les mécanismes chimiques de pyrolyse est essentielle car la plupart des biomasses susceptibles d'être utilisées dans des procédés de transformation thermochimique présentent des taux d'inorganiques importants (plantes herbacées et résidus forestiers)<sup>145</sup>. Les modèles de prédiction des produits de pyrolyse ne prennent pas en compte l'influence des inorganiques ce qui a pour conséquence de diminuer leur efficacité.

## II.5 Organisation de la démarche de la thèse

L'étude bibliographique a montré que les études sur les mécanismes chimiques de pyrolyse de la biomasse ne permettent pas de les décrire de façon précise. De plus, il n'existe pas de modèle cinétique capable de prédire la composition des produits de pyrolyse pour des biomasses avec des compositions variées (notamment effet des minéraux). Il est par conséquent crucial de développer de nouvelles techniques analytiques permettant d'améliorer la caractérisation chimique des produits de pyrolyse et ainsi de définir l'influence de la composition initiale de la biomasse sur les mécanismes chimiques de pyrolyse. De nombreuses techniques analytiques<sup>149</sup> sont utilisées dans la littérature mais la grande hétérogénéité des biomasses et des procédés de pyrolyse utilisés rend difficile une approche globale de ces mécanismes.

L'objectif de cette thèse est justement de réaliser des analyses complémentaires des produits de pyrolyses (charbon, goudrons et gaz) par de nombreuses méthodes physico-chimiques : Résonance magnétique nucléaire RMN du proton  $^1\text{H}$  et du carbone  $^{13}\text{C}$  ; Calorimétrie (DSC) ; Thermogravimétrie ; GC/MS (*Gas Chromatography and Mass spectrometry*) et LC/MS (*Liquid Chromatography and Mass Spectrometry*). Cette thèse a eu par conséquent l'objectif d'utiliser des techniques d'analyses dites *ex-situ* telles que l'analyse 2D RMN par la méthode HETCOR (*Heteronuclear correlation*)  $^1\text{H}$ - $^{13}\text{C}$  ainsi que des analyses *in-situ* en RMN  $^1\text{H}$  Haute Température ou dites PMRTA (*proton magnetic resonance thermal analysis*). Les analyses ont été conduites pour une large gamme de températures (200°C à 500°C) en pyrolyse lente pour différentes biomasses (miscanthus, chêne et douglas). Afin d'élargir le champ des investigations, ces techniques d'analyses ont aussi été employées sur des échantillons déminéralisés et imprégnés avec des minéraux pour obtenir des données originales sur l'influence des minéraux lors de la pyrolyse de la biomasse. Toutes ces analyses ont pour objectif final de développer un modèle cinétique détaillé pour prédire la composition des produits de pyrolyse et optimiser des réacteurs de transformation thermochimique notamment en orientant leur sélectivité vers des produits à forte valeur ajoutée.

Pour cette étude, les expériences de pyrolyses de biomasses ont été réalisées au sein d'un lit fixe permettant un contrôle optimal des phénomènes de transfert de chaleur et de matière en pyrolyse lente (5K/min). Ce dispositif nous a permis d'obtenir des échantillons de charbons, de goudrons et de gaz sur une large gamme de température (200-500°C) dans des quantités suffisantes afin de multiplier les analyses. Ces échantillons ont été réalisés principalement à partir de *Miscanthus x Giganteus* (MxG). Cette plante présente un grand potentiel dans le domaine de la valorisation énergétique<sup>150</sup> et demeure en cette occasion un sujet d'étude intéressant.

Ce travail réalisé de Novembre 2011 à Juillet 2015 est présenté sous la forme d'une thèse sur travaux. La thèse s'articule ainsi autour de cinq articles. Le plan s'articule en quatre chapitres qui présentent chacun un aspect différent de cette étude.

### Chapitre III :

Dans ce chapitre, nous nous sommes intéressés à l'étude de la structure chimique du charbon en Résonance Magnétique Nucléaire du carbone (RMN  $^{13}\text{C}$ ) afin d'identifier les espèces chimiques formées et converties lors de la pyrolyse du MxG. Afin d'élargir le champ d'investigation, nous avons procédé à l'étude de la structure du charbon de la pyrolyse des macromolécules (cellulose, holocellulose, lignine) extraites du miscanthus. Cette étude a permis de définir une évolution de la structure de la biomasse en fonction de la température. Nous avons également utilisé une technique de RMN dite à deux dimensions faisant intervenir la résonance magnétique nucléaire du proton  $^1\text{H}$  et du carbone  $^{13}\text{C}$  au sein de la même analyse permettant ainsi d'obtenir une caractérisation plus poussée de la structure du charbon. Ces analyses dites à deux dimensions (2D RMN  $^1\text{H}$ - $^{13}\text{C}$ ) ont été réalisées à l'aide de la technique HETCOR (*HETeronuclear CORrelation*) sur un appareil de

mesure à très haut champ (750MHz) permettant de mettre en évidence des caractéristiques chimiques, à notre connaissance, inconnues.

**Chapitre IV :** Ce chapitre porte sur l'étude de l'influence des minéraux et notamment du potassium (K) dans les mécanismes chimiques de pyrolyse. Ce chapitre présente une étude originale notamment réalisée à l'aide d'analyses en RMN « *in situ* »  $^1\text{H}$  haute température et en chromatographie d'exclusion stérique (SEC). Notre compréhension des mécanismes de pyrolyse est également complétée par des analyses globales (perte de masse par thermogravimétrie, chaleur de réaction par calorimétrie).

**Chapitre V :** Les chapitres III et IV ont donc portés sur la formation du solide (biochar) avec le passage par une phase « intermédiaire liquide ». Ce chapitre V traite de la formation des composés volatils (goudrons, gaz) formés durant la pyrolyse. La compréhension des mécanismes de formation des goudrons/volatils lors de la pyrolyse demeure un défi majeur pour la valorisation de la matière lignocellulosique dans les procédés de transformation thermique. La compréhension et la prédiction de la formation de ces goudrons permettraient de diriger les procédés vers la production de composés chimiques à forte valeur ajoutée ou vers une réduction des goudrons polluants. Les mécanismes de formation de ces goudrons ont été étudiés par des analyses « *en ligne* » à l'aide d'un spectromètre de masse à ionisation douce (*Single Photo Ionisation SPI*) couplé à un détecteur de masse à temps de vol (*Time Of Flight TOF*). Les goudrons générés ont également été condensés et analysés (hors-ligne) en chromatographie en phase gaz (GC/MS) La combinaison de ces deux analyses (SPI-TOFMS et GC/MS) apporte des données nouvelles sur les mécanismes de formation des goudrons primaires.

**Chapitre VI :** Ce chapitre présente une combinaison des principales techniques analytiques afin de déterminer un bilan global des mécanismes chimiques intervenant lors de la pyrolyse du miscanthus. Nous résumons les différentes techniques employées dans les chapitres précédents et discutons les apports complémentaires de celles-ci.

## Références

- (1) Mosseri, R.; Jeandel, C. *L'énergie à Découvert*, CNRS EDITIONS.; 2013.
- (2) Rowell, R., M.; Le Van-Green, S. L. Handbook of Wood Chemistry and Wood Composites. In *Handbook of Wood Chemistry and Wood Composites*; Rowell R.M., 2005; pp 121–138.
- (3) Eliaers, P.; Ranjan Pati, J.; Dutta, S.; De Wilde, J. Modeling and Simulation of Biomass Drying in Vortex Chambers. *Chem. Eng. Sci.* **2015**, *123*, 648–664.
- (4) Fahmi, R.; Bridgwater, A. V.; Darvell, L. I.; Jones, J. M.; Yates, N.; Thain, S.; Donnison, I. S. The Effect of Alkali Metals on Combustion and Pyrolysis of Lolium and Festuca Grasses, Switchgrass and Willow. *Fuel* **2007**, *86* (10-11), 1560–1569.
- (5) Saleh, S. B.; Hansen, B. B.; Jensen, P. A.; Dam-Johansen, K. Influence of Biomass Chemical Properties on Torrefaction Characteristics. *Energy Fuels* **2013**, *27* (12), 7541–7548.
- (6) Melkior, T.; Jacob, S.; Gerbaud, G.; Hediger, S.; Le Pape, L.; Bonnefois, L.; Bardet, M. NMR Analysis of the Transformation of Wood Constituents by Torrefaction. *Fuel* **2012**, *92* (1), 271–280.
- (7) Eom, I.-Y.; Kim, K.-H.; Kim, J.-Y.; Lee, S.-M.; Yeo, H.-M.; Choi, I.-G.; Choi, J.-W. Characterization of Primary Thermal Degradation Features of Lignocellulosic Biomass after Removal of Inorganic Metals by Diverse Solvents. *Bioresour. Technol.* **2011**, *102* (3), 3437–3444.
- (8) Park, J.; Meng, J.; Lim, K. H.; Rojas, O. J.; Park, S. Transformation of Lignocellulosic Biomass during Torrefaction. *J. Anal. Appl. Pyrolysis* **2013**, *100*, 199–206.
- (9) Wang, S.; Wang, K.; Liu, Q.; Gu, Y.; Luo, Z.; Cen, K.; Fransson, T. Comparison of the Pyrolysis Behavior of Lignins from Different Tree Species. *Biotechnol. Adv.* **2009**, *27* (5), 562–567.
- (10) Sticklen, M. B. Plant Genetic Engineering for Biofuel Production: Towards Affordable Cellulosic Ethanol. *Nat. Rev. Genet.* **2010**, *11* (4), 308–308.
- (11) Dufour, A.; Castro-Diaz, M.; Brosse, N.; Bouroukba, M.; Snape, C. The Origin of Molecular Mobility During Biomass Pyrolysis as Revealed by In Situ <sup>1</sup>H NMR Spectroscopy. *ChemSusChem* **2012**, *5* (7), 1258–1265.
- (12) Ragauskas, A. J.; Beckham, G. T.; Bidy, M. J.; Chandra, R.; Chen, F.; Davis, M. F.; Davison, B. H.; Dixon, R. A.; Gilna, P.; Keller, M.; Langan, P.; Naskar, A. K.; Saddler, J. N.; Tschaplinski, T. J.; Tuskan, G. A.; Wyman, C. E. Lignin Valorization: Improving Lignin Processing in the Biorefinery. *Science* **2014**, *344* (6185).
- (13) Stevanovic, T.; Perrin, D. *Chimie Du Bois*, Presses Polytechniques et universitaires romandes.; 2009.
- (14) Deglise, X.; Donnot, A. Bois énergie. Techniques de l'ingénieur 2004.
- (15) Cheng, J. *Biomass to Renewable Energy Processes*, CRC Press, Taylor and Francis group.; 2010.
- (16) Nishiyama, Y. Structure and Properties of the Cellulose Microfibril. *J. Wood Sci.* **2009**, *55* (4), 241–249.
- (17) O'Sullivan, A. C. Cellulose: The Structure Slowly Unravels. *Cellulose* **1997**, *4* (3), 173–207.
- (18) Park, S.; Baker, J. O.; Himmel, M. E.; Parilla, P. A.; Johnson, D. K. Cellulose Crystallinity Index: Measurement Techniques and Their Impact on Interpreting Cellulase Performance. *Biotechnol. Biofuels* **2010**, *3*.
- (19) El Hage, R. Prétraitement Du Miscanthus X Giganteus. Vers Une Valorisation Optimale de La Biomasse Lignocellulosique, Université de Nancy, 2010.
- (20) Pandey, M. P.; Kim, C. S. Lignin Depolymerization and Conversion: A Review of Thermochemical Methods. *Chem. Eng. Technol.* **2011**, *34* (1), 29–41.
- (21) Villaverde, J. J.; Li, J.; Ek, M.; Ligerio, P.; de Vega, A. Native Lignin Structure of *Miscanthus X Giganteus* and Its Changes during Acetic and Formic Acid Fractionation. *J. Agric. Food Chem.* **2009**, *57* (14), 6262–6270.
- (22) del Río, J. C.; Rencoret, J.; Prinsen, P.; Martínez, Á. T.; Ralph, J.; Gutiérrez, A. Structural Characterization of Wheat Straw Lignin as Revealed by Analytical Pyrolysis, 2D-NMR, and Reductive Cleavage Methods. *J. Agric. Food Chem.* **2012**, *60* (23), 5922–5935.
- (23) del Río, J. C.; Rencoret, J.; Marques, G.; Gutiérrez, A.; Ibarra, D.; Santos, J. I.; Jiménez-Barbero, J.; Zhang, L.; Martínez, Á. T. Highly Acylated (Acetylated And/or P-Coumaroylated) Native Lignins from Diverse Herbaceous Plants. *J. Agric. Food Chem.* **2008**, *56* (20), 9525–9534.

- (24) Zakzeski, J.; Bruijninx, P. C. A.; Jongerijs, A. L.; Weckhuysen, B. M. The Catalytic Valorization of Lignin for the Production of Renewable Chemicals. *Chem. Rev.* **2010**, *110* (6), 3552–3599.
- (25) Sette, M.; Wechselberger, R.; Crestini, C. Elucidation of Lignin Structure by Quantitative 2D NMR. *Chem. – Eur. J.* **2011**, *17* (34), 9529–9535.
- (26) Hon, D. N.-S.; Shiraishi, N. *Wood and Cellulosic Chemistry, Second Edition, Revised, and Expanded*; CRC Press, 2000.
- (27) Pan, W.-P.; Richards, G. N. Influence of Metal Ions on Volatile Products of Pyrolysis of Wood. *J. Anal. Appl. Pyrolysis* **1989**, *16* (2), 117–126.
- (28) Vassilev, S. V.; Baxter, D.; Andersen, L. K.; Vassileva, C. G. An Overview of the Composition and Application of Biomass Ash. Part 1. Phase–mineral and Chemical Composition and Classification. *Fuel* **2013**, *105*, 40–76.
- (29) Lorne, D. *Les Unités Pilotes de Biocarburants de Deuxième Génération Dans Le Monde-IFP Panorama*; IFP-, 2008.
- (30) Lorne, D.; Chabrelié, M.-F. *Les Nouvelles Technologies de Production de Biocarburants : états Des Lieux et Enjeux Des Filières En Développement-IFP Panaorama*; 2011.
- (31) Kuzhiyil, N.; Dalluge, D.; Bai, X.; Kim, K. H.; Brown, R. C. Pyrolytic Sugars from Cellulosic Biomass. *ChemSusChem* **2012**, *5* (11), 2228–2236.
- (32) Kambo, H. S.; Dutta, A. A Comparative Review of Biochar and Hydrochar in Terms of Production, Physico-Chemical Properties and Applications. *Renew. Sustain. Energy Rev.* **2015**, *45*, 359–378.
- (33) Butler, E.; Devlin, G.; Meier, D.; McDonnell, K. A Review of Recent Laboratory Research and Commercial Developments in Fast Pyrolysis and Upgrading. *Renew. Sustain. Energy Rev.* **2011**, *15* (8), 4171–4186.
- (34) Bridgwater, A. V. Review of Fast Pyrolysis of Biomass and Product Upgrading. *Biomass Bioenergy* **2012**, *38*, 68–94.
- (35) François, J. Modélisation et évaluation Environnementale Des Filières de Cogénération Par Combustion et Gazéification Du Bois, Université de Lorraine: Institut Jean Lamour, 2014.
- (36) Bhaskar, T.; Pandey, A. Chapter 1 - Advances in Thermochemical Conversion of Biomass—Introduction. In *Recent Advances in Thermo-Chemical Conversion of Biomass*; Sukumaran, A. P. B. S. K., Ed.; Elsevier: Boston, 2015; pp 3–30.
- (37) Zhang, L.; Xu, C. (Charles); Champagne, P. Overview of Recent Advances in Thermo-Chemical Conversion of Biomass. *Energy Convers. Manag.* **2010**, *51* (5), 969–982.
- (38) Doassans, N.; Mauviel, G.; Ferrasse, J.; Lede, J.; Boutin, O. Liquéfaction de Biomasse : Comparaison Des Procédés de Pyrolyse Rapide et de Liquéfaction - Posters, 2012.
- (39) Garcia-Perez, M.; Chaala, A.; Pakdel, H.; Kretschmer, D.; Roy, C. Characterization of Bio-Oils in Chemical Families. *Biomass Bioenergy* **2007**, *31* (4), 222–242.
- (40) Evans, R. J.; Milne, T. A. Molecular Characterization of the Pyrolysis of Biomass. 1. Fundamentals. *Energy Fuels* **1987**, *1* (2), 123–137.
- (41) Bridgwater, A. V. Renewable Fuels and Chemicals by Thermal Processing of Biomass. *Chem. Eng. J.* **2003**, *91* (2–3), 87–102.
- (42) Piskorz, J.; Majerski, P.; Radlein, D.; Vladars-Usas, A.; Scott, D. S. Flash Pyrolysis of Cellulose for Production of Anhydro-Oligomers. *J. Anal. Appl. Pyrolysis* **2000**, *56* (2), 145–166.
- (43) Dahiya, A. *Bioenergy: Biomass to Biofuels-Chapitre 26 Pyrolysis of Lignocellulosic Biomass*; Academic Press, 2014.
- (44) Dufour, A. Optimisation de La Production D'hydrogène Par Conversion Du Méthane Dans Les Procédés de Pyrolyse/gazéification de La Biomasse, 2007.
- (45) Lédé, J. Cellulose Pyrolysis Kinetics: An Historical Review on the Existence and Role of Intermediate Active Cellulose. *J. Anal. Appl. Pyrolysis*.
- (46) Molton, P. M.; Demmitt, T. F. *Reaction Mechanisms in Cellulose Pyrolysis: A Literature Review*; Battelle Pac. Northwest Lab., 1977; p 90 pp.
- (47) Broido, K.; Kilzer, F. J. A Critique of the Present State of Knowledge of the Mechanism of Cellulose Pyrolysis. *Fire Res.* **1963**, No. 5, 157.
- (48) Pictet, A.; Sarasin, J. Distillation of Cellulose and Starch in Vacuo. *Helv. Chim. Acta* **1**. 1918.

- (49) Holmes, F. H.; Shaw, C. J. G. The Pyrolysis of Cellulose and the Action of Flame-Retardants. I. Significance and Analysis of the Tar. *J. Appl. Chem.* **1961**, *11*, 210–216.
- (50) Dobeles, G. Production, Properties and Use of Wood Pyrolysis - A Brief of the Work Carried out at Research and Production Centres of the Former USSR from 1960 to 1990. In *Fast Pyrolysis of Biomass: A Handbook*; Bridgwater.
- (51) Pacault, A.; Sauret, G. The Thermal Depolymerization of Cellulose. *Compt Rend* **1958**, *246*, 608–611.
- (52) Chatterjee, P. K.; Conrad, C. M. Kinetics of the Pyrolysis of Cotton Cellulose. *Text. Res. J.* **1966**, *36* (6), 487–494.
- (53) Beall, F. C.; Eickner, H. W. *Thermal Degradation of Wood Components: A Review of the Literature*; U.S.D.A Forest service research paper, 1970.
- (54) Halpern, Y.; Riffer, R.; Broido, A. Levoglucosenone (1,6-Anhydro-3,4-Dideoxy- $\Delta^3$ - $\beta$ -D-Pyranosen-2-One). Major Product of the Acid-Catalyzed Pyrolysis of Cellulose and Related Carbohydrates. *J. Org. Chem.* **1973**, *38* (2), 204–209.
- (55) Kilzer, F. J.; Broido, A. Speculations on the Nature of Cellulose Pyrolysis. *Pyrolytics* **1965**, *2* (2-3), 151–163.
- (56) Arseneau, D. F. Competitive Reactions in the Thermal Decomposition of Cellulose. *Can. J. Chem.* **1971**, *49* (4), 632–638.
- (57) Shafizadeh, F. Pyrolysis and Combustion of Cellulosic Materials. *Adv. Carbohydr. Chem.* **1968**, *23*, 419–474.
- (58) Piskorz, J.; Radlein, D.; Scott, D. S. On the Mechanism of the Rapid Pyrolysis of Cellulose. *J. Anal. Appl. Pyrolysis* **1986**, *9* (2), 121–137.
- (59) Piskorz, J.; Radlein, D. S. A. G.; Scott, D. S.; Czernik, S. Pretreatment of Wood and Cellulose for Production of Sugars by Fast Pyrolysis. *J. Anal. Appl. Pyrolysis* **1989**, *16* (2), 127–142.
- (60) Richards, G. N. Glycolaldehyde from Pyrolysis of Cellulose. *J. Anal. Appl. Pyrolysis* **1987**, *10* (3), 251–255.
- (61) Garcia-Perez, M. The Formation of Polyaromatic Hydrocarbons and Dioxins During Pyrolysis. 2008.
- (62) Radlein, D.; Piskorz, J.; Scott, D. S. Fast Pyrolysis of Natural Polysaccharides as a Potential Industrial Process. *J. Anal. Appl. Pyrolysis* **1991**, *19*, 41–63.
- (63) Piskorz, J.; Radlein, D. S. A. G.; Scott, D. S.; Czernik, S. Liquid Products from the Fast Pyrolysis of Wood and Cellulose. In *Research in Thermochemical Biomass Conversion*; A.V. Bridgwater, J.L. Kuester: New York, 1988.
- (64) Diebold, J. P. A Unified, Global Model for the Pyrolysis of Cellulose. *Biomass Bioenergy* **1994**, *7* (1-6), 75–85.
- (65) Banyasz, J. L.; Li, S.; Lyons-Hart, J.; Shafer, K. H. Gas Evolution and the Mechanism of Cellulose Pyrolysis. *Fuel* **2001**, *80* (12), 1757–1763.
- (66) Banyasz, J. L.; Li, S.; Lyons-Hart, J. L.; Shafer, K. H. Cellulose Pyrolysis: The Kinetics of Hydroxyacetaldehyde Evolution. *J. Anal. Appl. Pyrolysis* **2001**, *57* (2), 223–248.
- (67) Bradbury, A. G. W.; Sakai, Y.; Shafizadeh, F. Kinetic Model for Pyrolysis of Cellulose. *J Appl Polym Sci* **1979**, *23* (11), 3271–3280.
- (68) Mettler, M. S.; Paulsen, A. D.; Vlachos, D. G.; Dauenhauer, P. J. Pyrolytic Conversion of Cellulose to Fuels: Levoglucosan Deoxygenation via Elimination and Cyclization within Molten Biomass. *Energy Environ. Sci.* **2012**, *5* (7), 7864–7868.
- (69) Várhegyi, G.; Jakab, E.; Antal Jr., M. J. Is the Broido-Shafizadeh Model for Cellulose Pyrolysis True? *Energy Fuels* **1994**, *8* (6), 1345–1352.
- (70) Antal Jr., M. J.; Várhegyi, G.; Jakab, E. Cellulose Pyrolysis Kinetics: Revisited. *Ind. Eng. Chem. Res.* **1998**, *37* (4), 1267–1275.
- (71) Lede, J. Comparison of Contact and Radiant Ablative Pyrolysis of Biomass. *J. Anal. Appl. Pyrolysis* **2003**, *70* (2), 601–618.
- (72) Lede, J.; Li, H. Z.; Villermaux, J. Fusion-like Behavior of Biomass Pyrolysis. *Prepr. Pap. - Am. Chem. Soc. Div. Fuel Chem.* **1987**, *32* (2), 59–67.
- (73) Boutin, O.; Ferrer, M.; Lede, J. Radiant Flash Pyrolysis of Cellulose -- Evidence for the Formation of Short-Lifetime Intermediate Liquid Species. *J. Anal. Appl. Pyrolysis* **1998**, *47* (1), 13–31.

- (74) Broido, A.; Javier-Son, A. C.; Ouano, A. C.; Barrall, E. M. Molecular Weight Decrease in the Early Pyrolysis of Crystalline and Amorphous Cellulose. **1973**.
- (75) Yu, Y.; Liu, D.; Wu, H. Characterization of Water-Soluble Intermediates from Slow Pyrolysis of Cellulose at Low Temperatures. *Energy Fuels* **2012**, *26* (12), 7331–7339.
- (76) Liu, D.; Yu, Y.; Wu, H. Differences in Water-Soluble Intermediates from Slow Pyrolysis of Amorphous and Crystalline Cellulose. *Energy Fuels* **2013**, *27* (3), 1371–1380.
- (77) Wang, Z.; McDonald, A. G.; Westerhof, R. J. M.; Kersten, S. R. A.; Cuba-Torres, C. M.; Ha, S.; Pecha, B.; Garcia-Perez, M. Effect of Cellulose Crystallinity on the Formation of a Liquid Intermediate and on Product Distribution during Pyrolysis. *J. Anal. Appl. Pyrolysis* **2013**, *100*, 56–66.
- (78) Wang, Z.; Pecha, B.; Westerhof, R. J. M.; Kersten, S. R. A.; Li, C.-Z.; McDonald, A. G.; Garcia-Perez, M. Effect of Cellulose Crystallinity on Solid/Liquid Phase Reactions Responsible for the Formation of Carbonaceous Residues during Pyrolysis. *Ind. Eng. Chem. Res.* **2014**, *53* (8), 2940–2955.
- (79) Chaiwat, W.; Hasegawa, I.; Tani, T.; Sunagawa, K.; Mae, K. Analysis of Cross-Linking Behavior during Pyrolysis of Cellulose for Elucidating Reaction Pathway. *Energy Fuels* **2009**, *23* (12), 5765–5772.
- (80) Wooten, J. B.; Seeman, J. I.; Hajaligol, M. R. Observation and Characterization of Cellulose Pyrolysis Intermediates by <sup>13</sup>C CPMAS NMR. A New Mechanistic Model. *Energy Fuels* **2004**, *18* (1), 1–15.
- (81) Ranzi, E.; Cuoci, A.; Faravelli, T.; Frassoldati, A.; Migliavacca, G.; Pierucci, S.; Sommariva, S. Chemical Kinetics of Biomass Pyrolysis. *Energy Fuels* **2008**, *22* (6), 4292–4300.
- (82) Trendewicz, A.; Evans, R.; Dutta, A.; Sykes, R.; Carpenter, D.; Braun, R. Evaluating the Effect of Potassium on Cellulose Pyrolysis Reaction Kinetics. *Biomass Bioenergy* **2015**, *74*, 15–25.
- (83) Bradbury, A. G. W.; Sakai, Y.; Shafizadeh, F. Kinetics Model for Pyrolysis of Cellulose. *J Appl Polym Sci* **1979**, *23* (11), 3271–3280.
- (84) Goring, D. A. I. Thermal Softening of Lignin, Hemicellulose, and Cellulose. *Pulp Pap. Mag. Can.* **1963**, *64* (12), T517–T527.
- (85) Diebold, J. P. *Ablative Pyrolysis of Macroparticles of Biomass*; Solar Energy Res. Inst., 1980; pp 237–252.
- (86) Boutin, O.; Ferrer, M.; Lédé, J. Flash Pyrolysis of Cellulose Pellets Submitted to a Concentrated Radiation: Experiments and Modelling. *Chem. Eng. Sci.* **2002**, *57* (1), 15–25.
- (87) Luo, Z.; Wang, S.; Liao, Y.; Cen, K. Mechanism Study of Cellulose Rapid Pyrolysis. *Ind. Eng. Chem. Res.* **2004**, *43* (18), 5605–5610.
- (88) Liu, Q.; Wang, S.; Wang, K.; Guo, X.; Luo, Z.; Cen, K. Mechanism of Formation and Consequent Evolution of Active Cellulose during Cellulose Pyrolysis. *Acta Phys.-Chim. Sin.* **2008**, *24* (11), 1957–1963.
- (89) Schroeter, J.; Felix, F. Melting Cellulose. *Cellulose* **2005**, *12* (2), 159–165.
- (90) Liu, D.; Yu, Y.; Hayashi, J.; Moghtaderi, B.; Wu, H. Contribution of Dehydration and Depolymerization Reactions during the Fast Pyrolysis of Various Salt-Loaded Celluloses at Low Temperatures. *Fuel* **2014**, *136*, 62–68.
- (91) Julien, S.; Chornet, E.; Tiwari, P. K.; Overend, R. P. Vacuum Pyrolysis of Cellulose: Fourier Transform Infrared Characterization of Solid Residues, Product Distribution and Correlations. *J. Anal. Appl. Pyrolysis* **1991**, *19* (0), 81–104.
- (92) Scheirs, J.; Camino, G.; Tumiatti, W. Overview of Water Evolution during the Thermal Degradation of Cellulose. *Eur. Polym. J.* **2001**, *37* (5), 933–942.
- (93) Antal, J. Biomass Pyrolysis: A Review of the Literature Part 1—Carbohydrate Pyrolysis. In *Advances in Solar Energy*; Böer, K. W., Duffie, J. A., Eds.; Springer New York, 1983; pp 61–111.
- (94) Patwardhan, P. R.; Dalluge, D. L.; Shanks, B. H.; Brown, R. C. Distinguishing Primary and Secondary Reactions of Cellulose Pyrolysis. *Bioresour. Technol.* **2011**, *102* (8), 5265–5269.
- (95) Mamliev, V.; Bourbigot, S.; Le Bras, M.; Yvon, J. The Facts and Hypotheses Relating to the Phenomenological Model of Cellulose Pyrolysis: Interdependence of the Steps. *J. Anal. Appl. Pyrolysis* **2009**, *84* (1), 1–17.
- (96) Shen, D. K.; Gu, S. The Mechanism for Thermal Decomposition of Cellulose and Its Main Products. *Bioresour. Technol.* **2009**, *100* (24), 6496–6504.

- (97) Mettler, M. S.; Mushrif, S. H.; Paulsen, A. D.; Javadekar, A. D.; Vlachos, D. G.; Dauenhauer, P. J. Revealing Pyrolysis Chemistry for Biofuels Production: Conversion of Cellulose to Furans and Small Oxygenates. *Energy Env. Sci* **2011**, *5* (1), 5414–5424.
- (98) Essig, M. ; Richards, G. N. Mechanisms of Formation of the Major Volatile Products from the Pyrolysis Cellulose. In *Chemistry and Wood chemistry technology*; Wiley and Sons New York, 1989; pp 841–862.
- (99) Pastorova, I.; Botto, R.; Arisz, P.; Boon, J. Cellulose Char Structure - a Combined Analytical Py-Gc- Ms, Ftir, and Nmr-Study. *Carbohydr. Res.* **1994**, *262* (1), 27–47.
- (100) Zhang, X.; Golding, J.; Burgar, I. Thermal Decomposition Chemistry of Starch Studied by <sup>13</sup>C High-Resolution Solid-State NMR Spectroscopy. *Polymer* **2002**, *43* (22), 5791–5796.
- (101) Piskorz, J.; Radlein, D. S. A. G.; Scott, D. S.; Czernik, S. Pretreatment of Wood and Cellulose for Production of Sugars by Fast Pyrolysis. *J. Anal. Appl. Pyrolysis* **1989**, *16* (2), 127–142.
- (102) Aubert, M. Effet Catalytique de Certains Inorganiques Sur La Sélectivité Des Réactions de Pyrolyse Rapide de Biomasses et de Leurs Constituants, Institut National Polytechnique de Lorraine: Nancy, 2009.
- (103) Hodgson, E. M.; Nowakowski, D. J.; Shield, I.; Riche, A.; Bridgwater, A. V.; Clifton-Brown, J. C.; Donnison, I. S. Variation in Miscanthus Chemical Composition and Implications for Conversion by Pyrolysis and Thermo-Chemical Bio-Refining for Fuels and Chemicals. *Bioresour. Technol.* **2011**, *102* (3), 3411–3418.
- (104) Hosoya, T.; Kawamoto, H.; Saka, S. Cellulose–hemicellulose and Cellulose–lignin Interactions in Wood Pyrolysis at Gasification Temperature. *J. Anal. Appl. Pyrolysis* **2007**, *80* (1), 118–125.
- (105) Dufour, A.; Weng, J.; Jia, L.; Tang, X.; Sirjean, B.; Fournet, R.; Le Gall, H.; Brosse, N.; Billaud, F.; Mauviel, G.; Qi, F. Revealing the Chemistry of Biomass Pyrolysis by Means of Tunable Synchrotron Photoionisation-Mass Spectrometry. *Rsc Adv.* **2013**, *3* (14), 4786–4792.
- (106) Shafizadeh, F.; Stevenson, T.; Cochran, T.; Furneaux, R. 1,5-Anhydro-4-Deoxy-D-Glycero-Hex-1-En-3-Ulose and Other Pyrolysis Products of Cellulose. *Carbohydr. Res.* **1978**, *67* (2), 433–447.
- (107) Werner, K.; Pommer, L.; Broström, M. Thermal Decomposition of Hemicelluloses. *J. Anal. Appl. Pyrolysis* **2014**, 130–137.
- (108) Shen, D. K.; Gu, S.; Bridgwater, A. V. Study on the Pyrolytic Behaviour of Xylan-Based Hemicellulose Using TG–FTIR and Py–GC–FTIR. *J. Anal. Appl. Pyrolysis* **2010**, *87* (2), 199–206.
- (109) Worasuwannarak, N.; Sonobe, T.; Tanthapanichakoon, W. Pyrolysis Behaviors of Rice Straw, Rice Husk, and Corncob by TG-MS Technique. *J. Anal. Appl. Pyrolysis* **2007**, *78* (2), 265–271.
- (110) Collard, F.-X.; Blin, J. A Review on Pyrolysis of Biomass Constituents: Mechanisms and Composition of the Products Obtained from the Conversion of Cellulose, Hemicelluloses and Lignin. *Renew. Sustain. Energy Rev.* **2014**, *38*, 594–608.
- (111) Peng, Y.; Wu, S. The Structural and Thermal Characteristics of Wheat Straw Hemicellulose. *J. Anal. Appl. Pyrolysis* **2010**, *88* (2), 134–139.
- (112) Hosoya, T.; Kawamoto, H.; Saka, S. Pyrolysis Behaviors of Wood and Its Constituent Polymers at Gasification Temperature. *J. Anal. Appl. Pyrolysis* **2007**, *78* (2), 328–336.
- (113) Jensen, A.; Dam-Johansen, K.; Wójtowicz, M. A.; Serio, M. A. TG-FTIR Study of the Influence of Potassium Chloride on Wheat Straw Pyrolysis. *Energy Fuels* **1998**, *12* (5), 929–938.
- (114) Ponder, G. R.; Richards, G. N. Thermal Synthesis and Pyrolysis of a Xylan. *Carbohydr. Res.* **1991**, *218*, 143–155.
- (115) Pouwels, A. D.; Tom, A.; Eijkel, G. B.; Boon, J. J. Characterisation of Beech Wood and Its Holocellulose and Xylan Fractions by Pyrolysis-Gas Chromatography-Mass Spectrometry. *J. Anal. Appl. Pyrolysis* **1987**, *11*, 417–436.
- (116) Ponder, G. R.; Richards, G. N. A Review of Some Recent Studies on Mechanisms of Pyrolysis of Polysaccharides. *Biomass Bioenergy* **1994**, *7* (1-6), 1–24.
- (117) Ponder, G. R.; Richards, G. N.; Stevenson, T. T. Influence of Linkage Position and Orientation in Pyrolysis of Polysaccharides: A Study of Several Glucans. *J. Anal. Appl. Pyrolysis* **1992**, *22* (3), 217–229.
- (118) Ohnishi, A.; Katō, K.; Takagi, E. Pyrolytic Formation of 3-Hydroxy-2-Penteno-1,5-Lactone from Xylan, Xylo-Oligosaccharides, and Methyl Xylopyranosides. *Carbohydr. Res.* **1977**, *58* (2), 387–395.

- (119) Yang, H.; Yan, R.; Chen, H.; Lee, D. H.; Zheng, C. Characteristics of Hemicellulose, Cellulose and Lignin Pyrolysis. *Fuel* **2007**, *86* (12–13), 1781–1788.
- (120) Jakab, E.; Faix, O.; Till, F.; Székely, T. Thermogravimetry/mass Spectrometry Study of Six Lignins within the Scope of an International Round Robin Test. *J. Anal. Appl. Pyrolysis* **1995**, *35* (2), 167–179.
- (121) Wang, S.; Ru, B.; Lin, H.; Sun, W.; Luo, Z. Pyrolysis Behaviors of Four Lignin Polymers Isolated from the Same Pine Wood. *Bioresour. Technol.* **2015**, *182*, 120–127.
- (122) Kawamoto, H.; Horigoshi, S.; Saka, S. Pyrolysis Reactions of Various Lignin Model Dimers. *J. Wood Sci.* **2007**, *53* (2), 168–174.
- (123) Liu, Q.; Wang, S.; Zheng, Y.; Luo, Z.; Cen, K. Mechanism Study of Wood Lignin Pyrolysis by Using TG–FTIR Analysis. *J. Anal. Appl. Pyrolysis* **2008**, *82* (1), 170–177.
- (124) Nakamura, T.; Kawamoto, H.; Saka, S. Pyrolysis Behavior of Japanese Cedar Wood Lignin Studied with Various Model Dimers. *J. Anal. Appl. Pyrolysis* **2008**, *81* (2), 173–182.
- (125) Brosse, N.; El Hage, R.; Chaouch, M.; Pétrissans, M.; Dumarçay, S.; Gérardin, P. Investigation of the Chemical Modifications of Beech Wood Lignin during Heat Treatment. *Polym. Degrad. Stab.* **2010**, *95* (9), 1721–1726.
- (126) Sharma, R. K.; Wooten, J. B.; Baliga, V. L.; Lin, X. H.; Chan, W. G.; Hajaligol, M. R. Characterization of Chars from Pyrolysis of Lignin. *Fuel* **2004**, *83* (11–12), 1469–1482.
- (127) Brebu, M.; Tamminen, T.; Spiridon, I. Thermal Degradation of Various Lignins by TG-MS/FTIR and Py-GC-MS. *J. Anal. Appl. Pyrolysis*.
- (128) Müller-Hagedorn, M.; Bockhorn, H.; Krebs, L.; Müller, U. A Comparative Kinetic Study on the Pyrolysis of Three Different Wood Species. *J. Anal. Appl. Pyrolysis* **2003**, *68–69*, 231–249.
- (129) Kim, U.-J.; Eom, S. H.; Wada, M. Thermal Decomposition of Native Cellulose: Influence on Crystallite Size. *Polym. Degrad. Stab.* **2010**, *95* (5), 778–781.
- (130) Liu, Q.; Wang, S.; Luo, Z.; Cen, K. Catalysis Mechanism Study of Potassium Salts on Cellulose Pyrolysis by Using TGA-FTIR Analysis. *J. Chem. Eng. Jpn.* **2008**, *41* (12), 1133–1142.
- (131) Nowakowski, D. J.; Jones, J. M. Uncatalysed and Potassium-Catalysed Pyrolysis of the Cell-Wall Constituents of Biomass and Their Model Compounds. *J. Anal. Appl. Pyrolysis* **2008**, *83* (1), 12–25.
- (132) Wang, S.; Ru, B.; Lin, H.; Sun, W. Pyrolysis Behaviors of Four O-Acetyl-Preserved Hemicelluloses Isolated from Hardwoods and Softwoods. *Fuel* **2015**, *150*, 243–251.
- (133) Zhou, S.; Pecha, B.; van Kuppevelt, M.; McDonald, A. G.; Garcia-Perez, M. Slow and Fast Pyrolysis of Douglas-Fir Lignin: Importance of Liquid-Intermediate Formation on the Distribution of Products. *Biomass Bioenergy* **2014**, *66*, 398–409.
- (134) Shen, D.; Xiao, R.; Gu, S.; Luo, K. The Pyrolytic Behavior of Cellulose in Lignocellulosic Biomass: A Review. *Rsc Adv.* **2011**, *1* (9), 1641–1660.
- (135) Couhert, C.; Commandre, J.-M.; Salvador, S. Is It Possible to Predict Gas Yields of Any Biomass after Rapid Pyrolysis at High Temperature from Its Composition in Cellulose, Hemicellulose and Lignin. *Fuel* **2009**, *88* (3), 408–417.
- (136) Wang, S.; Guo, X.; Wang, K.; Luo, Z. Influence of the Interaction of Components on the Pyrolysis Behavior of Biomass. *J. Anal. Appl. Pyrolysis* **2011**, *91* (1), 183–189.
- (137) Sun, R.; Lawther, J. M.; Banks, W. B. A Tentative Chemical Structure of Wheat Straw Lignin. *Ind. Crops Prod.* **1997**, *6* (1), 1–8.
- (138) Fushimi, C.; Katayama, S.; Tsutsumi, A. Elucidation of Interaction among Cellulose, Lignin and Xylan during Tar and Gas Evolution in Steam Gasification. *J. Anal. Appl. Pyrolysis* **2009**, *86* (1), 82–89.
- (139) Ranzi, E.; Cuoci, A.; Faravelli, T.; Frassoldati, A.; Migliavacca, G.; Pierucci, S.; Sommariva, S. Chemical Kinetics of Biomass Pyrolysis. *Energy Fuels* **2008**, *22* (6), 4292–4300.
- (140) Kohler, S. Pyrolyse Rapide de Biomasses et de Leurs Constituants, INPL: LSGC-Nancy, 2009.
- (141) Ranzi, E.; Corbetta, M.; Manenti, F.; Pierucci, S. Kinetic Modeling of the Thermal Degradation and Combustion of Biomass. *Chem. Eng. Sci.* **2014**, *110*, 2–12.
- (142) Patwardhan, P. R.; Satrio, J. A.; Brown, R. C.; Shanks, B. H. Influence of Inorganic Salts on the Primary Pyrolysis Products of Cellulose. *Bioresour. Technol.* **2010**, *101* (12), 4646–4655.

- (143) Szabó, P.; Várhegyi, G.; Till, F.; Faix, O. Thermogravimetric/mass Spectrometric Characterization of Two Energy Crops, *Arundo Donax* and *Miscanthus Sinensis*. *J. Anal. Appl. Pyrolysis* **1996**, *36* (2), 179–190.
- (144) Nik-Azar, M.; Hajaligol, M. R.; Sohrabi, M.; Dabir, B. Mineral Matter Effects in Rapid Pyrolysis of Beech Wood. *Fuel Process. Technol.* **1997**, *51* (1–2), 7–17.
- (145) Jiang, L.; Hu, S.; Sun, L.-S.; Su, S.; Xu, K.; He, L.-M.; Xiang, J. Influence of Different Demineralization Treatments on Physicochemical Structure and Thermal Degradation of Biomass. *Bioresour. Technol.* **2013**, *146*, 254–260.
- (146) Michel, R.; Kaknics, J.; Bouchetou, M. L.; Gratuze, B.; Balland, M.; Hubert, J.; Poirier, J. Physicochemical Changes in *Miscanthus* Ash on Agglomeration with Fluidized Bed Material. *Chem. Eng. J.* **2012**, *207–208*, 497–503.
- (147) Kleen, M.; Gellerstedt, G. Influence of Inorganic Species on the Formation of Polysaccharide and Lignin Degradation Products in the Analytical Pyrolysis of Pulps. *J. Anal. Appl. Pyrolysis* **1995**, *35* (1), 15–41.
- (148) Jakab, E.; Faix, O.; Till, F.; Székely, T. The Effect of Cations on the Thermal Decomposition of Lignins. *J. Anal. Appl. Pyrolysis* **1993**, *25*, 185–194.
- (149) Bahng, M.-K.; Mukarakate, C.; Robichaud, D. J.; Nimlos, M. R. Current Technologies for Analysis of Biomass Thermochemical Processing: A Review. *Anal. Chim. Acta* **2009**, *651* (2), 117–138.
- (150) Brosse, N.; Dufour, A.; Meng, X.; Sun, Q.; Ragauskas, A. *Miscanthus*: A Fast-Growing Crop for Biofuels and Chemicals Production. *Biofuels Bioprod. Biorefining-Biofpr* **2012**, *6* (5), 580–598.

### **III. Etude des mécanismes de formation du biochar par RMN haute résolution**



### **III.1 Article 1: High resolution solid state 2D NMR analysis of biomass and biochar**

Yann Le Brech<sup>1</sup>, Luc Delmotte<sup>2,†</sup>, Jesus Raya<sup>3,‡</sup>, Nicolas Brosse<sup>4</sup>, Roger Gadiou<sup>2</sup>, Anthony Dufour<sup>1\*</sup>

<sup>1</sup> LRGP, CNRS, Université de Lorraine, 1 rue Grandville 54000 Nancy, France

<sup>2</sup> IS2M, CNRS, Université de Haute Alsace, 15, rue Jean Starcky BP 2488 68057 Mulhouse cedex, France

<sup>3</sup> ICS, CNRS, Université de Strasbourg, 1 rue Blaise Pascal BP 296 R8 67008 Strasbourg Cedex, France

<sup>4</sup> LERMAB, Université de Lorraine, BP239 54506 Vandoeuvre les Nancy cedex, France.

**Article paru dans *Analytical Chemistry*, 2015, 87 (2), pp 843–847.**

#### **III.1.1 Abstract**

Solid state NMR methods are required to analyse biomass as a function of its chemical or biological treatment for biofuels, chemicals or biochar production. The native polymers network in lignocellulosic biomass and other solid materials, such as coal, coke or biochar, can hardly be analyzed by liquid state NMR due to their poor swelling ability without chemical modification. A <sup>1</sup>H-<sup>13</sup>C two dimensional heteronuclear correlation (HETCOR) experiment with frequency-switched Lee-Goldburg (FSLG) irradiation is performed on a high field spectrometer (750MHz). This method leads to previously unattained resolution for biomass and biochar and offers a unique ability to reveal their chemical composition. The formation of aromatic moieties from carbohydrates and lignin thermal conversion is clearly distinguished. This method can be applied to all other carbonaceous materials.

#### **III.1.2 Main text**

The worldwide growing demand of energy and the necessity to reduce greenhouse gas emissions lead to the increasing valorization of lignocellulosic biomass. Bioethanol from cellulosic feedstock and the thermochemical conversion of biomass are promising solutions to produce energy and green chemicals<sup>1,2</sup>. Lignin, cellulose and hemicelluloses form a complex network in the cell walls of biomass. There is a strong need for advanced analysis of the chemical functions involved in this network to better understand the composition of native biomass, as a function of growing conditions or genetic engineering<sup>3</sup>, and the conversion mechanism of these materials, as a function of the thermochemical, biochemical or chemical pre-treatment. NMR methods are non-destructive and have been used in many investigations for the analysis of coal, biomass polymers or char.<sup>4–23</sup> Some NMR characterizations were made by using isolated fractions of the plant cell wall polymers which requires tedious separation and isolation techniques of cellulose, lignin and hemicelluloses. This approach is not only time-consuming but also is likely to alter the native structure of the polymers. Recently, the solution state NMR spectroscopy of whole plant cell was reported by employing ionic liquids<sup>24,25</sup>, acetylated cell wall or swelled cell wall in a solvent to produce gel<sup>26,27</sup>. These methods require long preparation time and can alter the chemical structure of native polymers as well (e.g. lignin in ionic liquids). In addition, they are not adapted to study the chemical structure of cross-linked materials such as chars which

cannot be swelled by a solvent without chemical modification. Solid state NMR is a promising method for the analysis of chemical structures of insoluble materials. Nevertheless, 1D solid-state NMR applied to whole plant material or to char is often limited by poor resolution and overlapping caused by the complex structure of the biomass. Advanced two-dimensional solid-state NMR methods have been previously used on biomass in extensive works<sup>17,28–30</sup> but at relative low field. The aim of the present work is to develop high resolution solid state 2D NMR methods which could be applied on biomass and biochar for revealing the mechanism of biomass thermal conversion. Here we show the outstanding benefit of using a high field (17.6 tesla) 2D <sup>1</sup>H-<sup>13</sup>C heteronuclear correlation (HETCOR) experiments with frequency-switched Lee-Goldburg (FSLG) irradiation during the evolution time<sup>31</sup> for the analysis of biomass and biochar. The dramatic increase of resolution in the proton dimension obtained by FSLG homonuclear decoupling together with a high field makes this technique a unique choice for proton-carbon analysis in the solid state. De Groot and coworkers demonstrated the interest of this kind of approach on fully labelled <sup>13</sup>C bacteriochlorophyll<sup>32</sup>. We show here that the FSLG <sup>1</sup>H-<sup>13</sup>C HETCOR technique can be successfully applied without <sup>13</sup>C labelling, leading to previously unattained resolution for biomass and biochar samples. In order to sort out even most of the unprotonated carbons we found that a Cross-Polarization (CP) contact-time of 4ms was optimal. In those conditions even the weakly proton dipolar coupled rare spins like carbonyls give rise to rather well detectable cross-peaks despite their expected reduction by the « dipolar truncation » phenomenon<sup>33</sup> due to the stronger dipolar interactions like CH involving the same protons. The different kinds of sugar and lignin carbons analyzed by this method are named in a standard way (Figure III-1). The whole cell wall of miscanthus straw was analyzed in situ by solid state FSLG <sup>1</sup>H-<sup>13</sup>C HETCOR (Figure III-2). The NMR procedure and chemical characterizations of biomass are presented in supplementary materials<sup>34–36</sup>. The spectrum was compared with those obtained from raw miscanthus and isolated lignin through 1D, HSQC, HMQC and HMBC spectras<sup>12,15,25,37,38</sup> (see supplementary material). The HETCOR NMR spectrum of untreated miscanthus exhibits characteristic cross peaks for cellulose, hemicelluloses and lignin. The clusters of cross peaks at  $\delta C/\delta H$  64.4/3.6; 74.9-72.3/3.6; 83.6/3.6; 87.9/3.6; 104.8/3.6 are assigned to C<sub>6</sub> (CH<sub>2</sub>OH in glucose unit), C<sub>2,3,5</sub>, C<sub>4</sub> disordered structure, C<sub>4</sub> ordered structure, and C<sub>1</sub> carbons of polysaccharides respectively. These carbons seem to correlate with their own protons<sup>29</sup>. But in this range of <sup>13</sup>C chemical shift (105-64 ppm) there is also <sup>13</sup>C signal from aliphatic lignin<sup>39</sup>. Correlation between these carbons with O-alkyl protons and aromatic protons is shown in the area of  $\delta C/\delta H$  50.0-110/3-7 ppm. Concerning lignin, correlations are observed at  $\delta C/\delta H$  56.2/3.6 and 56.2/6.35-7 ppm corresponding respectively to O-alkyl protons from CH<sub>3</sub>O and aromatic protons from lignin aromatic rings. According to the <sup>13</sup>C chemical shift 74 ppm and 104 ppm, correlation with aromatic protons (6-7 ppm) could be due to interaction between carbohydrate carbons and lignin aromatic protons<sup>40</sup> or into lignin structure. Indeed solid state HETCOR measurement allows correlations between carbon and proton through the space. These correlations indicate that carbohydrates are closely associated with lignin in biomass structures.

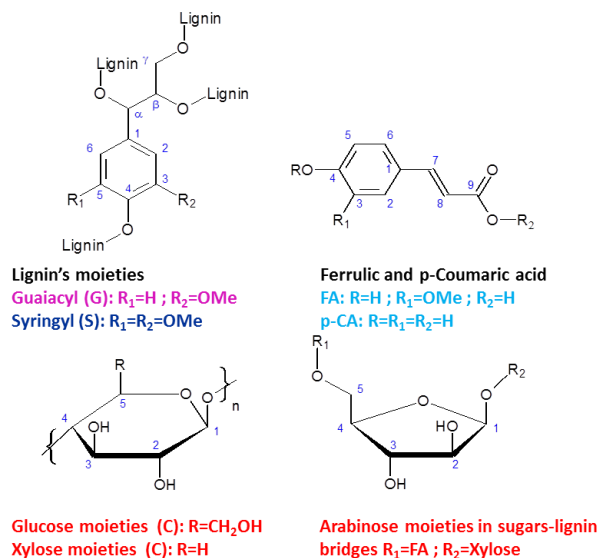


Figure III-1: Schematic representation of the main moieties of miscanthus giganteus2 and notations for carbon atoms

Cross signals corresponding to aromatic protons ( $C_{Ar}-H$ ) at  $\delta C/\delta H$  110-122/6.3-6.9 ppm were observed in this region of the FSLG  $^1H-^{13}C$  HETCOR spectrum. These signals corresponding to correlations between  $G_2$ ,  $G_5$  and  $G_6$  to their own protons, there were observed at  $\delta C/\delta H$  110-112/6.7-7.5 ppm, 113-115/6.5-7.5 ppm and 118-120/6.3-7.0 ppm respectively. Cross signal observed at 111.5/3.6 could be attributed to a correlation between  $G_2$  and methoxyl protons. Para-coumarate group was also detected at  $\delta C/\delta H$  116.9/6.9 ppm ( $p-CA_3$  and  $p-CA_5$ ). Signals for correlations of  $S_1$  and  $G_1$  units (aromatic carbons) with aliphatic CH-O protons were detected at  $\delta C/\delta H$  132-136/3.0-4.0 ppm. Cross signals of aromatic C-O carbons with aliphatic CH-O protons corresponding to  $S_4$ ,  $G_{3,4}$  and  $S_{3,5}$  etherified were observed at  $\delta C/\delta H$  138.0-140.0/3.2-4.0 ppm, 146.0-149.5/3.1-4.0 ppm and 150.0-154.0/3.2-4.0 ppm respectively. Long-range correlations between aromatic C-O carbons with aromatic protons were also observed at  $\delta C/\delta H$  145-147/6.8-7.2 ppm ( $G_4$ ),  $\delta C/\delta H$  147-149/7.0-7.5 ppm ( $G_3$ ). The region at  $\delta C/\delta H$  168-174/1.5-7.0 ppm (Figure III-2 1b) also gives valuable information concerning the carbonyl groups and their environment. The acetate group is unambiguously identified through the correlation signal at  $\delta C/\delta H$  172-173/1.9-2.1 ppm ( $CH_3-CO$ ). The chemical shifts of the cross signals 167-168/3.6-4.0 ppm could be consistent with those of carbonyl group with ferulate (Figure III-2) involved in lignin – hemicelluloses cross-linking<sup>41</sup>.

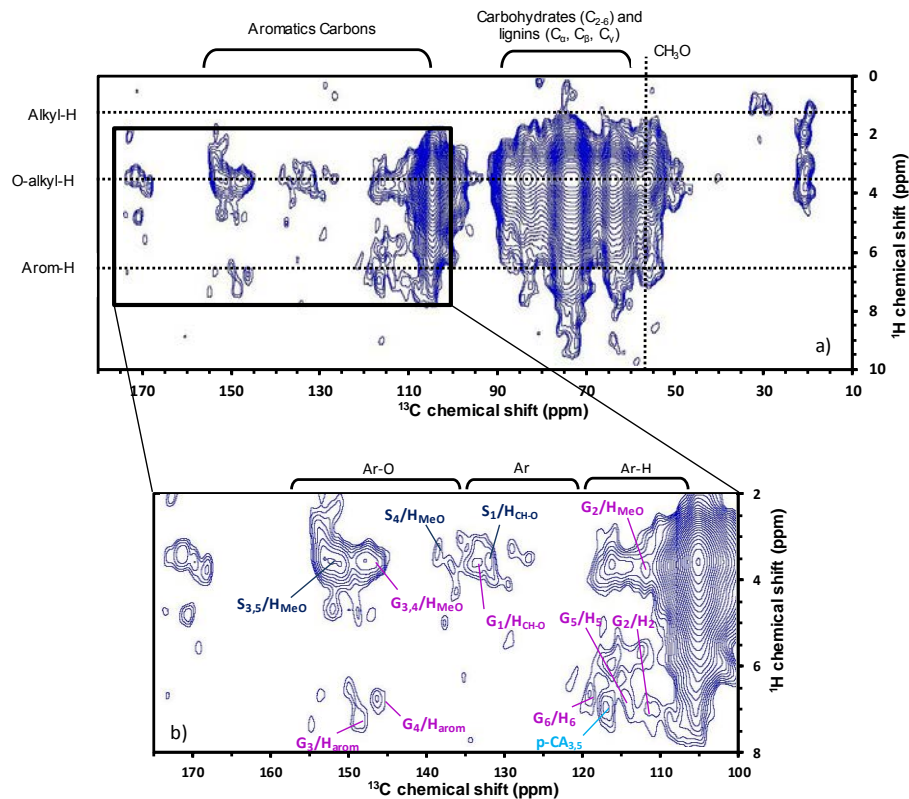


Figure III-2: a)  $^1\text{H}$ - $^{13}\text{C}$  2D HETCOR spectra of miscanthus, b) zoom on 175-100ppm zone

To illustrate the capability of this analytical method to unravel biomass conversion as a function of process conditions, the spectra of native miscanthus and char produced at 300°C are compared on Figure III-3. In supplementary material, 1D  $^{13}\text{C}$  CPMAS NMR spectra of different pyrolysis temperatures are presented and the choice of 300°C for the 2D NMR investigation is justified.

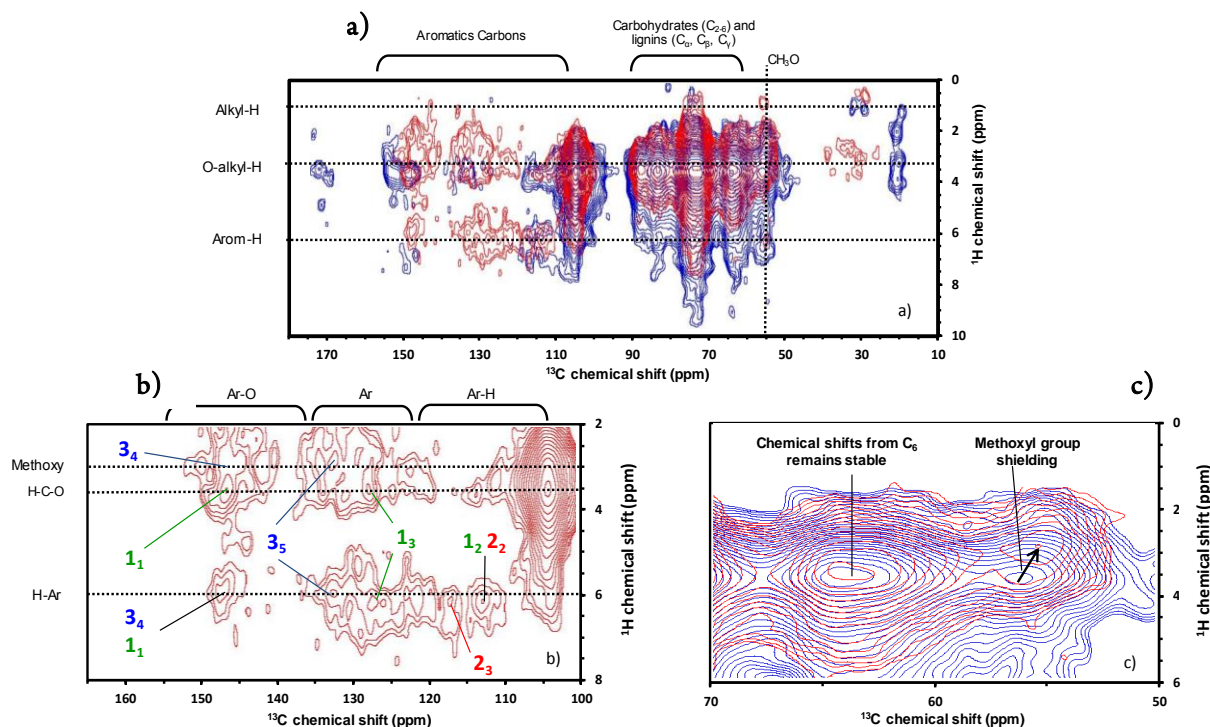


Figure III-3:  $^1\text{H}$ - $^{13}\text{C}$  2D HETCOR spectra a) comparison between native miscanthus and biochar produced at  $300^\circ\text{C}$ , b) zoom on 165-100 ppm  $\delta^{13}\text{C}$  zone of biochar, c) zoom on 70-50 ppm  $\delta^{13}\text{C}$  comparison between native miscanthus and biochar highlighting the shielding of methoxyl group in lignin-based aromatic clusters

Upon heating, the network of polymers in miscanthus undergoes competitive bond breaking and cross-linking reactions to form mobile species, volatiles and char.<sup>42</sup> The cross-linked network produced in char requires the use of solid-state NMR to understand the chemical mechanisms involved in thermal conversion. The high resolution of our NMR method enables to reveal some typical chemical moieties in the char (Figure III-4), in agreement with previous works<sup>43,44</sup>. The conversion of carbonyl functions is observed in the region of 165-173 ppm, indicating the cleavage between ferulic acid (in lignin) and arabinose (Figure III-3) in the network. The shoulder at around 100 ppm on the  $\text{C}_1$  sugars strongly decreases pointing out the degradation of carbohydrates in agreement with previous works<sup>17,45</sup>. Concerning the aromatic carbons, signals from  $\text{S}_3$  and  $\text{S}_5$  are no more present at  $300^\circ\text{C}$ . It can be explained by the cleavage of  $\beta\text{-O-4}$  functions or by demethoxylation of  $\text{S}_5$  carbons. The methoxyl groups undergo a shielding due to the formation of aromatic clusters in the char (Figure III-3c)<sup>11</sup>. Hence the  $\delta^1\text{H}$  chemical shift from methoxyl groups (2.7-3ppm) can be distinguished from other  $\delta^1\text{H}$  from carbohydrates (3.2-3.6ppm) (Figure III-3b). This finding is of tremendous importance to understand the chemistry of lignin and carbohydrates pyrolysis in the network and is enabled by our high magnetic field combined with the FSLG method. The formation of aromatic moieties from carbohydrates and lignin conversion is thus clearly distinguished. The peak at 146-147ppm could be furanic moieties cross-linked from the conversion of carbohydrates<sup>43</sup>. The furanic carbons correlate with aromatic (146-147/5.6-5.9 ppm) and aliphatic protons (146-147/3.3-3.7 ppm) (Figure III-4, structure 1, carbon 1). This 1<sub>1</sub> carbon signal is overlapped by the 3<sub>4</sub>  $^{13}\text{C}$  signal which correlates with aromatic  $^1\text{H}$  from aromatic clusters and  $^1\text{H}$  from methoxyl functions (146-147/6.0 ppm and 3.0 ppm).

The important peak at 132/6.0 ppm related to aromatic clusters<sup>43,46</sup> could be assigned to the aromatic carbons (3<sub>5</sub>) formed from lignin<sup>44</sup> or from carbohydrates<sup>45</sup>. Correlations at 132-133/2.7-3 ppm highlight the methoxyl groups remaining in the char from lignin. Carbon peaks at 127.5-128.5 ppm could be assigned to aromatics

carbons from carbohydrates<sup>47</sup> (structure 1) because these carbons seem to be correlated with aliphatic protons (3.2-3.6 ppm) from sugars and aromatics protons (6.1-6.4 ppm).

The signal at 117.5-118/6-6.5 ppm (Figure III-3b) can be assigned to 2<sub>3</sub> carbons (correlation with aromatic <sup>1</sup>H from furanic moieties). It can be observed that this signal is not correlated with any aliphatic or methoxyl proton, demonstrating the absence of aliphatic moieties in the structure 2. The signal at 113-114/6-6.3 ppm could be assigned to 1<sub>2</sub> and 2<sub>2</sub> with a direct correlation with aromatic <sup>1</sup>H.

All these structures evidenced in this work reveal the different mechanisms of aromatization during carbohydrates and lignin pyrolysis in the network of biomass cell walls.

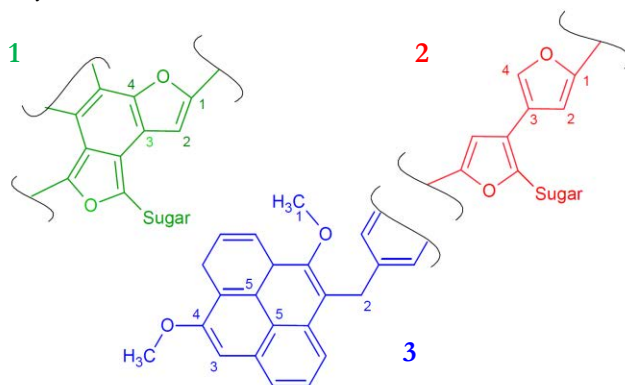


Figure III-4: Representation of some chemical moieties in char

This 2D NMR method is powerful to analyse solid materials hardly soluble or with labile moieties without any sample preparation, thanks to the high magnetic field and the FSLG method. It can be combined with quantitative 1D NMR for solid analysis<sup>18</sup> and high resolution mass spectrometry for liquid products analysis<sup>48</sup> to achieve a complete outlook of products from the chemical or biological conversion of any kind of carbonaceous materials.

### III.1.3 References

- (1) Ragauskas, A. J.; Williams, C. K.; Davison, B. H.; Britovsek, G.; Cairney, J.; Eckert, C. A.; Frederick, W. J.; Hallett, J. P.; Leak, D. J.; Liotta, C. L.; Mielenz, J. R.; Murphy, R.; Templer, R.; Tschaplinski, T. The Path Forward for Biofuels and Biomaterials. *Science* **2006**, *311* (5760), 484–489.
- (2) Brosse, N.; Dufour, A.; Meng, X.; Sun, Q.; Ragauskas, A. Miscanthus: A Fast-Growing Crop for Biofuels and Chemicals Production. *Biofuels Bioprod. Biorefining* **2012**, *6* (5), 580–598.
- (3) Vanholme, R.; Morreel, K.; Darrah, C.; Oyarce, P.; Grabber, J. H.; Ralph, J.; Boerjan, W. Metabolic Engineering of Novel Lignin in Biomass Crops. *New Phytol.* **2012**, *196* (4), 978–1000.
- (4) Haw, J. F.; Maciel, G. E.; Schroeder, H. A. Carbon-13 Nuclear Magnetic Resonance Spectrometric Study of Wood and Wood Pulping with Cross Polarization and Magic-Angle Spinning. *Anal. Chem.* **1984**, *56* (8), 1323–1329.
- (5) Tekely, P.; Nicole, D.; Delpuech, J. -j.; Totino, E.; Muller, J. F. Chemical Structure Changes in Coals after Low-Temperature Oxidation and Demineralization by Acid Treatment as Revealed by High Resolution Solid State <sup>13</sup>C NMR. *Fuel Process. Technol.* **1987**, *15* (C), 225–231.
- (6) Hatcher, P. G. *Energy Fuels* **1988**, *2* (1), 48–58.
- (7) Brosse, N.; El Hage, R.; Chaouch, M.; Pétrissans, M.; Dumarçay, S.; Gérardin, P. Investigation of the Chemical Modifications of Beech Wood Lignin during Heat Treatment. *Polym. Degrad. Stab.* **2010**, *95* (9), 1721–1726.
- (8) Love, G. D.; Law, R. V.; Snape, C. E. Determination of Nonprotonated Aromatic Carbon Concentrations in Coals by Single Pulse Excitation <sup>13</sup>C NMR. *Energy Fuels* **1993**, *7* (5), 639–644.
- (9) Atalla, R. H.; VanderHart, D. L. The Role of Solid State <sup>13</sup>C NMR Spectroscopy in Studies of the Nature of Native Celluloses. *Solid State Nucl. Magn. Reson.* **1999**, *15* (1), 1–19.
- (10) Sivonen, H.; Maunu, S. L.; Sundholm, F.; Jämsä, S.; Viitaniemi, P. Magnetic Resonance Studies of Thermally Modified Wood. *Holzforschung* **2002**, *56* (6), 648–654.
- (11) Bardet, M.; Hediger, S.; Gerbaud, G.; Gambarelli, S.; Jacquot, J. F.; Foray, M. F.; Gabelle, A. Investigation with <sup>13</sup>C NMR, EPR and Magnetic Susceptibility Measurements of Char Residues Obtained by Pyrolysis of Biomass. *Fuel* **2007**, *86* (12-13), 1966–1976.
- (12) Villaverde, J. J.; Li, J.; Ek, M.; Ligeró, P.; De Vega, A. Native Lignin Structure of Miscanthus X Giganteus and Its Changes during Acetic and Formic Acid Fractionation. *J. Agric. Food Chem.* **2009**, *57* (14), 6262–6270.
- (13) Salmon, E.; Behar, F.; Lorant, F.; Hatcher, P. G.; Marquaire, P.-M. Early Maturation Processes in Coal. Part 1: Pyrolysis Mass Balance and Structural Evolution of Coalified Wood from the Morwell Brown Coal Seam. *Org. Geochem.* **2009**, *40* (4), 500–509.
- (14) Mao, J.-D.; Schimmelmänn, A.; Mastalerz, M.; Hatcher, P. G.; Li, Y. Structural Features of a Bituminous Coal and Their Changes during Low-Temperature Oxidation and Loss of Volatiles Investigated by Advanced Solid-State NMR Spectroscopy. *Energy Fuels* **2010**, *24* (4), 2536–2544.
- (15) Del Río, J. C.; Rencoret, J.; Prinsen, P.; Martínez, A. T.; Ralph, J.; Gutiérrez, A. Structural Characterization of Wheat Straw Lignin as Revealed by Analytical Pyrolysis, 2D-NMR, and Reductive Cleavage Methods. *J. Agric. Food Chem.* **2012**, *60* (23), 5922–5935.
- (16) Mao, J.-D.; Johnson, R. L.; Lehmann, J.; Olk, D. C.; Neves, E. G.; Thompson, M. L.; Schmidt-Rohr, K. Abundant and Stable Char Residues in Soils: Implications for Soil Fertility and Carbon Sequestration. *Environ. Sci. Technol.* **2012**, *46* (17), 9571–9576.
- (17) Melkior, T.; Jacob, S.; Gerbaud, G.; Hediger, S.; Le Pape, L.; Bonnefois, L.; Bardet, M. NMR Analysis of the Transformation of Wood Constituents by Torrefaction. *Fuel* **2012**, *92* (1), 271–280.
- (18) Cao, X.; Pignatello, J. J.; Li, Y.; Lattao, C.; Chappell, M. A.; Chen, N.; Miller, L. F.; Mao, J. Characterization of Wood Chars Produced at Different Temperatures Using Advanced Solid-State <sup>13</sup>C NMR Spectroscopic Techniques. *Energy Fuels* **2012**, *26* (9), 5983–5991.
- (19) Foston, M. Advances in Solid-State NMR of Cellulose. *Curr. Opin. Biotechnol.* **2014**, *27*, 176–184.
- (20) Brewer, C. E.; Schmidt-Rohr, K.; Satrio, J. A.; Brown, R. C. Characterization of Biochar from Fast Pyrolysis and Gasification Systems. *Environ. Prog. Sustain. Energy* **2009**, *28* (3), 386–396.

- (21) Cho, J.; Chu, S.; Dauenhauer, P. J.; Huber, G. W. Kinetics and Reaction Chemistry for Slow Pyrolysis of Enzymatic Hydrolysis Lignin and Organosolv Extracted Lignin Derived from Maplewood. *Green Chem.* **2012**, *14* (2), 428–439.
- (22) Baccile, N.; Falco, C.; Titirici, M.-M. Characterization of Biomass and Its Derived Char Using  $^{13}\text{C}$ -Solid State Nuclear Magnetic Resonance. *Green Chem* **2014**.
- (23) Johnson, R. L.; Schmidt-Rohr, K. Quantitative Solid-State  $^{13}\text{C}$  NMR with Signal Enhancement by Multiple Cross Polarization. *J. Magn. Reson.*
- (24) Samuel, R.; Foston, M.; Jaing, N.; Cao, S.; Allison, L.; Studer, M.; Wyman, C.; Ragauskas, A. J. HSQC (heteronuclear Single Quantum Coherence)  $^{13}\text{C}$ -  $^1\text{H}$  Correlation Spectra of Whole Biomass in Perdeuterated Pyridinium Chloride-DMSO System: An Effective Tool for Evaluating Pretreatment. *Fuel* **2011**, *90* (9), 2836–2842.
- (25) Foston, M.; Samuel, R.; Ragauskas, A. J.  $^{13}\text{C}$  Cell Wall Enrichment and Ionic Liquid NMR Analysis: Progress towards a High-Throughput Detailed Chemical Analysis of the Whole Plant Cell Wall. *Analyst* **2012**, *137* (17), 3904–3909.
- (26) Kim, H.; Ralph, J. Solution-State 2D NMR of Ball-Milled Plant Cell Wall Gels in DMSO- $d_6$ /pyridine- $d_5$ . *Org. Biomol. Chem.* **2010**, *8* (3), 576–591.
- (27) Wen, J.-L.; Sun, S.-L.; Xue, B.-L.; Sun, R.-C. Recent Advances in Characterization of Lignin Polymer by Solution-State Nuclear Magnetic Resonance (NMR) Methodology. *Materials* **2013**, *6* (1), 359–391.
- (28) Bardet, M.; Emsley, L.; Vincendon, M. Two-Dimensional Spin-Exchange Solid-State NMR Studies of  $^{13}\text{C}$ -Enriched Wood. *Solid State Nucl. Magn. Reson.* **1997**, *8* (1), 25–32.
- (29) Mao, J. D.; Holtman, K. M.; Franqui-Villanueva, D. Chemical Structures of Corn Stover and Its Residue after Dilute Acid Prehydrolysis and Enzymatic Hydrolysis: Insight into Factors Limiting Enzymatic Hydrolysis. *J. Agric. Food Chem.* **2010**, *58* (22), 11680–11687.
- (30) Bardet, M.; Gerbaud, G.; Giffard, M.; Doan, C.; Hediger, S.; Pape, L. L.  $^{13}\text{C}$  High-Resolution Solid-State NMR for Structural Elucidation of Archaeological Woods. *Prog. Nucl. Magn. Reson. Spectrosc.* **2009**, *55* (3), 199–214.
- (31) vanRossum, B. J.; Forster, H.; Forster, H. J. M. High-Field and High-Speed CP-MAS C-13 NMR Heteronuclear Dipolar-Correlation Spectroscopy of Solids with Frequency-Switched Lee-Goldburg Homonuclear Decoupling. *J. Magn. Reson.* **1997**, *124*, 516–519.
- (32) Egorova-Zachernyuk, T.; Van Rossum, B.; Erkelens, C.; De Groot, H. Characterisation of Uniformly  $^{13}\text{C}$ ,  $^{15}\text{N}$  Labelled Bacteriochlorophyll a and Bacteriopheophytin a in Solution and in Solid State: Complete Assignment of the  $^{13}\text{C}$ ,  $^1\text{H}$  and  $^{15}\text{N}$  Chemical Shifts. *Magn. Reson. Chem.* **2008**, *46* (11), 1074–1083.
- (33) Hologne, M.; Bertani, P.; Azaïs, T.; Bonhomme, C.; Hirschinger, J.  $^1\text{H}/^{31}\text{P}$  Distance Determination by Solid State NMR in Multiple-Spin Systems. *Solid State Nucl. Magn. Reson.* **2005**, *28* (1), 50–56.
- (34) Hediger, S.; Meier, B. H.; Kurur, N. D.; Bodenhausen, G.; Ernst, R. R. NMR Cross Polarization by Adiabatic Passage through the Hartmann—Hahn Condition (APHH). *Chem. Phys. Lett.* **1994**, *223* (4), 283–288.
- (35) Raya, J.; Perrone, B.; Hirschinger, J. Chemical Shift Powder Spectra Enhanced by Multiple-Contact Cross-Polarization under Slow Magic-Angle Spinning. *J. Magn. Reson. San Diego Calif 1997* **2013**, *227*, 93–102.
- (36) Fung, B. M.; Khitrin, A. K.; Ermolaev, K. An Improved Broadband Decoupling Sequence for Liquid Crystals and Solids. *J. Magn. Reson.* **2000**, *142* (1), 97–101.
- (37) Samuel, R.; Foston, M.; Jiang, N.; Allison, L.; Ragauskas, A. J. Structural Changes in Switchgrass Lignin and Hemicelluloses during Pretreatments by NMR Analysis. *Polym. Degrad. Stab.* **2011**, *96* (11), 2002–2009.
- (38) Fernández-Costas, C.; Gouveia, S.; Sanromán, M. A.; Moldes, D. Structural Characterization of Kraft Lignins from Different Spent Cooking Liquors by 1D and 2D Nuclear Magnetic Resonance Spectroscopy. *Biomass Bioenergy* **2014**, *63*, 156–166.
- (39) Liitiä, T.; Maunu, S. L.; Hortling, B. Solid-State NMR Studies of Residual Lignin and Its Association with Carbohydrates. *J. Pulp Pap. Sci.* **2009**, *26* (9), 323–330.

- (40) Maunu, S. NMR Studies of Wood and Wood Products. *Prog. Nucl. Magn. Reson. Spectrosc.* **2002**, *40* (2), 151–174.
- (41) Ralph, J.; Grabber, J. H.; Hatfield, R. D. Lignin-Ferulate Cross-Links in Grasses: Active Incorporation of Ferulate Polysaccharide Esters into Ryegrass Lignins. *Carbohydr. Res.* **1995**, *275* (1), 167–178.
- (42) Dufour, A.; Castro-Daz, M.; Marchal, P.; Brosse, N.; Olcese, R.; Bouroukba, M.; Snape, C. In Situ Analysis of Biomass Pyrolysis by High Temperature Rheology in Relations with <sup>1</sup>H NMR. *Energy Fuels* **2012**, *26* (10), 6432–6441.
- (43) Baccile, N.; Laurent, G.; Babonneau, F.; Fayon, F.; Titirici, M.-M.; Antonietti, M. Structural Characterization of Hydrothermal Carbon Spheres by Advanced Solid-State MAS <sup>13</sup>C NMR Investigations. *J. Phys. Chem. C* **2009**, *113* (22), 9644–9654.
- (44) Chu, S.; Subrahmanyam, A. V.; Huber, G. W. The Pyrolysis Chemistry of a B-O-4 Type Oligomeric Lignin Model Compound. *Green Chem.* **2013**, *15* (1), 125.
- (45) Inari, G. N.; Mounquengui, S.; Dumarçay, S.; Pétrissans, M.; Gérardin, P. Evidence of Char Formation during Wood Heat Treatment by Mild Pyrolysis. *Polym. Degrad. Stab.* **2007**, *92* (6), 997–1002.
- (46) Falco, C.; Baccile, N.; Titirici, M.-M. Morphological and Structural Differences between Glucose, Cellulose and Lignocellulosic Biomass Derived Hydrothermal Carbons. *Green Chem.* **2011**, *13* (11), 3273–3281.
- (47) Falco, C.; Perez Caballero, F.; Babonneau, F.; Gervais, C.; Laurent, G.; Titirici, M.-M.; Baccile, N. Hydrothermal Carbon from Biomass: Structural Differences between Hydrothermal and Pyrolyzed Carbons via <sup>13</sup>C Solid State NMR. *Langmuir* **2011**, *27* (23), 14460–14471.
- (48) Olcese, R.; Carré, V.; Aubriet, F.; Dufour, A. Selectivity of Bio-Oils Catalytic Hydrotreatment Assessed by Petroleomic and GC\*GC/MS-FID Analysis. *Energy Fuels* **2013**, *27* (4), 2135–2145.

### III.1.4 Supporting information

#### Pyrolysis procedure for char production

Miscanthus was harvested in 2011 in France. Pyrolysis of miscanthus was conducted in a vertical U-shape quartz fixed bed reactor as those employed in catalytic studies. The miscanthus particles (800 mg, sieved between 40 and 100  $\mu\text{m}$ ) were supported on a quartz sintered plate (20mm internal diameter). This geometry allows a good control of temperature, with a thermocouple inside the fixed bed of biomass, and of mass transfer by flushing the fixed bed with a given flow rate of Argon (300 NmL min<sup>-1</sup>). The reactor was heated by an electrical furnace from 20°C to 300°C at a heating rate of 5K min<sup>-1</sup>. Once 300°C was reached, the furnace was immediately moved down and the reactor was immediately immersed in water. The cooling time from 300 to 200°C (thermocouple inside the fixed bed) is of about 30 seconds. Char was cooled under Argon down to 30°C and then collected for further analysis. The char yield was 63%mas.

#### Composition of miscanthus and char

The chemical analysis of miscanthus and ash and elemental compositions of miscanthus and the char are given in the following tables.

*Table III-1: Elemental composition of miscanthus*

Sample (%wt.)	N	C	H	S	ash	O (by difference)
Raw miscanthus	0.23	42.8	5.5	0.00	7.0	44.4
300°C char	0.26	48.2	4.8	0.00	9.7	37.1

*Table III-2: Ash composition of miscanthus*

Ash content %wt on dry biomass											
Sample	Si	Al	Fe	Mn	Mg	Ca	Na	K	Ti	P	Total
Miscanthus	1.66	0.16	0.09	0.02	0.10	0.37	0.01	0.65	0.01	0.00	3.06

*Table III-3: Composition of miscanthus*

%wt on dry biomass									
Sample	Main components				Sugar contents				
	Extractibles	Sugars	Klason lignin	Minerals	Glucose	Xylose	Mannose	Galactose	Arabinose
Miscanthus	3.1	68.0	28.9	7.0	47.4	17.7	0.0	0.5	2.2

**Analytical procedure for NMR analysis of miscanthus and char**

Solid-state NMR experiments were performed on an AVANCE 750 MHz wide bore spectrometer (Bruker™) operating at a frequency of 188.5 MHz for  $^{13}\text{C}$  and equipped with a triple resonance MAS probe designed for 3.2 mm od zirconia rotors (closed with Kel-F caps). Approximately 19.5 mg of materials was put inside the rotor without any physical or chemical treatment of biomass and char. All the samples were spun at 18 kHz spinning frequency. 2D  $^1\text{H}$ - $^{13}\text{C}$  heteronuclear correlation (HETCOR) experiments with frequency-switched Lee-Goldburg (FSLG) irradiation during the evolution time<sup>1</sup> were obtained with the first CP step following the Adiabatic Passage through the Hartmann-Hahn (HH) conditions scheme<sup>2</sup>. The latter conditions were set to 93 kHz and 111 kHz  $B_1$  fields for  $^{13}\text{C}$  and  $^1\text{H}$  respectively. The  $^1\text{H}$  RF field was swept from 96 to 126 kHz through the HH condition using the tangential time dependence and defined by the shape angle  $\phi = at_{cp}/2$  where  $a$  is the rate of angular change<sup>3</sup>.  $\phi$  and  $t_{cp}$  (contact time) were set to  $88^\circ$  and 4ms after optimization<sup>4</sup>. Proton decoupling during acquisition was obtained by using SPINAL-64<sup>5</sup> at a 80 kHz RF field while the recycle time was set to 4 s. The duration of the successive FSLG pulses was 8.05  $\mu\text{s}$  and the magic-angle pulse length was 2.01  $\mu\text{s}$ . 64 complex data points were acquired in the  $^1\text{H}$  indirect dimension and for each  $t_1$  increment 1024 scans were accumulated. The corresponding spectral widths were 10.75 kHz for  $^1\text{H}$  (331.31ppm) and 62.5 kHz for  $^{13}\text{C}$  (14.33ppm), leading to a time resolution of 2.9763ms and 16.434ms respectively. Prior to Fourier transformation, a Lorentzian line broadening of 150 Hz was applied in the direct dimension while the proton dimension apodization was done with a  $90^\circ$  shifted squared sine-bell function.

**Assignments of the main  $^1\text{H}$ - $^{13}\text{C}$  correlations signals found in the HETCOR spectrum of Native Miscanthus**

Miscanthus native		
$\delta\text{C}/\delta\text{H}$ (ppm)	Assignments	References
20.3/1.17	$\text{C}_{\text{Methyl acetates}}/\text{H}_{\text{aliphatics}}$	6
21.3/1.2		
21/3.2		
21.2/3.85		
56.2/3.6	$\text{C}_{\text{MeO}}/\text{H}_{\text{MeO}}$	6-8
56.2/6.35-7	$\text{C}_{\text{MeO}}/\text{H}_{2,6}$	<sup>9</sup> for $\delta\text{C}$
64.4/3.6	$\text{C}_6/\text{H}_6$ (carbohydrates)	10-12
74.9-72.3/3.6	$\text{C}_2, \text{C}_3, \text{C}_5/\text{H}_2, \text{H}_3, \text{H}_5$ (carbohydrates)	
83.6/3.6	$\text{C}_4$ (disord)/ $\text{H}_4$ (carbohydrates)	
87.9/3.6	$\text{C}_4$ (ord) / $\text{H}_4$ (carbohydrates)	
104.8/3.6	$\text{C}_1/\text{H}_1$ (carbohydrates)	
111.5/3.6	$\text{G}_2/\text{H}_{\text{MeO}}$	<sup>9</sup> for $\delta\text{C}$
110-112/6.7-7.5	$\text{G}_2/\text{H}_2$ (aromatics)	13,14
113-115/6.5-7.5	$\text{G}_5/\text{H}_5$ (aromatics)	8,15
116.9/6.9	$\text{C}_{3,5}/\text{H}_{3,5}$ in p-coumaroylated structure	13
118-120/6.3-7.0	$\text{G}_6/\text{H}_6$ (aromatics)	8,14,15
132-134/3.0-4.0	$\text{S}_1/\text{H}_{\text{alkyl-O}}$	<sup>9</sup> for $\delta\text{C}$ and <sup>11</sup>
134-136/3.0-4.0	$\text{G}_1/\text{H}_{\text{alkyl-O}}$	<sup>9</sup> for $\delta\text{C}$ and <sup>11</sup>
138-140/3.2-4.0	$\text{S}_4/\text{H}_{\text{MeO}}$	<sup>9</sup> for $\delta\text{C}$
145-147/6.8-7.2	$\text{G}_4/\text{H}_{\text{arom}}$	<sup>9</sup> for $\delta\text{C}$
146-149.5/3.1-4.1	$\text{G}_4/\text{H}_{\text{MeO}}$	<sup>9</sup> for $\delta\text{C}$
146-149.5/3.1-4.0	$\text{G}_3/\text{H}_{\text{MeO}}$	6
147-149/7.0-7.5	$\text{G}_5/\text{H}_{\text{arom}}$	<sup>9</sup> for $\delta\text{C}$
150.0-154.0/3.2-4.0	$\text{S}_{3,5}(\text{e})/\text{H}_{\text{MeO}}$	6

**Assignments of the main  $^1\text{H}$ - $^{13}\text{C}$  correlation signals found in the HETCOR spectrum of 300°C Miscanthus Char**

The  $^1\text{H}$ - $^{13}\text{C}$  correlations were assigned based on reference work and on modeling under the software ACD NMR.

300°C Miscanthus char		
$\delta\text{C}/\delta\text{H}$ (ppm)	Assignments	References
31/3.0	Caliphatics/Haliphatics	<sup>16</sup> and ACD NMR modeling
33.1/2.65		
35.5/2.64		
55.6/2.83	C <sub>MeO</sub> /H <sub>MeO</sub>	<sup>6-8</sup>
64.4/3.6	C <sub>6</sub> /H <sub>6</sub> (carbohydrates)	<sup>10-12</sup>
74.9-72.3/3.6	C <sub>2</sub> ,C <sub>3</sub> ,C <sub>5</sub> /H <sub>2</sub> ,H <sub>3</sub> ,H <sub>5</sub> (carbohydrates)	
83.6/3.6	C <sub>4</sub> (disord)/H <sub>4</sub> (carbohydrates)	
87.9/3.6	C <sub>4</sub> (ord)/H <sub>4</sub> (carbohydrates)	
104.8/3.6	C <sub>1</sub> /H <sub>1</sub> (carbohydrates)	
111.4/3.38	G <sub>2</sub> /H <sub>MeO</sub>	<sup>9</sup> for $\delta\text{C}$
111.4/6.04	G <sub>2</sub> /H <sub>2</sub> (aromatics)	<sup>13</sup>
113-114/6-6.3	C <sub><math>\beta</math>fur (c=c)</sub> /H <sub>arom</sub> structure 1 and 2, Carbon 2	ACD NMR for $\delta\text{H}$
117.5-118/6-6.5	C <sub><math>\beta</math>fur (c=c)</sub> /H <sub>arom</sub> structure 2, Carbon 3	<sup>16</sup> and ACD NMR modeling for $\delta\text{H}$
127.5-128.5/3.2-3.6	C <sub>arom c=c</sub> /H <sub>carbohyd</sub> structure 1	<sup>16</sup>
127.5-128.5/6.1-6.4	C <sub>arom c=c</sub> /H <sub>arom</sub> structure 1	<sup>16</sup>
132-133/2.7-3	C <sub>arom (c=c)</sub> /H <sub>MeO</sub> Aromatic clusters	<sup>17</sup>
132-133/5.9	C <sub>arom (c=c)</sub> /H <sub>arom</sub> Aromatic clusters	<sup>17</sup>
146-147/2.83	C <sub>arom</sub> /H <sub>MeO</sub> structure 3, Carbon 4	
146-147/3.3-3.7	C <sub><math>\alpha</math>fur</sub> /H <sub>carbohyd</sub> structure 1, Carbon 1	<sup>16,17</sup>
146-147/5.6-5.9	C <sub><math>\alpha</math>fur</sub> /H <sub>arom</sub> structure 1, Carbon 1 and structure 3, Carbon 4	<sup>16,17</sup>

**$^{13}\text{C}$  solid state NMR spectra for different chars produced at different temperatures**

300°C was chosen as the most appropriate temperature to investigate the intermediate chemical mechanism of biomass pyrolysis and to conduct further 2D high resolution NMR. Indeed the char yield is 63%wt at 300°C and the 1D  $^{13}\text{C}$  CPMAS NMR analysis shows the formation of aromatics and a significant conversion of the carbohydrates at 300°C.

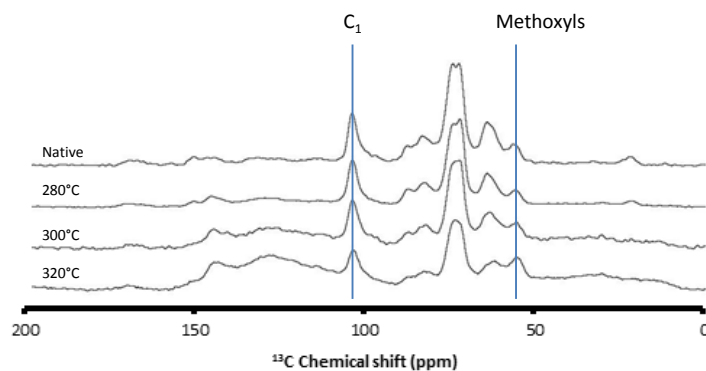


Figure III-5:  $^{13}\text{C}$  solid state NMR spectra for different char

 **$^{13}\text{C}$  solid state NMR spectra for the effect of contact time**

Figure III-6. highlights the effect of the mixing time from 1 to 4ms in 1D  $^{13}\text{C}$  CP/MAS method. The signal on lignin is enhanced by 4ms contact time without any loss of signal compared to short contact time, and far connectivities was preferred for this 2D analysis because this 2D method was specifically design to analyse the aromatic structure in biomass and char. In this aromatic structure, the connectivities between protons and carbons are longer, for this reason one needs long contact time to detect even the aromatic carbons far from protons. With a contact time of 4ms we attempted to investigate distant nuclei.

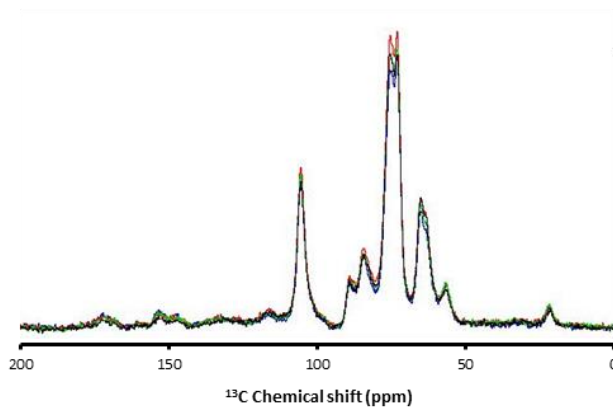


Figure III-6: Effect of contact time on 1D  $^{13}\text{C}$  CP/MAS analysis of miscanthus (green curve: 1ms, red: 2ms, black: 3ms, blue: 4ms)

Figure III-7 highlights a better sensitivity for aromatic carbons with a contact time of 4ms (blue) compared to 2ms (red) on a char produced at 350°C.

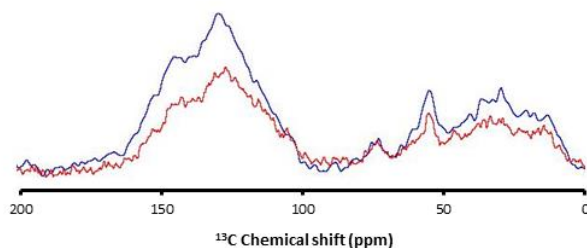


Figure III-7: Effect of contact time on 1D  $^{13}\text{C}$  CP/MAS analysis of 350°C char

### 2D $^1\text{H}$ - $^{13}\text{C}$ Hectcor spectrum of Cellulose

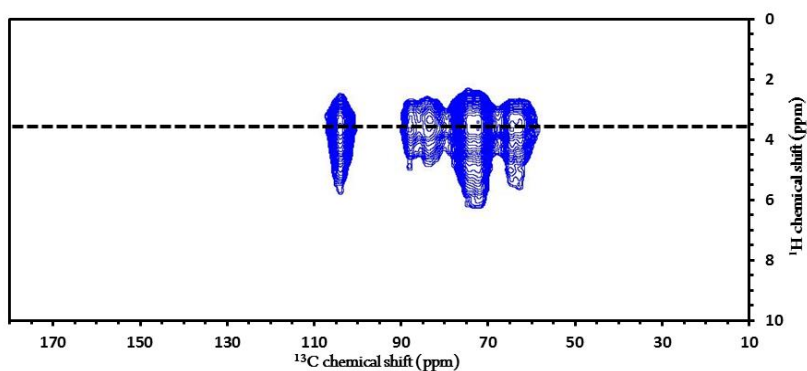


Figure III-8:  $^1\text{H}$ - $^{13}\text{C}$  Hectcor spectrum for cellulose extracted from *Miscanthus*

Even if the carbons in cellulose ( $\text{C}_1$ ,  $\text{C}_2$ ,  $\text{C}_3$ ,  $\text{C}_4$ ,  $\text{C}_5$  and  $\text{C}_6$  as illustrated in Figure III-2 in the main text) have different connectivities with protons, this is not analyzed by our method because of the long contact time which leads to a loss in selectivity for these carbons. The scope here was rather to detect aromatic carbons. We are aware that much more selective methods have been developed for carbons in carbohydrates<sup>18</sup>.

### 2D $^1\text{H}$ - $^{13}\text{C}$ Hectcor spectrum of Miscanthus 300°C char

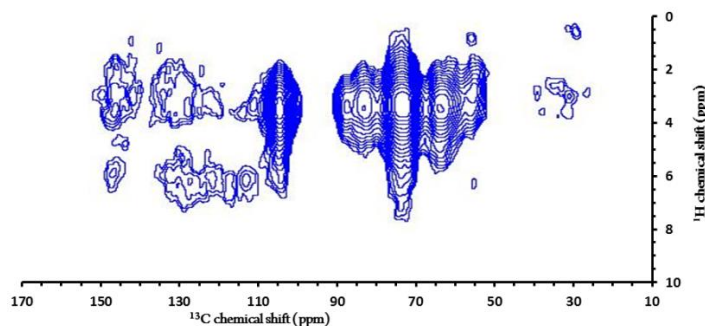


Figure III-9:  $^1\text{H}$ - $^{13}\text{C}$  Hectcor spectrum for 300°C Miscanthus char

### Thermo-gravimetric analysis of miscanthus

Thermo-gravimetric analysis obtained at a heating rate of the TGA at 5 K min<sup>-1</sup> on about 5 mg of biomass.

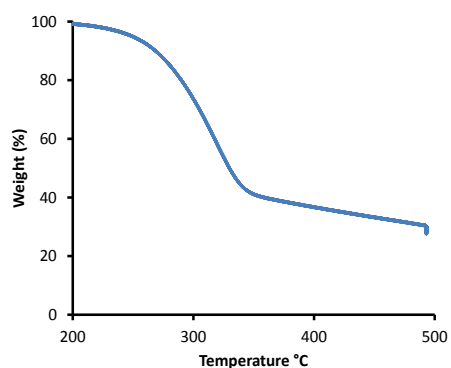


Figure III-10 : Thermo-gravetric analysis of miscanthus

### References of the supporting information

- (1) Van Rossum, B.-J.; Förster, H.; de Groot, H. J. M. High-Field and High-Speed CP-MAS  $^{13}\text{C}$  NMR Heteronuclear Dipolar-Correlation Spectroscopy of Solids with Frequency-Switched Lee–Goldburg Homonuclear Decoupling. *J. Magn. Reson.* **1997**, *124* (2), 516–519.
- (2) Hologne, M.; Bertani, P.; Azais, T.; Bonhomme, C.; Hirschinger, J.  $^1\text{H}/^{31}\text{P}$  Distance Determination by Solid State NMR in Multiple-Spin Systems. *Solid State Nucl. Magn. Reson.* **2005**, *28* (1), 50–56.
- (3) Hediger, S.; Meier, B. H.; Kurur, N. D.; Bodenhausen, G.; Ernst, R. R. NMR Cross Polarization by Adiabatic Passage through the Hartmann—Hahn Condition (APHH). *Chem. Phys. Lett.* **1994**, *223* (4), 283–288.
- (4) Raya, J.; Perrone, B.; Hirschinger, J. Chemical Shift Powder Spectra Enhanced by Multiple-Contact Cross-Polarization under Slow Magic-Angle Spinning. *J. Magn. Reson. San Diego Calif 1997* **2013**, *227*, 93–102.
- (5) Fung, B. M.; Khitrin, A. K.; Ermolaev, K. An Improved Broadband Decoupling Sequence for Liquid Crystals and Solids. *J. Magn. Reson.* **2000**, *142* (1), 97–101.
- (6) Fernández-Costas, C.; Gouveia, S.; Sanromán, M. A.; Moldes, D. Structural Characterization of Kraft Lignins from Different Spent Cooking Liquors by 1D and 2D Nuclear Magnetic Resonance Spectroscopy. *Biomass Bioenergy* **2014**, *63*, 156–166.

- (7) Samuel, R.; Foston, M.; Jaing, N.; Cao, S.; Allison, L.; Studer, M.; Wyman, C.; Ragauskas, A. J. HSQC (heteronuclear Single Quantum Coherence)  $^{13}\text{C}$ - $^1\text{H}$  Correlation Spectra of Whole Biomass in Perdeuterated Pyridinium Chloride-DMSO System: An Effective Tool for Evaluating Pretreatment. *Fuel* **2011**, *90* (9), 2836–2842.
- (8) Wen, J.-L.; Sun, S.-L.; Xue, B.-L.; Sun, R.-C. Recent Advances in Characterization of Lignin Polymer by Solution-State Nuclear Magnetic Resonance (NMR) Methodology. *Materials* **2013**, *6* (1), 359–391.
- (9) Brosse, N.; El Hage, R.; Chaouch, M.; Pétrissans, M.; Dumarçay, S.; Gérardin, P. Investigation of the Chemical Modifications of Beech Wood Lignin during Heat Treatment. *Polym. Degrad. Stab.* **2010**, *95* (9), 1721–1726.
- (10) Melkior, T.; Jacob, S.; Gerbaud, G.; Hediger, S.; Le Pape, L.; Bonnefois, L.; Bardet, M. NMR Analysis of the Transformation of Wood Constituents by Torrefaction. *Fuel* **2012**, *92* (1), 271–280.
- (11) Mao, J. D.; Holtman, K. M.; Franqui-Villanueva, D. Chemical Structures of Corn Stover and Its Residue after Dilute Acid Prehydrolysis and Enzymatic Hydrolysis: Insight into Factors Limiting Enzymatic Hydrolysis. *J. Agric. Food Chem.* **2010**, *58* (22), 11680–11687.
- (12) Maunu, S. L. NMR Studies of Wood and Wood Products. *Prog. Nucl. Magn. Reson. Spectrosc.* **2002**, *40* (2), 151–174.
- (13) Villaverde, J. J.; Li, J.; Ek, M.; Ligeró, P.; De Vega, A. Native Lignin Structure of Miscanthus X Giganteus and Its Changes during Acetic and Formic Acid Fractionation. *J. Agric. Food Chem.* **2009**, *57* (14), 6262–6270.
- (14) Foston, M.; Samuel, R.; Ragauskas, A. J.  $^{13}\text{C}$  Cell Wall Enrichment and Ionic Liquid NMR Analysis: Progress towards a High-Throughput Detailed Chemical Analysis of the Whole Plant Cell Wall. *Analyst* **2012**, *137* (17), 3904–3909.
- (15) Del Río, J. C.; Rencoret, J.; Prinsen, P.; Martínez, A. T.; Ralph, J.; Gutiérrez, A. Structural Characterization of Wheat Straw Lignin as Revealed by Analytical Pyrolysis, 2D-NMR, and Reductive Cleavage Methods. *J. Agric. Food Chem.* **2012**, *60* (23), 5922–5935.
- (16) Falco, C.; Perez Caballero, F.; Babonneau, F.; Gervais, C.; Laurent, G.; Titirici, M.-M.; Baccile, N. Hydrothermal Carbon from Biomass: Structural Differences between Hydrothermal and Pyrolyzed Carbons via  $^{13}\text{C}$  Solid State NMR. *Langmuir* **2011**, *27* (23), 14460–14471.
- (17) Baccile, N.; Laurent, G.; Babonneau, F.; Fayon, F.; Titirici, M.-M.; Antonietti, M. Structural Characterization of Hydrothermal Carbon Spheres by Advanced Solid-State MAS  $^{13}\text{C}$  NMR Investigations. *J. Phys. Chem. C* **2009**, *113* (22), 9644–9654.
- (18) Cheng, K.; Sorek, H.; Zimmermann, H.; Wemmer, D. E.; Pauly, M. Solution-State 2D NMR Spectroscopy of Plant Cell Walls Enabled by a Dimethylsulfoxide- $d_6$  /1-Ethyl-3-Methylimidazolium Acetate Solvent. *Anal. Chem.* **2013**, *85* (6), 3213–3221.

## **III.2 Article 2: Mechanism of biomass char formation investigated by advanced solid state NMR**

Yann Le Brech<sup>1</sup>, Jesus Raya<sup>2‡</sup>, Luc Delmotte<sup>3‡</sup>, Nicolas Brosse<sup>4</sup>, Roger Gadiou<sup>3</sup>, Anthony Dufour<sup>1\*</sup>

<sup>1</sup> LRGP, CNRS, Université de Lorraine, 1 rue Grandville 54000 Nancy, France

<sup>2</sup> ICS, CNRS, Université de Strasbourg, 1 rue Blaise Pascal BP 296 R8 67008 Strasbourg Cedex, France

<sup>3</sup> IS2M, CNRS, Université de Haute Alsace, 15, rue Jean Starcky BP 2488 68057 Mulhouse cedex, France

<sup>4</sup> LERMAB, Université de Lorraine, BP239 54506 Vandoeuvre les Nancy cedex, France.

**Article à soumettre au journal ChemSusChem.**

### **III.2.1 Abstract**

The pyrolysis of ligno-cellulosic biomass is the key first phenomena in all thermochemical processes. Char is produced during pyrolysis and it could be valorised as soil amendment, activated carbon or to produce syngas or heat by further oxidation. The mechanisms of char formation have to be better understood to target the chemistry of biomass pyrolysis and the properties of char. The pyrolysis was conducted in a fixed bed reactor allowing a good control of char temperature. Miscanthus and the macromolecules extracted from miscanthus (holocellulose, cellulose, ethanol organosolv lignin) were pyrolysed at 5 K/min to various final temperatures (250 to 500°C). The chemical moieties formed in the chars were studied by solid state <sup>13</sup>C NMR. Spectra obtained by Cross Polarization at the Magic Angle Spinning with Adiabatic Passage through Hartmann-Hahn conditions (CP/MAS APHH) were compared with the Direct Polarization (DP) method. A quantitative study of the formation of aromatic structures in the network of macromolecules in miscanthus and in the extracted macromolecules was done. It was shown that below 300 °C, xylan is the main source of aromatic formation while above this temperature aromatization of cellulose occurs.

### **III.2.2 Introduction**

The lignocellulosic biomass, including woody or herbaceous biomass, has a huge potential as a renewable starting material in the context of the reduction of greenhouse gas emissions<sup>1</sup>. The thermochemical conversion of biomass is a promising route to produce energy and green chemicals<sup>2</sup>. Pyrolysis is the first step in all thermochemical process and for this reason it has been extensively studied<sup>3</sup>. Upon pyrolysis, mass and heat transfers and complex chemical reactions are occurring in biomass and they lead to the formation of the volatile compounds (or primary tar), gases and char. Many analytical methods (Mass Spectrometry, Nuclear Magnetic Resonance-NMR, Infra-red, etc.) have been used in order to understand the chemical mechanisms occurring during biomass pyrolysis<sup>4</sup>. Despite all these studies, these chemical mechanisms are still not well understood and remains a major challenge to optimise thermochemical biorefineries<sup>2</sup>.

The three macromolecules in biomass have their own pyrolysis mechanisms<sup>5-7</sup>. They are organised in a complex network in the cell wall and interactions between them occur during biomass pyrolysis<sup>8,9</sup>. The minerals (K, Mg, Ca, etc.), present in the natural biomass structure, have an important catalytic effect and modify considerably the pyrolysis reactions<sup>10,11</sup>. The thermal decomposition of hemicelluloses starts at relative low temperature, around 200°C<sup>12</sup>, and the mechanisms are poorly understood. The rupture of the glycosidic

links, dehydration and fragmentation seem to be the main degradation pathway. Lignin is a phenolic macromolecule constituted of phenylpropane units linked together through various ether and carbon-carbon linkages<sup>13,14</sup>. Thermal degradation starts around 150°C and proceeds on a broad range of temperature (150-600°C)<sup>15</sup>. The main degradation pathways are  $\beta$ -ether bond scissions, C-C ruptures and demethoxylation<sup>16</sup>. Concerning cellulose, its pyrolysis mechanisms have been studied in more details. Degradation starts at higher temperature (around 300°C) compared to lignin and hemicelluloses. Cellulose is mainly converted through an intermediate active cellulose (cellulose with a low degree of polymerisation) and converted by three main pathways, namely: transglycosylation, fragmentation and dehydration<sup>3,17,18</sup>. These paths are likely to occur preferentially depending on the conditions (minerals contents, heat flux density, etc.).

The analysis of chars obtained after various pyrolysis conditions has given new insight into the mechanism of biomass pyrolysis. Solid state <sup>13</sup>C NMR analysis has been widely used to investigate the structure of char or of others aromatic materials<sup>19–25</sup> because it is a nondestructive method, not limited by sample insolubility (as for liquid-state NMR) and it can provide detailed structural information<sup>26</sup>. The Cross Polarization/Magic Angle Spinning (CP/MAS) method is the most used NMR technique to provide structural information of chars<sup>19,20,22–33</sup>. CP/MAS experiments give chemical information in a short analysis time and with good signal-to-noise ratio. The indirect excitation of <sup>13</sup>C nuclei through dipolar interaction with protons enhances the response of the signal compared to the direct excitation of <sup>13</sup>C nuclei (Direct Polarization, DP/MAS)<sup>27</sup>. However, it does not afford a reliable quantitative analysis of the different moieties because the CP/MAS efficiency is related to the magnetization transfer rate from <sup>1</sup>H to <sup>13</sup>C which is different depending on the <sup>13</sup>C nuclei environment. Moreover, the lack of protons in the biochar<sup>33</sup> and the presence of paramagnetic centers<sup>23</sup> could limit the CP efficiency. The CP/MAS method is not an accurate quantitative method<sup>16,32</sup>. DP/MAS method overcomes these problems<sup>22,23,25,27</sup> but it requires longer recycle delays, which lead to time consuming experiments and to weaker sensitivity than the CP method. Despite the numerous works on <sup>13</sup>C NMR analysis of biomass char, there is still a lack in analysis of char over a wide range of temperature to follow the aromatization and with a well-known temperature. Moreover, as far as we know, no work has been conducted on the macromolecules carefully extracted and characterized from the same, well-defined, biomass.

In this study, a detailed characterization by <sup>13</sup>C NMR of biochars produced by slow pyrolysis was investigated using an original fixed-bed set-up designed to reduce the secondary reactions that may occur (cracking of tar in the nascent char)<sup>34</sup>. The goal of the study is a better understanding of the primary mechanisms of aromatic structures formation from (1) the macromolecular network of biomass (miscanthus straw) and (2) the isolated macromolecules (cellulose, holocellulose, lignin) extracted from the same biomass in order to highlight the effect of the inter-macromolecular interactions. Despite the fact that Cross-Polarization techniques are known to be non-quantitative and playing around the APHH<sup>35,36</sup> CP scheme (Adiabatic Passage through Hartman Hahn conditions) we were able to experimentally find conditions giving in very short times spectra that mimics very well the quantitative ones (error less than 7%). This exceptional behavior were in scarce occasions already observed<sup>37</sup> and after systematic verifications for a number of typical combination of samples/temperatures<sup>37</sup> (APHH vs DP) we did take advantage of this unusual finding, undoubtedly specific to this class of samples, to highly speed-up our <sup>13</sup>C NMR quantitative study.

### III.2.3 Material and methods

#### Production and characterization of biomass samples

In this study, *Miscanthus x Giganteus* (MxG) has been used because of its high production yields and its low need in fertilizers<sup>38,39</sup>. MxG used in these experiments was harvested in Lorraine (France) in 2011, then milled and sieved to a particle size between 40  $\mu\text{m}$  and 100  $\mu\text{m}$ . Natural polymers (Figure III-11) were extracted based on previous investigation procedures<sup>8,40</sup> (detailed in Supplementary material).

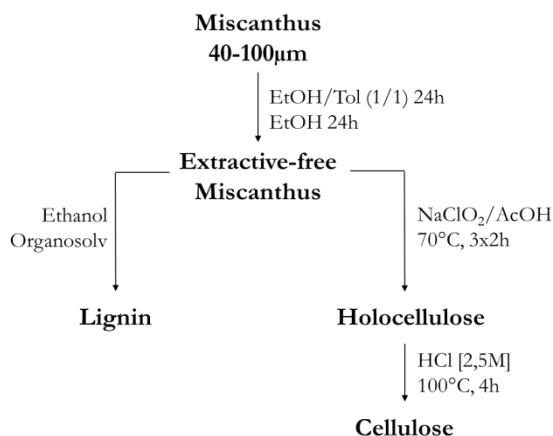


Figure III-11: Procedure for lignin, holocellulose and cellulose extractions from *Miscanthus x Giganteus*

The carbohydrates and Klason lignin contents in the three samples (MxG, holocellulose, cellulose) were measured on extractive free material, according to the NREL procedure<sup>41</sup> (results presented in supplementary material). Samples were hydrolyzed by concentrated sulfuric acid (72 %wt.) for 1h in a rotary water bath at 30°C and then autoclaved during 1h30 after being diluted to 3% sulfuric acid through addition of water. The autoclaved sample were filtered, and then dried to give the Klason lignin content. Monosaccharides in the filtrate were quantified using high-performance anion-exchange chromatography with pulsed amperometric detection (HPAEC-PAD)<sup>42</sup>. Samples have been analyzed by ICP-OES and ICP-MS following the CNRS-SARM procedure<sup>43</sup> in order to characterize their mineral and organic matter contents. These results are presented in the Supporting information. The purity of the different fractions extracted from MxG was verified by different characterizations techniques like DRIFT or Raman spectrometry<sup>44</sup>.

The pyrolysis behaviours of MxG and its extracted macromolecules were compared by thermogravimetric analysis using a Mettler Toledo set-up (TGA/DSC Stare system). These analyses were conducted on 5 mg of each sample at 5°C/min up to 500°C. The carrier gas (purified Argon) was set at 100 Nml/min. Elemental analysis of *Miscanthus*, extracted polymers and produced chars were performed on a Thermo Fisher (Flash EA 1112) apparatus. Each sample was dried at 105°C during several hours before experiments. All results are presented in the Supporting Materials (S3).

### Pyrolysis procedure for the production of chars

Pyrolysis of miscanthus, holocellulose and cellulose (800 mg) was conducted in a vertical U-shape quartz fixed bed reactor (Figure III-12). The particles (40-100  $\mu\text{m}$ ) were supported on a quartz sintered plate (20 mm internal diameter). This geometry allows a good control of temperature, thanks to a thermocouple (0,5 mm diameter) placed inside the fixed bed of biomass, and of mass transfer by flushing the fixed bed with a given flow rate of Argon (300 NmL min<sup>-1</sup>). The reactor was heated by an electrical furnace from 20°C to 500°C at a heating rate of 5 °C/min. The radial temperature gradient in the fixed bed was studied (by various thermocouples positioned along the diameter of the fixed bed) and was below 10°C between the middle and the border of the fixed bed of particles. Once the set temperature was achieved, the furnace was immediately moved down and the reactor was immediately immersed in ice-water in order to stop any reaction by a rapid cooling (2 minutes from 500°C to 150°C). Char was cooled down under Argon until 30°C and then collected for further analysis. Water content of each sample was determined by heating sample into an oven at 105°C during 30 minutes.

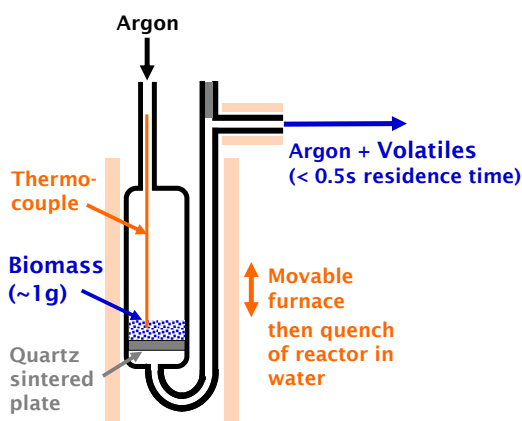


Figure III-12: Fixed bed pyrolysis reactor

Lignin pyrolysis was conducted in a tubular reactor<sup>45,46</sup> because the fixed bed could be plugged by the melted and swelled lignin. The apparatus consist of a steel tubular reactor heated by an electrical oven. The lignin sample (600 mg) was positioned inside a sample boat and flushed by inert nitrogen (900 Nml/min). The temperature of lignin and chars was analyzed by a thermocouple positioned inside the sample. A heating rate of the furnace of 5 °C/min was also set. One the set temperature was reached, the sample boat was fastly removed out of the furnace in a cooling zone and flushed by N<sub>2</sub> until 30°C.

### NMR methods

1D <sup>13</sup>C CP/MAS and DP/MAS experiments were performed on Bruker 500 MHz in order to get chemical information on biomass, extracted macromolecules and chars. In order to speed-up the acquisition of CP/MAS spectra we did use the CP scheme that is known to be among the best for getting the higher signal possible : the APHH scheme developed by R.R. Ernst and coworkers<sup>36</sup>. Analytical and experimental procedure is available in supporting material.

A <sup>1</sup>H-<sup>13</sup>C two dimensional heteronuclear correlation (HETCOR) experiment with frequency-switched Lee-Goldburg (FSLG) irradiation on high field spectrometer (750 MHz) as previously introduced by our group<sup>47</sup> was performed on biomass chars in order to get a better understanding of the biochar chemical structure. Analytical and experimental procedures are available in the supporting information.

The interpretation of the  $^{13}\text{C}$  NMR spectra presents a major difficulty due to the signal overlapping caused by superimposed and broad peaks. Spectral deconvolution is needed to overcome this problem. Therefore deconvolutions were performed by the DMFIT Software developed by Massiot et al.<sup>48</sup> and previously used for biomass chars<sup>49,50</sup>. Peaks were assigned based on literature<sup>31,32,51-53</sup>. The NMR spectrum of raw Miscanthus was first fitted and the parameters (chemical shift and linewidth) were saved in order to deconvolute NMR spectra of the pyrolysed samples in a similar and reproducible way. New peaks were added in order to take into account of the formation of new moieties. The deconvolutions were processed only with Gaussian lineshape. After deconvolution, quantitative evolution of the different moieties as function of temperature was performed. The different percentages relative to each carbons (or moieties) have been determined following several hypotheses: 1) NMR methods permit to see all the carbons in the sample ; 2) signal intensity response is similar for each detected carbon ; 3)  $^{13}\text{C}$  is heterogeneously spread in the sample. We calculated the percentage of each carbon moieties, presented in Table III-4, based on the original molar amount of carbon in the native sample. For each carbon moieties/function the %Original carbon at temperature Tx was calculated as follows:

$$\%Original\ Carbon(Tx) = \frac{\%A_{fit}(Tx) \times n_{Ctot}(Tx)}{\%C_{mass}(20^{\circ}C) \times \frac{msample(20^{\circ}C)}{12}} \times 100$$

Where  $\%A_{fit}$  is the percentage of the area for specific moieties (*fit*) at the temperature Tx,  $n_{Ctot}(Tx)$  is the total carbon moles in the char at temperature Tx (determined with the char yield at Tx).  $\%C_{mass}(20^{\circ}C)$  the mass percentage of carbon before pyrolysis analysis.  $msample(20^{\circ}C)$  is the mass of the sample introduced in the quartz reactor.

### III.2.4 Results and discussion

#### Mass loss in fixed bed compared with thermogravimetric analysis

The thermogravimetric analyses of the native MxG and of the cellulose, holocellulose and lignin extracted from MxG are presented on Figure III-13. The thermogram of MxG is in agreement with previous investigations<sup>54,55</sup>. The mass loss mainly occurs between 220°C and 350°C. The thermal degradation ranges for lignin, holocellulose and cellulose are 200-450°C, 220°C-350°C, 250-350°C respectively. The temperature for the maximum mass loss rate for MxG, lignin, holocellulose and cellulose are 315-320°C, 250-350°C, 315-320°C, 315-320°C, respectively.

The char yields obtained after experiments at different final temperatures from the fixed bed are plotted on the same figures (Figure III-13). The comparison between char yields obtained from fixed bed and TGA demonstrate that the experiments conducted in the fixed bed are close to the chemical regime (thanks to the efficient flushing of the bed and to its design).

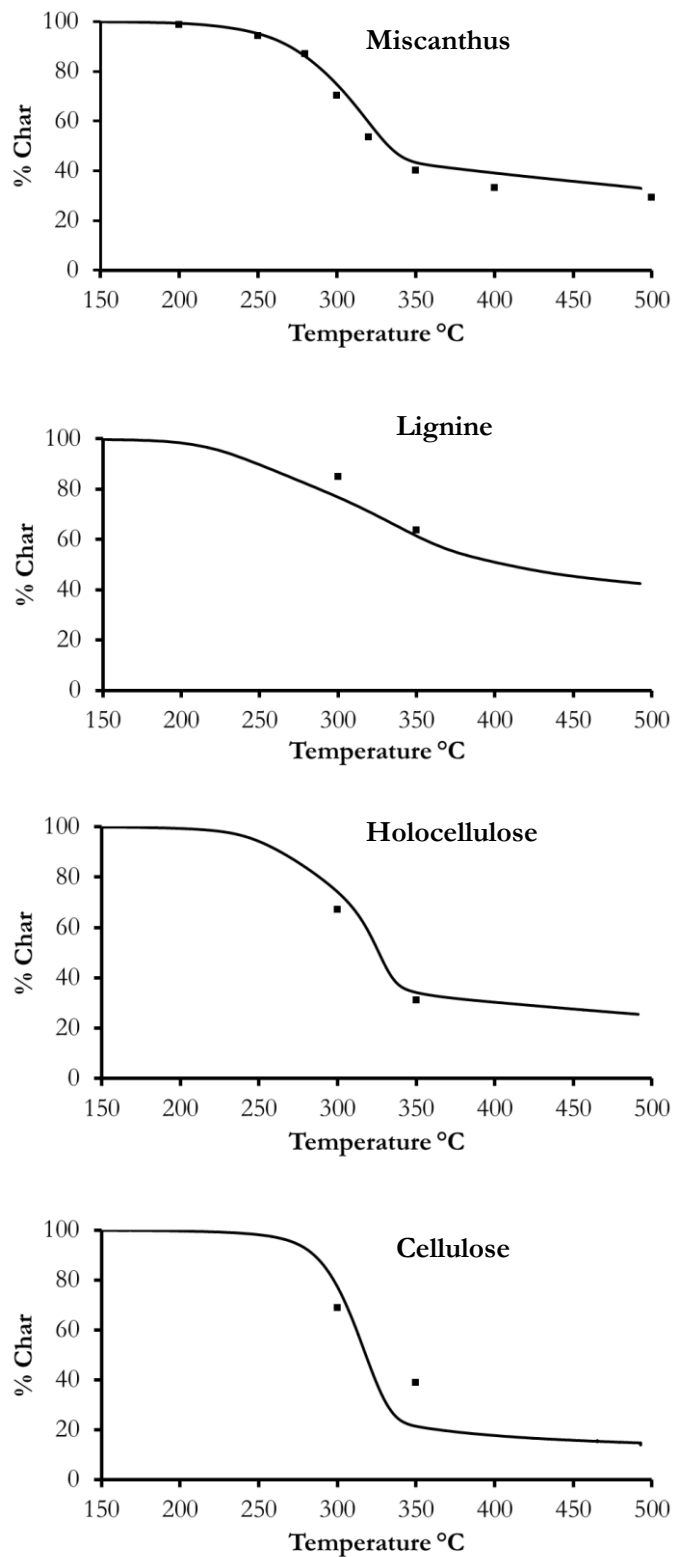


Figure III-13: Thermo-gravimetric analysis (lines) compared to char mass yield from fixed bed experiments (points)

### Comparison between CP and DP-MAS $^{13}\text{C}$ NMR analysis of the chars

In this study CP/MAS APHH<sup>36</sup> technique was used to increase the signal to noise ratio and shorten experiment time. The main concern about NMR biomass and char structure investigations is the quantitative reliability of the experiment. For this reason, we have verified that the CP/MAS APHH technique used in this study led to spectra almost identical than DP/MAS signals.

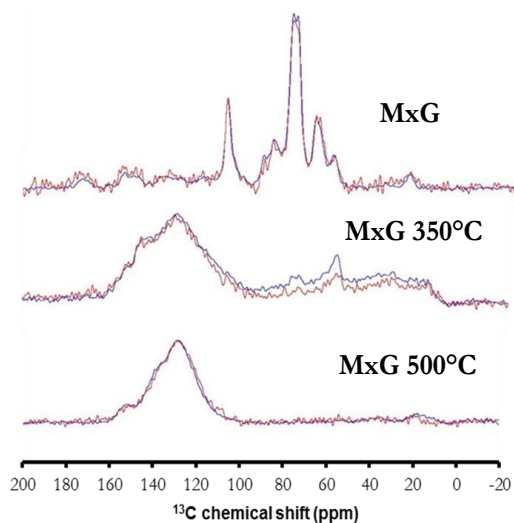


Figure III-14: Comparison of NMR signal from CP/MAS APHH (in blue) and DP/MAS APHH (in red)

Figure III-14 presents the comparison between CP/MAS APHH and DP/MAS spectra for MxG native and chars produced at 350°C and 500°C. It shows that the spectra obtained by the two different techniques are close. It could be concluded that: 1) the proton concentration in the MxG native is high enough and the proton dispersion in the material is homogeneous so that a complete transfer of the magnetization with a contact time of 2ms is obtained 2) Spin-diffusion phenomenon is enough effective to ensure a good transfer into MxG chars wherein the protons/carbons ratio is lower. In conclusion, the present NMR CP/MAS APHH method was used in the quantitative analysis of MxG, extracted macromolecules and produced chars. Thanks to this unexpected feature we could speed the experiment by a factor of 50 (4 s repetition time instead of 225 s for a really quantitative one as the longer  $^{13}\text{C}$  T1 we did measure was about ca 45 s.

### Effect of pyrolysis temperature on the composition of miscanthus biochar

The composition of the raw miscanthus and resultant chars were investigated by  $^{13}\text{C}$  CP/MAS APHH. The main chemical moieties present in miscanthus and their notations for carbon atoms are displayed in Figure III-15.  $^{13}\text{C}$  CP/MAS APHH spectra of raw miscanthus and chars are presented in Figure III-16 and the assignment of the bands is given in Table III-4.

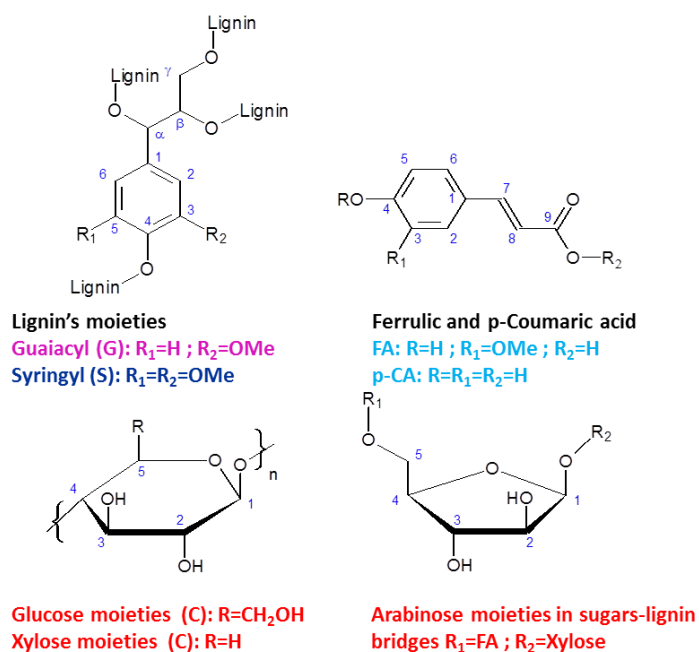


Figure III-15: Schematic representation of the main moieties in *Miscanthus x Giganteus*<sup>38</sup> and notations for carbon atoms

Table III-4 : Assignments of  $^{13}\text{C}/\text{MAS}$  APHH bands on miscanthus and extracted macromolecules and chars (band numbers are reported in Figures III-16 and III-18 on the NMR spectra, see Figure III-15 for the nomenclature of carbon notations)<sup>31,32,51-53</sup>

N°	Band (ppm)	Components	Origin
1	172	Carbonyls and Acetates	Lignin and hemicelluloses
2	154-152	Aromatic carbons with methoxyl groups	Lignin S <sub>3</sub> /S <sub>5</sub> etherified
3	150-144	Aromatic carbons link to oxygen	Lignin G <sub>4</sub> /G <sub>3</sub> , S <sub>3</sub> /S <sub>5</sub> nonetherified
4	141-120	Aromatic carbons (nonprotonated, protonated, oxygenated)	Lignin S <sub>4</sub> , G <sub>1</sub> , S <sub>1</sub> , G <sub>6</sub>
5	116-110	Protonated aromatic carbons	Lignin G <sub>5</sub> , G <sub>2</sub>
6	108-106	Protonated aromatic carbons	Lignin S <sub>2</sub> , S <sub>6</sub>
7	105	Carbohydrates	Cellulose C <sub>1</sub>
8	104-96	Carbohydrates	Hemicelluloses C <sub>1</sub>
9	88,5	Carbohydrates	Cellulose (ordered) C <sub>4</sub> <sup>a</sup>
10	84	Carbohydrates	Cellulose (disordered) C <sub>4</sub> <sup>a</sup>
11	74	Carbohydrates	Cellulose C <sub>2</sub> , C <sub>3</sub> , C <sub>5</sub> <sup>a</sup>
12	64	Carbohydrates	Cellulose C <sub>6</sub> <sup>a</sup>
13	56,2	Methoxyl groups	Lignin
14	30	Methylene groups	Lignin
15	21	Methyl acetates	Hemicelluloses

#### Clusters in chars

155-142	Aromatics C-O
142-124	Aromatics C-C
124-102	Aromatics C-H
90-50	Alkyl-O
50-10	Aliphatics

<sup>a</sup>Signals overlapped with hemicelluloses and lignin moieties

At 172 ppm, the signal n°1 was assigned to acetate groups which are present in lignin and hemicelluloses structures. The signal n°2 is assigned to carbons from syringyl units (S<sub>3</sub> and S<sub>5</sub>) involved in  $\beta$ -O-4 structures in lignin. The broad signal n°3 is assigned to guaiacyl units (G<sub>3</sub> and G<sub>4</sub>) and syringyl units non etherified (S<sub>3</sub> and S<sub>5</sub>). Broad and not very well-defined peaks between 142 and 105 ppm can be associated to other aromatic carbons of lignin (signals n°4 to 6).

Very intense signal at 105 ppm (n°7) refers to C<sub>1</sub> hemiacetallic carbons of cellulose. A broad and weak signal is observed between 104 and 96 ppm due to hemicelluloses C<sub>1</sub> hemiacetal carbon (n°8). The broadness can be attributed to their amorphous character. Signals n°9 (88.5 ppm) and n°10 (84 ppm) are assigned to carbohydrate carbons C<sub>4</sub> from cellulose in the ordered part of cellulose (88.5ppm) and in the disordered part (84ppm). These bands are overlapped with some signals belonging to lignin oxygenated aliphatic carbons (C <sub>$\beta$</sub> ) and xylan C<sub>4</sub>. For this reason, we did not deconvolute this zone of the spectra to calculate the ratio between

disordered and ordered cellulose in miscanthus but we did it for the extracted cellulose. The very intense signal, noted n°11, centered at 74 ppm can be mainly assigned to cellulose carbons C<sub>2</sub>, C<sub>3</sub> and C<sub>5</sub> but also to oxygenated aliphatic carbons (C<sub>α</sub>) in lignin and C<sub>2</sub> and C<sub>3</sub> in xylan. The signal n°12 at 64 ppm is attributed to cellulose carbons C<sub>6</sub> with two contributions corresponding to ordered and disordered cellulose. It is overlapped with signals from lignin oxygenated aliphatic carbons (C<sub>δ</sub>) and xylan C<sub>5</sub>. At 56 ppm, the signal n°13 corresponding to carbons from methoxyl groups in the lignin aromatic network is observed. At 21 ppm the signal n°15 can be attributed to methyl carbons in acetyl functions of hemicelluloses.

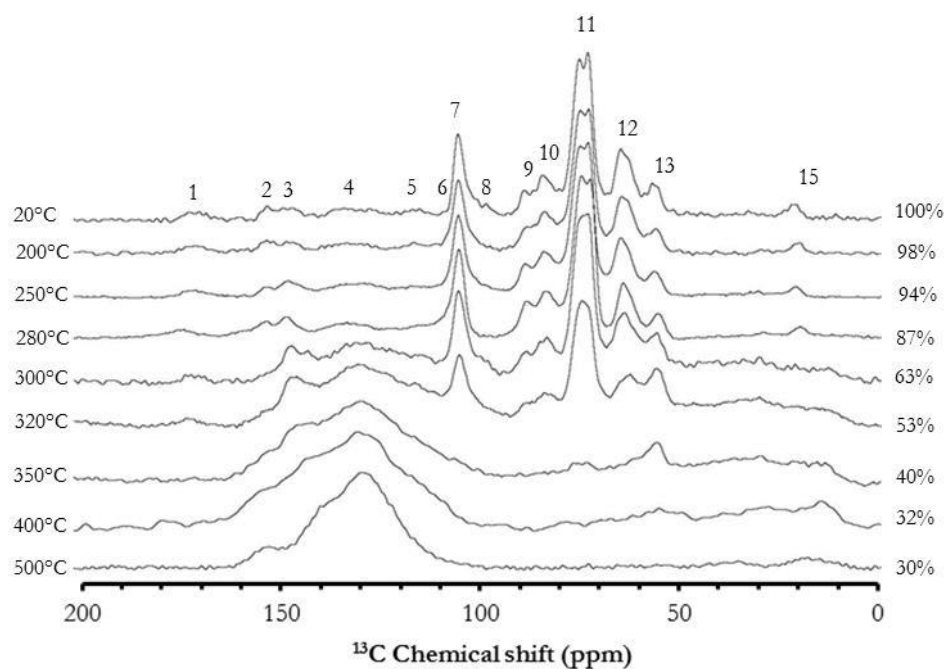


Figure III-16: <sup>13</sup>C NMR CP/MAS APHH spectra of native miscanthus (20°C) and chars produced after different final temperature (fixed bed, 5 K/min). Char yields are recalled at the right of each spectrum. See table III-4 for the assignment of the main bands.

The evolution of miscanthus carbon structure is presented as a function of temperature in Figure III-16. All spectra have been deconvoluted and the quantification of the different moieties is presented in Figure III-17. For a final pyrolysis temperature of 200°C, no obvious evolution is observable for all moieties. No variation of the peak at 154-152 ppm is observed, indicating the presence of intact β-O-4 linkages and methoxyl groups in syringyl units. Indeed, the aromatic carbons content remains stable from 20°C to 200°C.

It clearly appears from the Figure III-16 that between 200°C to 300°C, an increase of the pyrolysis temperature resulted in a decrease in etherified syringyl units (signal n°2, S<sub>3/5</sub> e) associated with an increase in non etherified units (signal n°3, G<sub>4</sub>/G<sub>3</sub>, S<sub>3/5</sub> ne). This observation is in agreement with an increasing degradation of the lignin network through β-O-4 linkage cleavages in this range of temperatures. However no significant variation of the methoxyl and aromatic content was observed.

The conversion of the carbohydrate carbons start at around 280°C. Up to this temperature, the signal of C<sub>1</sub> (peak n°7), which could be attributed especially to cellulose, remains stable. Therefore, the decrease in the carbohydrate carbons content is due to the degradation of hemicelluloses. This conversion of the hemicellulosic sugars is also accompanied with a decrease of the acetyl content (signals n° 1 and 15) detected from 250°C, indicating the cleavage of acetyl groups in xylan. The signal n°15 could also be assigned to the

ester linkages between *p*-coumaric and ferulic acids and hemicelluloses<sup>56</sup>. The thermal conversion of lignin-hemicelluloses linkages has been examined in our previous work based on 2D <sup>1</sup>H-<sup>13</sup>C NMR<sup>47</sup>.

A significant modification of the carbohydrate structure is observed from 300°C. At this temperature, roughly 50% of the carbohydrates carbons are converted. Simultaneously, an important increase in the aromatic and aliphatic contents is observed, most probably due to the conversion of xylan. The assignments of aromatic carbons could be questionable for temperature above 280 °C because of the overlap between aromatics from lignin and carbohydrate conversion. For this reason, we have previously used 2D solid-state NMR <sup>1</sup>H-<sup>13</sup>C HETCOR in order to better identify the origin of these aromatic moieties<sup>47</sup>. From 300°C, the aromatic oxygenated carbons from lignin (154-144ppm, S<sub>3</sub>, S<sub>5</sub>, G<sub>3</sub>, G<sub>4</sub>) cannot be clearly distinguished from the aromatics formed from the carbohydrates<sup>47</sup>. At 350°C, the chemical structure is mostly composed of aromatic and aliphatic carbons. Carbohydrates are totally converted in agreement with previous work<sup>23</sup>. An important methoxyl signal is still present in the char produced at 350°C. Above 350°C, the entire structure is dominated by aromatic carbons and a decrease of aliphatic content in the char is observed.

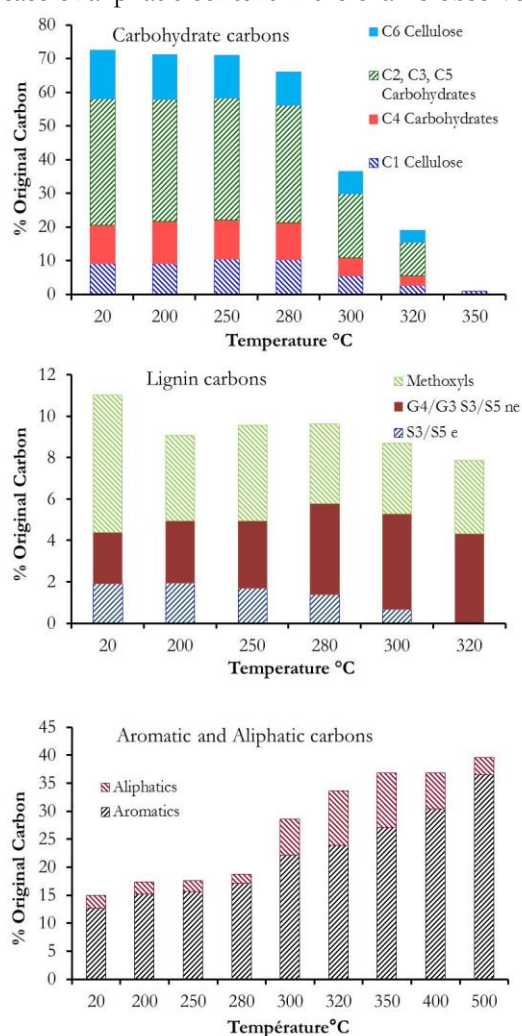


Figure III-17: Evolution of main moieties (%mol of original carbon) during pyrolysis of MxG as a function of temperature

**Effect of pyrolysis temperature on chars composition from fractionated polymers**

Different biochars have been produced from lignin, cellulose and holocellulose (isolated from MxG) at 300°C and 350°C. The objective here was to compare the chemical evolution in chars from the raw miscanthus and from its fractionated components. This approach could reveal the interactions between the components in the native network of miscanthus. The evolution of NMR spectra for lignin, cellulose and holocellulose chars is presented as a function of temperature in Figure III-18. The quantitative determination of the different moieties (after deconvolution) is presented in Figure III-19.

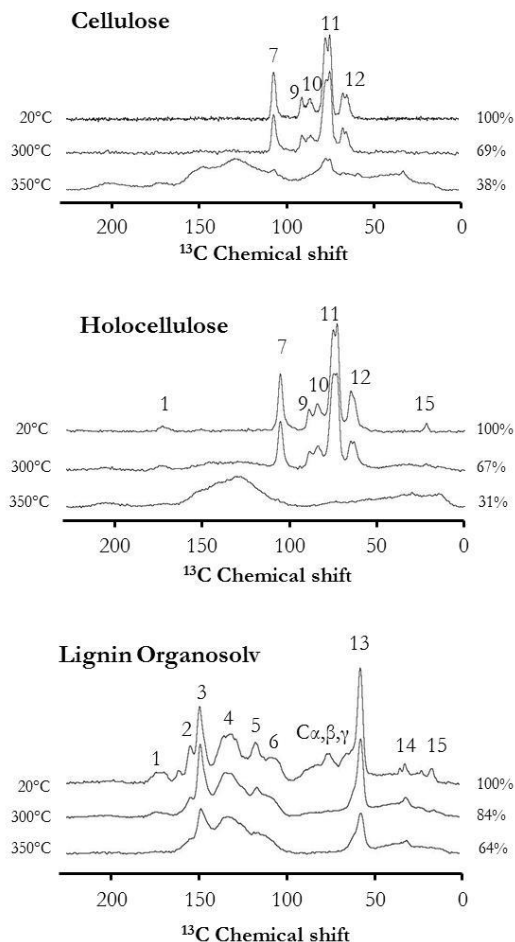


Figure III-18: Solid-state NMR  $^{13}\text{C}$  CPMAS spectra evolution for fractionated macromolecules as a function of temperature

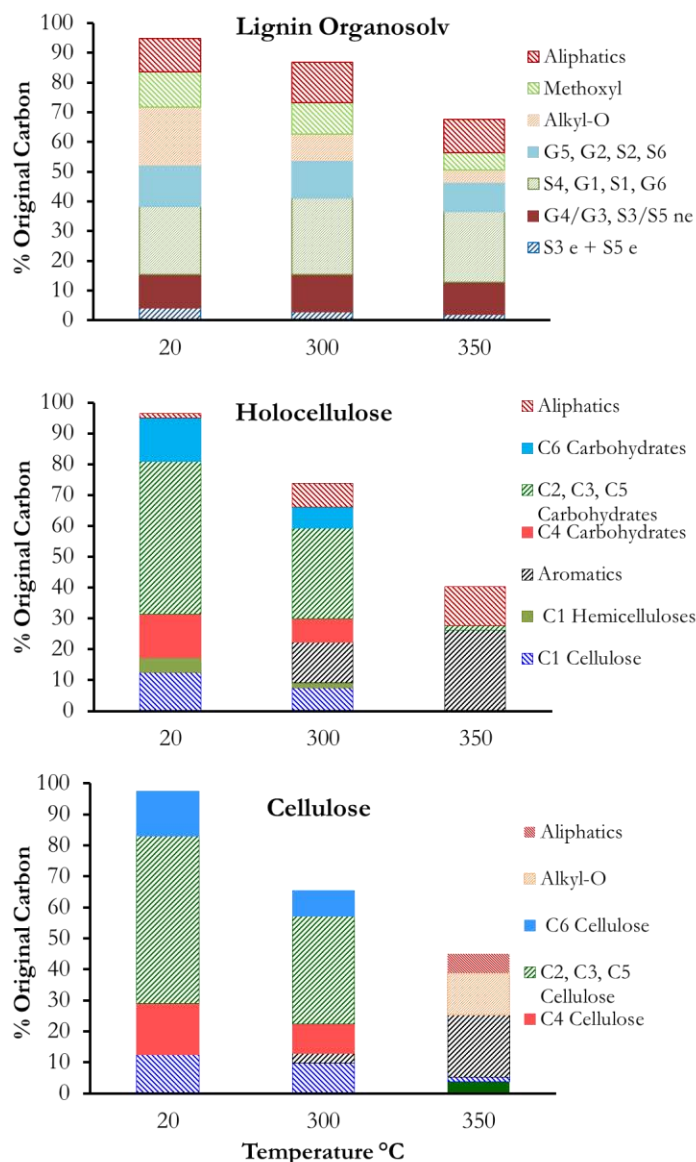


Figure III-19: Evolution of main moieties (% Original Carbons) during pyrolysis for extracted macromolecules as a function of temperature

### Evolution of cellulose chars

Concerning cellulose, the  $^{13}\text{C}$  CP-MAS APHH spectra of the fractionated cellulose before pyrolysis (Figure III-18) shows a typical carbon structure of cellulose<sup>24</sup>. Chemical shift ranges of 103-107, 80-90, 60-67 ppm are respectively attributed to C<sub>1</sub>, C<sub>4</sub> (ordered and disordered) and C<sub>6</sub> (Table III-4). The region of 68 to 80 ppm is assigned to C<sub>2</sub>, C<sub>3</sub> and C<sub>5</sub>. After heat treatment until 300°C, an important weight loss is observed (~30%) but the formation of aromatic carbons is not significant. This observation is in accordance with previous investigations<sup>28,29</sup>. The weight loss is due to the escape of primary volatiles and does not lead to important aromatic structures in the solid. Nevertheless the structure of cellulose is modified. The broadening of the signal at 75 ppm could be explained by an increase in the disorder of the cellulose due to the dispersion of the

chemical shift and non-uniform chemical environment. It is important to note that this effect could be also due to the paramagnetic centres<sup>24,29,57</sup>. The increase of disorder in cellulose is measured at the atomic scale by the NMR and it cannot be related to the evolution of crystallinity determined by XRD<sup>58</sup>. Indeed, the crystallinity index analysed by XRD was similar between 20 and 300°C.

At 300°C, weak signals observed at 130 and 146 ppm could be attributed to the beginning of the formation of aromatic carbons. The first signal could be assigned to the formation of furanic structures<sup>28,50</sup> and the second to the formation of aromatic rings.

At 350°C, important changes occur in the composition of cellulose char. Indeed, only peaks at 105ppm (C<sub>1</sub> cellulose) and 75ppm (C<sub>2</sub>, C<sub>3</sub>, C<sub>5</sub> carbohydrates) from the native carbon structure can be distinguished. The formation of aromatic and aliphatic moieties is clearly observable. The signal in the range of 155-105 ppm has been deconvoluted following the method proposed by Falco et al<sup>50</sup> in order to segregate furan moieties from arene ones. Signals at 151 and 142 ppm could correspond to non-protonated  $\alpha$ -carbon of furan rings and the signals at 118 and 110 ppm can be assigned to substituted and protonated  $\beta$ -carbon of furan rings respectively. Signals at 132 and 126 ppm correspond to aromatic rings. The resonance region between 151 and 142 ppm could also correspond to C=C-O present in phenolic structures. However the conversion of MxG cellulose (with minerals, see supplementary information) leads to the formation of furanic molecules (5-hydroxymethylfurfural, furfuraldehyde, etc.) as evidenced in our group by mass spectrometry analysis of the volatiles<sup>59</sup>. For this reason, the chemical shift band of 151-105 ppm is most probably assigned to furanic structure in char instead of phenolic structures, as already proposed in literature<sup>50,60</sup>. The formation of carbonyls (170 ppm) and ketones (200 ppm) carbons is also observed for cellulose at 350°C. C=O functions could be formed by the dehydration of glucose units. These moieties could be present in intermediate liquid compounds which could remain entrapped in the char structure<sup>3,9,18</sup> after the fast quenching. The formation of aliphatic moieties is also observed at 350°C (range of 33 to 10 ppm). These signals could be attributed to the formation of methylene bridges<sup>30</sup> between aromatic and furanic rings.

To sum-up, the analysis of char from the isolated cellulose reveals the following points:

- 1) Cellulose generates a furanic-aromatic char structure which is also observed in MxG chars;
- 2) Cellulose aromatization occurs only above 300°C indicating that aromatic structures formed at lower temperatures from carbohydrates in the raw miscanthus are mainly attributed to the conversion of hemicelluloses in miscanthus.

### **Evolution of holocellulose chars**

The NMR signal of holocellulose is not significantly different than those of cellulose. The main difference is the presence of hemicelluloses signals mixed with cellulose ones. Hemicelluloses are mainly composed of xylan in MxG<sup>61</sup> (Table III-4). The xylan network includes acetyl functions with signals corresponding to carbonyl carbons (n°1) and methyl carbons (n°15). Signals of hemiacetalic carbons of cellulose (n°7) and xylan C<sub>1</sub> (n°8) are also found. The presence of ordered and disordered cellulose is indicated by carbohydrate carbons C<sub>4</sub> (signals n°9 and n°10, respectively). These signals are overlapped by the ones from xylan C<sub>4</sub>. Cellulose fraction leads also to signals related to carbons C<sub>2</sub>, C<sub>3</sub> and C<sub>5</sub> (n°11) and C<sub>6</sub> (n°12). These two peaks are also overlapped by signals corresponding to xylan carbons C<sub>2</sub>, C<sub>3</sub> and xylan carbons C<sub>5</sub>, respectively.

At 300°C, the intensity of carbohydrate peaks decreases showing that hemicelluloses and cellulose were partially converted. Unlike cellulose, much more aromatic carbons are formed from holocellulose at 300°C. This result confirms that aromatic carbons formed from carbohydrates during the raw miscanthus pyrolysis at 300°C are mainly due to xylan conversion. Xylan is less stable than cellulose and its char yield is higher than cellulose, due to the different thermal stability of the monomer units and to the different crystallinity of the

polymers<sup>62</sup>. The formation of aliphatic moieties (peak centered at 35 ppm<sup>30</sup>) and ketones (200 ppm) are also observed in holocellulose biochars.

Signal from aromatic carbons could be divided in two main peaks:

- 1) One peak centered at 147 ppm which refers to oxygenated aromatic carbons probably included in furanic-aromatic structure;
- 2) Second peak centered at 125 ppm attributed to non-oxygenated aromatic carbons.

In order to have a better understanding of holocellulose char, a 2D solid state NMR <sup>1</sup>H-<sup>13</sup>C HETCOR experiment has been performed (presented in Figure III-20).

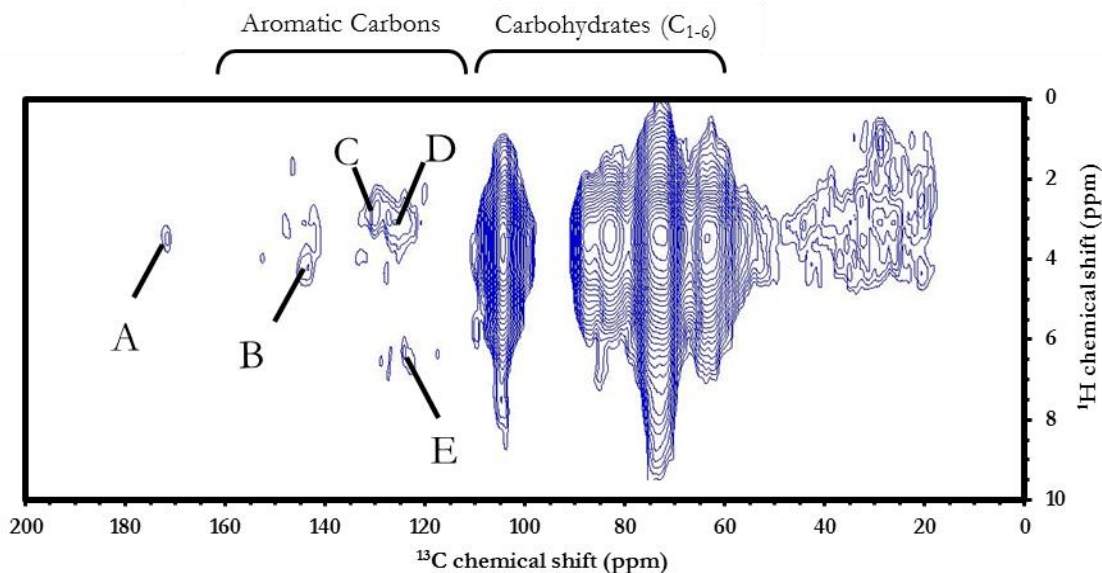


Figure III-20: <sup>1</sup>H-<sup>13</sup>C HETCOR spectra from holocellulose biochar produced at 300°C

It appears from Figure III-20 that carbonyl functions assigned to acetate moieties (peak labeled A, 173-172/3.7-3.1) are not totally converted at 300°C while they are completely converted in miscanthus at this same temperature<sup>47</sup>. This difference may be explained by the effect of the network in native miscanthus or by the higher content in minerals in miscanthus which may promote the conversion of acetate moieties. Different correlations are detected in the range of aromatic carbon chemical shift (155-110 ppm) and they are tentatively assigned in table III-5.

Table III-5: Tentative assignment of 2D <sup>1</sup>H-<sup>13</sup>C correlations analysed in holocellulose char at 300°C

N°	δC/δH (ppm)	Assignements
A	172-170/3.1-3.7	C <sub>Acetyl</sub> /H <sub>CH-O</sub>
B	145-142/4.5-3.75	C <sub>α-furan</sub> /H <sub>CH-O</sub>
C	130.5-128/3.2-2.5	C <sub>Arom</sub> /H <sub>CH-O</sub>
D	126-122/3.5-2.75	C <sub>Arom</sub> /H <sub>CH-O</sub>
E	124.2-122.5/6.75-6	C <sub>Arom</sub> /H <sub>arom</sub>

At 350°C, the carbohydrates are completely converted and the char is mainly composed of aromatic and aliphatic carbons (Figures III-18 and III-19).

### Evolution of lignin chars

The quantitative evolution of chemical moieties in lignin organosolv (EOL) as a function of temperature is given in Figures III-18 and III-19. The carbon structure of EOL (at 20°C) is quite similar than other studies<sup>16,31</sup>. Carbonyl signal is observed at 170 ppm. These carbons correspond to acetate or *p*-coumarate groups consequent to the acetylation of the lignin propyl side chain. Concerning aromatic carbons (154-104 ppm), carbons S<sub>3</sub> and S<sub>5</sub> from etherified syringyl (signal n°2 in Table III-4 and Figure III-18) were detected in the range of 154-152 ppm. Guaiacyl units (G<sub>3</sub> and G<sub>4</sub>) and syringyl units (S<sub>3</sub> and S<sub>5</sub> non-etherified) are observed between 150-144 ppm (n°3). Carbons G<sub>1</sub> and G<sub>6</sub> from guaiacyl units and carbons S<sub>1</sub> and S<sub>4</sub> were detected in the range of 141-120 ppm (n°4). Broad signal at 116-104 ppm is attributed to carbons G<sub>5</sub> and G<sub>2</sub> from guaiacyl units and carbons S<sub>2</sub> and S<sub>6</sub> from syringyl units (n°5 and 6). Signals between 90 and 59 ppm were assigned to lignin oxygenated aliphatic carbons (C<sub>α</sub>, C<sub>β</sub>, C<sub>γ</sub>). Methoxyl groups of lignin phenolic units appear at 56 ppm (n°13). Methylene carbons, CH<sub>3</sub> in acetyl groups and δ methyl in n-propyl chains are assigned to peaks at 30, 20, and 15 ppm, respectively.

Concerning lignin char produced at 300°C, the main changes occur on carbons from the oxygenated propyl chain (C<sub>α</sub>, C<sub>β</sub>, C<sub>γ</sub>). The cleavage of the α and β-aryl-ether linkages<sup>14,31</sup> in the lignin network is observed. This cleavage should lead to the formation of alkene carbons<sup>63</sup> in the range of 140-110 ppm. However due to important overlap, it is difficult to evidence them. Ether linkages at γ position on the propyl chain seem to be more stable because of the significant peak observed at 59 ppm. This finding is in agreement with previous works<sup>13,16</sup>. The cleavage of aryl-ether linkages is confirmed by the decrease of the carbons S<sub>3</sub> and S<sub>5</sub> from etherified syringyl units. Moreover the signal in the range of 150-144 ppm increases highlighting the formation of S<sub>3</sub> and S<sub>5</sub> from non-etherified syringyl units<sup>49,64</sup>. The methoxyl groups remain stable in the char. Thus it appears that no obvious demethoxylation is observed at 300°C. This result is not in agreement with previous studies performed using Kraft lignin<sup>16</sup>. This discrepancy could be explained by the different composition of the lignins. The EOL lignin studied here has a very low mineral content. The presence of sodium or potassium, which are present in Kraft lignin, could catalyze the demethoxylation and the demethylation of lignin during pyrolysis<sup>65,66</sup>.

Carbonyl carbons in lignin decrease at 300°C, showing the cleavage of acetylated linkages which are present in our lignin. The amount of aliphatic carbons is roughly constant but their nature is modified. Methyl acetates (20 ppm) and methyl in n-propyl chain (15 ppm) have been converted.

At 350°C, signals from S<sub>3</sub> and S<sub>5</sub> have almost disappeared, showing that the β-O-4 linkages between syringyl units and propyl chain are almost completely converted at this temperature. Moreover, the content in methoxyl groups decreases between 300 and 350°C. This could be explained by: (1) demethoxylation of the aromatics, (2) demethylation, (3) the release of volatile compounds composed of methoxyl groups (e.g. guaiacol, syringol, etc.). The decrease in aromatic carbons in the char is much lower (-7.4% mol. based on the original carbon) than the decrease in the methoxyl groups (-50% mol.). Moreover, no significant evolution of the oxygenated aromatic carbons and of the protonated aromatic carbons can be observed. Consequently, the decrease in methoxyl content can rather be attributed to demethylation instead of demethoxylation reactions. This finding is consistent with theoretical chemistry studies on lignin model compounds<sup>63,67</sup> which reveal that the dissociation energy of the O-CH<sub>3</sub> bonds is weaker than the one of the C<sub>ar</sub>-O bonds. We observed a higher decrease in methoxyl groups at 350°C in miscanthus than in lignin most probably because of a higher content in minerals in miscanthus. Ether linkages at γ position on the propyl chain seem to be present at 350°C. The yields in aliphatic and methylene carbons are stable between 300 and 350°C.

**Interactions inside the network of biomass for aromatic structure formation**

Potential interactions between the different polymers may occur in the native network of miscanthus and affect the yield in aromatic carbons formation. To investigate this hypothesis, the yields in aromatic carbons (mole of C arom/ g of biomass) produced during the pyrolysis of miscanthus (carbohydrates+lignin together in the same network of native biomass) and of the sum of holocellulose+lignin (fractionated from Miscanthus and pyrolysed at different temperatures) are compared in Figure III-21. The yield corresponding to the sum of aromatic carbons holocellulose+lignin is noted as nCaf (a for aromatic and f for “fractionated” biomass), it is calculated as:

$$nCaf(Tx) = \frac{nCaL(Tx) \times \%wtKlason\ Lignin + nCaH(Tx) \times \%wtSugar}{100}$$

nCaf(Tx) is the amount (mmol) of aromatic carbons present in “fractionated” biomass at the temperature Tx. nCaL(Tx) and nCaH(Tx) are the amount (mmol) of aromatic carbons for 1g of non-pyrolyzed material present in Lignin Organosolv and Holocellulose respectively at the temperature Tx.

Before pyrolysis, only lignin contributes to the yield in aromatic carbons for the fractionated biomass (no aromatic carbons present in holocellulose). A difference between aromatic yield in native MxG (4.5 mmol arom/g of biomass) and fractionated biomass (7.6 mmol/g) can be observed in Figure III-21. This could be explained by the impact of the Organosolv extraction which increases significantly the “aromatization” of lignin through degradation and dehydration on the lignin side chains<sup>40</sup>. As can be seen in Figure III-21, 1) the aromatic contents in fractionated biomass are more important compared to raw MxG ; 2) the aromatic content increases with the pyrolysis temperature. Nevertheless, it appears that the yields in aromatic carbons formed during the thermal treatment from fractionated or native biomass are similar: 3.3 and 5.2 mmol/g formed at 300 and 350°C respectively for the fractionated biomass and 3.4 and 5.1 mmol/g for the native biomass. However, based on the yield in aromatic in the materials, much more aromatic carbons are formed during the pyrolysis of the native biomass. At 300°C the increase is about 80 % of the starting content for the native biomass (3.4/4.2 mmol/g) whereas it is only 43 % for the fractionated one (3.3/7.8 mmol/g). At 350°C, this is about 113 % for the native biomass and 69 % for the fractionated one. Based on Figure III-17 and our previous discussion, the increase in the aromatic carbons is mainly attributed to the conversion of holocellulose. The conversion of lignin (in the native network or fractionated) does not create an important yield in new aromatic carbons, compared to the aromatic carbons formed by the pyrolysis of holocellulose. Consequently, the difference between the fractionated and native biomass may be mainly explained by the fact that the extracted lignin is more aromatic than the native one in the network.

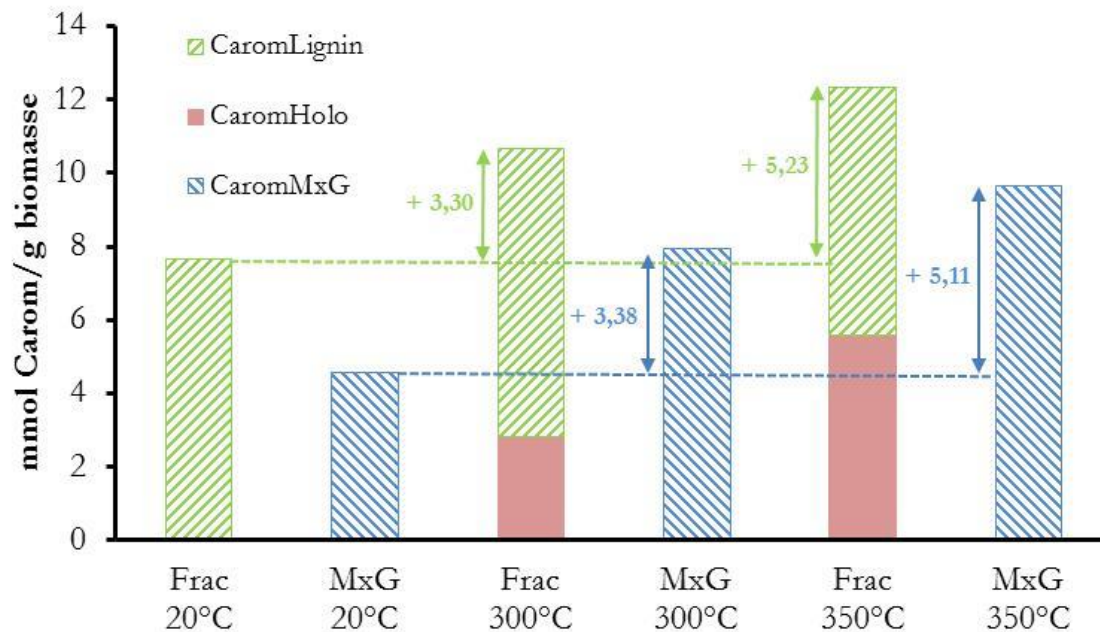


Figure III-21: Quantitative evolution of aromatic carbons (mmolC/g biomass) into MxG char and fractionated biomass as a function of temperature

### III.2.5 Conclusion

Thanks to the peculiar behavior of the chars under carefully set APHH CP/MAS conditions we were able to highly speed-up the  $^{13}\text{C}$  NMR quantitative analysis of carbon moieties in char, reducing significantly the accumulation time compared to DP/MAS. The evolution of chemical moieties in chars derived from miscanthus and macromolecules fractionated from the miscanthus network (cellulose, holocellulose and lignin) was studied based on this CP/MAS APHH method as a function of temperature. This allowed obtaining a detailed and quantitative analysis of the different kinds of carbon structures in the pristine biomass, in the extracted macromolecules and in the chars produced at various temperatures. We were then able to follow quantitatively the mechanisms of biomass pyrolysis.

### III.2.6 References

- (1) Ragauskas, A. J. The Path Forward for Biofuels and Biomaterials. *Science* **2006**, *311* (5760), 484–489.
- (2) Mettler, M. S.; Vlachos, D. G.; Dauenhauer, P. J. Top Ten Fundamental Challenges of Biomass Pyrolysis for Biofuels. *Energy Environ. Sci.* **2012**, *5* (7), 7797–7809.
- (3) Lédé, J. Cellulose Pyrolysis Kinetics: An Historical Review on the Existence and Role of Intermediate Active Cellulose. *J. Anal. Appl. Pyrolysis* **2012**, No. 0.
- (4) Bahng, M.-K.; Mukarakate, C.; Robichaud, D. J.; Nimlos, M. R. Current Technologies for Analysis of Biomass Thermochemical Processing: A Review. *Anal. Chim. Acta* **2009**, *651* (2), 117–138.
- (5) Shen, D. K.; Gu, S. The Mechanism for Thermal Decomposition of Cellulose and Its Main Products. *Bioresour. Technol.* **2009**, *100* (24), 6496–6504.
- (6) Nowakowski, D. J.; Bridgwater, A. V.; Elliott, D. C.; Meier, D.; de Wild, P. Lignin Fast Pyrolysis: Results from an International Collaboration. *J. Anal. Appl. Pyrolysis* **2010**, *88* (1), 53–72.
- (7) Shen, D. K.; Gu, S.; Bridgwater, A. V. Study on the Pyrolytic Behaviour of Xylan-Based Hemicellulose Using TG–FTIR and Py–GC–FTIR. *J. Anal. Appl. Pyrolysis* **2010**, *87* (2), 199–206.
- (8) Dufour, A.; Castro-Diaz, M.; Brosse, N.; Bouroukba, M.; Snape, C. The Origin of Molecular Mobility During Biomass Pyrolysis as Revealed by In Situ <sup>1</sup>H NMR Spectroscopy. *ChemSusChem* **2012**, *5* (7), 1258–1265.
- (9) Dufour, A.; Castro-Diaz, M.; Marchal, P.; Brosse, N.; Olcese, R.; Bouroukba, M.; Snape, C. In Situ Analysis of Biomass Pyrolysis by High Temperature Rheology in Relations with <sup>1</sup>H NMR. *Energy Fuels* **2012**, *26* (10), 6432–6441.
- (10) Nowakowski, D. J.; Jones, J. M. Uncatalysed and Potassium-Catalysed Pyrolysis of the Cell-Wall Constituents of Biomass and Their Model Compounds. *J. Anal. Appl. Pyrolysis* **2008**, *83* (1), 12–25.
- (11) Eom, I.-Y.; Kim, J.-Y.; Lee, S.-M.; Cho, T.-S.; Choi, I.-G.; Choi, J.-W. Study on the Thermal Decomposition Features and Kinetics of Demineralized and Inorganic Metal-Impregnated Lignocellulosic Biomass. *J. Ind. Eng. Chem.* **2012**, *18* (6), 2069–2075.
- (12) Shen, D. K.; Gu, S.; Bridgwater, A. V. Study on the Pyrolytic Behaviour of Xylan-Based Hemicellulose Using TG–FTIR and Py–GC–FTIR. *J. Anal. Appl. Pyrolysis* **2010**, *87* (2), 199–206.
- (13) Pandey, M. P.; Kim, C. S. Lignin Depolymerization and Conversion: A Review of Thermochemical Methods. *Chem. Eng. Technol.* **2011**, *34* (1), 29–41.
- (14) Kawamoto, H.; Horigoshi, S.; Saka, S. Pyrolysis Reactions of Various Lignin Model Dimers. *J. Wood Sci.* **2007**, *53* (2), 168–174.
- (15) Jakab, E.; Faix, O.; Till, F. Thermal Decomposition of Milled Wood Lignins Studied by Thermogravimetry/mass Spectrometry. *J. Anal. Appl. Pyrolysis* **1997**, *40–41*, 171–186.
- (16) Sharma, R. K.; Wooten, J. B.; Baliga, V. L.; Lin, X. H.; Chan, W. G.; Hajaligol, M. R. Characterization of Chars from Pyrolysis of Lignin. *Fuel* **2004**, *83* (11–12), 1469–1482.
- (17) Broido, A.; Javier-Son, A. C.; Ouano, A. C.; Barrall, E. M. Molecular Weight Decrease in the Early Pyrolysis of Crystalline and Amorphous Cellulose. *J. Appl. Polym. Sci.* **1973**, *17* (12), 3627–3635.
- (18) Mamleev, V.; Bourbigot, S.; Le Bras, M.; Yvon, J. The Facts and Hypotheses Relating to the Phenomenological Model of Cellulose Pyrolysis. *J. Anal. Appl. Pyrolysis* **2009**, *84* (1), 1–17.
- (19) Sivonen, H.; Maunu, S. L.; Sundholm, F.; Jämsä, S.; Viitaniemi, P. Magnetic Resonance Studies of Thermally Modified Wood. *Holzforschung* **2002**, *56* (6).
- (20) Freitas, Cunha; Emmerich. Solid-State Nuclear Magnetic Resonance (NMR) Methods Applied to the Study of Carbon Materials. In *Chemistry & Physics of Carbon*; Chemistry and Physics of Carbon; CRC Press, 2012; pp 85–170.
- (21) Mao, J.-D.; Holtman, K. M.; Franqui-Villanueva, D. Chemical Structures of Corn Stover and Its Residue after Dilute Acid Prehydrolysis and Enzymatic Hydrolysis: Insight into Factors Limiting Enzymatic Hydrolysis. *J. Agric. Food Chem.* **2010**, *58* (22), 11680–11687.
- (22) Melkior, T.; Jacob, S.; Gerbaud, G.; Hediger, S.; Le Pape, L.; Bonnefois, L.; Bardet, M. NMR Analysis of the Transformation of Wood Constituents by Torrefaction. *Fuel* **2012**, *92* (1), 271–280.

- (23) Cao, X.; Pignatello, J. J.; Li, Y.; Latta, C.; Chappell, M. A.; Chen, N.; Miller, L. F.; Mao, J. Characterization of Wood Chars Produced at Different Temperatures Using Advanced Solid-State  $^{13}\text{C}$  NMR Spectroscopic Techniques. *Energy Fuels* **2012**, *26* (9), 5983–5991.
- (24) Foston, M. Advances in Solid-State NMR of Cellulose. *Curr. Opin. Biotechnol.* **2014**, *27*, 176–184.
- (25) Brewer, C. E.; Schmidt-Rohr, K.; Satrio, J. A.; Brown, R. C. Characterization of Biochar from Fast Pyrolysis and Gasification Systems. *Environ. Prog. Sustain. Energy* **2009**, *28* (3), 386–396.
- (26) Mao, J.; Hu, W.; Ding, G.; Schmidt-Rohr, K.; Davies, G.; Ghabbour, E.; Xing, B. Suitability of Different  $^{13}\text{C}$  Solid-State NMR Techniques in the Characterization of Humic Acids. *Int. J. Environ. Anal. Chem.* **2002**, *82* (4), 183–196.
- (27) Freitas, J. C. C.; Bonagamba, T. J.; Emmerich, F. G.  $^{13}\text{C}$  High-Resolution Solid-State NMR Study of Peat Carbonization. *Energy Fuels* **1999**, *13* (1), 53–59.
- (28) Zhang, X.; Golding, J.; Burgar, I. Thermal Decomposition Chemistry of Starch Studied by  $^{13}\text{C}$  High-Resolution Solid-State NMR Spectroscopy. *Polymer* **2002**, *43* (22), 5791–5796.
- (29) Wooten, J. B.; Seeman, J. I.; Hajaligol, M. R. Observation and Characterization of Cellulose Pyrolysis Intermediates by  $^{13}\text{C}$  CPMAS NMR. A New Mechanistic Model. *Energy Fuels* **2004**, *18* (1), 1–15.
- (30) Inari, G. N.; Mounquengui, S.; Dumarçay, S.; Pétrissans, M.; Gérardin, P. Evidence of Char Formation during Wood Heat Treatment by Mild Pyrolysis. *Polym. Degrad. Stab.* **2007**, *92* (6), 997–1002.
- (31) Brosse, N.; El Hage, R.; Chaouch, M.; Pétrissans, M.; Dumarçay, S.; Gérardin, P. Investigation of the Chemical Modifications of Beech Wood Lignin during Heat Treatment. *Polym. Degrad. Stab.* **2010**, *95* (9), 1721–1726.
- (32) Ben, H.; Ragauskas, A. J. Torrefaction of Loblolly Pine. *Green Chem.* **2012**, *14* (1), 72–76.
- (33) Baccile, N.; Falco, C.; Titirici, M.-M. Characterization of Biomass and Its Derived Char Using  $^{13}\text{C}$ -Solid State Nuclear Magnetic Resonance. *Green Chem.* **2014**, *16* (12), 4839–4869.
- (34) Boroson, M. L.; Howard, J. B.; Longwell, J. P.; Peters, W. A. Heterogeneous Cracking of Wood Pyrolysis Tars over Fresh Wood Char Surfaces. *Energy Fuels* **1989**, *3* (6), 735–740.
- (35) Hologne, M.; Bertani, P.; Azais, T.; Bonhomme, C.; Hirschinger, J.  $^1\text{H}/^{31}\text{P}$  Distance Determination by Solid State NMR in Multiple-Spin Systems. *Solid State Nucl. Magn. Reson.* **2005**, *28* (1), 50–56.
- (36) Hediger, S.; Meier, B. H.; Kurur, N. D.; Bodenhausen, G.; Ernst, R. R. NMR Cross Polarization by Adiabatic Passage through the Hartmann—Hahn Condition (APHH). *Chem. Phys. Lett.* **1994**, *223* (4), 283–288.
- (37) Hervé, M.; Hirschinger, J.; Granger, P.; Gilard, P.; Deflandre, A.; Goetz, N. A  $^{13}\text{C}$  Solid-State NMR Study of the Structure and Auto-Oxidation Process of Natural and Synthetic Melanins. *Biochim. Biophys. Acta BBA - Protein Struct. Mol. Enzymol.* **1994**, *1204* (1), 19–27.
- (38) Brosse, N.; Dufour, A.; Meng, X.; Sun, Q.; Ragauskas, A. Miscanthus: A Fast-Growing Crop for Biofuels and Chemicals Production. *Biofuels Bioprod. Biorefining* **2012**, *6* (5), 580–598.
- (39) Hodgson, E. M.; Nowakowski, D. J.; Shield, I.; Riche, A.; Bridgwater, A. V.; Clifton-Brown, J. C.; Donnison, I. S. Variation in Miscanthus Chemical Composition and Implications for Conversion by Pyrolysis and Thermo-Chemical Bio-Refining for Fuels and Chemicals. *Bioresour. Technol.* **2011**, *102* (3), 3411–3418.
- (40) El Hage, R.; Brosse, N.; Chrusciel, L.; Sanchez, C.; Sannigrahi, P.; Ragauskas, A. Characterization of Milled Wood Lignin and Ethanol Organosolv Lignin from Miscanthus. *Polym. Degrad. Stab.* **2009**, *94* (10), 1632–1638.
- (41) Goh, C. S.; Tan, H. T.; Lee, K. T.; Brosse, N. Evaluation and Optimization of Organosolv Pretreatment Using Combined Severity Factors and Response Surface Methodology. *Biomass Bioenergy* **2011**, *35* (9), 4025–4033.
- (42) Brosse, N.; Sannigrahi, P.; Ragauskas, A. Pretreatment of Miscanthus X Giganteus Using the Ethanol Organosolv Process for Ethanol Production. *Ind. Eng. Chem. Res.* **2009**, *48* (18), 8328–8334.
- (43) Carignan, J.; Hild, P.; Mevelle, G.; Morel, J.; Yeghicheyan, D. Routine Analyses of Trace Elements in Geological Samples Using Flow Injection and Low Pressure On-Line Liquid Chromatography Coupled to ICP-MS: A Study of Geochemical Reference Materials BR, DR-N, UB-N, AN-G and GH. *Geostand. Newsl.* **2001**, *25* (2-3), 187–198.

- (44) Elmay, Y.; Brech, Y. L.; Delmotte, L.; Dufour, A.; Brosse, N.; Gadiou, R. Characterization of Miscanthus Pyrolysis by DRIFTS, UV Raman Spectroscopy and Mass Spectrometry. *J. Anal. Appl. Pyrolysis*.
- (45) Baumlin, S.; Broust, F.; Ferrer, M.; Meunier, N.; Marty, E.; Lédé, J. The Continuous Self Stirred Tank Reactor: Measurement of the Cracking Kinetics of Biomass Pyrolysis Vapours. *Chem. Eng. Sci.* **2005**, *60* (1), 41–55.
- (46) Olcese, R. N.; Lardier, G.; Bettahar, M.; Ghanbaja, J.; Fontana, S.; Carré, V.; Aubriet, F.; Petitjean, D.; Dufour, A. Aromatic Chemicals by Iron-Catalyzed Hydrotreatment of Lignin Pyrolysis Vapor. *ChemSusChem* **2013**, *6* (8), 1490–1499.
- (47) Le Brech, Y.; Delmotte, L.; Raya, J.; Brosse, N.; Gadiou, R.; Dufour, A. High Resolution Solid State 2D NMR Analysis of Biomass and Biochar. *Anal. Chem.* **2015**, *87* (2), 843–847.
- (48) Massiot, D.; Fayon, F.; Capron, M.; King, I.; Le Calv, S.; Alonso, B.; Durand, J.-O.; Bujoli, B.; Gan, Z.; Hoatson, G. Modelling One- and Two-Dimensional Solid-State NMR Spectra. *Magn. Reson. Chem.* **2002**, *40* (1), 70–76.
- (49) Melkior, T.; Jacob, S.; Gerbaud, G.; Hediger, S.; Le Pape, L.; Bonnefois, L.; Bardet, M. NMR Analysis of the Transformation of Wood Constituents by Torrefaction. *Fuel* **2012**, *92* (1), 271–280.
- (50) Falco, C.; Perez Caballero, F.; Babonneau, F.; Gervais, C.; Laurent, G.; Titirici, M.-M.; Baccile, N. Hydrothermal Carbon from Biomass: Structural Differences between Hydrothermal and Pyrolyzed Carbons via <sup>13</sup>C Solid State NMR. *Langmuir* **2011**, *27* (23), 14460–14471.
- (51) Bardet, M.; Gerbaud, G.; Giffard, M.; Doan, C.; Hediger, S.; Pape, L. L. <sup>13</sup>C High-Resolution Solid-State NMR for Structural Elucidation of Archaeological Woods. *Prog. Nucl. Magn. Reson. Spectrosc.* **2009**, *55* (3), 199–214.
- (52) Lahaye, M.; Rondeau-Mouro, C.; Deniaud, E.; Buléon, A. Solid-State <sup>13</sup>C NMR Spectroscopy Studies of Xylans in the Cell Wall of *Palmaria Palmata* (L. Kuntze, Rhodophyta). *Carbohydr. Res.* **2003**, *338* (15), 1559–1569.
- (53) Bardet, M.; Lundquist, K.; Parkäs, J.; Robert, D.; von Unge, S. <sup>13</sup>C Assignments of the Carbon Atoms in the Aromatic Rings of Lignin Model Compounds of the Arylglycerol B-Aryl Ether Type. *Magn. Reson. Chem.* **2006**, *44* (10), 976–979.
- (54) Collura, S.; Azambre, B.; Weber, J.-V. Thermal Behaviour of Miscanthus Grasses, an Alternative Biological Fuel. *Environ. Chem. Lett.* **2007**, *5* (1), 49–49.
- (55) Szabó, P.; Várhegyi, G.; Till, F.; Faix, O. Thermogravimetric/mass Spectrometric Characterization of Two Energy Crops, *Arundo Donax* and *Miscanthus Sinensis*. *J. Anal. Appl. Pyrolysis* **1996**, *36* (2), 179–190.
- (56) Ralph, J.; Grabber, J. H.; Hatfield, R. D. Lignin-Ferulate Cross-Links in Grasses: Active Incorporation of Ferulate Polysaccharide Esters into Ryegrass Lignins. *Carbohydr. Res.* **1995**, *275* (1), 167–178.
- (57) Atalla, R. H.; VanderHart, D. L. The Role of Solid-State Carbon-13 NMR Spectroscopy in Studies of the Nature of Native Celluloses. *Solid State Nucl. Magn. Reson.* **1999**, *15* (1), 1–19.
- (58) Park, S.; Baker, J. O.; Himmel, M. E.; Parilla, P. A.; Johnson, D. K. Cellulose Crystallinity Index: Measurement Techniques and Their Impact on Interpreting Cellulase Performance. *Biotechnol. Biofuels* **2010**, *3*.
- (59) Dufour, A.; Weng, J.; Jia, L.; Tang, X.; Sirjean, B.; Fournet, R.; Gall, H. L.; Brosse, N.; Billaud, F.; Mauviel, G.; Qi, F. Revealing the Chemistry of Biomass Pyrolysis by Means of Tunable Synchrotron Photoionisation-Mass Spectrometry. *RSC Adv.* **2013**, *3* (14), 4786–4792.
- (60) Aydıncak, K.; Yumak, T.; Sınağ, A.; Esen, B. Synthesis and Characterization of Carbonaceous Materials from Saccharides (Glucose and Lactose) and Two Waste Biomasses by Hydrothermal Carbonization. *Ind. Eng. Chem. Res.* **2012**, *51* (26), 9145–9152.
- (61) Lygin, A. V.; Upton, J.; Dohleman, F. G.; Juvik, J.; Zabolina, O. A.; Widholm, J. M.; Lozovaya, V. V. Composition of Cell Wall Phenolics and Polysaccharides of the Potential Bioenergy Crop -Miscanthus: *GCB Bioenergy* **2011**, *3* (4), 333–345.
- (62) Collard, F.-X.; Blin, J. A Review on Pyrolysis of Biomass Constituents: Mechanisms and Composition of the Products Obtained from the Conversion of Cellulose, Hemicelluloses and Lignin. *Renew. Sustain. Energy Rev.* **2014**, *38*, 594–608.

- (63) Faravelli, T.; Frassoldati, A.; Migliavacca, G.; Ranzi, E. Detailed Kinetic Modeling of the Thermal Degradation of Lignins. *Biomass Bioenergy* **2010**, *34* (3), 290–301.
- (64) Wikberg, H.; Lüsamaunu, S. Characterisation of Thermally Modified Hard- and Softwoods by C CPMAS NMR. *Carbohydr. Polym.* **2004**, *58* (4), 461–466.
- (65) Kleen, M.; Gellerstedt, G. Influence of Inorganic Species on the Formation of Polysaccharide and Lignin Degradation Products in the Analytical Pyrolysis of Pulps. *J. Anal. Appl. Pyrolysis* **1995**, *35* (1), 15–41.
- (66) Sharma, R. K.; Hajaligol, M. R. Effect of Pyrolysis Conditions on the Formation of Polycyclic Aromatic Hydrocarbons (PAHs) from Polyphenolic Compounds. *J. Anal. Appl. Pyrolysis* **2003**, *66* (1–2), 123–144.
- (67) Nowakowska, M.; Herbinet, O.; Dufour, A.; Glaude, P.-A. Detailed Kinetic Study of Anisole Pyrolysis and Oxidation to Understand Tar Formation during Biomass Combustion and Gasification. *Combust. Flame* **2014**, *161* (6), 1474–1488.

### **III.2.7 Supporting information**

#### **Mechanism of biomass char formation investigated by advanced solid state NMR**

Yann Le Brech<sup>1</sup>, Jesus Raya<sup>2‡</sup>, Luc Delmotte<sup>3‡</sup>, Nicolas Brosse<sup>4</sup>, Roger Gadiou<sup>3</sup>, Anthony Dufour<sup>1\*</sup>

<sup>1</sup> LRGP, CNRS, Université de Lorraine, 1 rue Grandville 54000 Nancy, France

<sup>2</sup> ICS, CNRS, Université de Strasbourg, 1 rue Blaise Pascal BP 296 R8 67008 Strasbourg Cedex, France

<sup>3</sup> IS2M, CNRS, Université de Haute Alsace, 15, rue Jean Starcky BP 2488 68057 Mulhouse cedex, France

<sup>4</sup> LERMAB, Université de Lorraine, BP239 54506 Vandoeuvre les Nancy cedex, France.

#### **Extraction procedure**

##### **Lignin extraction by the ethanol organosolv process**

25 g dry matter of Miscanthus (extractive-free and milled) was treated with aqueous ethanol (65 %Ethanol v/v) and sulfuric acid as a catalyst (1 %w/w). The solid to liquid ratio used was 1:8. The treatment was carried out in a 0.6 L Parr Reactor (Parr 4836). The reaction mixture was heated (180°C/60 min) with continuous stirring. The pressure increased to 20-25 bars. The pretreated Miscanthus was filtered and washed with 60°C ethanol/water (80/20 3\*50 ml) and then dried over the night (oven at 40°C/12 h). Three volumes of water were added to the filtrate in order to precipitate the Ethanol Organosolv Lignin. The mixtures were kept in a fridge over the night (5°C/12 h) in order to improve precipitation. The precipitate Ethanol Organosolv Lignin was collected by centrifugation (4000 rtm/20 min) and dried over the night (40°C/12 h).

##### **Holocellulose extraction**

80 g oven dried Miscanthus (extractive-free and milled) was dispersed in to 6 L de-ionized water. The reaction mixture was put in a 10 L jacketed glass reactor. 48 ml glacial acetic acid (CH<sub>3</sub>COOH) and 48 g sodium chlorite (NaClO<sub>2</sub>) were added. Mixture was stirred and heated to 70°C for 6 h. Each 2 hours 48 ml glacial acetic acid and 48 g sodium chlorite were added to the mixture. The solid holocellulose was collected by filtration (using a Buchner funnel and filter paper), vigorously washed with water and dried overnight in a fume hood (40°C).

##### **Cellulose extraction**

8 g of dried holocellulose was treated with 0.5 L of HCl solution (2.5 M) for 4 hours at the temperature of 100°C. The solid cellulose was collected by filtration (using a Buchner funnel and filter paper), vigorously washed with water and dried overnight in a fume hood (40°C).

**Composition**

The carbohydrates, Klason lignin and Organic matter contents have been determined and are presented in Table III-6.

*Table III-6: Composition of Miscanthus and extracted polymers*

Samples	%wt dry biomass Extractive free							
	Total Sugars	Klason Lignin	Organic matter	Glucose	Xylose	Mannose	Galactose	Arabinose
<b>Miscanthus</b>	70,2	29,8	92,4	48,9	18,3	0,0	0,6	2,3
STD	1,8	1,8	3,3	1,3	1,4	0,0	0,0	0,1
<b>Holocellulose</b>	94,8	5,2	96,2	63,7	27,5	0,0	0,4	2,9
STD	0,6	0,6	n.a	0,5	0,7	0,0	0,0	0,1
<b>Cellulose</b>	96,2	3,8	94,2	93,3	2,8	0,0	0,0	0,0
STD	1,7	1,7	n.a	1,6	0,1	0,0	0,0	0,0

The extraction procedure for holocellulose preserves a similar composition in carbohydrates than in the native biomass. The extracted cellulose is mainly composed of glucose.

**ICP analysis**

Samples have been analyzed by ICP-OES and ICP-MS following the CNRS-SARM procedure<sup>1</sup> in order to characterize their mineral. These results are presented Table III-7.

*Table III-7: Inorganics content in the different samples*

	%wt dry basis										
	Si	Al	Fe	Mn	Mg	Ca	Na	K	Ti	P	Total
<b>Miscanthus</b>	1.66	0.16	0.09	0.02	0.10	0.37	0.01	0.65	0.01	0.00	3.06
<b>Holocellulose</b>	1.51	0.09	0.06	0.00	0.02	0.05	0.42	0.04	0.00	0.00	2.19
<b>Cellulose</b>	2.27	0.09	0.00	0.00	0.00	0.00	0.02	0.06	0.00	0.00	2.44
<b>Lignine</b>	0.01	0.00	0.02	0.00	0.00	0.00	0.01	0.06	0.00	0.00	0.11

**Molecular weight distribution analysis***Table III-8: Molecular weight distribution analysis*

<b>Molecular weight distribution</b>			
<b>Samples</b>	<b>Weight average</b>	<b>Number average</b>	<b>Polydispersity</b>
<b>Cellulose</b>	595012	62713	9.5
STD	9496	1899	0.4
<b>Lignine</b>	6891	4956	1.4
STD	31	40	0

The Ethanol Organosolv Lignin was purified with pentane in a Soxhlet apparatus (12 h). The extractive free was dried in an oven overnight. 2ml of acetic anhydride/pyridine (1:1) mixture were added to 20 mg of EOL extractive free. The mixture was kept at room temperature with stirring for 24 hrs. 25 ml of Ethanol were added to the reaction mixture and kept for 30 min. Then ethanol was evaporated. This step was repeated until the acetic anhydride and pyridine were evaporated. Acetylated lignin is dissolved in 2 ml of Chloroform and added solution drop wise to 100 ml magnetically stirred diethyl ether. Precipitated acetylated lignin was collected after centrifugation. Then dissolved in 25 ml THF for GPC investigations.

The dried cellulose samples were derivatized with phenyl isocyanate. About 15 mg of dry cellulose sample was soaked in 4 ml anhydrous pyridine in 25 ml flask, and 0.5 ml phenyl isocyanate was added. The flask was sealed with Teflon-lined cap. The reaction mixture was kept at 65°C in oil bath for 2 ~ 3 days until the cellulose was completely dissolved. The mixture was stirred with magnetic stirring bar. After the reaction completed, the solution was cooled and 1 ml methanol was added to eliminate the unreacted phenyl isocyanate. The mixture was then poured into 100 ml water-methanol (3:7). The precipitated cellulose tricarbanilates were purified through centrifuging at 8000 rpm by repeated washing with water-methanol 3 times, and water 2 times. The cellulose tricarbanilates were then freeze-dried and vacuum dried for analysis. The cellulose tricarbanilates were analyzed for molecular weights (MW) and molecular weight distribution analysis using a Hewlett Packard 1090 series HPLC system consisting of in-line filter and an auto-sampler, a UV detector. The system was calibrated with standard narrow polystyrene samples. The number-average molecular weight (Mn), weight-average molecular weight (Mw) and polydispersity index were calculated by GPC software.

**Elemental analysis**

Elemental analysis of Miscanthus, extracted macromolecules and produced chars were performed on a Thermo Fisher apparatus. Each sample was dried at 105°C during several hours before experiments.

*Table III-9: Elemental analysis of miscanthus and extracted macromolecules*

Samples	T (°C)	%wt (oven dried values)			
		%C	%C <sub>STD</sub>	%H	%H <sub>STD</sub>
Miscanthus	20	42.8	0.6	5.5	0.1
	200	44.1	1.2	5.5	0.2
	250	45.0	0.8	5.4	0.1
	280	45.8	1.1	5.1	0.1
	300	48.9	1.0	4.9	0.1
	320	50.2	1.6	4.3	0.2
	350	54.0	0.5	3.7	0.2
	400	54.6	0.3	2.9	0.2
	500	56.2	0.0	2.4	0.0
Cellulose	20	42.0	0.5	6.0	0.0
	300	43.2	1.0	5.5	0.0
	350	51.1	1.3	3.7	0.0
Holocellulose	20	41.3	0.9	5.7	0.1
	300	47.2	0.1	5.6	0.0
	350	59.7	1.2	3.9	0.2
Lignine Organosolv	20	62.5	1.2	6.0	0.0
	300	66.6	1.5	5.4	0.1
	350	70.4	0.5	5.0	0.1

**Solid-state 1D  $^{13}\text{C}$  NMR deconvolution illustrations**

Deconvolution procedures have been proceed with DMFIT Software developed by Massiot et al.<sup>2</sup>.

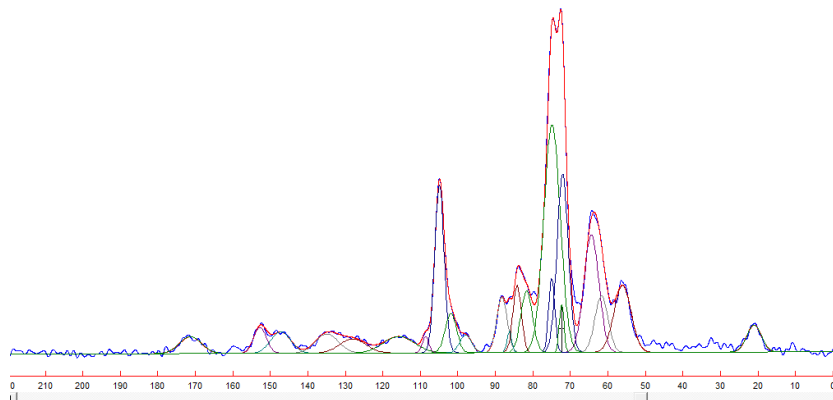


*Figure III-22: Solid-state 1D  $^{13}\text{C}$  CPMAS APHH spectrum of Miscanthus with spectral deconvolution*

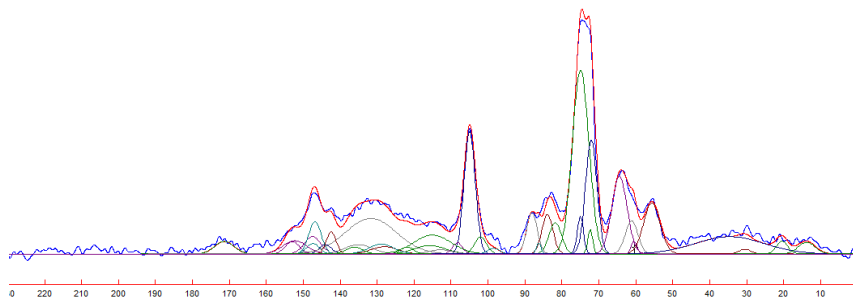


*Figure III-23: Solid-state 1D  $^{13}\text{C}$  CPMAS APHH spectrum of Miscanthus char 300°C with spectral deconvolution*

**Analytical procedure for NMR analysis****1D DP and APHH-CP  $^{13}\text{C}\{^1\text{H}\}$  experiments**

All 1D spectra were obtained on a Bruker™ AVANCE 500MHz wide bore spectrometer operating at a  $^{13}\text{C}$  frequency of 125MHz. Samples were spun in 3.2 mm od zirconia rotors (closed with KeI-F caps) at 18 kHz spinning frequency on a triple resonance MAS 3.2mm Bruker™ probe operating in double mode ( $^1\text{H}$ - $^{13}\text{C}$ ) for better RF performances. Under those conditions (125MHz and 18 kHz spinning speed) any rotational side bands were thrown out of the spectral region of interest thus allowing proper deconvolution of spectra. Proton decoupling during acquisition was obtained by using SPINAL-64 at a 90 kHz RF field. All spectra were performed within a 35714 Hz spectral window (284 ppm) and 1024 time domain acquisition points (70 Hz spectral resolution). Recycle times were dependent on the acquisition method (CP or DP).

**APHH-CP/MAS  $^{13}\text{C}\{^1\text{H}\}$  experiments conditions**

Cross Polarization from  $^1\text{H}$  to  $^{13}\text{C}$  was performed following the Adiabatic Passage through the Hartmann-Hahn (HH) conditions scheme. The latter HH conditions were set to 80 kHz and 98 kHz  $B_1$  fields for  $^{13}\text{C}$  and  $^1\text{H}$  respectively. The  $^1\text{H}$  RF field was swept from 84 to 122 kHz through the HH condition using the tangential time dependence and defined by the shape angle  $\phi = \alpha t_{\phi}/2$  where  $\alpha$  is the rate of angular change.  $\phi$  and  $t_{\phi}$  (contact time) were set to  $88^\circ$  and 2ms after optimization. We did try various  $\phi$  angles until we were able to get 1D spectra very close to those obtained in quantitative conditions, ie DP/MAS with recycle times equal to  $3 \cdot T_1$ . Recycle time was set here to 4 seconds.

**DP/MAS  $^{13}\text{C}\{^1\text{H}\}$  experiments conditions**

Quantitative Direct Polarization (DP) is a rather simple experiment where a single RF pulse ( $P_{90^\circ}$  pulse) is directly followed by acquisition with proton decoupling as stated previously. The experiment is then repeated  $N$  times with a recycle delay corresponding to at least 3 times the longer  $T_1$  (spin-lattice relaxation time) inside the sample. Those  $T_1$  were measured following saturation recuperation (sat-rec) method<sup>3</sup> and lead us to set up Direct Polarization experiments (DP) with recycle delays equal to 300s. Correct Signal/Noise ratio was obtained adding 3072 transients by FID, therefore each DP spectrum needed ca. 10 days for acquisition.

**2D  $^1\text{H}$ - $^{13}\text{C}$  heteronuclear correlation (HETCOR) experiments**

Solid-state NMR experiments were performed on an AVANCE III 750 MHz wide bore spectrometer (Bruker™) operating at a frequency of 188.5 MHz for  $^{13}\text{C}$  and equipped with a triple resonance MAS probe designed for 3.2 mm od zirconia rotors (closed with Kel-F caps). Approximately 19.5 mg of materials was put inside the rotor without any physical or chemical treatment of biomass and char. All the samples were spun at 18 kHz spinning frequency. 2D  $^1\text{H}$ - $^{13}\text{C}$  heteronuclear correlation (HETCOR) experiments with frequency-switched Lee-Goldburg (FSLG) irradiation during the evolution time<sup>4</sup> were obtained with the first CP step following the Adiabatic Passage through the Hartmann-Hahn (HH) conditions scheme<sup>5</sup>. The latter conditions were set to 93 kHz and 111 kHz  $B_1$  fields for  $^{13}\text{C}$  and  $^1\text{H}$  respectively. The  $^1\text{H}$  RF field was swept from 96 to 126 kHz through the HH condition using the tangential time dependence and defined by the shape angle  $\phi = \alpha t_{\phi}/2$  where  $\alpha$  is the rate of angular change<sup>6</sup>.  $\phi$  and  $t_{\phi}$  (contact time) were set to  $88^\circ$  and 4ms after optimization<sup>7</sup>. Proton decoupling during acquisition was obtained by using SPINAL-64<sup>8</sup> at a 80 kHz RF

field while the recycle time was set to 4 s. The duration of the successive FSLG pulses was  $8.05 \mu\text{s}$  and the magic-angle pulse length was  $2.01 \mu\text{s}$ . 128 complex data points were acquired in the  $^1\text{H}$  indirect dimension and for each  $t_1$  increment 1024 scans were accumulated. The corresponding spectral widths were 10.75 kHz for  $^1\text{H}$  (14.33 ppm) and 62.5 kHz for  $^{13}\text{C}$  (331.31 ppm), leading to a time resolution of 5.9526 ms and 16.434 ms respectively. Prior to Fourier transformation, a Lorentzian line broadening of 150 Hz was applied in the direct dimension while the proton dimension apodization was done with a  $90^\circ$  shifted squared sine-bell function.

### **2D $^1\text{H}$ - $^{13}\text{C}$ Hetcor spectrum of Holocellulose**

2D  $^1\text{H}$ - $^{13}\text{C}$  Hetcor spectrum of untreated Holocellulose performed on an AVANCE 750 MHz is presented Figure III-24. The clusters of cross peaks at  $\delta\text{C}/\delta\text{H}$  63.5/3.5; 74.9-72.3/3.5; 83.1/3.5; 87.9/3.5; 104.8/3.5 are assigned to  $\text{C}_6$  ( $\text{CH}_2\text{OH}$  in glucose unit),  $\text{C}_{2,3,5}$ ,  $\text{C}_4$  disordered structure,  $\text{C}_4$  ordered structure, and  $\text{C}_1$  carbons of polysaccharides respectively. These signals are overlapped by signal from hemicelluloses (xylan). The acetyl function is unambiguously identified through the correlation signal at  $\delta\text{C}/\delta\text{H}$  171-173/2.9-3.6 ppm. This highlights a long-range correlation between carbonyl carbons, present in acetyl function, with O-alkyl protons from carbohydrate structure. Direct correlations between alkyl carbons and alkyl protons from acetyl function ( $\text{CH}_3\text{-CO}$ ) are detected at  $\delta\text{C}/\delta\text{H}$  19.5-21.5/1.3-2 ppm. Concerning these carbons a long-range correlation with O-alkyl protons from carbohydrate structure is observed at  $\delta\text{C}/\delta\text{H}$  19.5-21.5/3-4 ppm.

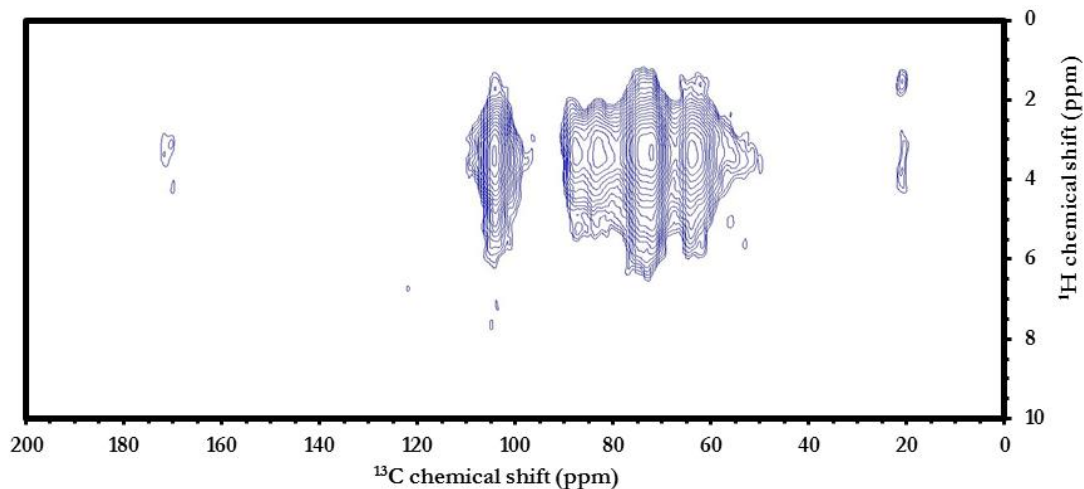


Figure III-24: 2D  $^1\text{H}$ - $^{13}\text{C}$  Hetcor spectrum of Holocellulose

**References for the supporting information**

- (1) Carignan, J.; Hild, P.; Mevelle, G.; Morel, J.; Yeghicheyan, D. Routine Analyses of Trace Elements in Geological Samples Using Flow Injection and Low Pressure On-Line Liquid Chromatography Coupled to ICP-MS: A Study of Geochemical Reference Materials BR, DR-N, UB-N, AN-G and GH. *Geostand. Newsl.* **2001**, *25* (2-3), 187–198.
- (2) Massiot, D.; Fayon, F.; Capron, M.; King, I.; Le Calv, S.; Alonso, B.; Durand, J.-O.; Bujoli, B.; Gan, Z.; Hoatson, G. Modelling One- and Two-Dimensional Solid-State NMR Spectra. *Magn. Reson. Chem.* **2002**, *40* (1), 70–76.
- (3) Fukushima, E.; Roeder, S. *Experimental Pulse NMR: A Nuts and Bolts Approach, Chap III.D Measurement of Spin-Lattice Relaxation*; Addison-Wesley, 1996.
- (4) vanRossum, B. J.; Forster, H.; Forster, H. J. M. High-Field and High-Speed CP-MAS C-13 NMR Heteronuclear Dipolar-Correlation Spectroscopy of Solids with Frequency-Switched Lee-Goldburg Homonuclear Decoupling. *J. Magn. Reson.* **1997**, *124*, 516–519.
- (5) Hologne, M.; Bertani, P.; Azaïs, T.; Bonhomme, C.; Hirschinger, J.  $^1\text{H}/^{31}\text{P}$  Distance Determination by Solid State NMR in Multiple-Spin Systems. *Solid State Nucl. Magn. Reson.* **2005**, *28* (1), 50–56.
- (6) Hediger, S.; Meier, B. H.; Kurur, N. D.; Bodenhausen, G.; Ernst, R. R. NMR Cross Polarization by Adiabatic Passage through the Hartmann—Hahn Condition (APHH). *Chem. Phys. Lett.* **1994**, *223* (4), 283–288.
- (7) Raya, J.; Perrone, B.; Hirschinger, J. Chemical Shift Powder Spectra Enhanced by Multiple-Contact Cross-Polarization under Slow Magic-Angle Spinning. *J. Magn. Reson. San Diego Calif 1997* **2013**, *227*, 93–102.
- (8) Fung, B. M.; Khitritin, A. K.; Ermolaev, K. An Improved Broadband Decoupling Sequence for Liquid Crystals and Solids. *J. Magn. Reson.* **2000**, *142* (1), 97–101.



#### **IV. Etude de l'influence du potassium sur les mécanismes de pyrolyse de la biomasse**



#### **IV.1 Article 3: Effect of potassium on the mechanisms of biomass pyrolysis as studied by in-situ $^1\text{H}$ NMR, TG-DSC and LC/MS**

Yann Le Brech<sup>1</sup>, Thierry Ghislain<sup>1</sup>, Sébastien Leclerc<sup>2</sup>, Mohamed Bouroukba<sup>1</sup>, Luc Delmotte<sup>3</sup>, Nicolas Brosse<sup>4</sup>, Colin Snape<sup>5</sup>, Anthony Dufour<sup>1</sup>

<sup>1</sup> LRGP, CNRS, Université de Lorraine, 1 rue Grandville 54000 Nancy, France

<sup>2</sup> LEMTA, CNRS, Université de Lorraine, BP 54506 Vandoeuvre lès Nancy

<sup>3</sup> IS2M, CNRS, Université de Haute Alsace, 15 rue Jean Starcky BP 2488 68057 Mulhouse cedex, France

<sup>4</sup> LERMAB, Université de Lorraine, BP239 54506 Vandoeuvre lès Nancy cedex, France

<sup>5</sup> Faculty of Engineering, The University of Nottingham, Energy Technologies Building, Nottingham NG2 2 TU, United Kingdom

**Article à soumettre au journal ChemSusChem.**

##### **IV.1.1 Abstract**

Complementary analytical methods have been used to study the effect of potassium on the primary pyrolysis mechanisms of cellulose and miscanthus. Thermogravimetry, calorimetry, high temperature  $^1\text{H}$  NMR (in-situ and real time analysis of the fluid phase formed during pyrolysis) and water extraction of quenched char followed by SEC/MS-ELSD (size exclusion chromatography coupled with mass spectrometry and evaporative light scattering detector have been combined). Pyrolysis was conducted under fixed bed conditions to impose similar mass transfer conditions in the analytical devices (calorimetry,  $^1\text{H}$  NMR and char production for SEC analysis). Potassium impregnated in cellulose suppresses the formation of anhydro-sugars measured by SEC/MS, reduces the formation of mobile protons as observed by in-situ  $^1\text{H}$  NMR and gives rise to a mainly exothermic signal (by calorimetry). Interestingly, the evolution of mobile protons formed from K-impregnated cellulose follows with a very similar pattern the evolution of the mass loss rate while the mobile protons are formed before mass loss for pure cellulose pyrolysis. This methodology has been also applied to miscanthus, demineralised miscanthus, potassium re-impregnated miscanthus after demineralization, raw oak and douglas fir. We discuss the mechanism of primary pyrolysis of biomass and notably highlight the importance of the intermediate liquid phase.

#### IV.1.2 Introduction

Faced with growing concern over the excessive emissions of greenhouse gases lignocellulosic biomass has been recognized as a promising alternative and carbon-neutral renewable source for biofuels and chemicals<sup>1</sup>. Thermo-chemical processes (gasification, pyrolysis, combustion and liquefaction) are serious options in order to transform biomass into energy or materials.<sup>2</sup> All of these transformation technologies involve pyrolysis as the initial transformation step.<sup>3,4</sup> For this reason, the chemical mechanism of biomass pyrolysis have been extensively studied for over a century.<sup>5,6</sup> Lignocellulosic biomass composition varies among biomass species and growing conditions but it consists generally of carbohydrates (~70 wt%), lignin (10-30 wt%), extractibles, and ashes. Inorganic materials come mainly from mineral nutrients necessary for plant growth and life. The mineral content depends on genotype, harvest time, location and also fertilization.<sup>2,7</sup> Basically, minerals represent less than 1 wt% of dry biomass, however the content can reach 15 wt% in some forestry residues or herbaceous biomass.<sup>8,9</sup> The major inorganic elements are silicon, alkali, alkaline earth metallic and transition metals<sup>10</sup>, which could have significant catalytic effects on the chemical mechanisms of biomass pyrolysis and for this reason they have been extensively studied.<sup>9,11-18</sup> Furthermore, inorganic constituents significantly modify the pyrolysis products (char, bio-oil and gas) distribution and composition.<sup>15,19,20</sup> Their presence not only leads to catalytic effects but also contributes to several problems in the thermo-chemical processes such as a decrease in the quality of bio-oil, syngas or exhaust gas.<sup>8,21</sup>

In order to investigate the influence of inorganic constituents during biomass pyrolysis removal<sup>8,9,14,20,22-25</sup> and/or impregnation<sup>12,20,26</sup> of biomass with mineral matters have been studied by various treatments.

The most convenient method to remove inorganic materials from biomass is leaching with water or acids.<sup>9</sup> Treatments with strong acids (hydrochloric, sulfuric or nitric) are the most efficient techniques for removing inorganics but it could alter the biomass structure<sup>8,9,27</sup> and therefore it could be an important artifact leading to an incorrect conclusion about the effect of inorganic materials. On the other side water leaching and hydrofluoric acid treatment do not affect significantly the structure of biomass<sup>9,28</sup> albeit these treatments are not as efficient as strong acid ones concerning inorganic removal. Regards water leaching, previous investigations showed that this method is selective for potassium (K) and sodium (Na) removal.<sup>8,9,14,29</sup>

Potassium has an important catalytic role on the chemical mechanisms of biomass pyrolysis and it has been extensively investigated.<sup>23,28,30,31</sup> Based on previous thermo-gravimetric analysis (TGA) of different biomasses (Table IV-1), the main influences according to potassium are: 1) it lowers the initial temperature decomposition; 2) increases the char yield; 3) lowers the maximum degradation rate; 4) lowers the temperature for maximum degradation. Studies have also been conducted on individual biomass components indicating that potassium has a similar impact on cellulose.<sup>12,23</sup> These studies show that the influence on the hemicelluloses (xylan) is not so important<sup>12,23</sup>. TGA results about K-impregnated lignins show inconsistent results, however it is known that potassium could promotes several chemical reactions such as demethoxylation, demethylation, condensation and C<sub>γ</sub>-elimination during lignin pyrolysis.<sup>17,32,33</sup>

Potassium not only controls product distributions but it also significantly impacts the composition of the products. Pyrolysis combined with Gas Chromatography (Py-GC)<sup>15,33</sup>, GC/Mass Spectrometry (MS)<sup>28</sup>, TG-MS<sup>19,34</sup>, on-line MS<sup>35,36</sup>, TGA-FTIR<sup>23,37,38</sup> have been used in order to investigate the effect of potassium on the composition of volatiles. Nuclear Magnetic Resonance (NMR) has been also used for char analysis.<sup>39</sup> All these investigations confirm that K-impregnation of cellulose or biomass has the following effect on pyrolysis: 1) it increases char and gas yield at the expense of bio-oils; 2) higher yields in lower molecular weight species (aldehydes and acid light compounds) and lower yields in levoglucosan are produced. During pyrolysis,

potassium increases the formation of this lower molecular weight species by fragmentation, ring opening and dehydration<sup>38</sup> reactions and inhibits the formation of anhydrosugars.<sup>36,40</sup>

Table IV-1: Initial temperature decomposition ( $T_i$ ), maximum degradation rate temperature ( $T_{max}$ ) and char weight yield (%char) for different biomass samples and various potassium contents

Sample	Raw			K-doped			Water leached			heating rate °C/min	ref
	$T_i$	$T_{max}$	%char	$T_i$	$T_{max}$	%char	$T_i$	$T_{max}$	%char		
Wheat straw	225	342	22% (700°C)				397		12,3% (700°C)	10	23
Yellow poplar wood		356	6,8% (800°C)				374		4,4% (800°C)	10	28
Willow, 1wt%K (KC <sub>2</sub> H <sub>3</sub> O <sub>2</sub> )		374	12,3% (900°C)	313		19,8% (900°C)				25	37
Miscanthus Giganteus	200	355	28,1% (900°C)				250	365	18,6% (900°C)	10	27
Poplar wood	220	362	14,9% (700°C)				220	376	11,4% (700°C)	10	9
Wheat straw	200	320	75,3% (300°C)				200	354	79,9% (300°C)	5	41
Miscanthus Sinensis			22% (900°C)						14,5% (900°C)	20	19
Cellulose cotton 1wt%K (K <sub>2</sub> CO <sub>3</sub> )	263	372	9% (600°C)	185	357	21,6% (600°C)				20	38
Cellulose, 1wt%K (KC <sub>2</sub> H <sub>3</sub> O <sub>2</sub> )		368	7,7% (900°C)		325	27,7% (900°C)				25	12

During biomass pyrolysis, the formation of a liquid intermediate phase has been observed.<sup>42–45</sup> This intermediate is very important for chemical mechanisms occurring during pyrolysis because it is a precursor of gas/volatiles/char and it can strongly control the composition of products. The composition of the liquid intermediate phase produced during cellulose fast pyrolysis has been analysed by Lédé and al.<sup>46</sup> and Piskorz and al.<sup>47</sup> A recent work<sup>48</sup> provides an experimental evidence and quantification of this intermediate liquid-phase by *in-situ* <sup>1</sup>H NMR (or Proton magnetic resonance thermal analysis PMRTA<sup>49</sup>) during biomass pyrolysis. H transfer from H donor' intermediate products to H acceptors are important pyrolysis mechanisms<sup>35,50,51</sup>. For this reason, the analysis of mobile protons by *in situ* <sup>1</sup>H NMR investigation is an interesting method to better understand the mechanism of pyrolysis. This investigation shows that the presence of inorganic materials can reduce mobility development during biomass pyrolysis by the inhibition of cellulose depolymerization.<sup>48</sup> However, this study has been conducted on biomass treated by a strong acid inducing biomass structural degradation. The liquid intermediate phase during slow pyrolysis of cellulose have been investigated by water extraction and further analysis of water-soluble compounds (by using high-performance anion-exchange chromatography with pulsed amperometric detection HPAEC-PAD).<sup>52</sup> Similar studies have been performed on cellulose fast pyrolysis with different salt impregnations.<sup>53,54</sup> These experiments have been extensively discussed highlighting interesting effects on cellulose pyrolysis mechanisms. The depolymerization,

which occurs during pure cellulose pyrolysis and produces mainly anhydro-sugars, seems to be inhibited in the presence of salts whereas the pyrolysis of impregnated-cellulose leads to a more cross-linked structure. To the best of our knowledge and despite all these previous studies, the detailed chemical effects of inorganic materials and especially of potassium during pyrolysis are still poorly understood because of the heterogeneity of the various samples and conditions tested. The most advanced kinetic mechanisms does not yet take into account the role of inorganic materials<sup>55</sup>. Therefore, there is still a strong need to develop original experimental methods in order to better understand the effect of inorganic materials during pyrolysis.

The aim of this study is to provide a multi-analytical investigation combining TGA, Differential Scanning Calorimetry (DSC), *in-situ* <sup>1</sup>H NMR, Size Exclusion Chromatography (SEC)-MS in order to get a better understanding of the effect of potassium during biomass pyrolysis. It is important that these analyses are conducted under controlled mass and heat transfer conditions. This study focuses on well characterized biomasses (*Miscanthus x Giganteus*, Douglas fir and Oak) and on pure commercial cellulose. The influence of potassium during the fluid phase development is highlighted by our *in-situ* analysis. It confirms that minerals directly interact with the biomass structure and generate specific primary chemical pathways.

#### **IV.1.3 Material and methods**

##### **Characterization of biomass samples**

*Miscanthus x Giganteus* was harvested in Lorraine (France) in 2011. Douglas and oak were harvested in the Haut-Beaujolais area (South-East France). They were milled and sieved to a particle size between 40 and 100 $\mu$ m. This particle size was kept constant for all characterizations and pyrolysis experiments. Samples have been analyzed by ICP-OES and ICP-MS following the CNRS-SARM procedure<sup>56</sup> in order to characterize their mineral and organic matter contents.

Carbohydrates and Klason lignin contents were measured on extractive free material according to the NREL procedure<sup>57</sup> and the analysis was repeated at least three times (standard deviation presented in sup. information). Samples were hydrolyzed by concentrated sulfuric acid (72%) for 1h in a rotary water bath at 30°C and then autoclaved during 1h30 after being diluted to 3% sulfuric acid through addition of water. The autoclaved sample were filtered, and then dried to give the Klason lignin content. Monosaccharides in the filtrate were quantified using high-performance anion-exchange chromatography with pulsed amperometric detection (HPAEC-PAD). Microgranular cellulose was purchased from Sigma Aldrich (ref. C6413).

##### **Demineralization and impregnation procedures**

Biomass (10 g) was washed two times by ultra-pure water at 90°C for 2 hours.<sup>9</sup> The remaining inorganic materials were quantified by ICP-OES and ICP-MS following CNRS-SARM procedure.<sup>56</sup> Biomass, demineralized biomass and cellulose were impregnated by the incipient wetness method with potassium acetate to yield of 1 wt% of potassium based on dry biomass. 3 g of dry biomass were contacted with 1.27 mL of a potassium acetate solution in deionized water (0,06 g/ml). Biomass was carefully stirred to ensure a good distribution of potassium. Then, the sample was dried at 80°C for a night.

**Thermogravimetric and differential scanning calorimetry analysis**

Samples were analysed by thermo-gravimetric analysis using Mettler Toledo (Stare System) apparatus. These analyses were conducted on 5 mg of each sample, put into a graphite crucible, heated at 5 °C/min up to 500°C. The carrier gas was purified Argon at 100 Nml/min. Differential scanning calorimetry analysis were performed on a SETARAM DSC 111 calorimeter equipped by an original fixed bed set up (Figure IV-1) in order to better control mass transfer during analysis. Approximately 30 mg of each sample was heated at 5 K/min up to 500°C. The sample was flushed by purified argon gas at 20 Nml/min.<sup>58</sup>

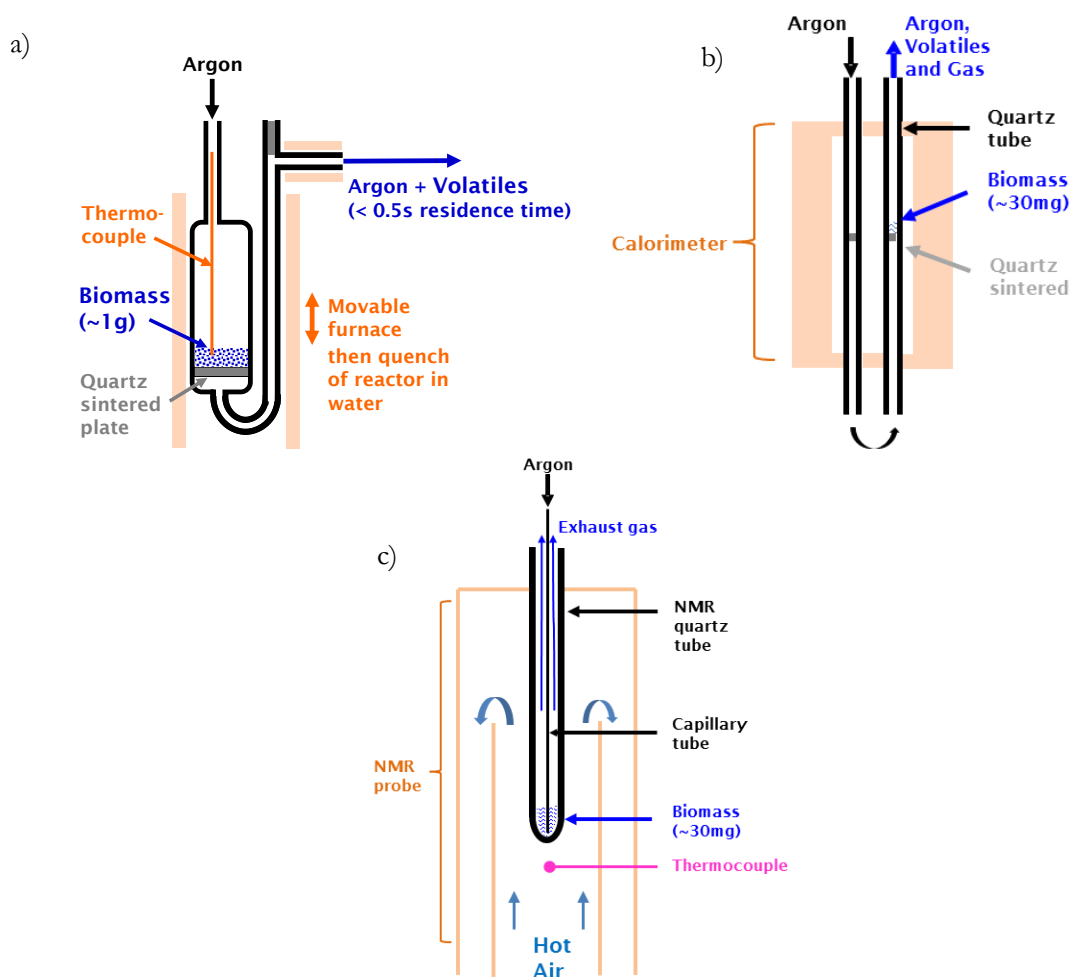


Figure IV-1: Simplified scheme of a) U-shape quartz fixed bed, b) calorimeter fixed bed, c) 1H NMR High temperature probe equipped with flushing gas  
 The carrier gas velocity was kept constant between the 3 devices to get similar mass transfers within the fixed beds of particles.

### **Pyrolysis experiments in fixed bed reactor**

A larger mass of biomass (800 mg) was pyrolysed in a vertical U-shape quartz fixed bed reactor (Figure IV-1) in order to extract from the char (quenched at various final temperatures) a sufficient amount of intermediate species for further analysis. Biomass particles were supported on quartz sintered plate (20 mm internal diameter). This geometry allows a good control of temperature, thanks to a thermocouple (0.5 mm diameter) inside the fixed bed of biomass particles, and of mass transfer by flushing the fixed bed with a given flow rate of Argon (300 NmL/min). The reactor was heated by an electrical furnace from 20°C to targeted temperature at a heating rate of 5 °C/min. The gradient inside sample was estimated to 10°C between the middle and the outer surface of the bed. Once the set temperature was achieved, the furnace was immediately moved down and the reactor was immediately immersed in ice-water in order to quench the char by a rapid cooling (maximum 2 minutes cooling from 500°C to 150°C). Char was cooled down under Argon until 30°C and then collected for further analysis such as water extraction and LC/MS analysis.

### **In-situ <sup>1</sup>H NMR analysis**

A Bruker 300 MHz NMR instrument was used in conjunction with a high temperature probe equipped by a proprietary device in order to improve mass transfer during pyrolysis inside the probe (Figure IV-1). Approximately 30 mg of each sample were put inside the NMR quartz tube which was equipped by a thin glass capillary line in order to flush the sample inside the tube with purified argon during pyrolysis, in a similar way than in all the other fixed bed devices (Figure IV-1). The flow rate was set at 10 Nml/min. A piece of quartz wool was placed on the top of the sample in order to avoid any particles entrainment. A temperature calibration was realized by comparing temperature given by the probe and temperature inside the sample. A thermocouple was put inside the sample during a blank test and temperature was increased to 500°C under inert atmosphere. Then the temperature correction factor has been established. As already described in previous investigation<sup>48</sup>, the spectra were deconvoluted using a Matlab program into Gaussian (solid-like) and Lorentzian (liquid-like) distribution functions (see ref. <sup>48</sup> for more details). The amount of fluid phase (% Mobility) is calculated from the following relation:

$$\%H_L = A_L / (A_L + A_G)$$

Where  $A_L$  and  $A_G$  are the areas of Lorentzian and Gaussian functions respectively.

All the carrier gas flow rates for fixed bed DSC, fixed bed U-shape reactor and *in-situ* <sup>1</sup>H NMR tests were set to keep the same carrier gas velocity in each set-up.

### **Characterization of water-soluble fractions from biomass chars**

In this study, the solid residue (char) obtained after various final temperature by the fixed bed U-shape reactor was separated into water-soluble and water-insoluble fractions. Approximately 150 mg of the solid residue were immersed in demineralized water (10 ml) at ambient temperature during 30 minutes under stirring. The mixture was filtered to obtain the liquid containing soluble species. Aqueous solutions were analyzed by a total organic carbon analyzer (TOC Shimadzu V<sub>CSH</sub>) in order to determine the total carbon content in the solution. The yield of water soluble species was calculated on a carbon basis via normalizing the total water-soluble carbon in pyrolyzed cellulose to the total carbon in raw cellulose<sup>52</sup> (Yield %C). Water-soluble fractions were also analyzed by HPLC-SEC-MS/Evaporative Light Scattering Detector (ELSD) Separation was performed on a Shimadzu LC-MS 20 equipped with two SEC PL aquagel-OH 20 columns provided by Agilent. Mobile phase was composed of methanol/water 50:50 v/v, ammonium acetate (100 μM) and formic acid (0.1 %) were added to improve electrospray ionization. The flow rate was maintained at 0.4 mL/min, resulting pressure in the columns was 50 bar, oven temperature was set at 40°C. A split was placed after the separation and a flow of roughly 10 μL/min were sent to the mass spectrometer and the rest was diverted to the ELSD. Mass spectrometry settings were set as followed: interface voltage – 4.5 kV, interface temperature: 350 °C, heat block temperature: 150°C, nitrogen nebulization gas: 1.5 L/min, nitrogen drying gas: 3 L/min. Data from the Shimadzu ELSD were acquired at 10 Hz rate and temperature was set at 40°C.

## **IV.1.4 Results and discussion**

### **Characterization of biomass**

The inorganic metal contents for all the samples are presented in Table IV-2. Cellulose microgranular (Cel\_micro) shows absolutely no detectable inorganic material and Cellulose impregnated by 1 %wt of potassium (Cel\_1K) shows a content of 0.9 %wt of potassium. Miscanthus was treated with water as described previously in order to remove inorganic materials (Misc\_Demin). The mass loss occurring during this procedure was 5 %wt (on dry biomass basis). This loss could be due to smooth hemicellulose hydrolysis and/or extractible solubilization. In order to estimate the impact of the water treatment on biomass, carbohydrates, the Klason lignin and the inorganic metal contents were compared before and after the water treatment. The comparison of monomeric sugar contents (Table IV-3) shows that there is no significant effect on the composition of the raw material after the treatment and that the hemicellulosic sugars are well preserved after demineralization as described in the literature.<sup>9</sup> The investigation of the inorganic elemental contents after water treatment indicates that only potassium is removed from the biomass as already described.<sup>14,59</sup>

Table IV-2: Inorganic elemental contents in sample before and after mineralization/demineralization

	Si	Al	Fe	Mn	Mg	Ca	Na	K	Ti	P	Total
<b>Cellulose</b>	0.01	0.00	0.00	0.00	0.00	0.00	0.01	0.00	0.00	0.00	0.00
<b>K impregnated cellulose</b>	0.00	0.00	0.00	0.00	0.00	0.00	0.01	0.90	0.00	0.00	0.92
<b>Miscanthus</b>	1.66	0.16	0.09	0.02	0.10	0.37	0.01	0.65	0.01	0.00	3.06
<b>Misc_Demin</b>	0.88	0.11	0.07	0.01	0.06	0.26	0.01	0.04	0.01	0.01	1.47
<b>Douglas</b>	0.01	0.00	0.00	0.01	0.00	0.03	0.00	0.02	0.00	0.00	0.08
<b>Oak</b>	0.03	0.01	0.01	0.01	0.01	0.14	0.00	0.11	0.00	0.01	0.34

Table IV-3: Compositions before and after demineralization

Samples	%wt biomass (extractible free)							
	Klason lignin	Organic matter	Total Sugars	Arabinose	Galactose	Glucose	Xylose	Mannose
<b>Miscanthus</b>	29.8	92.4	70.2	2.3	0.6	48.9	18.3	0.0
<b>Misc_Demin</b>	28.3	94.8	71.7	2.9	0.7	46.6	20.9	0.0

### Effect of carrier gas velocity on the pyrolysis regimes

In order to reduce secondary reactions and to study primary mechanisms, the flow rate of carrier gas has been optimized for all fixed bed devices. The residence time is one of the most important parameters according to pyrolysis operations. For this reason, the influence of the flow rate have been investigated by DSC<sup>58</sup> and also by <sup>1</sup>H-NMR analysis. DSC analysis showed that there is no significant effect of flow rate (from 20 NmL/min) when a fixed bed is used. These results are confirmed by *in-situ* <sup>1</sup>H-NMR investigations. Figure IV-2 shows that the presence of carrier gas has an important effect on the fluidity development during miscanthus pyrolysis. Without carrier gas, the fluidity remains at higher temperatures because the carrier gas improves the devolatilisation of the intermediate liquid-phase. Mass transfer effects are very well known in pyrolysis<sup>60,61</sup> and is here demonstrated by our *in-situ* analysis. Different flow rates of carrier gas were studied up to 15 Nml/min. The effect of the gas flow is weak between 5 and 15 Nml/min (Figure IV-2). Consequently under these conditions the pyrolysis is conducted close to chemical regime conditions.

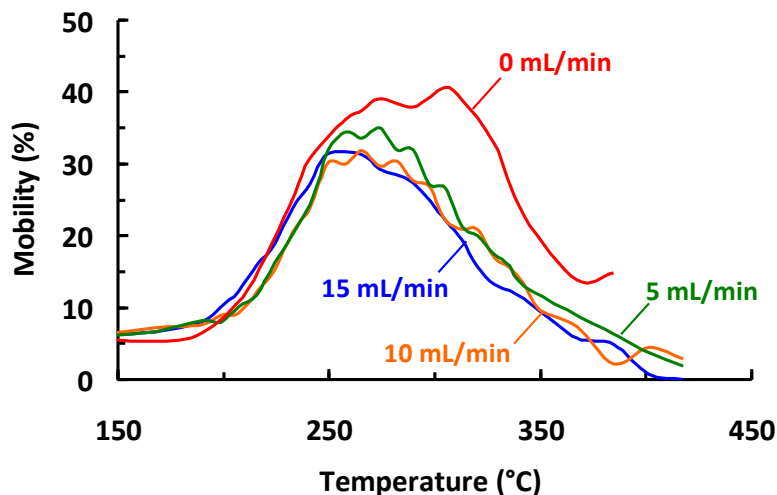


Figure IV-2: Effect of carrier gas flow rate on fluidity development during *Miscanthus* pyrolysis

The char yield is a good indicator of the heat and mass transfer conditions occurring during pyrolysis. The char yields obtained from the four devices are comparable (Table IV-4) except for the  $^1\text{H}$  NMR probe. In the latter case, the char yield is higher because the maximum temperature was limited to  $420^\circ\text{C}$  to protect the probe. Experiments with 800 mg sample mass (in the U-shape fixed bed reactor) gave the same char yield than experiments with 5 mg in the TGA. Char yields are very near for all methods at  $500^\circ\text{C}$  final temperature demonstrating that these experiments were conducted under similar mass and heat transfer conditions and thus very close to the pure chemical regime.

Table IV-4: Comparison of char yields for the different experimental techniques (\*NMR at  $420^\circ\text{C}$  final temperature)

Samples	%wt dry biomass at $500^\circ\text{C}$			
	Fixed bed	DSC	$^1\text{H}$ in situ NMR*	TG
Miscanthus	29	29	32	29
Misc_Demin	-	16	21	16
Cellulose	7	7	13	7
K-impregnated cellulose	-	21	28	26
Douglas	21	19	26	20
Oak	19	18	27	19

**Effect of potassium on cellulose pyrolysis**

In order to have a better understanding of the influence of potassium (K) during cellulose pyrolysis, the thermal behavior of cellulose microgranular and 1 %K-impregnated cellulose have been investigated by TGA, DSC and *in situ* <sup>1</sup>H NMR. Chars produced by the fixed bed pyrolysis at selected temperatures were submitted to aqueous extractions to identify and quantify the water-soluble pyrolysis products. Figure IV-3 presents the differential thermo-gravimetric (DTG) signal (% wt/s), the DSC results (mW/mg), the amount of fluid <sup>1</sup>H (% mobility) and the yield of water soluble species (yield % C, as analyzed by TOC) as a function of pyrolysis final temperature.

The comparison between the pure and the impregnated cellulose DTG signals indicates the important effect of the potassium during pyrolysis. These results are in close agreement with literature data<sup>12,38</sup>. Cellulose exhibits a degradation curve with one main peak which reaches a maximum decomposition rate at 330°C whereas impregnated cellulose shows a DTG curve with two peaks, at a maximum mass loss rate at 213°C and 320°C, respectively. Char yields from TGA, DSC and <sup>1</sup>H NMR analysis (Table IV-4) are much higher for the K-impregnated cellulose. The comparison between the two DSC analysis profiles (Figure IV-3) shows that the decomposition of cellulose which is mainly endothermic, becomes slightly exothermic with the addition of 1% wt K without any detectable endothermic peak. The pure cellulose gives an endothermic thermogram, it mostly undergoes depolymerization reactions which induce the formation of anhydro-sugars by transglycosylation.<sup>35,62</sup> Consequently, the overall reaction is mainly endothermic due to the rupture of glycosidic bonds and to the evaporation of depolymerized products.<sup>60,61,63</sup> This depolymerization may not involve mass loss because it produces oligomers which have a too high molecular weight to be devolatilised. At higher temperatures the polymerization degree is further reduced and lower molecular weight species (anhydro-sugars, mainly levoglucosan) can devolatilise. Concerning the impregnated cellulose, the first degradation step (213°C) observed in the DTG signal could be due to the production and volatilization of low molecular weight molecules (acids) and gas (CO<sub>2</sub> and CO).<sup>37,38</sup> At higher temperature, the transglycosylation reactions are inhibited by potassium and ring opening, fragmentation and dehydration are favoured<sup>33,36,40</sup>. Ab-initio modeling has shown that the complexation of potassium with cellulose hydroxyl and ether groups may stabilize a particular conformation of the glycosidic bond and therefore promote ring opening and cracking of glycosidic linkage<sup>25</sup>. Crosslinking reactions are promoted by potassium leading to a higher char yield and to an exothermic signal overall<sup>60,64</sup>. The exothermic signal is also promoted by the formation of a higher yield in aromatic structures<sup>39</sup>.

The inhibition of the transglycosylation, which leads to levoglucosan formation, has been highlighted recently by activation energies based on MBMS experiments<sup>36</sup>. The addition of potassium also induces a significant impact on fluidity development (Figure IV-3). The fluidity development of cellulose starts at 250°C and reaches its maximum at 300°C (20% of mobile H) and decreases to 5% at 400°C. The development occurs before any mass loss illustrating the formation of a “fluid phase cellulose” as already observed and discussed in our previous investigation<sup>48</sup>, which corresponds to the formation of an intermediate material extensively studied<sup>5</sup> and identified by several names (active cellulose<sup>65</sup>, intermediate carbohydrates<sup>39</sup>, depolymerized cellulose<sup>66</sup>). This active cellulose undergoes further depolymerization to generate a pool of intermediate species (levoglucosan, cellobiosan, etc.)<sup>46,47</sup> until the devolatilisation of the lighter ones. Conversely, the fluidity development of impregnated cellulose exhibits a very similar pattern compared to the mass loss probably because the small molecules formed by the fragmentation reactions give rise to a fluid phase which is easily devolatilised. Fewer mobile protons entrapped in the char are produced for the impregnated cellulose (Figure IV-3). The decrease in mobile protons by K-catalyzed pyrolysis could arise due to the enhancement of homolytic scission imposed by potassium due to the conformation of pyranose ring in the presence of

potassium<sup>67</sup>. Furthermore the mobile protons may stabilise the free radicals formed during pyrolysis<sup>51</sup>. In other words, the enhanced formation of radicals could reduce the number of mobile <sup>1</sup>H protons.

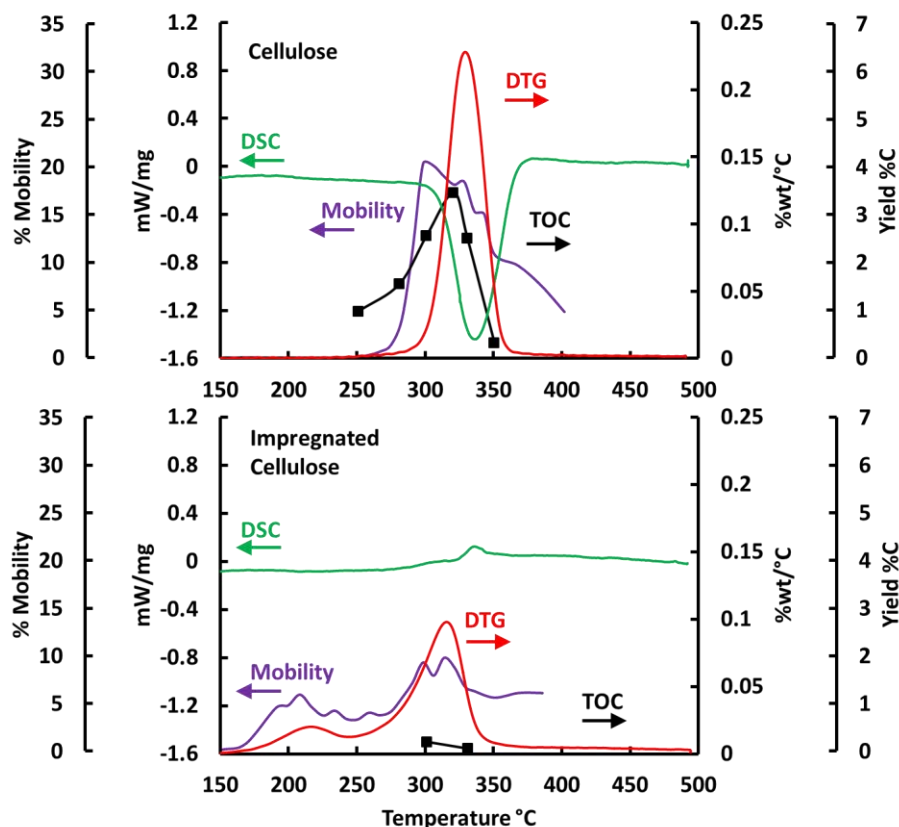


Figure IV-3: DSC, DTG, % Mobility and TOC evolution as function of temperature for Cellulose and Impregnated Cellulose

Chars produced at different temperatures with the U-shape fixed bed reactor have been separated into water-soluble and water-insoluble fractions. The water soluble fractions have been analyzed by SEC-MS/ELSD and the ELSD chromatograms are presented in Figure IV-4. The water-soluble levoglucosan and cellobiosan contents have been quantified at different temperatures and the yields obtained are presented in Figure IV-5. One can notice a similar pattern for levoglucosan and cellobiosan formation (Figure IV-5), both being formed after the formation of an intermediate liquid phase (as analysed by in-situ <sup>1</sup>H NMR) composed of depolymerized cellulose, confirming previous findings<sup>44,47,52</sup>. The formation of this intermediate liquid phase does depend on the crystallinity and degree of polymerisation of the cellulose.<sup>52,68,69</sup> Concerning the water-soluble fractions from the pure cellulose chars, only anhydro-sugars (DP 1-5) have been identified by mass spectrometry (see supplementary information for the mass spectra and major ions formed). No sugars (cellobiose, etc.) have been detected confirming that transglycosylation is the main chemical pathway occurring during pyrolysis of pure cellulose. Concerning K-impregnated cellulose, TOC values are much lower than for pure cellulose (Figure IV-3). The liquid intermediate species are devolatilised quickly and poorly retained in the char. The char structure is more “cross linked” due to the impact of potassium, also explaining the poor water solubility.<sup>54</sup> Furthermore, no anhydro-sugar has been detected in the water-soluble fraction from the impregnated cellulose char, confirming that transglycosylation is no longer occurring during pyrolysis. For all the samples, a peak is observed at a retention time of 34.5 minutes (Figure IV-4). This peak seems to be more important for the impregnated cellulose. Unfortunately the MS analysis did not allow us to

conduct any qualitative investigation about this peak (too high molecular weight). This peak could correspond to a high molecular weight intermediate which is water-soluble and composed of cross-linked glucose units.

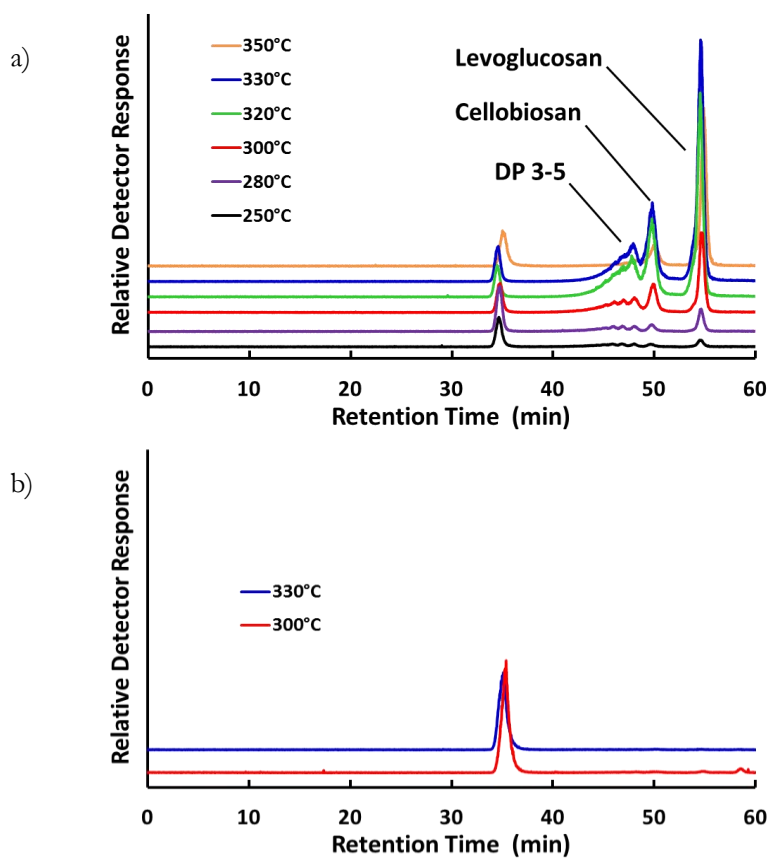


Figure IV-4: Effect of pyrolysis temperature on the composition of water soluble compounds extracted from char quenched at various pyrolysis temperatures for a) cellulose and b) K-impregnated cellulose

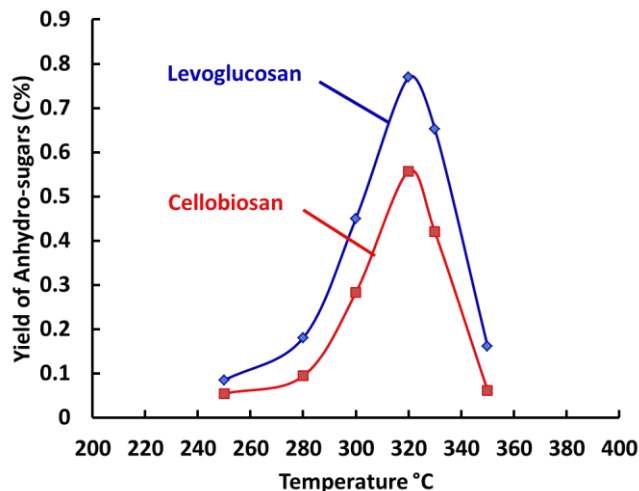


Figure IV-5: Quantification of the levoglucosan and cellobiosan in the water soluble fractions extracted from char quenched at various pyrolysis temperatures for pure cellulose

#### **Effect of demineralization and potassium impregnation on Miscanthus pyrolysis**

Figure IV-6 presents the DTG curve (%wt/s), DSC signal (mW/mg), amount of fluid  $^1\text{H}$  (% mobility) and the yield of water soluble species (Yield %C) as function of temperature for miscanthus, demineralized miscanthus (Misc\_Demin) and demineralized miscanthus followed by an impregnation with 1 %wt. of potassium (Misc\_Demin\_1K). The miscanthus mass loss starts at 200°C and reaches a maximum at 320°C. The DSC profile exhibits a first exothermic peak and a second endothermic which give roughly a thermoneutral signal (compared to pure cellulose signals). Miscanthus is composed of hemicelluloses, lignin, cellulose and minerals involving various chemical reactions with a balance between endo- and exothermic reactions. The fluidity analyzed by in-situ  $^1\text{H}$  NMR starts to increase quickly at 200°C and reaches a maximum at 270°C.

Concerning demineralized miscanthus (Misc\_Demin), the mass loss starts at 220°C with a shoulder (295°C) more pronounced than for raw miscanthus and followed by a maximum at 340°C (320°C for raw miscanthus). The maximum mass loss rate (0.117 %wt/s) is higher than for raw miscanthus (0.068 %wt/s). These results are in close agreement with previous investigations.<sup>9,27,29</sup> The shoulder at 295°C could be attributed to hemicellulose degradations and the peak at 340°C to cellulose degradation. The shoulder is more pronounced after the demineralization because demineralization does not affect significantly the DTG signal for xylan and lignin but it increases the maximum mass loss rate of cellulose and shifts the maximum degradation to higher temperature. The fluidity starts to increase at 200°C and reaches a maximum at 270°C as already observed for miscanthus. The maximum value of the fluid phase is similar (around 30 %mobile H) for Misc\_Demin and miscanthus but the fluidity remains stable for Misc\_Demin until 350°C whereas it decreases for raw miscanthus from 300°C. The higher content in potassium in raw char leads to an important decrease of fluidity development from cellulose pyrolysis.

This observation is supported by the DSC investigation. The pyrolysis of demineralised miscanthus is mainly endothermic due to the removal of inorganic materials which promote crosslinking reactions. However the

analysis of water-soluble compounds by HPLC (Figure IV-7) does not reveal any anhydro-sugars formed during the pyrolysis of demineralised miscanthus unlike pure cellulose. Indeed it remains inorganic materials into biomass even after demineralization which could still inhibit transglycosylation reactions of cellulose.

When 1% wt K is added to the demineralized miscanthus, the behaviour becomes similar to those obtained for the raw miscanthus (Figure IV-6). The DTG profile shows one peak degradation step which reaches a maximum at 320°C and the DSC thermogram is very similar to the raw miscanthus one. However the % mobility profile is slightly different. The demineralization step has removed other inorganic materials than potassium (Ca, Mg, etc, see Table IV-2) and the impregnation by potassium (after demineralization) may involve different forms and locations of the potassium in the macromolecular network compared to the raw miscanthus. Although the maximum fluidity is different for the two samples, the shape of the mobility curve is similar. Indeed, the maximum fluidity and the decrease in fluidity development occur at the same temperatures (270 and 300°C respectively (Figure IV-6). When potassium is added, it modifies the degradation of cellulose as already discussed. The addition of potassium reduces the maximum fluidity (at 270°C) which is mainly developed in this temperature zone by hemicelluloses conversion<sup>48</sup>. TOC values are similar for the investigated temperatures.

Similarly to cellulose, a peak is observed by HPLC for the water soluble fractions in all cases at the retention time of 34.5 minutes. Although any investigation by MS were not possible, the evolution of the area is in agreement with previous results. The signal for this high molecular weight species increases with the presence of potassium in the sample.

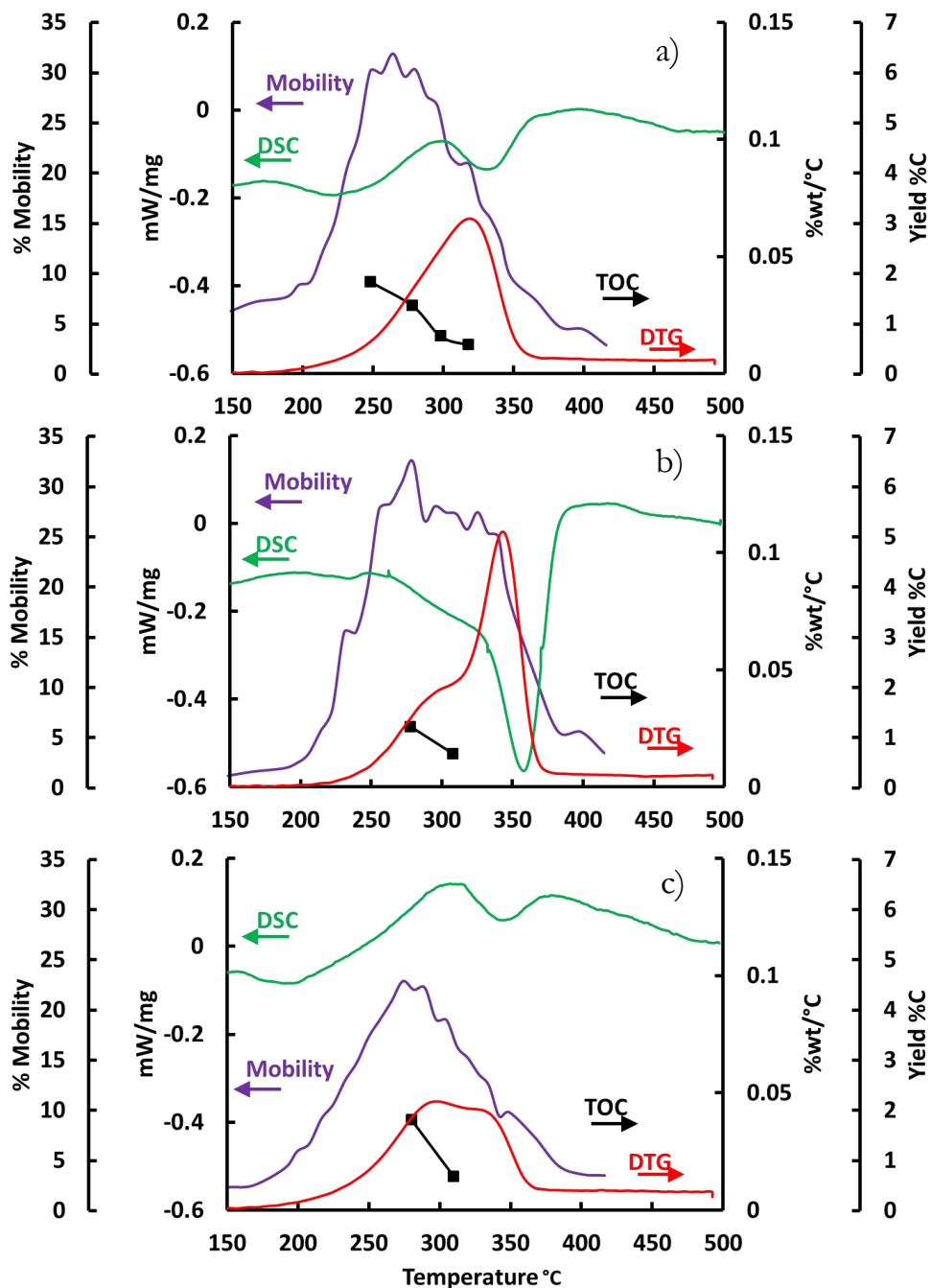


Figure IV-6: DSC, DTG,  $^1\text{H}$  NMR and TOC for a) *Miscanthus*, b) *Misc\_Demin*, c) *Misc\_Demin\_1K*

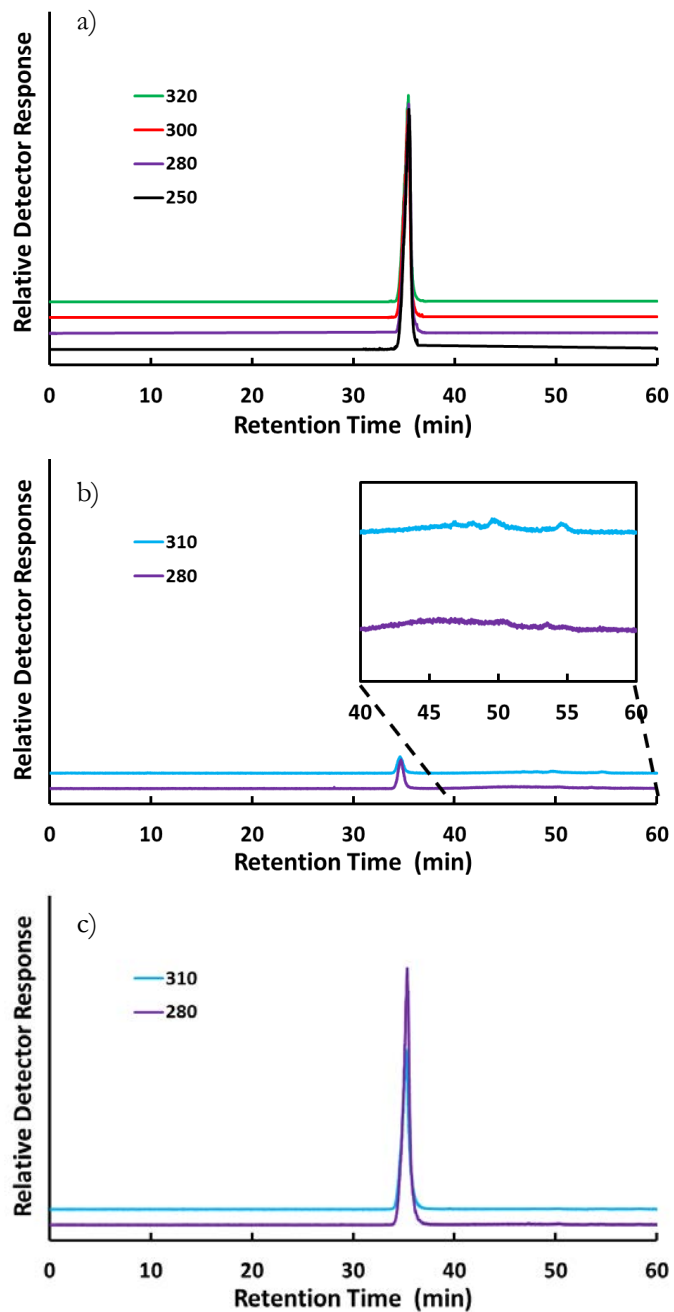


Figure IV-7: SEC-DEDL of water extracted Misc. a), water Misc\_Demin b), water Mis\_Demin\_1K c)

### **Pyrolysis behaviour of douglas fir and oak**

The same multi-analysis approach has been used on oak and douglas fir (Figure IV-8). Oak and douglas exhibit a global endothermic behavior whereas miscanthus is both slightly exothermic and then endothermic. A weak exothermic peak can also be detected for oak pyrolysis at about 300°C. These differences could be mainly attributed mainly to the different amounts of inorganic species present. Douglas fir and oak contain much lower concentrations of inorganic elements than miscanthus (Table IV-2). The higher concentrations in miscanthus (especially K, Ca, Mg, Fe) promotes cross-linking (exothermic) reactions. DTG curves of douglas and oak present a shoulder at 280°C and 310°C for oak and douglas respectively, which is attributed to hemicelluloses conversion. This difference can mainly be explained by the different compositions of the hemicelluloses. Douglas hemicelluloses are composed predominantly by glucomannan (C6 pyranose) whereas oak hemicelluloses are composed by xylan (C5 pyranose), therefore it induces different thermal stabilities.<sup>70</sup> Xylan is less stable than mannan exhibiting a more pronounced shoulder for oak pyrolysis. The peak of maximum mass loss rate (340 and 350°C for oak and douglas, respectively) is attributed to cellulose decomposition. Oak has a higher inorganic content (notably Ca<sup>2+</sup> and K<sup>+</sup>). It is known that ash content of coniferous trees is usually smaller than deciduous trees and coniferous wood often decomposes at higher temperature ranges in TG experiments.<sup>29</sup>

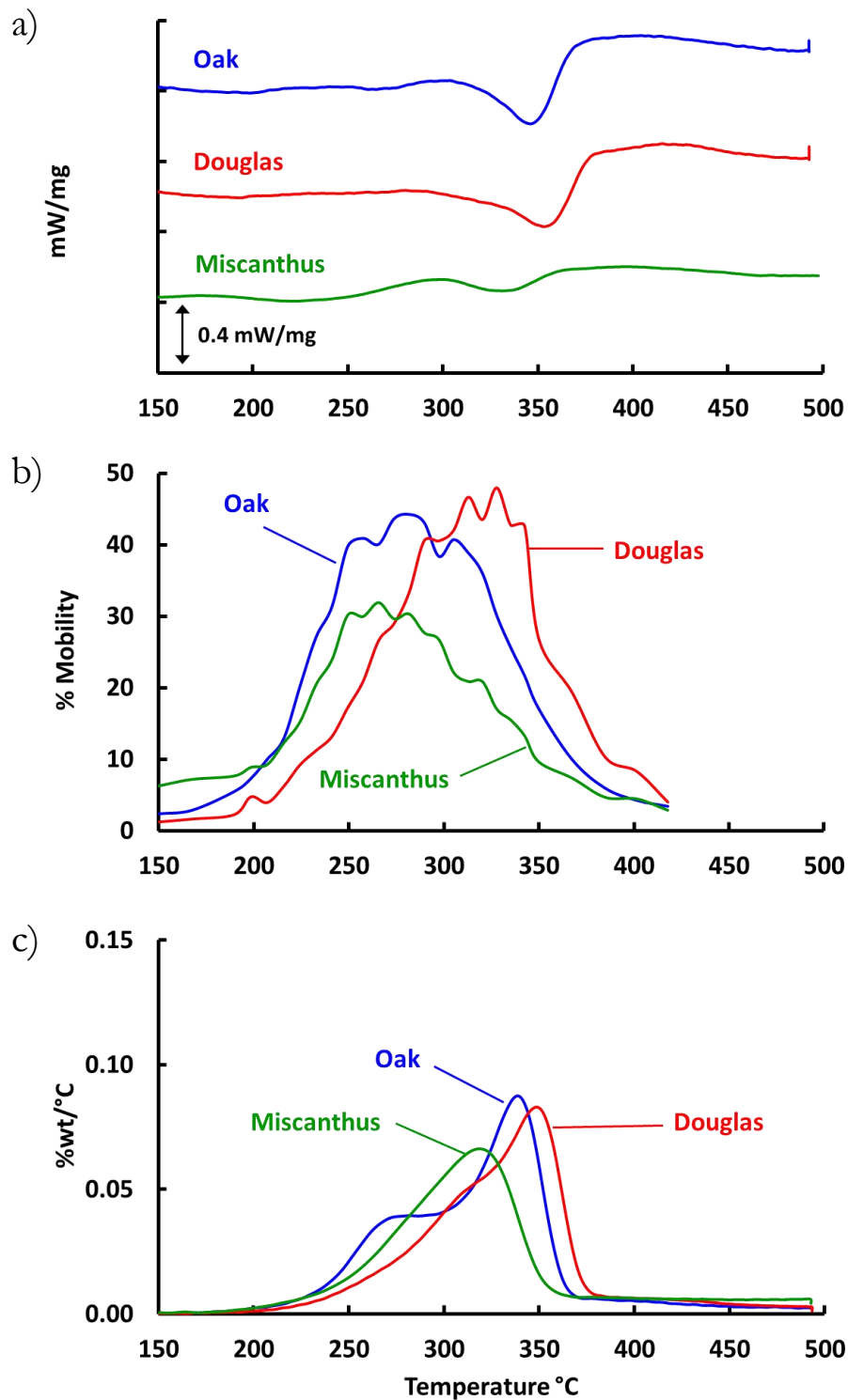


Figure IV-8: Miscanthus, douglas, oak : a) DSC, b) <sup>1</sup>H NMR c) DTG

Inorganic element and hemicelluloses contents also impact are the fluidity developments (Figure IV-8). The mobility development starts at 200°C (from lignin conversion<sup>48</sup>) for the three biomasses but the maximum fluidity occurs at higher temperature for douglas than for oak and miscanthus.

#### **IV.1.5 Conclusion**

As far as we know, this work presents for the first time the combination of: (1) TG-DSC, (2) in-situ  $^1\text{H}$  NMR analysis of mobile protons, (3) water extraction of chars followed SEC/MS-ELSD to analyse the intermediate species during primary pyrolysis of biomass. The complementary analytical methods are conducted under similar mass transfer effects very close to the pure chemical regime. They are used to better understand the impact of potassium on the pyrolysis mechanism of cellulose and of ligno-cellulosic biomass (miscanthus). This methodology is applied to other biomasses (oak and douglas fir) with different content in inorganic materials and different composition in the macromolecules (mainly hemicelluloses). Potassium inhibits mobile  $^1\text{H}$  formation by chemical interactions with the polysaccharide structure. Radicals formed by homolytic scissions due to potassium presence<sup>67</sup> during pyrolysis could reduce the  $^1\text{H}$  mobile content because of the fact that mobile protons stabilize the free radicals formed during pyrolytic chemical reactions<sup>48</sup>. Hydrogen transfer reactions are of high importance in the mechanisms of biomass pyrolysis and consequently the enhancement of homolytic scissions could induce different degradation pathways (cross linking) leading to a more aromatic structure. This phenomenon is correlated with a high cross-linked char formation highlighted by exothermic signal observed during calorimetry experiments and the losing of anhydrosugars in water soluble char fractions.

#### **Acknowledgments**

The authors gratefully acknowledge the financial support of the French research national through the project “PYRAIM” (ANR-11BS09-003) and of the CNRS interdisciplinary program through the project “FORÊVER”. F. Mathieu (LRGP-CNRS) is acknowledged for some help on the Matlab program used for deconvolution of  $^1\text{H}$  NMR spectra. S. Pontvianne (LRGP-CNRS) is acknowledged for the optimization of the total organic carbons method and for some help on the SEC/MS-ELSD method.

IV.1.6 **References**

- (1) Ragauskas, A. J.; Williams, C. K.; Davison, B. H.; Britovsek, G.; Cairney, J.; Eckert, C. A.; Frederick, W. J.; Hallett, J. P.; Leak, D. J.; Liotta, C. L.; Mielenz, J. R.; Murphy, R.; Templer, R.; Tschaplinski, T. The Path Forward for Biofuels and Biomaterials. *Science* **2006**, *311* (5760), 484–489.
- (2) Brosse, N.; Dufour, A.; Meng, X.; Sun, Q.; Ragauskas, A. Miscanthus: A Fast-Growing Crop for Biofuels and Chemicals Production. *Biofuels Bioprod. Biorefining* **2012**, *6* (5), 580–598.
- (3) Mettler, M. S.; Vlachos, D. G.; Dauenhauer, P. J. Top Ten Fundamental Challenges of Biomass Pyrolysis for Biofuels. *Energy Environ. Sci.* **2012**, *5* (7), 7797–7809.
- (4) Huber, G. W.; Iborra, S.; Corma, A. Synthesis of Transportation Fuels from Biomass: Chemistry, Catalysts, and Engineering. *Chem. Rev.* **2006**, *106* (9), 4044–4098.
- (5) Lédé, J. Cellulose Pyrolysis Kinetics: An Historical Review on the Existence and Role of Intermediate Active Cellulose. *J. Anal. Appl. Pyrolysis* **2012**, No. 0.
- (6) Klason, P.; Heidenstam, G. V.; Norlin, E. Investigations on the Charring of Wood. **1910**, *23*, 1252–1257.
- (7) Baxter, L. L.; Miles, T. R.; Miles Jr., T. R.; Jenkins, B. M.; Milne, T.; Dayton, D.; Bryers, R. W.; Oden, L. L. The Behavior of Inorganic Material in Biomass-Fired Power Boilers: Field and Laboratory Experiences. *Fuel Process. Technol.* **1998**, *54* (1–3), 47–78.
- (8) Jiang, L.; Hu, S.; Sun, L.-S.; Su, S.; Xu, K.; He, L.-M.; Xiang, J. Influence of Different Demineralization Treatments on Physicochemical Structure and Thermal Degradation of Biomass. *Bioresour. Technol.* **2013**, *146*, 254–260.
- (9) Eom, I.-Y.; Kim, K.-H.; Kim, J.-Y.; Lee, S.-M.; Yeo, H.-M.; Choi, I.-G.; Choi, J.-W. Characterization of Primary Thermal Degradation Features of Lignocellulosic Biomass after Removal of Inorganic Metals by Diverse Solvents. *Bioresour. Technol.* **2011**, *102* (3), 3437–3444.
- (10) Rutkowski, P. Pyrolysis of Cellulose, Xylan and Lignin with the K<sub>2</sub>CO<sub>3</sub> and ZnCl<sub>2</sub> Addition for Bio-Oil Production. *Fuel Process. Technol.* **2011**, *92* (3), 517–522.
- (11) Pan, W.-P.; Richards, G. N. Influence of Metal Ions on Volatile Products of Pyrolysis of Wood. *J. Anal. Appl. Pyrolysis* **1989**, *16* (2), 117–126.
- (12) Nowakowski, D. J.; Jones, J. M. Uncatalysed and Potassium-Catalysed Pyrolysis of the Cell-Wall Constituents of Biomass and Their Model Compounds. *J. Anal. Appl. Pyrolysis* **2008**, *83* (1), 12–25.
- (13) Halpern, Y.; Patai, S. Pyrolytic Reactions of Carbohydrates. VI. Isothermal Decomposition of Cellulose in Vacuo, in the Presence of Additives. *Isr. J. Chem.* **1969**, *7* (5), 685–690.
- (14) Fahmi, R.; Bridgwater, A. V.; Darvell, L. I.; Jones, J. M.; Yates, N.; Thain, S.; Donnison, I. S. The Effect of Alkali Metals on Combustion and Pyrolysis of Lolium and Festuca Grasses, Switchgrass and Willow. *Fuel* **2007**, *86* (10–11), 1560–1569.
- (15) Patwardhan, P. R.; Satrio, J. A.; Brown, R. C.; Shanks, B. H. Influence of Inorganic Salts on the Primary Pyrolysis Products of Cellulose. *Bioresour. Technol.* **2010**, *101* (12), 4646–4655.
- (16) Di Blasi, C.; Galgano, A.; Branca, C. Influences of the Chemical State of Alkaline Compounds and the Nature of Alkali Metal on Wood Pyrolysis. *Ind. Eng. Chem. Res.* **2009**, *48* (7), 3359–3369.
- (17) Kleen, M.; Gellerstedt, G. Influence of Inorganic Species on the Formation of Polysaccharide and Lignin Degradation Products in the Analytical Pyrolysis of Pulps. *J. Anal. Appl. Pyrolysis* **1995**, *35* (1), 15–41.
- (18) Dauenhauer, P. J.; Colby, J. L.; Balonek, C. M.; Suszynski, W. J.; Schmidt, L. D. Reactive Boiling of Cellulose for Integrated Catalysis through an Intermediate Liquid. *Green Chem* **2009**, *11* (10), 1555–1561.
- (19) Szabó, P.; Várhegyi, G.; Till, F.; Faix, O. Thermogravimetric/mass Spectrometric Characterization of Two Energy Crops, Arundo Donax and Miscanthus Sinensis. *J. Anal. Appl. Pyrolysis* **1996**, *36* (2), 179–190.
- (20) Nik-Azar, M.; Hajaligol, M. R.; Sohrabi, M.; Dabir, B. Mineral Matter Effects in Rapid Pyrolysis of Beech Wood. *Fuel Process. Technol.* **1997**, *51* (1–2), 7–17.

- (21) Michel, R.; Kaknics, J.; Bouchetou, M. L.; Gratuze, B.; Balland, M.; Hubert, J.; Poirier, J. Physicochemical Changes in Miscanthus Ash on Agglomeration with Fluidized Bed Material. *Chem. Eng. J.* **2012**, *207–208*, 497–503.
- (22) Davidsson, K. O.; Korsgren, J. G.; Pettersson, J. B. C.; Jäglid, U. The Effects of Fuel Washing Techniques on Alkali Release from Biomass. *Fuel* **2002**, *81* (2), 137–142.
- (23) Jensen, A.; Dam-Johansen, K.; Wójtowicz, M. A.; Serio, M. A. TG-FTIR Study of the Influence of Potassium Chloride on Wheat Straw Pyrolysis. *Energy Fuels* **1998**, *12* (5), 929–938.
- (24) Oudenhoven, S. R. G.; Westerhof, R. J. M.; Aldenkamp, N.; Brilman, D. W. F.; Kersten, S. R. A. Demineralization of Wood Using Wood-Derived Acid: Towards a Selective Pyrolysis Process for Fuel and Chemicals Production. *J. Anal. Appl. Pyrolysis* **2013**, *103*, 112–118.
- (25) Saddawi, A.; Jones, J. M.; Williams, A. Influence of Alkali Metals on the Kinetics of the Thermal Decomposition of Biomass. *Fuel Process. Technol.* **2012**, *104*, 189–197.
- (26) Zaror, C. A.; Hutchings, I. S.; Pyle, D. L.; Stiles, H. N.; Kandiyoti, R. Secondary Char Formation in the Catalytic Pyrolysis of Biomass. *Fuel* **1985**, *64* (7), 990–994.
- (27) Collura, S.; Azambre, B.; Weber, J.-V. Thermal Behaviour of Miscanthus Grasses, an Alternative Biological Fuel. *Environ. Chem. Lett.* **2007**, *5* (1), 49–49.
- (28) Hwang, H.; Oh, S.; Cho, T.-S.; Choi, I.-G.; Choi, J. W. Fast Pyrolysis of Potassium Impregnated Poplar Wood and Characterization of Its Influence on the Formation as Well as Properties of Pyrolytic Products. *Bioresour. Technol.* **2013**, *150C*, 359–366.
- (29) Müller-Hagedorn, M.; Bockhorn, H.; Krebs, L.; Müller, U. A Comparative Kinetic Study on the Pyrolysis of Three Different Wood Species. *J. Anal. Appl. Pyrolysis* **2003**, *68–69*, 231–249.
- (30) Di Blasi, C.; Galgano, A.; Branca, C. Analysis of the Physical and Chemical Mechanisms of Potassium Catalysis in the Decomposition Reactions of Wood. *Ind. Eng. Chem. Res.* **2011**, *50* (7), 3864–3873.
- (31) Julien, S.; Chornet, E.; Tiwari, P. K.; Overend, R. P. Vacuum Pyrolysis of Cellulose: Fourier Transform Infrared Characterization of Solid Residues, Product Distribution and Correlations. *J. Anal. Appl. Pyrolysis* **1991**, *19* (0), 81–104.
- (32) Sharma, R. K.; Wooten, J. B.; Baliga, V. L.; Lin, X. H.; Chan, W. G.; Hajaligol, M. R. Characterization of Chars from Pyrolysis of Lignin. *Fuel* **2004**, *83* (11-12), 1469–1482.
- (33) Eom, I.-Y.; Kim, J.-Y.; Kim, T.-S.; Lee, S.-M.; Choi, D.; Choi, I.-G.; Choi, J.-W. Effect of Essential Inorganic Metals on Primary Thermal Degradation of Lignocellulosic Biomass. *Bioresour. Technol.* **2012**, *104*, 687–694.
- (34) Sebestyén, Z.; May, Z.; Réczey, K.; Jakab, E. The Effect of Alkaline Pretreatment on the Thermal Decomposition of Hemp. *J. Therm. Anal. Calorim.* **2010**, *105* (3), 1061–1069.
- (35) Evans, R. J.; Milne, T. A. Molecular Characterization of the Pyrolysis of Biomass. 1. Fundamentals. *Energy Fuels* **1987**, *1* (2), 123–137.
- (36) Trendewicz, A.; Evans, R.; Dutta, A.; Sykes, R.; Carpenter, D.; Braun, R. Evaluating the Effect of Potassium on Cellulose Pyrolysis Reaction Kinetics. *Biomass Bioenergy* **2015**, *74*, 15–25.
- (37) Nowakowski, D. J.; Jones, J. M.; Brydson, R. M. D.; Ross, A. B. Potassium Catalysis in the Pyrolysis Behaviour of Short Rotation Willow Coppice. *Fuel* **2007**, *86* (15), 2389–2402.
- (38) Liu, Q.; Wang, S.; Luo, Z.; Cen, K. Catalysis Mechanism Study of Potassium Salts on Cellulose Pyrolysis by Using TGA-FTIR Analysis. *J. Chem. Eng. Jpn.* **2008**, *41* (12), 1133–1142.
- (39) Wooten, J. B.; Seeman, J. I.; Hajaligol, M. R. Observation and Characterization of Cellulose Pyrolysis Intermediates by <sup>13</sup>C CPMAS NMR. A New Mechanistic Model. *Energy Fuels* **2004**, *18* (1), 1–15.
- (40) Piskorz, J.; Radlein, D. S. A. G.; Scott, D. S.; Czernik, S. Pretreatment of Wood and Cellulose for Production of Sugars by Fast Pyrolysis. *J. Anal. Appl. Pyrolysis* **1989**, *16* (2), 127–142.
- (41) Saleh, S. B.; Hansen, B. B.; Jensen, P. A.; Dam-Johansen, K. Influence of Biomass Chemical Properties on Torrefaction Characteristics. *Energy Fuels* **2013**, *27* (12), 7541–7548.
- (42) Shafizadeh, F.; Fu, Y. L. Pyrolysis of Cellulose. *Carbohydr. Res.* **1973**, *29* (1), 113–122.
- (43) Lede, J.; Li, H. Z.; Villermaux, J. Fusion-like Behavior of Biomass Pyrolysis. *Prépr. Pap. - Am. Chem. Soc. Div. Fuel Chem.* **1987**, *32* (2), 59–67.
- (44) Boutin, O.; Ferrer, M.; Lede, J. Radiant Flash Pyrolysis of Cellulose -- Evidence for the Formation of Short-Lifetime Intermediate Liquid Species. *J. Anal. Appl. Pyrolysis* **1998**, *47* (1), 13–31.

- (45) Axelson, D. E.; Wooten, J. B. Magnetic Resonance Imaging Characterization of Intact Smoked Cigarettes. *J. Anal. Appl. Pyrolysis* **2007**, *78* (1), 214–227.
- (46) Lédé, J.; Blanchard, F.; Boutin, O. Radiant Flash Pyrolysis of Cellulose Pellets: Products and Mechanisms Involved in Transient and Steady State Conditions. *Fuel* **2002**, *81* (10), 1269–1279.
- (47) Piskorz, J.; Majerski, P.; Radlein, D.; Vladars-Usas, A.; Scott, D. . Flash Pyrolysis of Cellulose for Production of Anhydro-Oligomers. *J. Anal. Appl. Pyrolysis* **2000**, *56* (2), 145–166.
- (48) Dufour, A.; Castro-Diaz, M.; Brosse, N.; Bouroukba, M.; Snape, C. The Origin of Molecular Mobility During Biomass Pyrolysis as Revealed by In Situ <sup>1</sup>H NMR Spectroscopy. *ChemSusChem* **2012**, *5* (7), 1258–1265.
- (49) Mercedes Maroto-Valer, M.; Andrésen, J. M.; Snape, C. E. In Situ <sup>1</sup>H NMR Study of the Fluidity Enhancement for a Bituminous Coal by Coal Tar Pitch and a Hydrogen-Donor Liquefaction Residue. *Fuel* **1998**, *77* (9–10), 921–926.
- (50) Kotake, T.; Kawamoto, H.; Saka, S. Mechanisms for the Formation of Monomers and Oligomers during the Pyrolysis of a Softwood Lignin. *J. Anal. Appl. Pyrolysis*.
- (51) Solomon, P. R.; Hamblen, D. G.; Serio, M. A.; Yu, Z.-Z.; Charpenay, S. A Characterization Method and Model for Predicting Coal Conversion Behaviour. *Fuel* **1993**, *72* (4), 469–488.
- (52) Yu, Y.; Liu, D.; Wu, H. Characterization of Water-Soluble Intermediates from Slow Pyrolysis of Cellulose at Low Temperatures. *Energy Fuels* **2012**, *26* (12), 7331–7339.
- (53) Liu, D.; Yu, Y.; Long, Y.; Wu, H. Effect of MgCl<sub>2</sub> Loading on the Evolution of Reaction Intermediates during Cellulose Fast Pyrolysis at 325 °C. *Proc. Combust. Inst.* **2015**, *35* (2), 2381–2388.
- (54) Liu, D.; Yu, Y.; Hayashi, J.; Moghtaderi, B.; Wu, H. Contribution of Dehydration and Depolymerization Reactions during the Fast Pyrolysis of Various Salt-Loaded Celluloses at Low Temperatures. *Fuel* **2014**, *136*, 62–68.
- (55) Ranzi, E.; Corbetta, M.; Manenti, F.; Pierucci, S. Kinetic Modeling of the Thermal Degradation and Combustion of Biomass. *Chem. Eng. Sci.* **2014**, *110*, 2–12.
- (56) Carignan, J.; Hild, P.; Mevelle, G.; Morel, J.; Yeghicheyan, D. Routine Analyses of Trace Elements in Geological Samples Using Flow Injection and Low Pressure On-Line Liquid Chromatography Coupled to ICP-MS: A Study of Geochemical Reference Materials BR, DR-N, UB-N, AN-G and GH. *Geostand. Newsl.* **2001**, *25* (2-3), 187–198.
- (57) Brosse, N.; Sannigrahi, P.; Ragauskas, A. Pretreatment of Miscanthus X Giganteus Using the Ethanol Organosolv Process for Ethanol Production. *Ind. Eng. Chem. Res.* **2009**, *48* (18), 8328–8334.
- (58) Lardier, G.; Bouroukba, M.; Le Brech, Y.; Dufour, A. Intrinsic Heats of Celluloses, Xylan, Lignin and Biomasses Pyrolysis. *In Preparation*
- (59) Eom, I.-Y.; Kim, J.-Y.; Lee, S.-M.; Cho, T.-S.; Choi, I.-G.; Choi, J.-W. Study on the Thermal Decomposition Features and Kinetics of Demineralized and Inorganic Metal-Impregnated Lignocellulosic Biomass. *J. Ind. Eng. Chem.* **2012**, *18* (6), 2069–2075.
- (60) Mok, W. S.-L.; Antal Jr., M. J. Effects of Pressure on Biomass Pyrolysis. II. Heats of Reaction of Cellulose Pyrolysis. *Thermochim. Acta* **1983**, *68* (2–3), 165–186.
- (61) Suuberg, E. M.; Milosavljevic, I.; Oja, V. Two-Regime Global Kinetics of Cellulose Pyrolysis: The Role of Tar Evaporation. *Symp. Int. Combust.* **1996**, *26* (1), 1515–1521.
- (62) Mamleev, V.; Bourbigot, S.; Le Bras, M.; Yvon, J. The Facts and Hypotheses Relating to the Phenomenological Model of Cellulose Pyrolysis. Interdependence of the Steps. *J. Anal. Appl. Pyrolysis* **2009**, *84* (1), 1–17.
- (63) Arseneau, D. F. Competitive Reactions in the Thermal Decomposition of Cellulose. *Can. J. Chem.* **1971**, *49* (4), 632–638.
- (64) Milosavljevic, I.; Oja, V.; Suuberg, E. M. Thermal Effects in Cellulose Pyrolysis: Relationship to Char Formation Processes. *Ind. Eng. Chem. Res.* **1996**, *35* (3), 653–662.
- (65) Bradbury, A. G. W.; Sakai, Y.; Shafizadeh, F. Kinetics Model for Pyrolysis of Cellulose. *J Appl Polym Sci* **1979**, *23* (11), 3271–3280.
- (66) Mettler, M. S.; Paulsen, A. D.; Vlachos, D. G.; Dauenhauer, P. J. Pyrolytic Conversion of Cellulose to Fuels: Levoglucosan Deoxygenation via Elimination and Cyclization within Molten Biomass. *Energy Environ. Sci.* **2012**, *5* (7), 7864–7868.

- (67) Kuzhiyil, N.; Dalluge, D.; Bai, X.; Kim, K. H.; Brown, R. C. Pyrolytic Sugars from Cellulosic Biomass. *ChemSusChem* **2012**, *5* (11), 2228–2236.
- (68) Wang, Z.; Pecha, B.; Westerhof, R. J. M.; Kersten, S. R. A.; Li, C.-Z.; McDonald, A. G.; Garcia-Perez, M. Effect of Cellulose Crystallinity on Solid/Liquid Phase Reactions Responsible for the Formation of Carbonaceous Residues during Pyrolysis. *Ind. Eng. Chem. Res.* **2014**, *53* (8), 2940–2955.
- (69) Wang, Z.; McDonald, A. G.; Westerhof, R. J. M.; Kersten, S. R. A.; Cuba-Torres, C. M.; Ha, S.; Pecha, B.; Garcia-Perez, M. Effect of Cellulose Crystallinity on the Formation of a Liquid Intermediate and on Product Distribution during Pyrolysis. *J. Anal. Appl. Pyrolysis* **2013**, *100*, 56–66.
- (70) Collard, F.-X.; Blin, J. A Review on Pyrolysis of Biomass Constituents: Mechanisms and Composition of the Products Obtained from the Conversion of Cellulose, Hemicelluloses and Lignin. *Renew. Sustain. Energy Rev.* **2014**, *38*, 594–608.

#### IV.1.7 Supporting information

##### Sugar analysis

Standard deviations (STD) have been calculated for biomass components analysis.

*Table IV-5: Analysis of lignin and sugars composition in biomasses*

Samples	% wt biomass Extractible Free							
	Total Sugars	Klason Lignin	Organic matter	Glucose	Xylose	Mannose	Galactose	Arabinose
<b>Douglas</b>	65.6	34.4	99.8	43.7	5.8	8.5	5.1	1.5
<b>STD</b>	0.6	0.6	n.a	0.3	0.5	0.2	0.3	0.1
<b>Oak</b>	74.8	24.2	99.8	48.7	21.5	1.3	1.3	1.3
<b>STD</b>	0.1	0.1	n.a	0.2	0.0	0.0	0.0	0.0
<b>Miscanthus</b>	70.2	29.8	92.4	48.9	18.3	0.0	0.6	2.3
<b>STD</b>	0.0	0.0	0.9	1.3	1.4	0.0	0.0	0.1
<b>Misc_Demin</b>	71.7	28.3	94.8	46.6	20.9	0.0	0.7	2.9
<b>STD</b>	0.48	0.48	0.09	0.436	0.47	0.00	0.04	0.04

##### High temperature <sup>1</sup>H NMR analysis

For the NMR fluidity development studies, a Bruker SEI-HT <sup>1</sup>H NMR probe was used in conjunction with a Bruker DSX300. A flow of 535 L/h hot air was used to heat the sample (see Figure IV-1 in main text). The volatiles formed during pyrolysis were carried out from the remaining solid by a flow (10 Nml/min) of purified argon. The probe was connected with a cooling system provided by Bruker in order to protect the magnet and the shim system. The temperature was monitored by a thermocouple located below the NMR tube. The temperature was calibrated as described in the main text. In order to obtain a <sup>1</sup>H NMR spectrum and to refocus dipolar and quadrupolar couplings, solid echo pulse sequence (90°-τ-90°) was used. A pulse length of 8 μs was maintained throughout the test and 70 scans were accumulated using a recycle time of 0.3 s. For each experiment, a mass of approximately 30 mg was put down into a quartz NMR tube. The experiments were conducted from 25°C to 500°C. and samples were subsequently cooled to 25°C at the rate of 10 °C/min. The solid residue was removed from the tube and the weight of residue was determined to calculate the char ratio. The Fourier-transformed time domain decays of the solid echo pulse signal were deconvoluted into Gaussian and Lorentzian distribution functions by a home-made Matlab program. The fittings regression coefficients (R<sub>2</sub>) are most of the time better than 0.995 and always than 0.99. The program enables the calculation of the fraction of mobile hydrogen fraction (%H<sub>i</sub>).

### Reproducibility of NMR probe measurements

The reproducibility is highlighted in Figure IV-9 showing a good reproducibility for miscanthus and demineralized miscanthus.

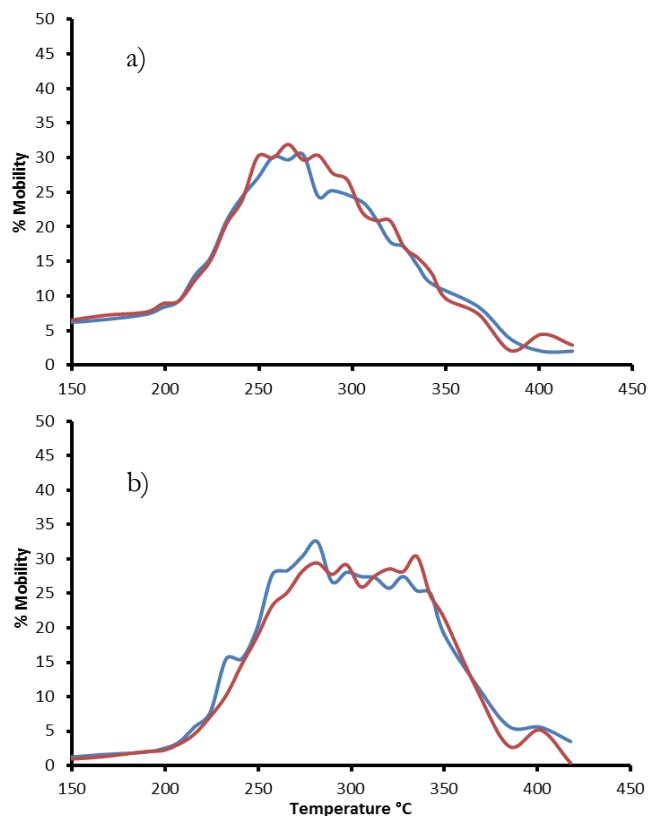


Figure IV-9: Evolution of the Mobile hydrogen fractions as function of temperature for a) miscanthus and b) demineralised miscanthus.

**Mass spectrometric investigations**

Water-soluble fractions have been separated and analyzed by SEC-MS/ELSD. Only anhydro-sugars (DP 1-5) have been identified by mass spectrometry. TIC(+) and ELSD chromatograms from the water-soluble fraction of cellulose char 300°C are presented on Figure IV-10.

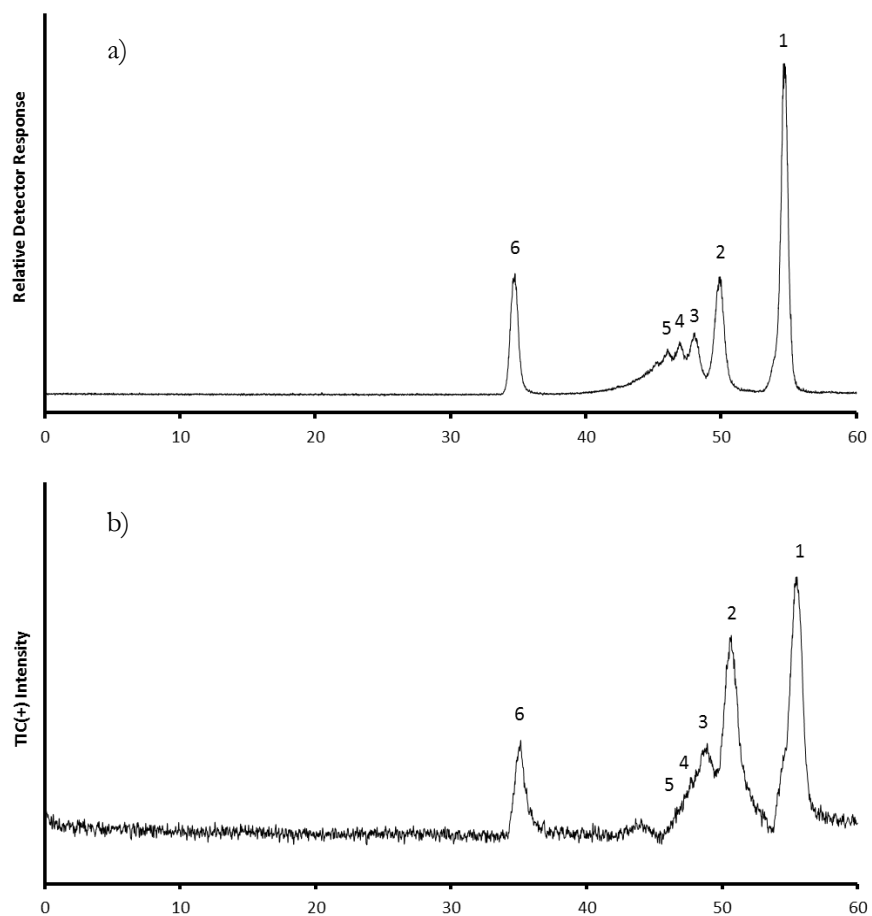


Figure IV-10: ELSD a) and TIC b) from the water-soluble fraction of cellulose char 300°C

Table IV-6: Identified compounds as function of samples

N° peak	5	4	3	2	1
Retention time	45.9	46.9	47.9	49.7	54.6
Cellulose 250°C		m/z 666: [Cellotetraosan+NH <sub>4</sub> ] <sup>+</sup> m/z 671: [Cellotetraosan+Na] <sup>+</sup>	m/z 504: [Cellotriosan+NH <sub>4</sub> ] <sup>+</sup> m/z 509: [Cellotriosan+Na] <sup>+</sup>	m/z 342: [Cellobiosan+NH <sub>4</sub> ] <sup>+</sup> m/z 347: [Cellobiosan+Na] <sup>+</sup>	m/z 185: [Levoglucosan+Na] <sup>+</sup> m/z 203: (H <sub>2</sub> O)[Levoglucosan+Na] <sup>+</sup> . m/z: 217: (MeOH)[Levoglucosan+Na] <sup>+</sup> . m/z 274: [Background]
Cellulose 280°C		m/z 666: [Cellotetraosan+NH <sub>4</sub> ] <sup>+</sup> m/z 671: [Cellotetraosan+Na] <sup>+</sup>	m/z 504: [Cellotriosan+NH <sub>4</sub> ] <sup>+</sup> m/z 509: [Cellotriosan+Na] <sup>+</sup>	m/z 342: [Cellobiosan+NH <sub>4</sub> ] <sup>+</sup> m/z 347: [Cellobiosan+Na] <sup>+</sup>	m/z 185: [Levoglucosan+Na] <sup>+</sup> m/z 203: (H <sub>2</sub> O)[Levoglucosan+Na] <sup>+</sup> . m/z: 217: (MeOH)[Levoglucosan+Na] <sup>+</sup> . m/z 274: [Background]
Cellulose 300°C	m/z 828: [Cellopentaosan+NH <sub>4</sub> ] <sup>+</sup> m/z 833: [Cellopentaosan+Na] <sup>+</sup>	m/z 666: [Cellotetraosan+NH <sub>4</sub> ] <sup>+</sup> m/z 671: [Cellotetraosan+Na] <sup>+</sup>	m/z 504: [Cellotriosan+NH <sub>4</sub> ] <sup>+</sup> m/z 509: [Cellotriosan+Na] <sup>+</sup>	m/z 342: [Cellobiosan+NH <sub>4</sub> ] <sup>+</sup> m/z 347: [Cellobiosan+Na] <sup>+</sup>	m/z 185: [Levoglucosan+Na] <sup>+</sup> m/z 203: (H <sub>2</sub> O)[Levoglucosan+Na] <sup>+</sup> . m/z: 217: (MeOH)[Levoglucosan+Na] <sup>+</sup> . m/z 274: [Background]
Cellulose 320°C	m/z 828: [Cellopentaosan+NH <sub>4</sub> ] <sup>+</sup> m/z 833: [Cellopentaosan+Na] <sup>+</sup>	m/z 666: [Cellotetraosan+NH <sub>4</sub> ] <sup>+</sup> m/z 671: [Cellotetraosan+Na] <sup>+</sup>	m/z 504: [Cellotriosan+NH <sub>4</sub> ] <sup>+</sup> m/z 509: [Cellotriosan+Na] <sup>+</sup>	m/z 342: [Cellobiosan+NH <sub>4</sub> ] <sup>+</sup> m/z 347: [Cellobiosan+Na] <sup>+</sup>	m/z 185: [Levoglucosan+Na] <sup>+</sup> m/z 203: (H <sub>2</sub> O)[Levoglucosan+Na] <sup>+</sup> . m/z: 217: (MeOH)[Levoglucosan+Na] <sup>+</sup> . m/z 274: [Background]
Cellulose 330°C		m/z 666: [Cellotetraosan+NH <sub>4</sub> ] <sup>+</sup> m/z 671: [Cellotetraosan+Na] <sup>+</sup>	m/z 504: [Cellotriosan+NH <sub>4</sub> ] <sup>+</sup> m/z 509: [Cellotriosan+Na] <sup>+</sup>	m/z 342: [Cellobiosan+NH <sub>4</sub> ] <sup>+</sup> m/z 347: [Cellobiosan+Na] <sup>+</sup>	m/z 185: [Levoglucosan+Na] <sup>+</sup> m/z 203: (H <sub>2</sub> O)[Levoglucosan+Na] <sup>+</sup> . m/z: 217: (MeOH)[Levoglucosan+Na] <sup>+</sup> . m/z 274: [Background]
Cellulose 350°C				m/z 342: [Cellobiosan+NH <sub>4</sub> ] <sup>+</sup> m/z 347: [Cellobiosan+Na] <sup>+</sup>	m/z 185: [Levoglucosan+Na] <sup>+</sup> m/z 203: (H <sub>2</sub> O)[Levoglucosan+Na] <sup>+</sup> . m/z: 217: (MeOH)[Levoglucosan+Na] <sup>+</sup> . m/z 274: [Background]

Table IV-6 summarizes the MS identifications according to water-soluble fraction from the different cellulose chars. For each peak and temperature different adducts have been identified by mass spectrometry. Most anhydro-sugars are detected by the association with NH<sub>4</sub><sup>+</sup> or Na<sup>+</sup> ions (Figure IV-10), whereas levoglucosan (54.6 min) mainly forms adduct with Na<sup>+</sup> (m/z 185) and Na<sup>+</sup> stabilized by a molecule of MeOH (m/z 217). An ion at m/z 203 is also detected. it could be associate to (H<sub>2</sub>O)[Levoglucosan+Na]<sup>+</sup>. Several small peaks at m/z 311, 329, 359 and 409 have been detected at the same retention time than levoglucosan but they haven't been identified. Extracted mass spectra for water extraction from cellulose char at 300°C are presented Figure IV-11. For all the samples, a peak is observed at a retention time of 34.5 minutes. This peak seems to be more important for the impregnated cellulose. Unfortunately the MS analysis did not allow us to make any qualitative investigation about this peak (too high molecular weight).

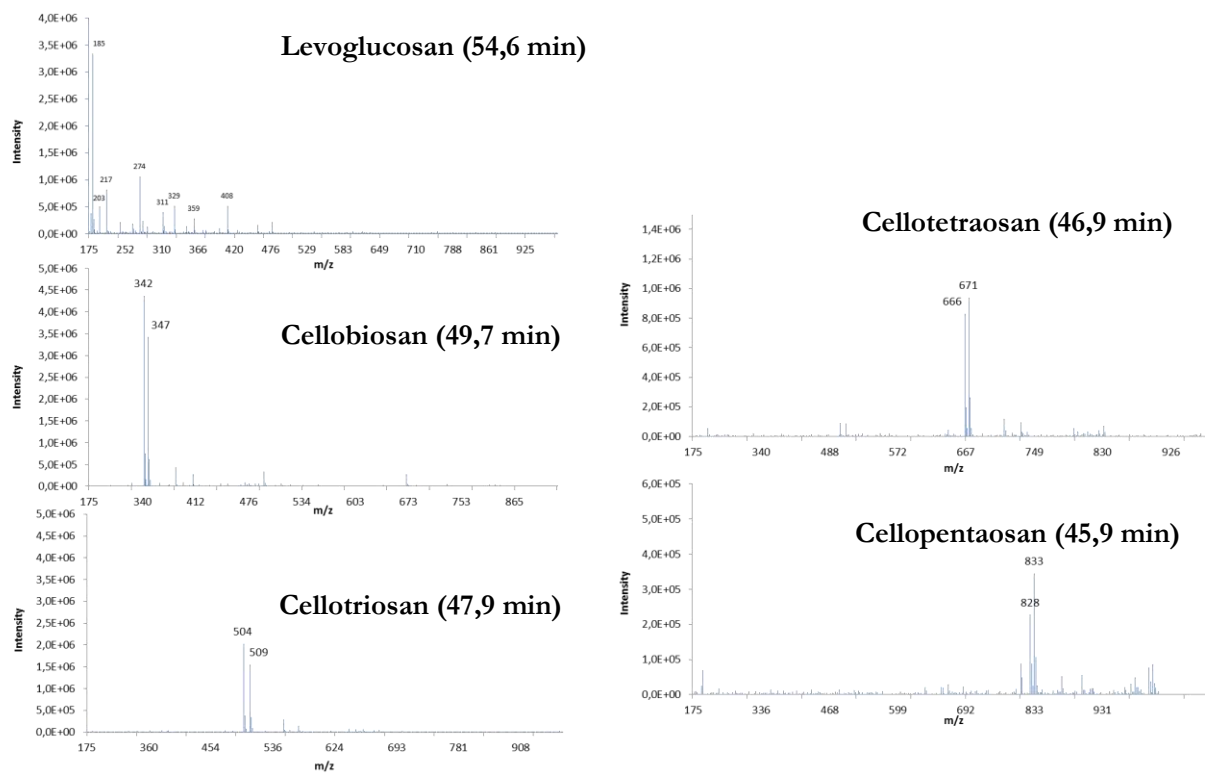


Figure IV-11: Anhydro-sugars MS spectra identified in water-soluble fractions

**V. Etude de la formation des composés volatils**



## **V.1 Article 4: Biomass slow pyrolysis in a fixed bed reactor: mass balance, gas composition and analysis of primary volatiles by on-line VUV photoionisation mass spectrometry and off-line GC\*GC/MS-FID**

Y. Le Brech<sup>1</sup>, L.Y. Jia<sup>1</sup>, S. Cissé<sup>1</sup>, G. Mauviel<sup>1</sup>, N. Brosse<sup>2</sup>, A. Dufour<sup>1</sup>

<sup>1</sup> LRGP, CNRS, Université de Lorraine, 1 rue Grandville 54000 Nancy, France

<sup>2</sup> LERMAB, Université de Lorraine, BP239 54506 Vandoeuvre les Nancy cedex, France.

### **Article à soumettre au journal Energy & Fuels**

#### **V.1.1 Abstract**

Slow pyrolysis of different biomasses (miscanthus, douglas fir and oak) was conducted in a fixed bed reactor swept by a carrier gas in order to suppress secondary reactions. The evolution of solid, condensable and gas phases are studied between 200°C and 500°C. The primary volatiles are analyzed on-line by single-photon ionization (SPI) using VUV light combined with a time-of-flight mass spectrometer (TOFMS). SPI-TOFMS gives the evolution of the main markers of volatiles produced in real-time as a function of the temperature. The chemical structure of the markers analyzed on-line by SPI-TOFMS is determined by GC\*GC/FID-MS analysis of the condensed bio-oils. The pyrolysis mechanisms of hemicelluloses, cellulose and lignin in the complex network of biomass (including minerals catalytic effect) are discussed.

#### **V.1.2 Introduction**

The energy growing demand and the increase of greenhouse gases due to the overexploitation of geological reserves make research in renewable and neutral-carbon resources one of the most crucial challenges for humanity. Since the last four decades<sup>1</sup>, many researches for the conversion of biomass resources into fuel and chemical products have been made. Therefore investigations concerning lignocellulosic biomass, such as wood and herbaceous biomass, have garnered much interest<sup>2</sup>. Thermo-chemical transformation processes (gasification and combustion) are promising option to convert biomass in both energy and biofuels<sup>3</sup>. Pyrolysis is the first step of these processes and consequently it is of tremendous importance to better understand the chemical mechanisms of pyrolysis in order to optimize the selectivity of these transformation processes. Pyrolysis is a primary decomposition step of biomass resulting in the formation of char, primary tars and gases<sup>4</sup>. It controls to a great extent the products distribution and composition<sup>5</sup>. Consequently pyrolysis primary chemical mechanisms have been extensively investigated<sup>6,7</sup> mainly by thermo-gravimetric analysis<sup>8-11</sup>, mass spectrometry analysis<sup>4,12-15</sup> and in-situ spectroscopic analysis<sup>5,16,17</sup>. These investigations have given important insights into the chemical mechanism of biomass pyrolysis. The analysis of the primary volatiles compounds formed during biomass pyrolysis is an important issue to reveal the chemistry of pyrolysis.

Lignocellulosic biomass including woody and herbaceous biomass are composed by three macromolecules (cellulose, hemicelluloses, lignin) organised in a complex network in the cell wall<sup>18</sup>. Cellulose is a polymer of  $\beta$ -D-glucopyranose. Its degradation occurs principally from 300°C to 400°C following different chemical mechanisms. These mechanisms are favoured or inhibited by the operating conditions (temperature, heat flux density) or the presence of inorganics. Cellulose can be converted by three main pathways:

- 1) transglycosylation<sup>4,19,20</sup> which leads to the formation of anhydro-sugars (levoglucosan);
- 2) dehydration<sup>21–23</sup> which induces the formation of insaturated bonds;
- 3) open-ring/fragmentation<sup>24–26</sup> reactions leading to the formation of light oxygenated compounds.

The compounds formed from cellulose (furans, methylglyoxal,...) are produced by combination of these different mechanisms. For instance the formation of furans needs open-ring reactions and dehydration in order to create furan ring from glucopyranose structure.

Hemicelluloses degradation occurs on a more expanded range of temperature than cellulose (from 200 to 350°C) because hemicelluloses are formed by different molecules linked by various chemical bonds which induce different thermal stabilities<sup>27</sup>. Xylan (the polymer of xylose) is the most studied polymer in reference to the hemicelluloses pyrolysis<sup>28,29</sup>. At low temperature (200-250°C) hemicelluloses undergo dehydration reactions<sup>6</sup> and specific chemical function fragmentations<sup>28</sup>. Acetyls, carboxylics and methoxyls moieties are converted into formic acid, acetic acid and methanol respectively<sup>28,30</sup>. For higher temperature (250-350°C) the formation of furanic compounds (furans and furanones) is observed from the combinaison of dehydration, open-ring and cyclization reactions. The formation of anhydro-sugars (levoglucosane, levogalactosane or 1,4-anhydro-D-xylopyranose...) from glycosidic ruptures is also described<sup>31</sup>. Furfural is one of the major compounds from xylan pyrolysis<sup>28</sup>. Pyranones are also described as a product of hemicelluloses pyrolysis<sup>32,33</sup>.

Lignin is a phenolic macromolecule constituted of phenylpropane units linked together through various ether and carbon-carbon linkages<sup>34,35</sup>. The main conversion step of lignin occurs over a large temperature range from 150 to 500°C.<sup>36,37</sup> At low temperature (150-300°C), oxygenated propyl chains are mainly converted in water by dehydration reactions<sup>36</sup> and formaldehydes by the release of carbonyl functions localized on carbon C $\gamma$ <sup>35</sup>. The ether linkages ( $\alpha$ -O-4 and  $\beta$ -O-4) can react from 200°C<sup>6</sup> leading to the formation of unsaturated chains or to the release of phenolic compounds with chemical structures close to the native network. Besides, these phenolic compounds are composed of oxygenated aromatic rings substituted by an alkyl chain with two or three carbons (eugenol, 4-vinyl-guaiacol). For temperature higher than 300°C, alkyl chain conversion is global<sup>38</sup> and phenolic compounds without or with a short alkyl chain (mainly one carbon such as methylguaiacol) are devolatilized<sup>4,39,40</sup>. Methoxyl moieties become reactive from approximately 370°C (depending on the inorganic content of lignins) leading to the formation of methanol and methane by demethoxylation and demethylation reactions respectively. Consequently, demethoxylated (phenol, methylphenol) and demethylated (catechol, cresol) phenolic compounds are also released.

In the present work, a fixed bed reactor was combined with on-line analysis of volatiles by single-photon ionization (SPI)-time of flight mass spectrometry (TOF-MS) and off-line analysis after condensation followed by GC\*GC/FID\*MS analysis. The U-shape fixed bed allows controlling external mass transfer, temperature of the bed, quenching char and quantifying mass balance. The main advantage of SPI-MS is that the ionisation is soft and leads to a more interpretable mass spectra with few or no fragment ions<sup>39</sup>.

### V.1.3 Material and methods

#### Characterization of biomass

In this study, *Miscanthus x Giganteus* has been used because of its high production yields and its low need in fertilizers. *Miscanthus* was harvested in Lorraine (France, Lorraine). Douglas and oak were harvested in the Haut-Beaujolais area (South-East France). They were milled and sieved to a particle size between 40 and 100  $\mu\text{m}$ . This particle size was kept constant for all characterizations and pyrolysis experiments. A complete characterization of these biomass is given in Supporting Material.

#### Pyrolysis procedure

The pyrolysis of *Miscanthus*, oak and douglas (800 mg) was conducted in a vertical U-shape quartz fixed bed reactor under atmospheric pressure. Figure V-1 presents the apparatus. The particles (40-100  $\mu\text{m}$ ) were supported on a quartz sintered plate (20 mm internal diameter). This geometry allows a good control of temperature, thanks to a thermocouple (0.5 mm diameter) placed inside the fixed bed of biomass, and of mass transfer by flushing the fixed bed with a given flow rate of argon (300  $\text{NmL min}^{-1}$ ). The reactor was heated by an electrical furnace from 20°C to various final set temperatures (between 280 and 500°C) at a heating rate of 5  $\text{K min}^{-1}$ . The radial temperature gradient in the fixed bed was studied (by various thermocouples positioned along the diameter of the fixed bed) and was below 10°C between the middle and the border of the fixed bed of particles. Once the final set temperature was achieved, the furnace was immediately moved down and the reactor was immediately immersed in ice-water in order to quench the reactions (2 minutes cooling time from 500°C to 150°C). Char was cooled down under argon until 30°C and then collected for further analysis. The traps used to collect condensable products were then weighted.

The pyrolysis experiments with the on-line SPI-MS and the condensation system were performed separately.

#### Analysis of condensables by GC\*GC/MS-FID

The off-gas line which connected the quartz reactor to the cold traps (Figure V-1) was heated at 350°C in order to prevent condensation. Cold traps were glass tube fitted with glass beads (without solvent). The first trap was put inside an ice-water bath (0°C) in order to condense the water and “heavy” compounds formed during pyrolysis. The two following traps were put in propanol-liquid nitrogen mix (-60°C). A bubbler with methanol was placed after the three cold traps. All traps were washed with a total of approximately 20mL of methanol. An internal standard (1  $\mu\text{l}$ , tetradecene, Sigma Aldrich ref 87187) was injected in the whole volume (~20mL methanol and condensables). The solution of condensed products (with the internal standard) was analysed by an Agilent 7890 gas chromatograph coupled to an Agilent 5975C MS analyser. The solution (1  $\mu\text{l}$ ) was injected with a split ratio of 10 into an Agilent HP-5MS connected with a heart-cutting system (Dean’s switch) to an Agilent DB-Wax123 column. These two columns were chosen because of their complementary polarities. More details on the calibration and predictive quantification method are available in the Supporting Material. More than 100 oxygenated compounds have been detected and 30 compounds have been clearly identified by MS and the NIST database. Between 25 and 30 compounds have been quantified for each biomass.

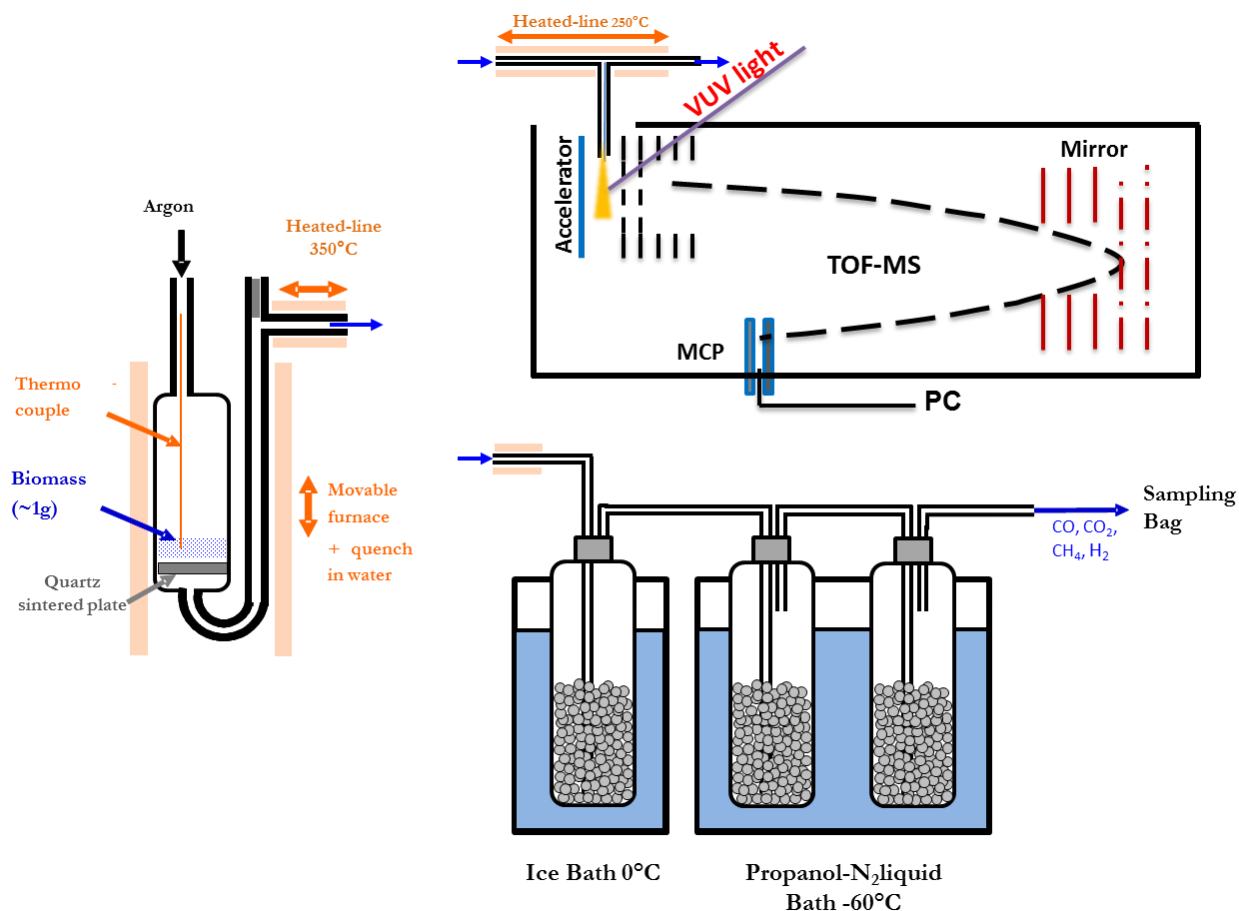


Figure V-1: Schematic of the fixed bed reactor

### Analysis of permanent gases

Incondensable gases were collected by a gas sampling bag positioned after the bubbler. They were analysed on a  $\mu$ GC-Varian 490 equipped with four modules, composed of two molecular sieves 5A, a PoraPlot U and a CP-Wax 52CB columns.  $\mu$ GC-490 signal was calibrated using standard bottles (Air Liquide, France). Four major gases ( $H_2$ , CO,  $CO_2$  and  $CH_4$ ) were quantitatively determined.

### On-line analysis of volatiles by SPI-MS

The on-line SPI-MS (developed by the Photonion company) was connected to the off-gas line of the quartz reactor. A small fraction of the gas phase products was sampled through a capillary line at  $250^\circ C$  and injected to the photoionisation region of the SPI-MS. The SPI-MS is composed of an orthogonal acceleration time-of-flight mass spectrometer (TOF-MS, resolution  $\sim 2000$  at  $m/z$  78) equipped with an argon-discharged vacuum ultraviolet (VUV) lamp system (*E-Lux 126, Optimare, Germany*). The photon energy of VUV light is 9.8 eV.

## V.1.4 Results

### Mass yields in gaseous, liquid and char

Figure V-2 presents the mass yields of gaseous, liquid and char products as a function of the final pyrolysis temperature for miscanthus. The global mass balance is between 95 and 108wt%. Char yield decreases sharply in the temperature range of 280 and 350°C (75 wt% to 40 wt%) whereas the condensable and gaseous yields increase from 25 wt% to 48 wt% and 3 wt% to 8 wt% respectively. From 350°C product yields evolve then slowly, char yield decreases until 30 wt%, condensable and gaseous yields slightly increase up to 56 wt% and 10 wt% respectively. The water content in the condensed phase was not determined since the amount of condensable was not sufficient. However, water was reported as a major component of the condensed phase<sup>41</sup>. The char yields obtained after rapid quenching in the fixed bed were in good agreement with thermogravimetry analysis (see Supporting Information).

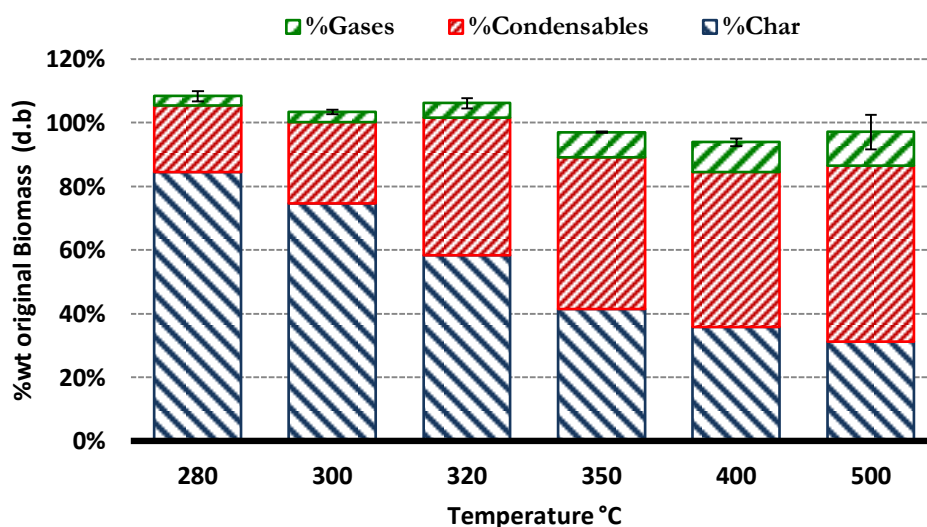


Figure V-2: Mass balances for miscanthus slow pyrolysis

Figure V-3 presents the yield of gaseous, liquid and char products as a function of temperature for oak and douglas. For these biomasses only the final temperatures of 300°C and 500°C have been investigated. At the temperature of 300°C, the yield of gases is very low (~1 wt% for douglas and ~1.5 wt% for oak) and the char yield from oak is lower compared to the char yield from douglas. This observation was confirmed by thermogravimetric analysis (See Supporting information). This could be explained by a different composition of oak, douglas and miscanthus. Douglas hemicelluloses are composed predominantly of glucomannan whereas oak hemicelluloses are composed of xylan, therefore this induces different thermal stabilities<sup>6</sup>. At the temperature of 500°C the char yield is quite similar between the two wood species (~23%). For miscanthus, char yields at 300°C and 500°C are higher mainly due to the higher inorganic content. The high condensable yields (~67%) and the low gas yields (~6%) indicate that the secondary reaction of volatiles was insignificant during fixed bed experiments.

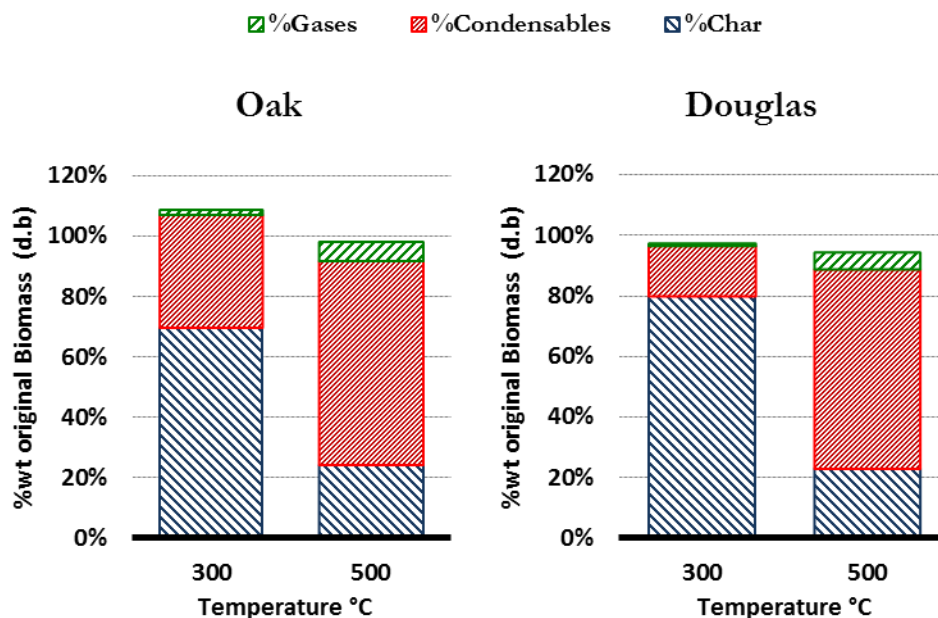


Figure V-3: Mass balances for oak and douglas slow pyrolysis

### Gas Compositions

Gases released during pyrolysis have been quantified as function of temperature and are presented in Figure V-4. CO<sub>2</sub> and CO display a similar pattern. H<sub>2</sub> was detected at the temperature of 500°C but not quantified because of a very low concentration. The formation of CH<sub>4</sub> starts at 350°C and increases until 500°C. The emission of CO<sub>2</sub> is mainly due to the cleavage of carboxyl function present in hemicelluloses and lignin.<sup>28,36</sup> The formation of CO arises from cleavage of carbonyl functions naturally present in hemicelluloses and lignin but also from the cleavage of C-O and C-O-C bonds. The production of methane (CH<sub>4</sub>) occurs at higher temperature highlighting the demethylation of lignin methoxyl groups remaining into the char and also the breaking of methylene groups.<sup>36</sup> Concerning douglas and oak, the amount of gas released during slow pyrolysis (shown in supplementary material) are smaller but in accordance with literature<sup>37,42</sup>.

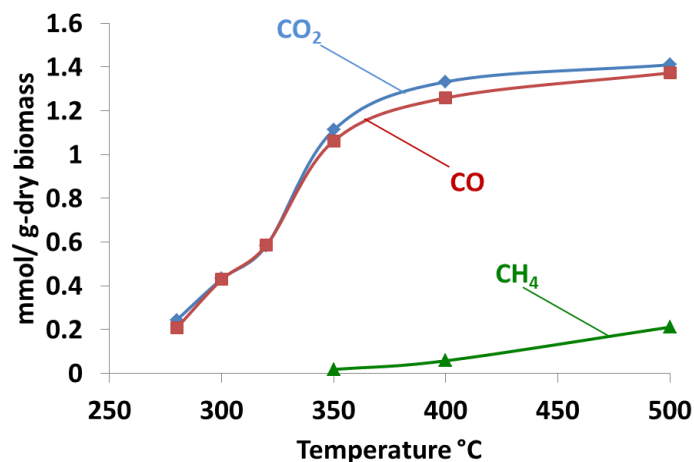


Figure V-4: The gas release from the slow primary pyrolysis of miscanthus

### **GC/MS analysis**

The condensed phase, as revealed by GC/MS analysis (Figure V-5) contains a wide variety of products. Their complete quantification appears to be very difficult, some compounds being too heavy to be quantified by GC. The GC-analysed products of miscanthus, oak and douglas represent about 8.2 %, 13.3 % and 11.7 % of the initial weight of dry biomass respectively. The more intense identified compounds have been quantified and they are presented in Table V-1. Their chemical structures are given in supporting information. Concerning miscanthus, the evolution profiles of key compounds as a function of temperature have been plotted on Figure V-6.

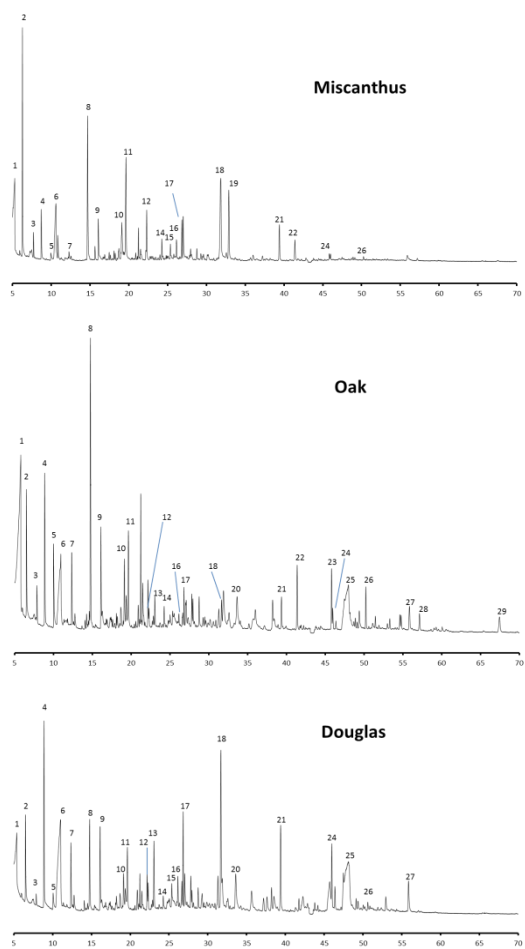


Figure V-5: Chromatogram for the condensable sampled from the three biomasses at 500°C final temperature

Table V-1: Main compounds quantified (mg/g dry biomass) by GC/MS-FID (\* n.q means not quantified)

N°	Compounds	N° CAS	Mw	Formula	Miscanthus	Oak	Douglas	Ref. for qualitative assignment
1	Acetic acid	64-19-7	60	C <sub>2</sub> H <sub>4</sub> O <sub>2</sub>	18.88	40.41	7.91	NIST
2	2-Propanone, 1-hydroxy	116-09-6	74	C <sub>3</sub> H <sub>6</sub> O <sub>2</sub>	10.25	4.38	3.60	NIST
3	Ethyl-1-propenyl ether	928-55-2	86	C <sub>5</sub> H <sub>10</sub> O	0.71	0.65	0.26	NIST
4	Methylglyoxal	78-98-8	72	C <sub>3</sub> H <sub>4</sub> O <sub>2</sub>	3.60	6.72	10.30	NIST
5	1-Penten-3-one	1629-58-9	84	C <sub>5</sub> H <sub>8</sub> O	0.00	2.25	0.58	NIST
6	Propanal, 2,3 dihydroxy	367-47-5	90	C <sub>3</sub> H <sub>6</sub> O <sub>3</sub>	14.24	17.39	29.49	NIST
7	Propanoic acid, 2-oxo-, methyl ester	600-22-6	102	C <sub>4</sub> H <sub>6</sub> O <sub>3</sub>	0.53	2.89	3.20	NIST
8	furfural	98-01-1	96	C <sub>5</sub> H <sub>4</sub> O <sub>2</sub>	6.82	9.19	3.71	NIST
9	2-Furanmethanol	98-00-0	98	C <sub>5</sub> H <sub>6</sub> O <sub>2</sub>	2.03	2.79	2.88	NIST
10	2(5H)-Furanone	497-23-4	84	C <sub>4</sub> H <sub>4</sub> O <sub>2</sub>	n.q*	2.99	2.15	NIST
11	2,cyclopenten-1-one, 2 hydroxy	10493-98-8	98	C <sub>5</sub> H <sub>6</sub> O <sub>2</sub>	6.42	4.05	2.94	NIST
12	Phenol	108-95-2	94	C <sub>6</sub> H <sub>6</sub> O	1.49	0.34	0.61	NIST
13	4-Hydroxy-5,6-dihydro-(2H)-pyran-2-one	-	114	C <sub>5</sub> H <sub>6</sub> O <sub>3</sub>	0.00	1.25	3.33	<sup>43</sup>
14	Corylon	80-71-7	112	C <sub>6</sub> H <sub>8</sub> O <sub>2</sub>	0.95	0.48	0.35	NIST
15	Phenol 2-methyl	95-48-7	108	C <sub>7</sub> H <sub>8</sub> O	0.43	n.q*	0.44	NIST
16	Phenol, 4-methyl-	106-44-5	108	C <sub>7</sub> H <sub>8</sub> O	0.61	0.17	0.57	NIST
17	Phenol, 2-methoxy-	90-05-1	124	C <sub>7</sub> H <sub>8</sub> O <sub>2</sub>	1.30	0.84	2.05	NIST
18	Phenol, 2 methoxy-4-methyl	93-51-6	138	C <sub>8</sub> H <sub>10</sub> O <sub>2</sub>	n.q*	0.82	5.34	NIST
19	4 vinyl phenol	496-16-2	120	C <sub>8</sub> H <sub>8</sub> O	3.48	0.00	0.00	<sup>44</sup>
20	2-Furaldehyde, 5-(hydroxymethyl)-	67-47-0	126	C <sub>6</sub> H <sub>6</sub> O <sub>3</sub>	0.00	3.32	2.79	NIST
21	2-Methoxy-4-vinylphenol	7786-61-0	150	C <sub>9</sub> H <sub>10</sub> O <sub>2</sub>	1.84	1.05	2.71	NIST
22	Phenol, 2,6-dimethoxy-	91-10-1	154	C <sub>8</sub> H <sub>10</sub> O <sub>3</sub>	1.34	1.91	0.00	NIST
23	vanillic acid	121-34-6	168	C <sub>8</sub> H <sub>8</sub> O <sub>4</sub>	0.00	1.79	0.00	NIST
24	Isoeugenol	5932-68-3	164	C <sub>10</sub> H <sub>12</sub> O <sub>2</sub>	n.q*	0.43	4.41	NIST
25	Levogluosane	498-07-7	162	C <sub>6</sub> H <sub>10</sub> O <sub>5</sub>	0.00	19.57	25.55	NIST
26	Coniferyl alcohol (Douglas)/ 4-vinyl syringol (Oak and Miscanthus)	458-35-5/ 28343-22-8	180	C <sub>10</sub> H <sub>12</sub> O <sub>3</sub>	n.q*	1.07	0.31	<sup>44</sup>
27	2-Propenal, 3-(4-hydroxy-3-methoxyphenyl)-	127321-19-1	178	C <sub>10</sub> H <sub>10</sub> O <sub>3</sub>	n.q*	0.96	0.04	<sup>44</sup>
28	Syringyl acetone	19037-58-2	210	C <sub>11</sub> H <sub>14</sub> O <sub>4</sub>	0.00	0.66	0.00	<sup>44</sup>
29	3,5-Dimethoxy-4-hydroxycinnamaldehyde	87345-53-7	208	C <sub>11</sub> H <sub>12</sub> O <sub>4</sub>	0.00	0.93	0.00	<sup>44</sup>

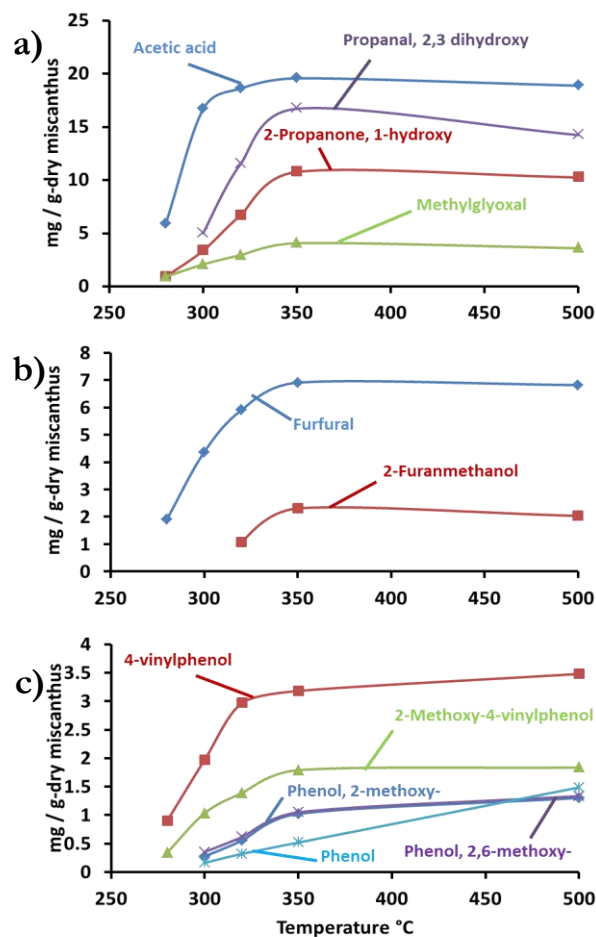


Figure V-6: Effect of the final pyrolysis temperature on the yield of some key primary tar compounds from miscanthus. a) Low molecular weight molecules, b) furan derivatives, c) phenol derivatives

Carbohydrates markers can be divided in different categories which showing the different chemical pathway for thermal degradation as function of temperature and biomass composition:

- 1) the light oxygenated compounds (acetic acid; 2-propanone,1-hydroxy; ethyl-1-propenyl ether; methylglyoxal; 1-penten-3-one; propanal 2,3, dihydroxy and propanoic acid, 2-oxo methyl ester) testify to the fragmentation/dehydration pathways;
- 2) the furanic compounds (furfural ; 2-furanmethanol ; 2-furaldehyde, 5-(hydroxymethyl)-), furanones (2(5H)-furanone) ; and cyclopentanone (2,cyclopenten-1-one, 2 hydroxy ; corylon) highlight the dehydration/open-ring/cyclisation mechanism;
- 3) Anhydro-sugars (levoglucosan) evidence the transglycosylation pathway.

Acetic acid is more important according to miscanthus and oak pyrolysis. Concerning miscanthus the evolution during pyrolysis occurs mainly in the range of 200 – 300°C (Figure V-6) corresponding to the degradation of hemicelluloses. For oak, acetic acid continue to be formed after 300°C, this observation is in agreement with TG analysis which shows that oak degradation occurs at higher temperature probably due to lower inorganics content. 2-propanone,1-hydroxy is more important for miscanthus pyrolysis whereas methylglyoxal is a major product of douglas pyrolysis. Propanal, 2,3, dihydroxy is an important product for miscanthus and oak but not for douglas. Levoglucosan is detected and quantified for oak and douglas but not

in miscanthus highlighting the catalytic effect of minerals which inhibit the transglycosylation pathway<sup>45,46</sup>. Before 300°C, no levoglucosan is observed for oak and douglas showing that transglycosylation reaction is not yet started at this temperature. All compounds assigned to carbohydrate products formed before this temperature (300°C) mainly come from hemicelluloses degradation. For instance, formation of furfural which is a good indicator of hemicelluloses degradation (for xylan mainly) is important for oak at 300°C indicating the hemicelluloses degradation starts before 300°C. Furfural is not so important in douglas products highlighting the low xylose content in the native biomass. However the formation of 4-hydroxy-5,6-dihydro-(2H)-pyran-2-one is more important in douglas and oak than in miscanthus. It could be explain by mineral catalytic effects<sup>33</sup>. The presence of an anhydrosugar compound (not identified clearly) at 45.72 min was only detected in douglas products highlighting the specific hemicelluloses composition of douglas as compared to miscanthus and oak. This compound which is formed from hemicelluloses evidence that hemicelluloses with a low mineral content undergo the formation of anhydrosugar.<sup>33</sup> Furthermore, the formation of 4-hydroxy-5,6-dihydro-(2H)-pyran-2-one which is a C<sub>5</sub> compound is observed for douglas whereas douglas hemicelluloses are mainly composed of C<sub>6</sub> sugars. Further investigations are necessary to understand its mechanism of formation.

The formation of cyclopentenones (2,cyclopenten-1-one, 2 hydroxy ; corylon) is enhanced in miscanthus whereas the formation of anhydrosugar (levoglucosan), furan (2-furaldehyde, 5-(hydroxymethyl)-) is more important for oak and douglas. Furthermore, a furanone is detected (m/z 128, retention time 26.64 min, not quantified) and appears to be an important compound for oak and douglas. This compound has been assigned to 5-methyl-4-oxotetrahydrofuran-2-carbaldehyde in a previous investigation from our by synchrotron SPI/MS\*MS<sup>39</sup>. The selectivity concerning the formation of these compounds seems to be led by the inorganic catalytic effects. As already described<sup>11</sup>, furanones and anhydro-sugars are more important from biomass with low mineral content whereas cyclopentanone derivatives and phenol are more important<sup>47</sup> for biomass with high inorganic content (especially potassium). Cyclopentenone could be formed by rearrangement (aldol reaction) and dehydration of carbohydrates. A global simplified mechanism for cellulose pyrolysis is proposed in Figure V-7.

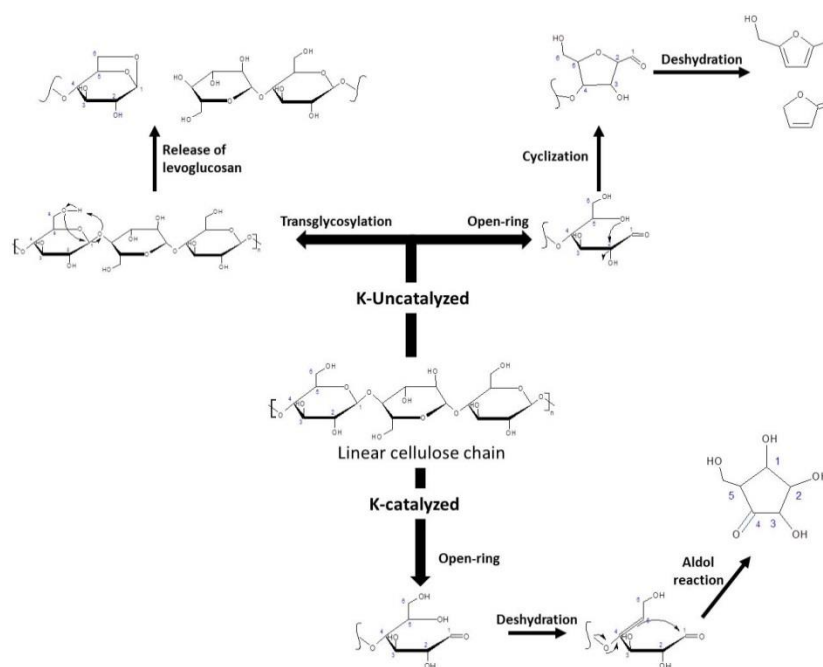


Figure V-7: Simplified mechanism of cellulose pyrolysis highlighting the main degradation pathways and key markers

Oxygenated aromatic compounds are good lignin markers and the substituted degree of these aromatic compounds is a good indicator of the thermal treatment severity. Concerning douglas, no syringyl derivative was detected which is in agreement with the low syringyl units content in coniferous woods. Concerning miscanthus, the evolution of phenol, 2,6-dimethoxy; 2-methoxy-4-vinylphenol; phenol, 2 methoxy-4-methyl; phenol, 2-methoxy- and 4-vinylphenol has been plotted in the Figure V-6. It is shown that these lignin products are mainly formed between 280 and 350°C. Phenol, 2,6-dimethoxy and phenol, 2-methoxy- exactly follow the same trend showing that they could be produced by the same chemical mechanism.

### SPI-TOFMS

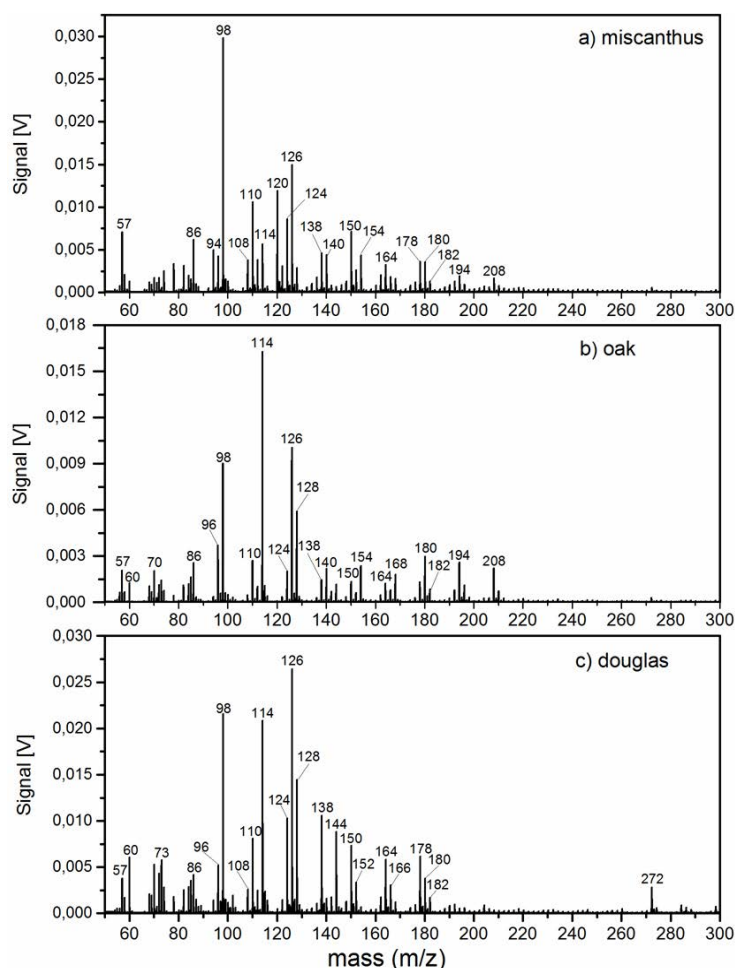


Figure V-8: Total mass spectra accumulated on whole experimental time until 500°C

Mass spectra obtained for the three investigated biomasses (fixed bed, 5°C/min, final temperature 500°C) are displayed in Figure V-8. By comparison with products identified in GC/MS and based on previous studies<sup>4,12,39,48</sup>, the main m/z which are molecular ions from the key markers of pyrolysis mechanisms have been identified. The main product from the pyrolysis of cellulose are furfuryl alcohol and 2-cyclopenten-1-one, 2 hydroxy (m/z 98); furfural (m/z 96); 2-furaldehyde, 5-(hydroxymethyl)- (m/z 126) and 5-methyl-4-oxotetrahydrofuran-2-carbaldehyde (m/z 128). Products from transglycosylation : levoglucosan (m/z 162) or levoglucosan fragments (m/z 144, 126, 98 and 97) induced by dissociative photoionisation as already

described<sup>39</sup> are observed. Peaks at  $m/z$  43, 57 and 73 are also observed and could mainly come from the fragmentations of carbohydrate products.<sup>13,49,50</sup> It corresponds mainly to low molecular weight carbonyl compounds<sup>13</sup> ( $m/z$  : 43  $C_2H_3O^+$ ). 3-Hydroxy-2-penteno-1,5-lactone ( $m/z$  114) which is a compound from hemicelluloses degradation is also observed. This compound has been identified in previous studies as a hemicelluloses marker<sup>39,51</sup>. It has been confirmed by GC/MS analysis and by comparison between literature data<sup>43</sup>.

Lignin markers are also detected for each biomass highlighting the difference in the native network. The main  $m/z$  ions were assigned to the following markers: Phenol ( $m/z$  94); phenol, 2-methoxy-4-methyl ( $m/z$  138); 2-methoxy-4-vinylphenol ( $m/z$  150); phenol, 4-ethyl-2-methoxy ( $m/z$  152, not quantified, 37.2 min); phenol, 2,6-dimethoxy- ( $m/z$  154); isoeugenol ( $m/z$  164); 2-Propenal 3-(4-hydroxy-3-methoxyphenyl)- ( $m/z$  178); coniferyl alcohol (Douglas) and 4-vinyl syringol (Oak) ( $m/z$  180); propenylsyringol ( $m/z$  194, not quantified, 61.4 min); 3,5-Dimethoxy-4-hydroxycinnamaldehyde ( $m/z$  208). The different profiles concerning different markers for cellulose, hemicelluloses and lignin have been plotted as function of temperature and are presented in Figure V-9,10 and 11 for miscanthus, oak, douglas respectively.

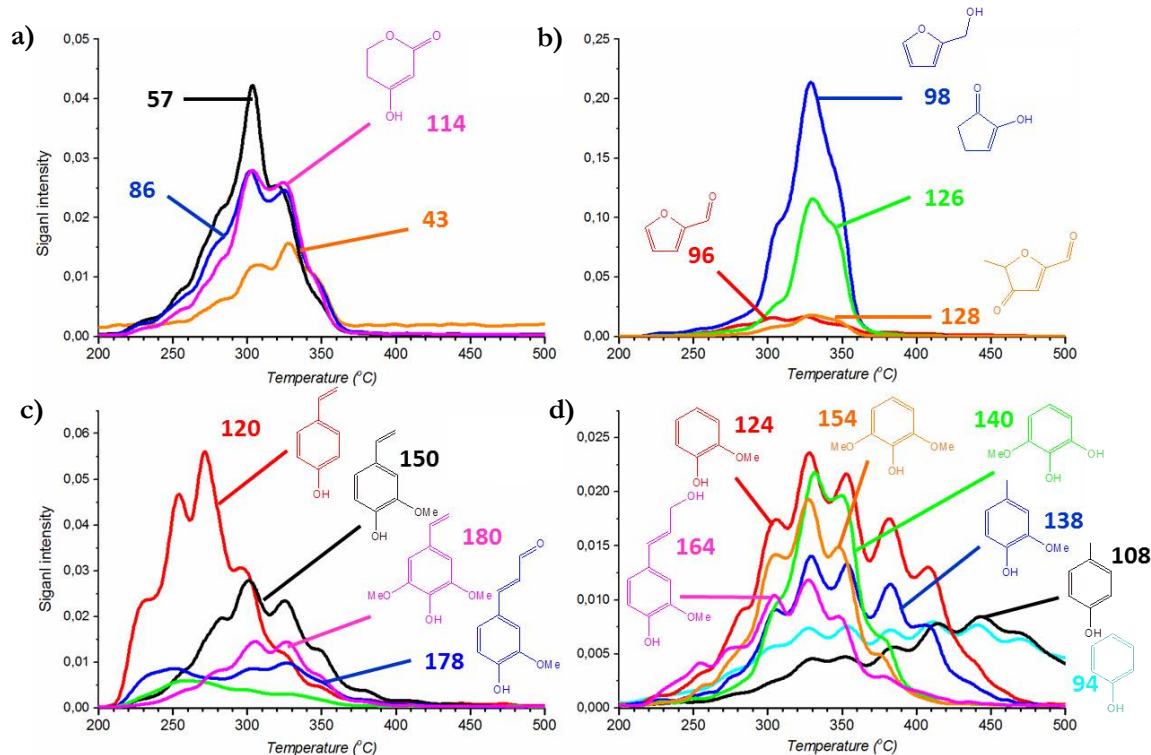


Figure V-9: On-line analysis of key markers by SPI-MS vs. temperature of pyrolysis for miscanthus, a) hemicelluloses and carbohydrate fragments, b) main cellulose markers, c) lignin markers at low temperature, d) lignin markers at high temperature.

Concerning miscanthus, the first products (from 220°C) analysed by SPI-MS are 4-vinylphenol ( $m/z$  120) and 2-propenal 3-(4-hydroxy-3-methoxyphenyl)- ( $m/z$  178) (Figure V-9c). These products could mainly come from the thermal degradation of the acetyl functions localized at C $\gamma$  of the propyl side chains of lignin monomers in the native network. The native lignin in *Miscanthus x Giganteus* is highly acetylated at the C $\gamma$  possibly with acetate or p-coumarate groups<sup>52</sup>. Consequently, the formation of 4-vinylphenol ( $m/z$  120) and 2-propenal 3-(4-hydroxy-3-methoxyphenyl)- ( $m/z$  178) could be due to the breaking of acetate functions. C $\gamma$  implied into carbonyl function is likely to break at temperature around 250°C.<sup>6</sup> The  $m/z$  at 150 (2-methoxy-4-

vinylphenol) and  $m/z$  180 (4-vinyl syringol), observed at slightly higher temperature, could be produced probably by the combination of dehydration and the breaking of ether bounds.<sup>6</sup> The carbohydrates degradation is highlighted by the evolution of 3-hydroxy-2-penteno-1,5-lactone ( $m/z$  114) which comes mainly from hemicelluloses thermal degradation<sup>33,39</sup> and carbohydrate fragments ( $m/z$  43, 57 and 86) from 220°C until 370°C with a maximum around 300°C. This degradation becomes more important at higher temperature (300°C-350°C) with the release of furfuryl alcohol and 2-cyclopenten-1-one, 2 hydroxy ( $m/z$  98) and the  $m/z$  126. The  $m/z$  126 may be assigned to levoglucosenone (detected by GC/MS but not quantified). The degradation of lignin structure is significant from 250°C to 450°C (Figure V-9, d)) with the release of many different compounds as phenol, 2-methoxy- ( $m/z$  124) ; phenol, 2,6-dimethoxy- ( $m/z$  154); catechol, 3-methoxy ( $m/z$  140, not quantified, 36.06 min); phenol, 2 methoxy-4-methyl ( $m/z$  138) ; isoeugenol ( $m/z$  164) ; methylphenol ( $m/z$  108) ; phenol ( $m/z$  94). These compounds come mainly from the conversion of the alkyl chain (phenol, 2-methoxy- ; phenol, 2,6-dimethoxy- ; phenol, 2 methoxy-4-methyl) which induce C-C linkage breaking. Compounds which require demethoxylation reaction are also observed. Indeed phenol ( $m/z$  94) and methylphenol ( $m/z$  108) were detected from 250°C to high temperature (500°C). The catechol, 3-methoxy is also observed but only from 270 to 400°C. This compound is formed by the demethylation of syringol units enhanced by minerals catalytic effect<sup>53</sup>.

The formation of volatiles starts at 220°C for oak slow pyrolysis (Figure V-10). Indeed, some lignin markers are detected 3,5-dimethoxy-4-hydroxycinnamaldehyde ( $m/z$  208) and 2-propenal, 3-(4-hydroxy-3-methoxyphenyl)- ( $m/z$  178). The formation of these phenolic aldehydes in the first step of pyrolysis has been already described<sup>54</sup>. It is due to ether  $\alpha$ -O-4 and/or  $\beta$ -O-4 splitting at about 200°C and 250°C respectively<sup>55</sup>. This reaction should be combined with the formation of C=O moieties on the  $C_\gamma$  of the propyl side chain probably by dehydration<sup>54</sup> of the  $C_\gamma H_2 OH$  moiety or conversion of the carboxyl group on  $\gamma$ -position. The formation of these aldehydes could be also due to the large quantities of radicals. Radicals are formed in the first step of lignin pyrolysis through the homolytic cleavage of the lignin ether linkages which react with the  $C_\gamma$ -hydrogen at the conjugated allyl position<sup>56</sup> to form aldehydes.

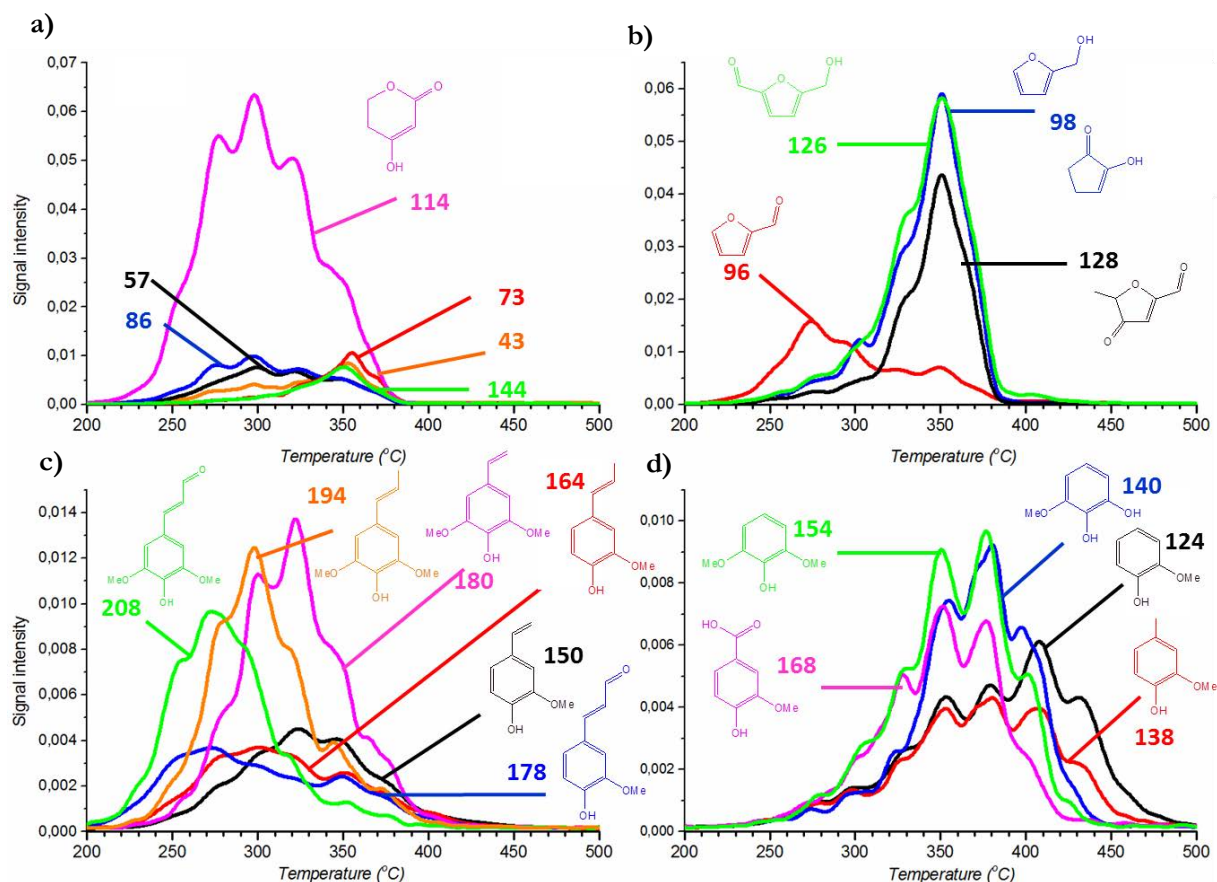


Figure V-10: On-line analysis of key markers by SPI-MS vs. temperature of pyrolysis for oak, a) hemicelluloses and carbohydrate fragments, b) main cellulose markers, c) lignin markers at low temperature, d) lignin markers at high temperature.

At slightly higher temperature, propenyl syringol (m/z 194, not quantified, at 54.6 min on GC chromatogram); 4 vinyl syringol (m/z 180); isoeugenol (m/z 164); 2-methoxy-4-vinylphenol (m/z 150) and 2-propenal, 3-(4-hydroxy-3-methoxyphenyl)- (m/z 178) are detected. These products are formed from ether-linkage (for propenyl phenolic compounds : m/z 164, m/z 194) combined to C-C breaking (for vinyl phenolic compounds m/z 150, m/z 180). These products highlight the formation of double bond in conjugation with the aromatic ring in the early stage of pyrolysis<sup>4</sup> which is described to come from the enhancement of H-donor species<sup>56</sup>. H-addition reactions<sup>57</sup> could provoke the formation of products with double bond in conjugation with the aromatic ring as isoeugenol and vinylguaiacol. H-donor species are formed from hydrogen radicals<sup>56</sup> during aromatization mechanisms. These radicals could come from the aromatization of hemicelluloses starting in the same range of temperature.

As for miscanthus pyrolysis, the degradation of carbohydrates in oak is highlighted by the evolution of 3-hydroxy-2-penteno-1,5-lactone (m/z 114) and carbohydrate fragments<sup>49</sup> (m/z 43, 73, 57). Ethyl-1-propenyl ether (m/z 86) are less significant compare to m/z 114. Hence the formation of 3-hydroxy-2-penteno-1,5-lactone is favoured for oak. Minor fragmentation reactions are induced in oak hemicelluloses probably due to the low concentration of inorganics. Furfural (m/z 96) is also detected from 220°C to 400°C with a maximum at 270°C highlighted that conversion of oak's hemicelluloses (mainly xylan) occurred at this temperature. This observation is in accordance with the thermogravimetric analysis (see supplementary material).

At higher temperature, the formation of phenolic compounds with small alkyl chain (with one carbon) or without alkyl side chain is observed. Vanillic acid (m/z 168, not quantified, at 45.81 min on GC chromatogram); phenol, 2,6-dimethoxy- (m/z 154), phenol, 2-methoxy- (m/z 124), phenol, 2 methoxy-4-methyl (m/z 138) are detected between 280 and 470°C. The catechol, 3-methoxy (m/z 140, not quantified, at 36.06 min on GC chromatogram) is also observed. This compound is formed by the demethylation of syringol units induced by mineral catalytic effects as for miscanthus.

The phenolic volatiles composed of S-units seem to be produced at lower temperature than G-units. Indeed, phenol, 2,6-dimethoxy- (m/z 154) and catechol, 3-methoxy (m/z 140) are formed at lower temperature as compared to phenol, 2-methoxy- (m/z 124) and phenol, 2 methoxy-4-methyl (m/z 138) (figure V-10). Syringyl units are described to be depolymerized at lower temperature range base on different studies comparing softwood and hardwood.<sup>54,58</sup> However, the signal at high temperature could be assigned to dihydroxytoluene (m/z 124, not quantified, 35.63 min on GC chromatogram) produced by demethylation of 2 methoxy-4-methyl (m/z 138). Further investigations are requires to understand this mechanism.

The m/z 126 is assigned to 2-furaldehyde, 5-(hydroxymethyl)-, m/z 98 to 2-cyclopenten-1-one, 2-hydroxy and 2-furanmethanol and the m/z 128 was assigned to 5-methyl-4-oxotetrahydrofuran-2-carbaldehyde. These compounds are markers of cellulose degradation on the range of 300-380°C. The m/z 128 was clearly relatively more important for oak than miscanthus probably due to lower inorganic catalytic effect as already discussed.

Concerning douglas pyrolysis, the formation of volatiles starts at 200°C (Figure V-11) with the release of 2-propenal, 3-(4-hydroxy-3-methoxyphenyl) (m/z 178). As for oak, the formation of this compound is in accordance with the formation of aldehyde compounds in the early stage of pyrolysis. At slightly higher temperatures, products formed by ether-linkage (coniferyl alcohol (m/z 180)) combined to C-C breaking (2-methoxy-4-vinylphenol (m/z 150); isoeugenol (m/z 164)) are observed. The m/z 272 is assigned to enol ether dimer<sup>4</sup> formed by C $\gamma$  elimination.<sup>35</sup> The formation of phenolic compounds with small alkyl chain (phenol, 2 methoxy-4-methyl (m/z 138)) or without alkyl chain (phenol, 2-methoxy- (m/z 124)) is observed.

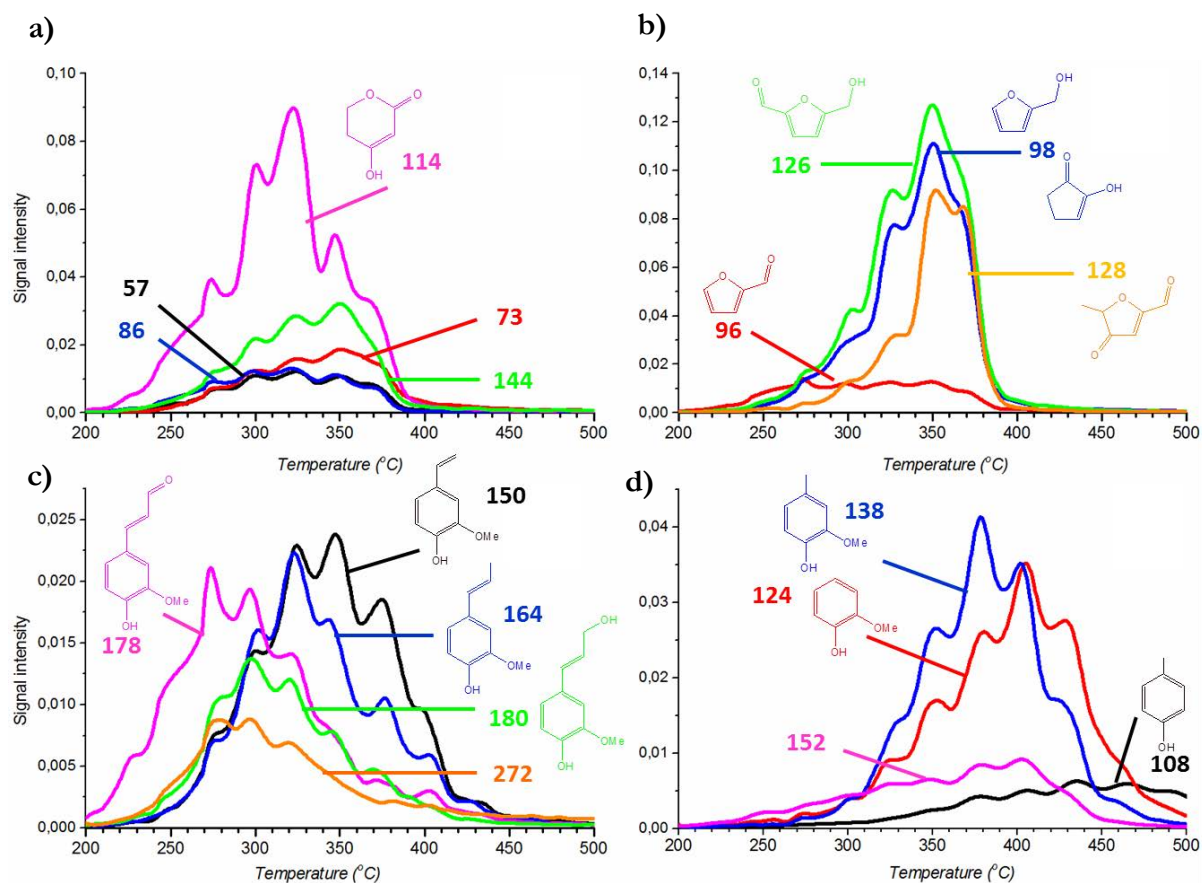


Figure V-11: On-line analysis vs. time of pyrolysis for douglas slow pyrolysis, a) hemicelluloses and carbohydrate fragments b) main cellulose markers c) lignin markers low temperature d) lignin markers high temperature.

The production of 3-hydroxy-2-penteno-1,5-lactone ( $m/z$  114) is observed from 220°C to 400°C indicating the degradation of the hemicelluloses. The  $m/z$  126 is assigned to 2-furaldehyde, 5-(hydroxymethyl)-,  $m/z$  98 to 2-cyclopenten-1-one, 2-hydroxy and 2-furanmethanol. The  $m/z$  128 may be assigned to 5-methyl-4-oxotetrahydrofuran-2-carbaldehyde. These compounds are markers of cellulose degradation on the range of 300-380°C.

Despite their different structural compositions, oak and douglas display relative similar pyrolysis profiles. Aldehyde phenolic (*i.e.* 2-propenal, 3-(4-hydroxy-3-methoxyphenyl)-) compounds start to be volatilized at low temperature (around 250°C to 400°C) followed at slightly higher temperature by alkyl phenolic compounds (*i.e.* methoxy-4-vinylphenol). The formation of phenolic compounds with small alkyl chain (*i.e.* phenol, 2-methoxy-4-methyl (m/z 138)) or without alkyl chain (*i.e.* phenol, 2-methoxy- (m/z 124)) is then observed at higher temperature (Figure V-12). Regarding miscanthus the formation of these volatiles is less distinguishable highlighting the catalytic effect of inorganic materials.

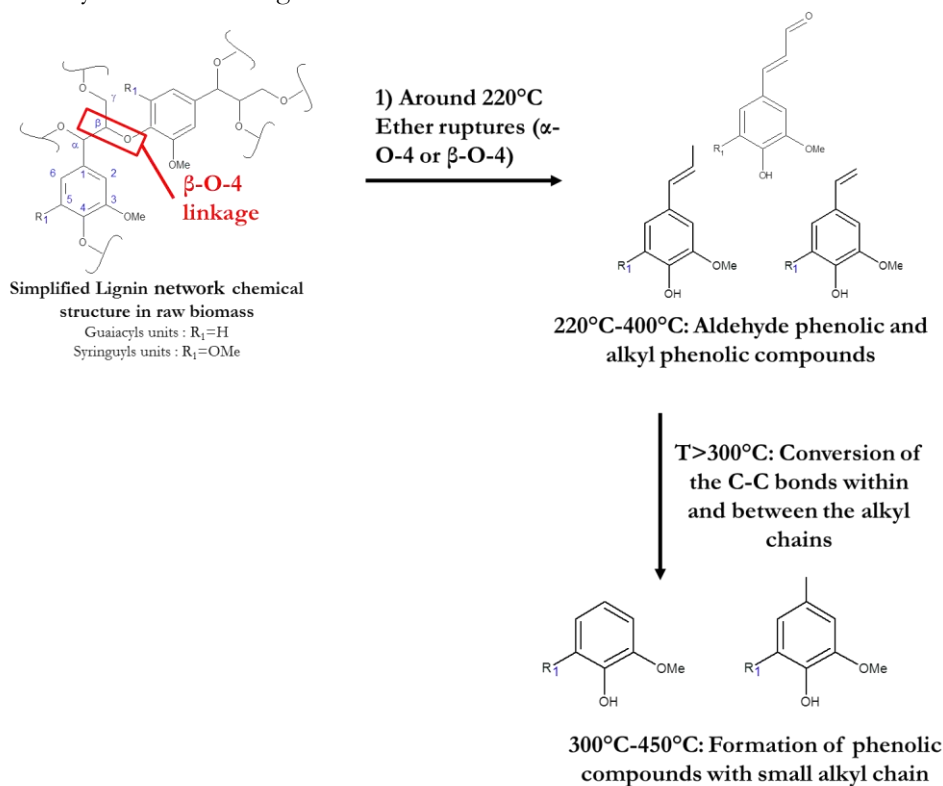


Figure V-12: Simplified mechanism of lignin pyrolysis highlighting the formation of the different markers as a function of temperature

### **V.1.5 Conclusion**

The geometry of the fixed bed reactor with a good control of temperature and mass transfers allows studying accurately the primary mechanisms of biomass pyrolysis. The combination of SPI/MS for on-line analysis with GC/MS for the assignment of the chemical structure of main m/z markers constitutes a pivotal approach to understand the chemistry of biomass pyrolysis and notably for the evolution of lignin markers. In other word, this investigation is interesting in order to unravel the different step of pyrolysis according to the different macromolecules (lignin, cellulose, hemicelluloses) present in the biomass network. The three investigated biomasses, namely grass (miscanthus) and wood (oak and douglas fir) exhibit different compositions (inorganics, sugars, lignin structure) and give rise to various volatiles. Inorganic presence inside the native biomass is the most important parameter that influences the chemical mechanism during pyrolysis. Nevertheless, there is still the need of a softer and more selective ionisation method than in the SPI (9.8eV) to detect anhydrosugars without any fragmentation. The data obtained in this work may be useful to develop a detailed kinetic mechanism for biomass pyrolysis.

### V.1.6 References

- (1) Mohan, D.; Pittman; Steele, P. H. Pyrolysis of Wood/Biomass for Bio-Oil: A Critical Review. *Energy Fuels* **2006**, *20* (3), 848–889.
- (2) Ragauskas, A. J.; Williams, C. K.; Davison, B. H.; Britovsek, G.; Cairney, J.; Eckert, C. A.; Frederick, W. J.; Hallett, J. P.; Leak, D. J.; Liotta, C. L.; Mielenz, J. R.; Murphy, R.; Templer, R.; Tschaplinski, T. The Path Forward for Biofuels and Biomaterials. *Science* **2006**, *311* (5760), 484–489.
- (3) Brosse, N.; Dufour, A.; Meng, X.; Sun, Q.; Ragauskas, A. Miscanthus: A Fast-Growing Crop for Biofuels and Chemicals Production. *Biofuels Bioprod. Biorefining* **2012**, *6* (5), 580–598.
- (4) Evans, R. J.; Milne, T. A. Molecular Characterization of the Pyrolysis of Biomass. 1. Fundamentals. *Energy Fuels* **1987**, *1* (2), 123–137.
- (5) Dufour, A.; Castro-Diaz, M.; Brosse, N.; Bouroukba, M.; Snape, C. The Origin of Molecular Mobility During Biomass Pyrolysis as Revealed by In Situ <sup>1</sup>H NMR Spectroscopy. *ChemSusChem* **2012**, *5* (7), 1258–1265.
- (6) Collard, F.-X.; Blin, J. A Review on Pyrolysis of Biomass Constituents: Mechanisms and Composition of the Products Obtained from the Conversion of Cellulose, Hemicelluloses and Lignin. *Renew. Sustain. Energy Rev.* **2014**, *38*, 594–608.
- (7) Lédé, J. Cellulose Pyrolysis Kinetics: An Historical Review on the Existence and Role of Intermediate Active Cellulose. *J. Anal. Appl. Pyrolysis*. **2011**
- (8) Jensen, A.; Dam-Johansen, K.; Wójtowicz, M. A.; Serio, M. A. TG-FTIR Study of the Influence of Potassium Chloride on Wheat Straw Pyrolysis. *Energy Fuels* **1998**, *12* (5), 929–938.
- (9) Jakab, E.; Faix, O.; Till, F. Thermal Decomposition of Milled Wood Lignins Studied by Thermogravimetry Mass Spectrometry. *J. Anal. Appl. Pyrolysis* **1997**, *40-1*, 171–186.
- (10) Antal, M. J. J.; Varhegyi, G. Cellulose Pyrolysis Kinetics: The Current State of Knowledge. *Ind. Eng. Chem. Res.* **1995**, *34* (3), 703–717.
- (11) Nowakowski, D. J.; Jones, J. M. Uncatalysed and Potassium-Catalysed Pyrolysis of the Cell-Wall Constituents of Biomass and Their Model Compounds. *J. Anal. Appl. Pyrolysis* **2008**, *83* (1), 12–25.
- (12) Faix, O.; Fortmann, I.; Bremer, J.; Meier, D. Thermal Degradation Products of Wood: A Collection of Electron-Impact (EI) Mass Spectra of Polysaccharide Derived Products. *Holz Als Rob- Werkst.* **1991**, *49* (7-8), 299–304.
- (13) Fendt, A.; Streibel, T.; Sklorz, M.; Richter, D.; Dahmen, N.; Zimmermann, R. On-Line Process Analysis of Biomass Flash Pyrolysis Gases Enabled by Soft Photoionization Mass Spectrometry. *Energy Fuels* **2012**, *26* (1), 701–711.
- (14) Genuit, W.; Boon, J. J.; Faix, O. Characterization of Beech Milled Wood Lignin by Pyrolysis-Gas Chromatography-Photoionization Mass Spectrometry. *Anal. Chem.* **1987**, *59* (3), 508–513.
- (15) Adam, T.; Baker, R. R.; Zimmermann, R. Investigation, by Single Photon Ionisation (SPI)–time-of-Flight Mass Spectrometry (TOFMS), of the Effect of Different Cigarette-Lighting Devices on the Chemical Composition of the First Cigarette Puff. *Anal. Bioanal. Chem.* **2006**, *387* (2), 575–584.
- (16) Zickler, G. A.; Wagermaier, W.; Funari, S. S.; Burghammer, M.; Paris, O. In Situ X-Ray Diffraction Investigation of Thermal Decomposition of Wood Cellulose. *J. Anal. Appl. Pyrolysis* **2007**, *80* (1), 134–140.
- (17) Kirtania, K.; Tanner, J.; Kabir, K. B.; Rajendran, S.; Bhattacharya, S. In Situ Synchrotron IR Study Relating Temperature and Heating Rate to Surface Functional Group Changes in Biomass. *Bioresour. Technol.*
- (18) Zakzeski, J.; Bruijninx, P. C. A.; Jongerius, A. L.; Weckhuysen, B. M. The Catalytic Valorization of Lignin for the Production of Renewable Chemicals. *Chem. Rev.* **2010**, *110* (6), 3552–3599.
- (19) Piskorz, J.; Radlein, D.; Scott, D. S. On the Mechanism of the Rapid Pyrolysis of Cellulose. *J. Anal. Appl. Pyrolysis* **1986**, *9* (2), 121–137.
- (20) Mamliev, V.; Bourbigot, S.; Le Bras, M.; Yvon, J. The Facts and Hypotheses Relating to the Phenomenological Model of Cellulose Pyrolysis: Interdependence of the Steps. *J. Anal. Appl. Pyrolysis* **2009**, *84* (1), 1–17.

- (21) Chaiwat, W.; Hasegawa, I.; Tani, T.; Sunagawa, K.; Mae, K. Analysis of Cross-Linking Behavior during Pyrolysis of Cellulose for Elucidating Reaction Pathway. *Energy Fuels* **2009**, *23* (12), 5765–5772.
- (22) Scheirs, J.; Camino, G.; Tumiatti, W. Overview of Water Evolution during the Thermal Degradation of Cellulose. *Eur. Polym. J.* **2001**, *37* (5), 933–942.
- (23) Kilzer, F. J.; Broido, A. The Nature of Cellulose Pyrolysis. *Pyrodynamic* **1965**, *2* (2-3), 151–163.
- (24) Richards, G. N. Glycolaldehyde from Pyrolysis of Cellulose. *J. Anal. Appl. Pyrolysis* **1987**, *10* (3), 251–255.
- (25) Shen, D. K.; Gu, S. The Mechanism for Thermal Decomposition of Cellulose and Its Main Products. *Bioresour. Technol.* **2009**, *100* (24), 6496–6504.
- (26) Piskorz, J.; Radlein, D. S. A. G.; Scott, D. S.; Czernik, S. Pretreatment of Wood and Cellulose for Production of Sugars by Fast Pyrolysis. *J. Anal. Appl. Pyrolysis* **1989**, *16* (2), 127–142.
- (27) Werner, K.; Pommer, L.; Broström, M. Thermal Decomposition of Hemicelluloses. *J. Anal. Appl. Pyrolysis*.
- (28) Shen, D. K.; Gu, S.; Bridgwater, A. V. Study on the Pyrolytic Behaviour of Xylan-Based Hemicellulose Using TG–FTIR and Py–GC–FTIR. *J. Anal. Appl. Pyrolysis* **2010**, *87* (2), 199–206.
- (29) Worasuwannarak, N.; Sonobe, T.; Tanthapanichakoon, W. Pyrolysis Behaviors of Rice Straw, Rice Husk, and Corncob by TG-MS Technique. *J. Anal. Appl. Pyrolysis* **2007**, *78* (2), 265–271.
- (30) Peng, Y.; Wu, S. The Structural and Thermal Characteristics of Wheat Straw Hemicellulose. *J. Anal. Appl. Pyrolysis* **2010**, *88* (2), 134–139.
- (31) Hosoya, T.; Kawamoto, H.; Saka, S. Pyrolysis Behaviors of Wood and Its Constituent Polymers at Gasification Temperature. *J. Anal. Appl. Pyrolysis* **2007**, *78* (2), 328–336.
- (32) Ohnishi, A.; Katō, K.; Takagi, E. Pyrolytic Formation of 3-Hydroxy-2-Penteno-1,5-Lactone from Xylan, Xylo-Oligosaccharides, and Methyl Xylopyranosides. *Carbohydr. Res.* **1977**, *58* (2), 387–395.
- (33) Ponder, G. R.; Richards, G. N. Thermal Synthesis and Pyrolysis of a Xylan. *Carbohydr. Res.* **1991**, *218*, 143–155.
- (34) Pandey, M. P.; Kim, C. S. Lignin Depolymerization and Conversion: A Review of Thermochemical Methods. *Chem. Eng. Technol.* **2011**, *34* (1), 29–41.
- (35) Kawamoto, H.; Horigoshi, S.; Saka, S. Pyrolysis Reactions of Various Lignin Model Dimers. *J. Wood Sci.* **2007**, *53* (2), 168–174.
- (36) Jakab, E.; Faix, O.; Till, F.; Székely, T. Thermogravimetry/mass Spectrometry Study of Six Lignins within the Scope of an International Round Robin Test. *J. Anal. Appl. Pyrolysis* **1995**, *35* (2), 167–179.
- (37) Wang, S.; Wang, K.; Liu, Q.; Gu, Y.; Luo, Z.; Cen, K.; Fransson, T. Comparison of the Pyrolysis Behavior of Lignins from Different Tree Species. *Biotechnol. Adv.* **2009**, *27* (5), 562–567.
- (38) Sharma, R. K.; Wooten, J. B.; Baliga, V. L.; Lin, X. H.; Chan, W. G.; Hajaligol, M. R. Characterization of Chars from Pyrolysis of Lignin. *Fuel* **2004**, *83* (11-12), 1469–1482.
- (39) Dufour, A.; Weng, J.; Jia, L.; Tang, X.; Sirjean, B.; Fournet, R.; Le Gall, H.; Brosse, N.; Billaud, F.; Mauviel, G.; Qi, F. Revealing the Chemistry of Biomass Pyrolysis by Means of Tunable Synchrotron Photoionisation-Mass Spectrometry. *Rsc Adv.* **2013**, *3* (14), 4786–4792.
- (40) Shen, D. K.; Gu, S.; Luo, K. H.; Wang, S. R.; Fang, M. X. The Pyrolytic Degradation of Wood-Derived Lignin from Pulping Process. *Bioresour. Technol.* **2010**, *101* (15), 6136–6146.
- (41) Butler, E.; Devlin, G.; Meier, D.; McDonnell, K. Fluidised Bed Pyrolysis of Lignocellulosic Biomasses and Comparison of Bio-Oil and Micropyrolyser Pyrolysate by GC/MS-FID. *J. Anal. Appl. Pyrolysis* **2013**, *103*, 96–101.
- (42) Williams, P. T.; Besler, S. The Influence of Temperature and Heating Rate on the Slow Pyrolysis of Biomass. *Renew. Energy* **1996**, *7* (3), 233–250.
- (43) Faix, O.; Fortmann, I.; Bremer, J.; Meier, D. Thermal Degradation Products of Wood. *Holz Als Rob-Werkst.* **1991**, *49* (5), 213–219.
- (44) Faix, O.; Meier, D.; Fortmann, I. Thermal Degradation Products of Wood. *Holz Als Rob-Werkst.* **1990**, *48* (9), 351–354.
- (45) Patwardhan, P. R.; Satrio, J. A.; Brown, R. C.; Shanks, B. H. Influence of Inorganic Salts on the Primary Pyrolysis Products of Cellulose. *Bioresour. Technol.* **2010**, *101* (12), 4646–4655.

- (46) Trendewicz, A.; Evans, R.; Dutta, A.; Sykes, R.; Carpenter, D.; Braun, R. Evaluating the Effect of Potassium on Cellulose Pyrolysis Reaction Kinetics. *Biomass Bioenergy* **2015**, *74*, 15–25.
- (47) Eom, I.-Y.; Kim, K.-H.; Kim, J.-Y.; Lee, S.-M.; Yeo, H.-M.; Choi, I.-G.; Choi, J.-W. Characterization of Primary Thermal Degradation Features of Lignocellulosic Biomass after Removal of Inorganic Metals by Diverse Solvents. *Bioresour. Technol.* **2011**, *102* (3), 3437–3444.
- (48) Hodgson, E. M.; Nowakowski, D. J.; Shield, I.; Riche, A.; Bridgwater, A. V.; Clifton-Brown, J. C.; Donnison, I. S. Variation in Miscanthus Chemical Composition and Implications for Conversion by Pyrolysis and Thermo-Chemical Bio-Refining for Fuels and Chemicals. *Bioresour. Technol.* **2011**, *102* (3), 3411–3418.
- (49) Jarvis, M. W.; Haas, T. J.; Donohoe, B. S.; Daily, J. W.; Gaston, K. R.; Frederick, W. J.; Nimlos, M. R. Elucidation of Biomass Pyrolysis Products Using a Laminar Entrained Flow Reactor and Char Particle Imaging. *Energy Fuels* **2011**, *25* (1), 324–336.
- (50) Sykes, R.; Kodrzycki, B.; Tuskan, G.; Foutz, K.; Davis, M. Within Tree Variability of Lignin Composition in Populus. *Wood Sci. Technol.* **2008**, *42* (8), 649–661.
- (51) Ponder, G. R.; Richards, G. N.; Stevenson, T. T. Influence of Linkage Position and Orientation in Pyrolysis of Polysaccharides: A Study of Several Glucans. *J. Anal. Appl. Pyrolysis* **1992**, *22* (3), 217–229.
- (52) El Hage, R.; Brosse, N.; Chrusciel, L.; Sanchez, C.; Sannigrahi, P.; Ragauskas, A. Characterization of Milled Wood Lignin and Ethanol Organosolv Lignin from Miscanthus. *Polym. Degrad. Stab.* **2009**, *94* (10), 1632–1638.
- (53) Kleen, M.; Gellerstedt, G. Influence of Inorganic Species on the Formation of Polysaccharide and Lignin Degradation Products in the Analytical Pyrolysis of Pulps. *J. Anal. Appl. Pyrolysis* **1995**, *35* (1), 15–41.
- (54) Nonier, M. F.; Vivas, N.; Vivas de Gaulejac, N.; Absalon, C.; Soulié, P.; Fouquet, E. Pyrolysis–gas Chromatography/mass Spectrometry of Quercus Sp. Wood. *J. Anal. Appl. Pyrolysis* **2006**, *75* (2), 181–193.
- (55) Collard, F.-X.; Blin, J.; Bensakhria, A.; Valette, J. Influence of Impregnated Metal on the Pyrolysis Conversion of Biomass Constituents. *J. Anal. Appl. Pyrolysis* **2012**, *95*, 213–226.
- (56) Kotake, T.; Kawamoto, H.; Saka, S. Mechanisms for the Formation of Monomers and Oligomers during the Pyrolysis of a Softwood Lignin. *J. Anal. Appl. Pyrolysis* **2014**, *105*, 309–316.
- (57) Kotake, T.; Kawamoto, H.; Saka, S. Pyrolysis Reactions of Coniferyl Alcohol as a Model of the Primary Structure Formed during Lignin Pyrolysis. *J. Anal. Appl. Pyrolysis* **2013**, *104*, 573–584.
- (58) Kotake, T.; Kawamoto, H.; Saka, S. Pyrolytic Formation of Monomers from Hardwood Lignin as Studied from the Reactivities of the Primary Products. *J. Anal. Appl. Pyrolysis* **2015**, *113*, 57–64.

### V.1.7 Supporting information

#### Thermo-gravimetric analysis

The pyrolysis behaviours of MxG, Oak and Douglas were compared by thermo-gravimetric using Mettler Toledo (Stare System) apparatus (Figure V-13). These analyses were conducted on 5mg of each sample at 5°C/min up to 500°C. The carrier gas (purified argon) was set at 100 Nml/min.

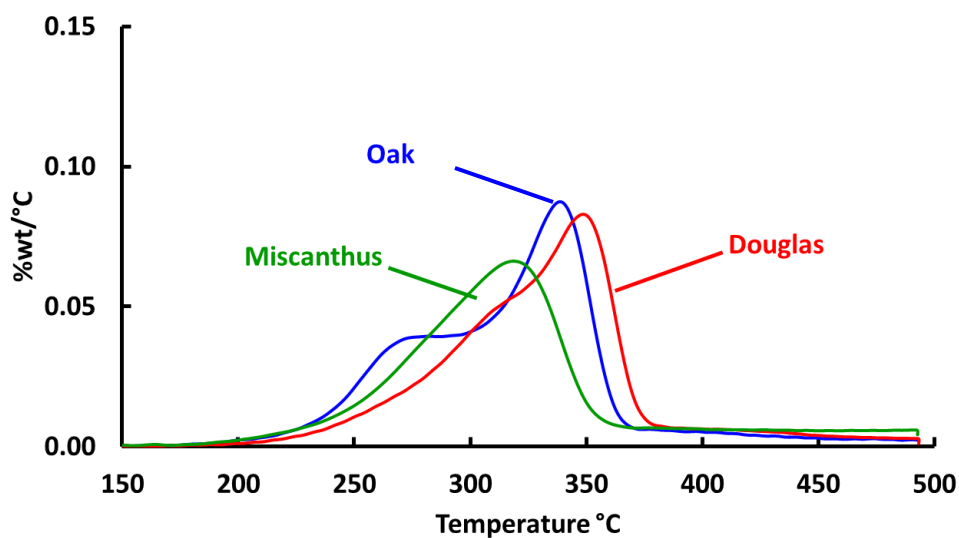


Figure V-13: DTG curves (5°C/min) of the TGA

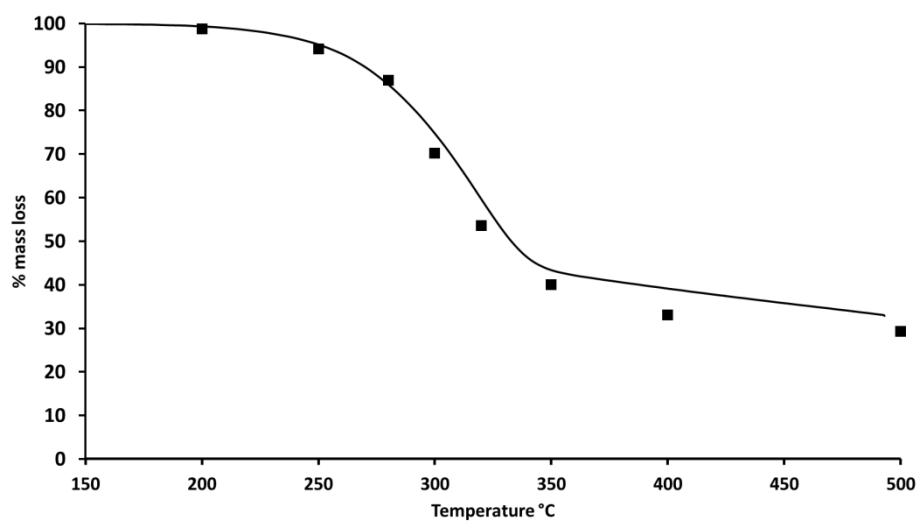


Figure V-14: Comparison between thermogravimetric analysis (line) and char yield obtained in the fixed bed reactor after char quenching (points) for miscanthus pyrolysis (5°C/min)

**Elemental analysis**

Elemental analysis of Miscanthus, Oak and Douglas and produced chars were performed on a Thermo Fisher apparatus. Each sample was dried at 105°C during several hours before experiments. Table V-2 presents the weight percentage for carbon (%C) and hydrogen (%H). The standard deviation is also presented for each element (%<sub>STD</sub>).

*Table V-2: Elemental analysis for miscanthus, oak and douglas*

Samples	T (°C)	%wt (oven dried values)			
		%C	%C <sub>STD</sub>	%H	%H <sub>STD</sub>
<b>Miscanthus</b>	20	42.8	0.6	5.5	0.1
	200	44.1	1.2	5.5	0.2
	250	45.0	0.8	5.4	0.1
	280	45.8	1.1	5.1	0.1
	300	48.9	1.0	4.9	0.1
	320	50.2	1.6	4.3	0.2
	350	54.0	0.5	3.7	0.2
	400	54.6	0.3	2.9	0.2
	500	56.2	0.0	2.4	0.0
<b>Oak</b>	20	47.1	0.3	6.1	0.1
	300	52.3	0.6	5.8	0.3
	500	78.2	1.3	3.0	0.1
<b>Douglas</b>	20	48.7	0.2	6.1	0.2
	300	54.5	0.3	5.9	0.1
	500	79.2	0.9	3.4	0.1

**Biomass composition**

The carbohydrates and Klason lignin contents in the three samples (MxG, holocellulose, cellulose) were measured on extractive free material, according to the NREL procedure<sup>1</sup>. Samples were hydrolyzed by concentrated sulfuric acid (72%wt.) for 1h in a rotary water bath at 30°C and then autoclaved during 1h30 after being diluted to 3% sulfuric acid through addition of water. The autoclaved sample were filtered, and then dried to give the Klason lignin content. Monosaccharides in the filtrate were quantified using high-performance anion-exchange chromatography with pulsed amperometric detection (HPAEC-PAD)<sup>1</sup>.

*Table V-3: Analysis of lignin and sugars composition in biomasses*

% wt biomass Extractible Free								
Samples	Total Sugars	Klason Lignin	Organic matter	Glucose	Xylose	Mannose	Galactose	Arabinose
<b>Douglas</b>	65.6	34.4	99.8	43.7	5.8	8.5	5.1	1.5
<b>STD</b>	0.6	0.6	n.a	0.3	0.5	0.2	0.3	0.1
<b>Oak</b>	74.8	24.2	99.8	48.7	21.5	1.3	1.3	1.3
<b>STD</b>	0.1	0.1	n.a	0.2	0.0	0.0	0.0	0.0
<b>Miscanthus</b>	70.2	29.8	92.4	48.9	18.3	0.0	0.6	2.3
<b>STD</b>	0.0	0.0	0.9	1.3	1.4	0.0	0.0	0.1
<b>Misc_Demin</b>	71.7	28.3	94.8	46.6	20.9	0.0	0.7	2.9
<b>STD</b>	0.48	0.48	0.09	0.436	0.47	0.00	0.04	0.04

Samples have been analyzed by ICP-OES and ICP-MS following the CNRS-SARM procedure<sup>2</sup> in order to characterize their mineral and organic matter contents.

*Table V-4: Organics content of the different biomasses*

	Si	Al	Fe	Mn	Mg	Ca	Na	K	Ti	P	Total
<b>Miscanthus</b>	1.66	0.16	0.09	0.02	0.10	0.37	0.01	0.65	0.01	0.00	3.06
<b>Douglas</b>	0.01	0.00	0.00	0.01	0.00	0.03	0.00	0.02	0.00	0.00	0.08
<b>Oak</b>	0.03	0.01	0.01	0.01	0.01	0.14	0.00	0.11	0.00	0.01	0.34

Gas composition for the pyrolysis of douglas and oak

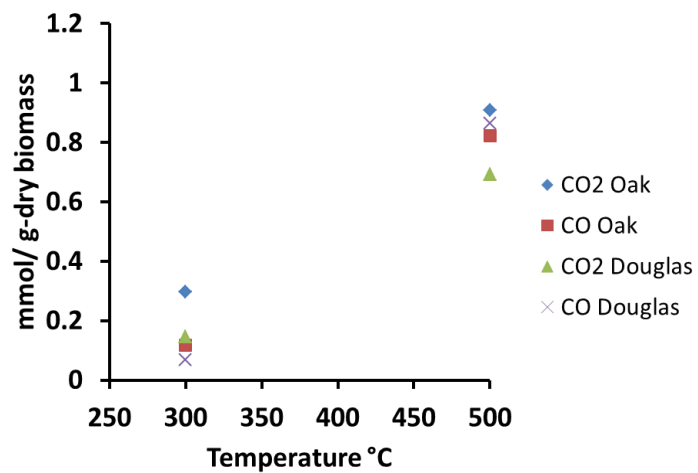


Figure V-15: The gas release from pyrolysis of oak and douglas

**Calibration of the GC\*GC/ MS-FID-FID heart-cutting method of some selected compounds**

A HP-5MS (diphenyl -5% - dimethylpolysiloxan -95%, not polar, 30m × 250µm × 0,25µm) column (0,93ml min<sup>-1</sup> of He) was coupled to a DB-WAX (polyethylenglycol, polar, 30m × 320µm × 0.25µm) column (3.44 ml min<sup>-1</sup> of He) with a Dean's switch (for heart-cutting). The complementary polarities of these two columns allow separating different compounds in a complex mixture. The HP-5MS was connected simultaneously to FID and MS which allows quantification on the FID and identification on the MS by the same injection. The DBWAX is connected to a FID for quantification of the heart-cut part of the HP-5MS. The response factors on the FID of compounds were predicted using the method reported by de Saint Laumer and al<sup>3</sup> as previously used in our group<sup>4</sup>. Calibration and comparison between experimental response factors and predicted by de Saint Laumer's method have been made with tetradecene as the internal standard (Sigma Aldrich ref 87189-25ml).

On a single FID, the area of product i (A<sub>i</sub>) divided by the area of 1-tetradecene (A<sub>i-Tetra</sub>), the internal standard, is proportional to the molar ratio between product i and tetradecene (n<sup>o</sup><sub>i</sub>/n<sup>o</sup><sub>Tetra</sub>). (α<sub>i</sub>/α<sub>Tetra</sub>) is the relative response factor.

$$n^{\circ}i/n^{\circ}_{\text{Tetra}} = (\alpha_i/\alpha_{\text{Tetra}}) \times A_i/A_{\text{Tetra}} \quad (1)$$

HP-5MS is connected simultaneously to MS and FID analysis and the outlet of the DB-WAX column is connected to a FID. Consequently the signal from HP-5MS-FID is lower than DB-WAX-FID. So an analytical partition coefficient is needed when heart cutting is used. This coefficient (fp) is defined as:

$$A_{\text{FID-DBWAX}} = fp \times A_{\text{FID-HP-5MS}} \quad (2)$$

Combining equation (1) and (2), we can calculate a relative corrected response factor even if the A<sub>Tetra</sub> is determined on DBWAX-FID and A<sub>i</sub> is determined on FID from HP-5MS column.

$$n^{\circ}i/n^{\circ}_{\text{Tetra}} = (\alpha_i/\alpha_{\text{Tetra}}) \times fp \times A_i/A_{\text{Tetra}} \quad (3)$$

Four solutions (20ml) of Naphthalene, Guaiacol, Syringaldehyde (all purchased from Sigma Aldrich) were prepared and 1 µl of Tetradecene (3,954µmol) was introduced in each solution. 1µL of solution was injected into GC with a split ratio of 10. On the HP-5MS FID the areas of the different compounds were measured. The experimental response factor relative to 1µL of Tetradecene was calculated by plotting the ratio of areas (A<sub>i</sub>/A<sub>Tetra</sub>) vs the n<sup>o</sup> of moles of i prepared (100% purity was considered) in standard solutions. Figure V-16 presents some plots for Naphthalene, Guaiacol and Syringaldehyde. The four points were fitted in Excel with a y=c.x formula (linear, forced to zero). C was then divided by 3,954µmols in order to calculate (α<sub>i</sub>/α<sub>Tetra</sub>) × fp. fp was next determined based on theoretical value of (α<sub>i</sub>/α<sub>Tetra</sub>). A value of fp=2 +/- 0,12. Finally a partition coefficient of 2 were kept in order to minimize the average deviation between predicted and measured response factor. Figure V-17 shows experimental response factor (n<sup>o</sup><sub>i</sub>/n<sup>o</sup><sub>Tetra</sub>)/(A<sub>i</sub>/A<sub>Tetra</sub>) vs predicted values from de Saint Laumer. It shows a good accordance.

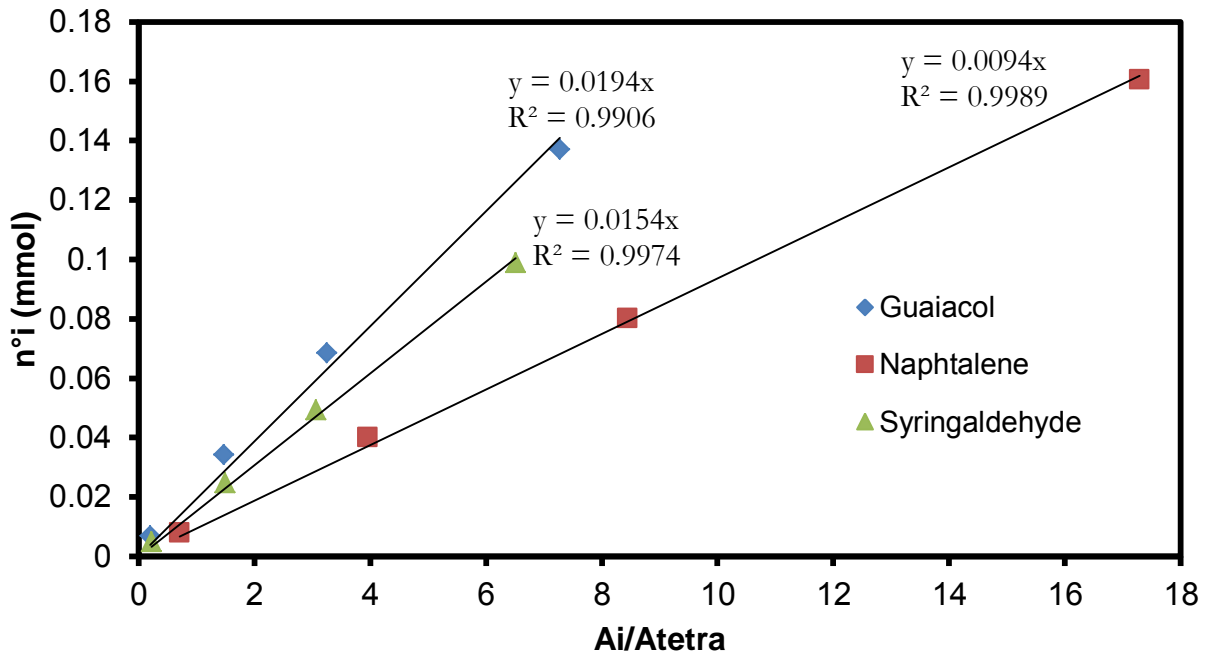


Figure V-16: Plots for calibration of compounds on de Saint Laumer heart-cutting method

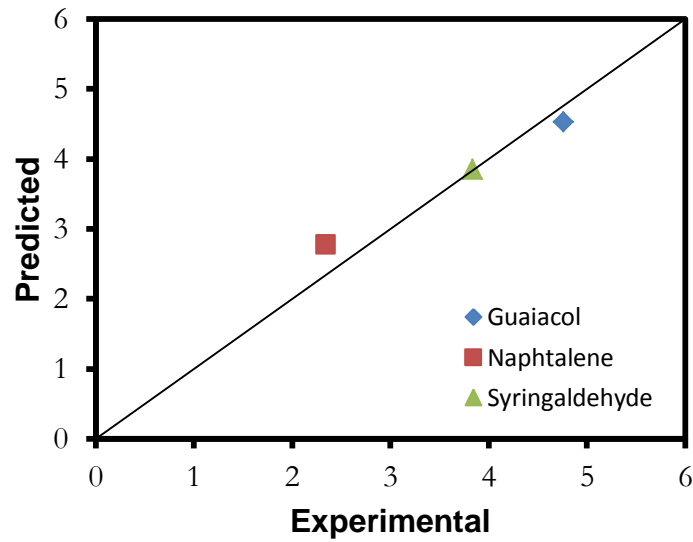
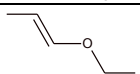
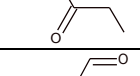
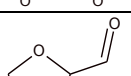
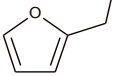
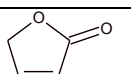
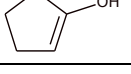
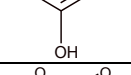
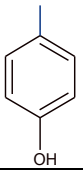
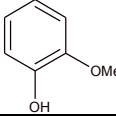
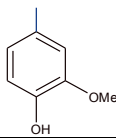
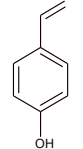
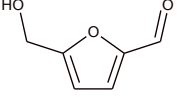
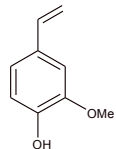
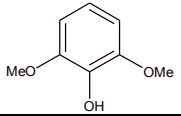
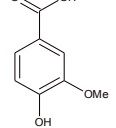
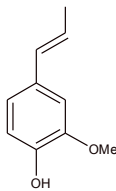
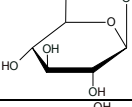
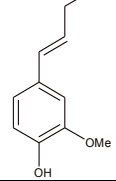


Figure V-17: Comparison between experimental response factors and predicted by de Saint Laumer method

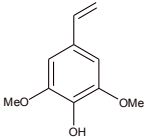
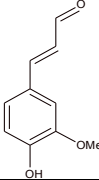
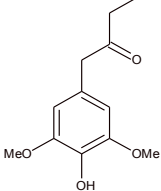
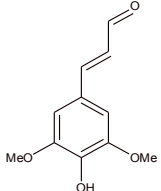
## Article4: Supporting information

	Compounds	N° CAS	Mw	Formula		ref
1	Acetic acid	0	60	C <sub>2</sub> H <sub>4</sub> O <sub>2</sub>		NIST
2	2-Propanone, 1-hydroxy	116-09-6	74	C <sub>3</sub> H <sub>6</sub> O <sub>2</sub>		NIST
3	Ethyl-1-propenyl ether	928-55-2	86	C <sub>5</sub> H <sub>10</sub> O		NIST
4	Methylglyoxal	78-98-8	72	C <sub>3</sub> H <sub>4</sub> O <sub>2</sub>		NIST
5	1-Penten-3-one	1629-58-9	84	C <sub>5</sub> H <sub>8</sub> O		NIST
6	Propanal, 2,3 dihydroxy	367-47-5	90	C <sub>3</sub> H <sub>6</sub> O <sub>3</sub>		NIST
7	Propanoic acid, 2-oxo-, methyl ester	600-22-6	102	C <sub>4</sub> H <sub>6</sub> O <sub>3</sub>		NIST
8	furfural	98-01-1	96	C <sub>5</sub> H <sub>4</sub> O <sub>2</sub>		NIST
9	2-Furanmethanol	98-00-0	98	C <sub>5</sub> H <sub>6</sub> O <sub>2</sub>		NIST
10	2(5H)-Furanone	497-23-4	84	C <sub>4</sub> H <sub>4</sub> O <sub>2</sub>		NIST
11	2,cyclopenten-1-one, 2 hydroxy	10493-98-8	98	C <sub>5</sub> H <sub>6</sub> O <sub>2</sub>		NIST
12	Phenol	108-95-2	94	C <sub>6</sub> H <sub>6</sub> O		NIST
13	4-Hydroxy-5,6-dihydro-(2H)-pyran-2-one	-	114	C <sub>5</sub> H <sub>6</sub> O <sub>3</sub>		5
14	Corylon	80-71-7	112	C <sub>6</sub> H <sub>8</sub> O <sub>2</sub>		NIST
15	Phenol 2-methyl	95-48-7	108	C <sub>7</sub> H <sub>8</sub> O		NIST

Article4: Supporting information

16	Phenol, 4-methyl-	106-44-5	108	C <sub>7</sub> H <sub>8</sub> O		NIST
17	Phenol, 2-methoxy-	90-05-1	124	C <sub>7</sub> H <sub>8</sub> O <sub>2</sub>		NIST
18	Phenol, 2 methoxy-4-methyl	93-51-6	138	C <sub>8</sub> H <sub>10</sub> O <sub>2</sub>		NIST
19	4-vinyl phenol	496-16-2	120	C <sub>8</sub> H <sub>8</sub> O		6
20	2-Furaldehyde, 5-(hydroxymethyl)-	67-47-0	126	C <sub>6</sub> H <sub>6</sub> O <sub>3</sub>		NIST
21	2-Methoxy-4-vinylphenol	7786-61-0	150	C <sub>9</sub> H <sub>10</sub> O <sub>2</sub>		NIST
22	Phenol, 2,6-dimethoxy-	91-10-1	154	C <sub>8</sub> H <sub>10</sub> O <sub>3</sub>		NIST
23	Benzoic acid, 4-hydroxy-3-methoxy-	121-34-6	168	C <sub>8</sub> H <sub>8</sub> O <sub>4</sub>		NIST
24	isoeugenol	5932-68-3	164	C <sub>10</sub> H <sub>12</sub> O <sub>2</sub>		NIST
25	Levoglucosane	498-07-7	162	C <sub>6</sub> H <sub>10</sub> O <sub>5</sub>		NIST
26	Coniferyl alcohol (Douglas)	458-35-5	180	C <sub>10</sub> H <sub>12</sub> O <sub>3</sub>		6

Article4: Supporting information

26	Syringol 4 vinyl Oak	28343-22-8	180	C <sub>10</sub> H <sub>12</sub> O <sub>3</sub>		
27	2-Propenal, 3-(4-hydroxy-3-methoxyphenyl)-	127321-19-1	178	C <sub>10</sub> H <sub>10</sub> O <sub>3</sub>		6
28	Syringyl acetone	19037-58-2	210	C <sub>11</sub> H <sub>14</sub> O <sub>4</sub>		6
29	3,5-Dimethoxy-4-hydroxycinnamaldehyde	87345-53-7	208	C <sub>11</sub> H <sub>12</sub> O <sub>4</sub>		6

**References of the supporting information**

- (1) Brosse, N.; Sannigrahi, P.; Ragauskas, A. Pretreatment of *Miscanthus X Giganteus* Using the Ethanol Organosolv Process for Ethanol Production. *Ind. Eng. Chem. Res.* **2009**, *48* (18), 8328–8334.
- (2) Carignan, J.; Hild, P.; Meville, G.; Morel, J.; Yeghicheyan, D. Routine Analyses of Trace Elements in Geological Samples Using Flow Injection and Low Pressure On-Line Liquid Chromatography Coupled to ICP-MS: A Study of Geochemical Reference Materials BR, DR-N, UB-N, AN-G and GH. *Geostand. Newsl.* **2001**, *25* (2-3), 187–198.
- (3) de Saint Laumer, J.-Y.; Cicchetti, E.; Merle, P.; Egger, J.; Chaintreau, A. Quantification in Gas Chromatography: Prediction of Flame Ionization Detector Response Factors from Combustion Enthalpies and Molecular Structures. *Anal. Chem.* **2010**, *82* (15), 6457–6462.
- (4) Olcese, R. N.; Lardier, G.; Bettahar, M.; Ghanbaja, J.; Fontana, S.; Carré, V.; Aubriet, F.; Petitjean, D.; Dufour, A. Aromatic Chemicals by Iron-Catalyzed Hydrotreatment of Lignin Pyrolysis Vapor. *ChemSusChem* **2013**, *6* (8), 1490–1499.
- (5) Faix, O.; Fortmann, I.; Bremer, J.; Meier, D. Thermal Degradation Products of Wood: A Collection of Electron-Impact (EI) Mass Spectra of Polysaccharide Derived Products. *Holz Als Roh- Werkst.* **1991**, *49* (7-8), 299–304.
- (6) Faix, O.; Meier, D.; Fortmann, I. Thermal Degradation Products of Wood. *Holz Als Roh- Werkst.* **1990**, *48* (7-8), 281–285.



## **VI. Multianalyse de la pyrolyse du miscanthus**



## Article 5: Multianalytical analysis of miscanthus pyrolysis

Short communication to be submitted.

Biomass pyrolysis leads to the conversion and formation of various chemical moieties. In order to better understand these mechanisms, we have undertaken the development of a multianalytical method. Primary pyrolysis of biomass forms char, primary tars and gases through the formation of an intermediate liquid. The different analytical methods which have been used to analyse these products are presented on Figure VI-1.

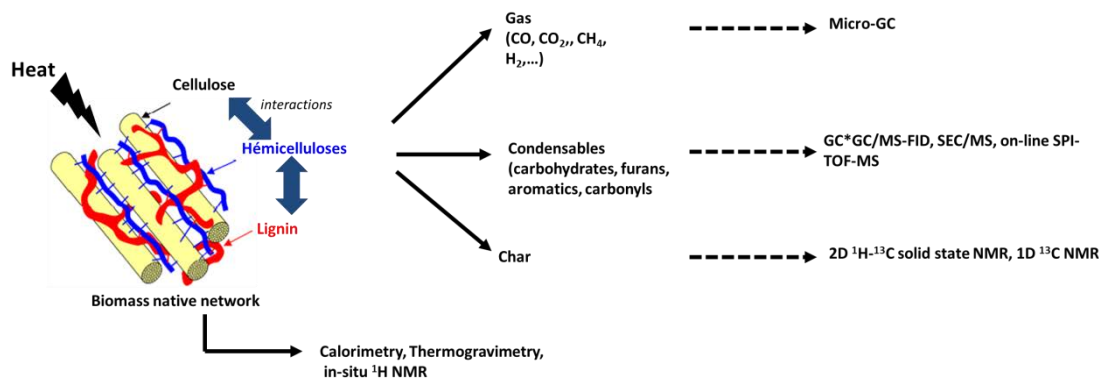


Figure VI-1: Multi-analytical study of biomass pyrolysis

According to miscanthus pyrolysis, the comparison between <sup>13</sup>C NMR investigation of the char (Figure VI-2), SPI/MS investigations of the volatiles (Figure VI-4) and in-situ <sup>1</sup>H NMR study (Figure VI-5) allows a global description of the chemical mechanisms.

Up to 200°C, no evolution of the carbon structure and volatiles are observed. Formation of volatiles is observed by SPI/MS from 220°C with the release of 4-vinylphenol (*m/z* 120) and the evolution of the <sup>1</sup>H mobility is detected by in-situ <sup>1</sup>H NMR. The production of 4-vinylphenol indicates the breaking of *p*-coumarate groups acetylated on C<sub>γ</sub> of lignin phenylpropane. The release of different compounds (2-Propenal 3-(4-hydroxy-3-methoxyphenyl)- (*m/z* 178); 2-methoxy-4-vinylphenol (*m/z* 150) and 4-vinyl syringol (*m/z* 180)) observed by SPI/MS from 250°C points out the cleavage of ether bonds ( $\alpha$ -O-4 and  $\beta$ -O-4) in the lignin network. But the formation of these compounds must include a C-C rupture in order to form vinyl compounds. This could be explained by the C<sub>γ</sub> elimination occurring before the cleavage of ether linkages<sup>1</sup>.

Simultaneously, the fluidity of the miscanthus analysed by in-situ <sup>1</sup>H NMR (Figure VI-5) increases showing that mobile molecules which are free to rotate are produced. This development could be attributed to the depolymerization of lignin but could be also due to the hydrogen link ruptures in carbohydrates. Kotake et al<sup>2</sup> described the importance of H-donor reactions in the side chain reduction to explain the formation of alkyl phenolic compounds. At the first step of pyrolysis, the pyrolysis environment is considered to be under radical conditions. These radicals come from the homolytic cleavage of the lignin ether linkages. Formed radicals could be stabilized by abstracting hydrogens from other molecules and led to the formation of, for instance, coniferyl aldehyde (Figure VI-3).

At higher temperature the presence of H-donor species provides the side chain reduction to enhance the formation of eugenol ( $m/z$  164) (for instance) by H-addition reactions. These H-donors could be provided by the pyrolysis of the other wood constituents<sup>3</sup> (hemicelluloses). This observation could be correlated to the enhancement of  $^1\text{H}$  mobility in this same range of temperature. In other word, the formation of a fluid phase could favor the transfer of hydrogen. These transfers could reduce condensation reaction and increase the volatilization of aromatics species<sup>4</sup>.

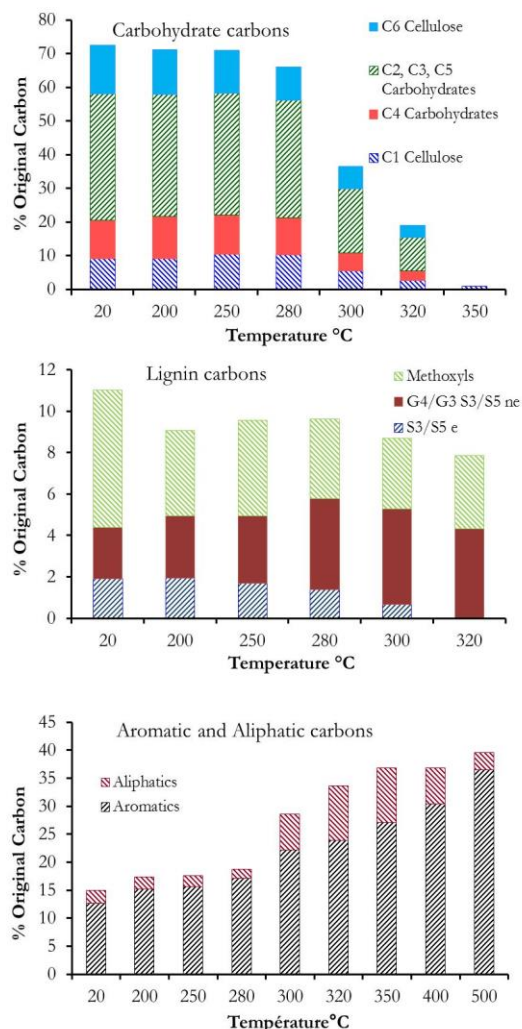


Figure VI-2: Evolution of main moieties (%mol of original carbon) during pyrolysis of Miscanthus

The  $^{13}\text{C}$  NMR investigation indicates that the decrease of etherified syringyl units is not so important until 280°C but become significant at 300°C (Figure VI-2). The temperature range between 280 and 300°C is pivotal for chemical mechanisms.  $^{13}\text{C}$  NMR analysis highlights that the conversion of carbohydrates is very important between 280°C and 300°C (Figure VI-2).

The carbohydrates starts to produce volatiles from 250°C based on the SPI/MS (Figure VI-4) with the detection of carbohydrates fragments ( $m/z$  43, 57 and 86) and 4-hydroxy-5,6-dihydro-(2H)-pyranone ( $m/z$  114). A maximum of release is observed at 300°C for the fragments  $m/z$  57, 86 and 114 but the release of cellulose pyrolysis products is not important. It means that aromatic formation into the char is mostly due to hemicelluloses conversion up to 300°C. The evolution of the carbon structure of lignin in miscanthus during

pyrolysis is difficult to be analysed solely with  $^{13}\text{C}$  NMR because of the important overlap of various moieties in the range of aromatic chemical shifts. The extraction of lignin from miscanthus has given good indications about the mechanisms of lignin pyrolysis by NMR (Article 2) but the extraction process induces some degradation of the native lignin structure. On-line SPI investigation during pyrolysis gives more accurate information according to lignin degradation in miscanthus network than NMR.

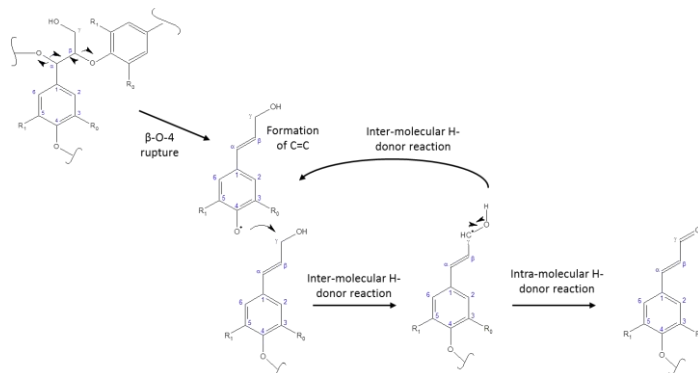


Figure VI-3: Formation of coniferaldehyde

At  $300^\circ\text{C}$  the formation of aliphatic moieties in the char is significant (Figure VI-2), mainly due to hemicelluloses conversion because cellulose is hardly converted and lignin alkyl chains are converted. The fluidity presents a maximum at  $270^\circ\text{C}$  (30% mobility) and stay relatively important until  $300^\circ\text{C}$  showing that for this range of temperature the biomass physical state is more “fluid” where molecules are free to rotate. It probably highlights the formation of some “liquid phase” inside the matrix which promotes the transfer of molecules and of H-species.

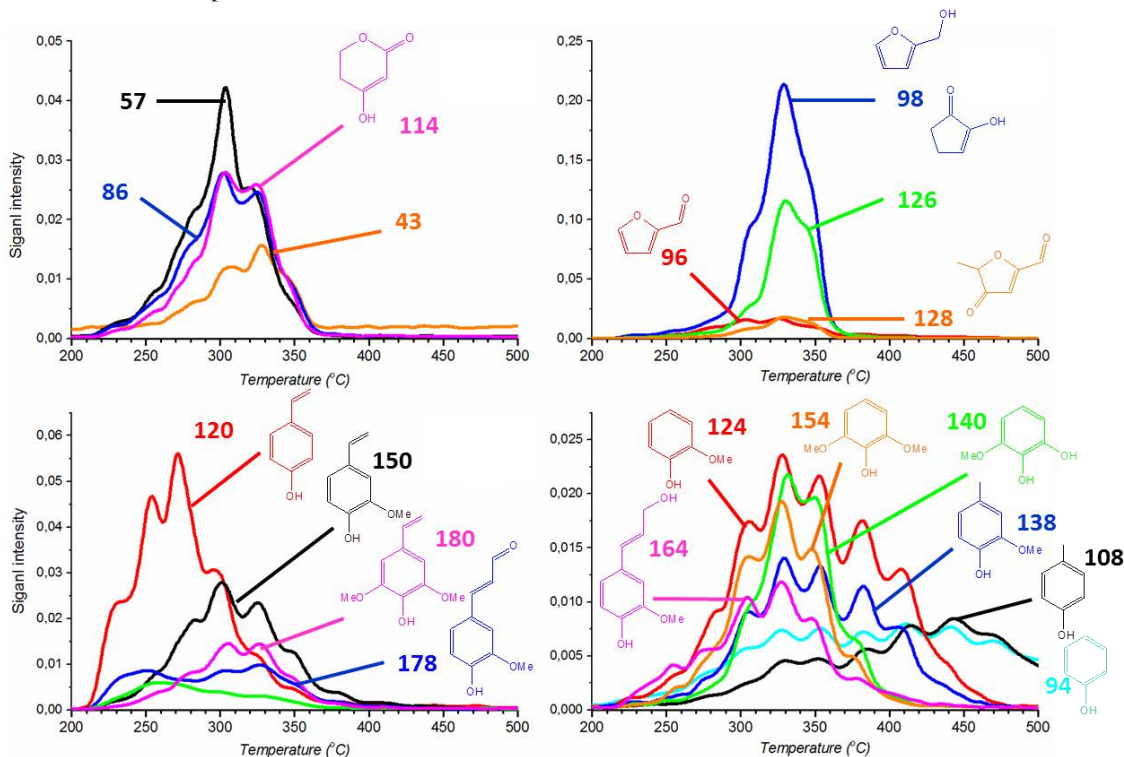


Figure VI-4: On-line analysis vs. time of pyrolysis for *Miscanthus slow*, a) hemicelluloses and carbohydrate fragments, b) main cellulose markers c) lignin markers low temperature d) lignin markers high temperature

This “softening” does not present any endothermic signal (by calorimetry in article 3) indicating that it is not a real melting but mostly a disruption of the biomass network (*i.e.* hydrogen bond disruption). Endothermic signals in biomass pyrolysis appear to be mainly correlated to volatilization of produced tars. The fluidity decreases sharply between 300°C and 350°C. It means that the physical state of the char evolves towards a more rigid (or cross-linked) structure. No evolution of the char structure (observed by <sup>13</sup>C NMR) is observed according to carbohydrate structure up to 300°C. Fluidity significantly decreases when aromaticity appears in the char induced mainly by xylan cross-linking reactions.

At the temperature of 320°C, the degradation of the carbohydrates is significant (as revealed by <sup>13</sup>C NMR) but the maximum of devolatilisation rate (by SPI) is not yet reached. Probably, the structure of carbohydrates is mainly converted to furanone, pyranone or furan derivatives but these compounds are still include in the char as revealed by 2D NMR investigation (Article 1).

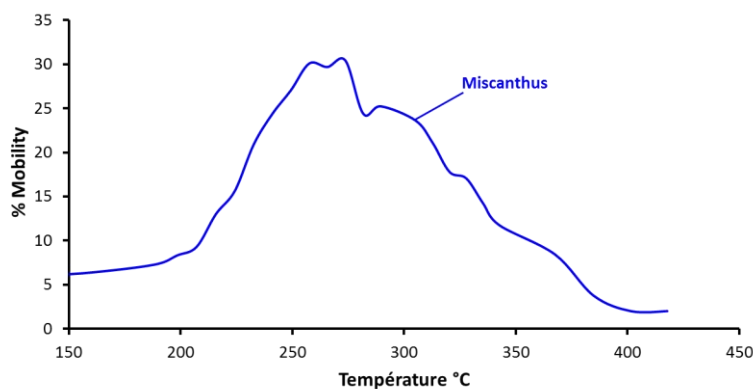


Figure VI-5: % Mobility determined by *in-situ* <sup>1</sup>H NMR as function of temperature during miscanthus pyrolysis

The formation of volatiles is observed mainly around 330°C when molecules are able to be released. The char is composed of aromatic carbons probably linked by aliphatic or ether bridges.

From 350°C to 500°C, a weak mass loss is detected and only some aromatic lignin compounds are detected by SPI/MS(phenol *m/z* 94 and methylphenol *m/z* 108) highlighting the organization of the aromatic char.

## Conclusion et perspectives

Face aux préoccupations relatives à l'épuisement et à l'impact environnemental des énergies fossiles, le développement de systèmes de productions énergétiques plus efficaces et durables apparaît comme une nécessité. La conversion thermochimique de la biomasse lignocellulosique en énergie et/ou en produits chimiques présente un fort potentiel comme alternative à l'énergie fossile. Cependant, la substitution de cette énergie fossile par des procédés de conversion de la biomasse présente à ce jour des limites technologiques et environnementales. La connaissance des mécanismes chimiques de pyrolyse de la biomasse apparaît comme nécessaire pour permettre l'optimisation des réacteurs de transformation thermochimique, notamment afin de guider leur sélectivité vers la production de produits à haute valeur ajoutée.

Depuis plus d'un siècle, les recherches portant sur la détermination des mécanismes chimiques de la pyrolyse de la biomasse ont suscité un grand intérêt. Cependant la diversité des études menées (analyses et biomasses) rend difficile une approche globale de ces mécanismes. Dans ces travaux de thèse, nous avons entrepris d'étudier ces mécanismes en utilisant diverses analyses présentant des conditions de pyrolyses proches (calorimétrie, « *in-situ* »  $^1\text{H}$  RMN, lit fixe). Les analyses ont été conduites pour une large gamme de température (200°C à 500°C) en pyrolyse lente pour différentes biomasses. D'autres essais ont été également conduits en conditions de pyrolyse rapide (pas décrits dans ce manuscrit).

Les analyses RMN (1D  $^{13}\text{C}$ ) sur les charbons issus de la pyrolyse en lit fixe nous ont permis d'observer et de quantifier l'évolution des fonctions chimiques au sein de la biomasse lors de la pyrolyse. Cependant la complexité de la structure chimique de la biomasse limite la pertinence de cette technique analytique. Par conséquent, nous avons réalisé une caractérisation par 2D  $^1\text{H}$ - $^{13}\text{C}$  Hetcor à haut champ (750 MHz) afin de pouvoir observer la formation de certaines fonctions chimiques de façon plus précise (*i.e.* furanes). Cependant, de nombreuses analyses RMN supplémentaires (*ie* déphasage dipolaire,  $^{13}\text{C}$ - $^{13}\text{C}$ ) semblent nécessaire afin d'améliorer la caractérisation de l'évolution de la structure chimique au sein de la biomasse lignocellulosique lors de la pyrolyse. Un des inconvénients de ces analyses RMN est qu'elles sont réalisées de façon *ex-situ* et qu'il advient important de s'abstraire des perturbations induites par les étapes d'échantillonnage qui peuvent par exemple provoquer des réactions chimiques supplémentaires. De plus la stabilité des espèces présentes au sein des charbons n'est pas déterminée de façon précise.

Les études RMN « *in-situ* » présente dans ce cas un fort potentiel mais requiert un développement important. Nous avons mis en place des analyses *in-situ*  $^1\text{H}$  RMN qui nous ont permis d'observer la formation d'une phase fluide au cours de la pyrolyse. Le développement de cette mobilité a été corrélé avec les autres analyses mettant en évidence l'importance de la phase fluide dans les mécanismes de pyrolyse. La compréhension des effets catalytiques des éléments inorganiques (potassium, sodium, calcium,...) demeure un enjeu important pour une meilleure compréhension des mécanismes de pyrolyse. De nouvelles caractérisations concernant l'influence de la présence de composés inorganiques lors de la pyrolyse ont été abordées grâce aux analyses « *in-situ* »  $^1\text{H}$  RMN. En effet la présence de potassium semble limiter la formation de la mobilité inhibant par conséquent les transferts de molécules au sein de la biomasse lors de la pyrolyse ce qui augmente la formation de charbon (structure aromatique). Ces investigations ont été supportées par la caractérisation à l'aide d'analyses en chromatographie liquide de la matière extractible des charbons (quantification des

anhydrosaccharides). La description des interactions biomasse-matière inorganique est un des points les plus importants afin de comprendre l'influence de ces inorganiques sur les mécanismes chimiques de pyrolyse.

L'évolution des structures chimiques au sein des charbons a également été corrélée avec la caractérisation des espèces volatiles formées lors de la pyrolyse. Nous avons développé des analyses en ligne via un spectromètre à ionisation douce (*Single Photo Ionisation*) couplées avec des analyses GC/MS après condensation des volatils. L'évolution de la structure des volatils formés est un témoin important des mécanismes chimiques se déroulant au sein de la matière lignocellulosique. Ces analyses sont notamment très perspicaces en ce qui concerne l'évolution des volatils provenant de la dégradation thermique de la lignine. En effet, l'évolution de la structure la lignine est difficilement caractérisable avec précision par RMN du fait de la trop grande similarité entre les composants du réseau ligneux. Ces analyses en ligne nous ont permis de voir l'enchaînement des diverses transformations s'opérant au sein de la biomasse. Cependant, cette technique présente également des limites à cause de la présence d'isomères au sein des volatils qui ne sont, par conséquent, pas discernables via la photoionisation à énergie constante. L'utilisation de sources d'ionisation provenant d'un rayonnement synchrotron permettrait de discerner ces différents isomères. L'utilisation d'autres sources d'ionisation (par exemple Resonance Enhanced Multi Photon Ionisation, disponible au LRGP) présente également un intérêt dans la caractérisation de la formation des volatils au cours de la pyrolyse. Les caractérisations GC\*GC/FID\*MS apporte une caractérisation supplémentaire et permettent également d'obtenir une évolution de la formation des volatils en fonction de la température. Cependant cette technique est dite « ex-situ » ou hors ligne, ce qui induit inévitablement des limites :

- 1) risque d'évolution des produits condensés au cours du temps après échantillonnage ;
- 2) la condensation préalable des volatils est nécessaire ce qui complexifie la mise en place de ces analyses ;
- 3) la difficulté de réaliser une séparation optimale sur une bio-huile présentant des centaines de composés.

Cette étude globale donne de nombreuses données sur les produits formés (charbon, condensables, gaz) lors de la pyrolyse lente de la biomasse. Ces données obtenues à partir de biomasses caractérisées par des techniques s'opérant dans des conditions de pyrolyse similaires apportent une meilleure mise en relation des techniques analytiques. L'influence des minéraux demeure un des points importants quant à l'optimisation des procédés de transformation thermochimique. Les modèles cinétiques devront prendre en compte leur influence. Ces techniques analytiques peuvent également être utilisées pour étudier/optimiser les procédés de pyrolyses rapides qui représentent un gros potentiel dans la valorisation de la biomasse. D'un point de vue fondamental, le rôle joué par les radicaux dans les mécanismes de pyrolyse semble être déterminant. Des analyses RPE (résonance paramagnétique électronique) « *in situ* » seraient intéressante à réaliser afin de compléter cette étude. Les analyses des bio-huiles formées est également un verrou important dans la compréhension des mécanismes chimiques. En effet, pour ces travaux, l'identification des espèces présentes dans les bio-huiles ne représente qu'une fraction assez faible (seulement 10% en masse).

## Liste des communications écrites et orales

### Communications écrites

- 1) **High Resolution Solid State 2D NMR Analysis of Biomass and Biochar**, Yann Le Brech, Luc Delmotte, Jesus Raya, Nicolas Brosse, Roger Gadiou, Anthony Dufour, Analytical Chemistry, 2015.
- 2) **Characterisation of Miscanthus pyrolysis by DRIFTS, UV Raman spectroscopy and Mass Spectrometry**, Y. Elmay, Y. Le Brech, L. Delmotte, A. Dufour, N. Brosse, R. Gadiou, Journal of Analytical and Applied Pyrolysis, 2015.
- 3) **Mechanism of biomass char formation investigated by advanced solid state NMR**, Yann Le Brech, Luc Delmotte, Jesus Raya, Nicolas Brosse, Roger Gadiou, Anthony Dufour, *A soumettre*.
- 4) **Effect of potassium on the mechanisms of biomass pyrolysis as studied by in-situ <sup>1</sup>H NMR, TG-DSC and LC/MS**, Yann Le Brech, Thierry Ghislain, Sébastien Leclerc, Mohammed Bouroukba, Luc Delmotte, Nicolas Brosse, Colin Snape, Anthony Dufour, *A soumettre*.
- 5) **Biomass slow pyrolysis in a fixed bed reactor: mass balance, gas composition and analysis of primary volatiles by on-line VUV photoionisation mass spectrometry and off-line GC\*GC/MS-FID**, Y. Le Brech, L.Y. Jia, S. Cissé, G. Mauviel, N. Brosse, A. Dufour, *A soumettre*.

### Communications orales

- 1) **Investigation of biomass pyrolysis by in-situ <sup>1</sup>H NMR, Rheology and ex-situ <sup>13</sup>C NMR**, Y. Le Brech, M.C. Diaz, C. Snape, N. Brosse, L. Delmotte, M. Bouroukba, P. Marchal, A. Dufour, 19th International Symposium on Analytical and Applied Pyrolysis, Linz, 2012.
- 2) **Effect of pyrolysis temperature on the property modifications of lignocellulosic biomass and its components**, Y. Elmay, L. Delmotte, R. Gadiou, Y. Le Brech, A. Dufour, N. Brosse, 2014 5TH INTERNATIONAL RENEWABLE ENERGY CONGRESS, 2014.
- 3) **Revealing the chemical structure of biomass and biochar by advanced solid state 2D NMR**, Yann Le Brech, Luc Delmotte, Jesus Raya, Nicolas Brosse, Roger Gadiou, Anthony Dufour, ACS Chemistry and Materials for Energy, Dallas, 2014.
- 4) **Pyrolysis of miscanthus and its biopolymers: characteristic of changes in biochars**, Y. Le Brech, Y. Elmay, L. Delmotte, A. Dufour, N. Brosse, R. Gadiou. 20<sup>th</sup> International Symposium on Analytical and Applied Pyrolysis, Birmingham, 2014.

## Annexes : Techniques d'analyses et de caractérisations

### Broyage de la biomasse

La biomasse a été broyée à l'aide d'un broyeur mécanique (*Retsch*®). Le broyage a été effectué en plusieurs étapes : 1) Broyage à l'aide d'une grille de 8 mm ; 2) Broyage avec une grille de 1 mm ; 3) Broyage avec une grille de 0,2 mm. La biomasse a été ensuite tamisée et deux fractions ont été séparées et récupérées : 0,1-0,2 mm et 0,04-0,1 mm.

### Détermination du taux de lignine de Klason

La technique de taux de lignine de Klason permet de déterminer la composition de la biomasse en sucres et en lignine (lignine de Klason). Elle consiste à évaluer le résidu solide obtenu après hydrolyse complète des chaînes polysaccharides (cellulose et hémicelluloses). Les extractibles de la biomasse étudiée sont extraits par extraction Soxhlet : 36 cycles (environ 24 h) avec pour solvant un mélange éthanol/toluène (50/50 en volume) et 36 cycles avec pour solvant de l'éthanol pur. Une masse anhydre de 0,175 g de biomasse est disposée dans un tube plastique conique. Un volume de 1,5 ml d'une solution d'acide sulfurique à 72 % (densité 1,6338) préalablement préparée est introduit. Le mélange est ensuite placé dans un bain marie agitant réglé à la température de 30 °C pendant 1 h. Le mélange est agité manuellement toutes les 5 minutes à l'aide d'une tige en verre. La solution est diluée avec 42 ml d'eau distillée pour obtenir une concentration en acide de 3 %. Les tubes sont scellés à l'aide de feuillets d'aluminium et placés dans une autoclave (121°C pendant 1 h). Le mélange obtenu est ensuite filtré sous Buchner sur un filtre *whatman*®. Le résidu est séché à 105 °C pendant 24h, refroidi jusqu'à température ambiante dans un dessiccateur. La masse de résidu est ensuite déterminée par pesée. Le volume du filtrat est complété jusqu'à 100 ml et environ 5 ml sont conservés (-5°C) afin d'analyser la teneur en différents saccharides (analyses en chromatographie ionique).

### Analyses par chromatographie ionique (IC) HPAEC-PAD

La chromatographie ionique permet de séparer les constituants d'un mélange en phase aqueuse. Le principe de la Chromatographie ionique est basé sur un échange d'ions sur résine. Les ions sont entraînés par une phase mobile et séparés par l'action de la phase stationnaire. Cette méthode permet après hydrolyse (technique « *Klason lignin* ») de caractériser les sucres constitutifs de biomasses lignocellulosiques. La chromatographie HPAEC-PAD est une séparation sur colonne échangeuse d'anions (HPAEC) et une détection ampérométrique pulsée (PAD). Pour ces travaux, la séparation et la quantification ont été effectuées en utilisant un système de chromatographie ionique de type Dionex ICS-300 qui contient un dispositif de pompage, un auto-injecteur, un détecteur électrochimique avec une électrode en or, une électrode de référence Ag/AgCl et un logiciel d'analyse et de traitement *Chromeleon*. Une pré-colonne (4 x 50 mm, Dionex) reliée à une colonne CarboPac PA1 (4 x 250 mm, Dionex) sont utilisées comme phase stationnaire, en présence d'une solution d'hydroxyde de sodium 1mM. L'éluant est une solution de soude à 48% dans de l'eau ultra pure qui est dégazée avec de l'hélium pendant 20 minutes avant utilisation. Après chaque analyse, la colonne est lavée et rééquilibrée. Les échantillons sont injectés (25 µl) à l'aide d'un passeur automatique et la séparation est effectuée à 25°C pour un débit de 1ml/min. Différents standards (arabinose, galactose, glucose, mannose,

rhamnose et le xylose) sont utilisés afin d'établir des droites d'étalonnage permettant de déterminer la teneur en sucre des différentes biomasses.

## Analyses élémentaires

Les analyses élémentaires ont été réalisées sur un appareil de type Thermo Fisher. Les résultats sont présentés dans chaque « Supporting information ».

## Analyses Organique Carbone Total (TOC)

L'appareil TOC-Shimadzu-V<sub>CSH</sub> a été utilisé afin de déterminer la quantité de carbone organique dissout dans les extractions aqueuses réalisées sur les charbons de pyrolyse (voir Chapitre 3). Une droite de calibration a été réalisée pour chaque série d'essais (Septembre 2015 et Février 2015).

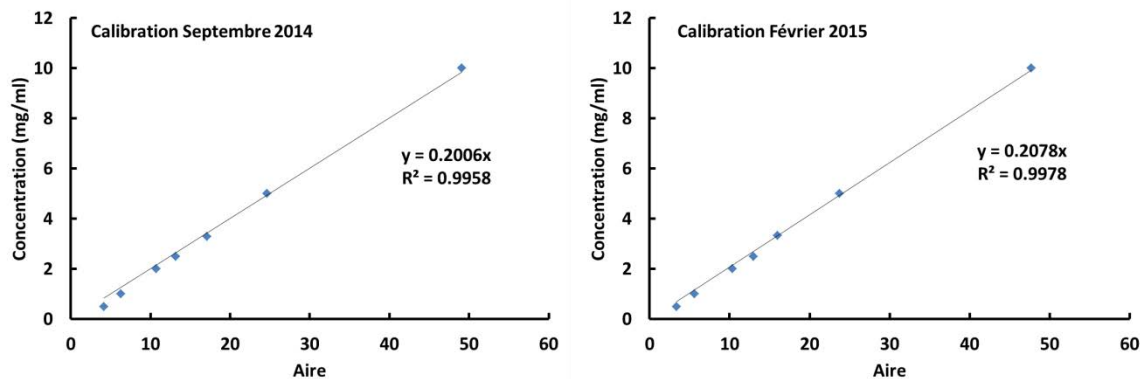


Figure A-1 : Calibration pour analyses Total Organique Carbone

Pour chaque charbon, 150 mg ont été immergés dans 10 ml d'eau ultra pure (H<sub>2</sub>O LC/MS Sigma Aldrich) pendant 30 minutes sous agitation à l'aide d'un barreau aimanté. Le charbon résiduel et la solution ont été séparés à l'aide d'une filtration Buchner avec un papier filtre *whatman*®. 4 ml de chaque filtrat ont été prélevés et dilués par 10 avec de l'eau ultra pure. Cette solution a été filtrée à l'aide de filtre en cellulose régénérée 0,45µm afin d'éviter que de fines particules soient présentes dans la solution. L'appareil TOC Shimadzu est équipé d'un système de dilution automatique si l'échantillon analysé se trouve hors gamme.

Tableau A-1 : Résultats des analyses TOC des extraits de charbon

	T (°C)	C (mg/L)	Quantité de Carbone extrait (mg)	%Charbon lit fixe	mC soluble Tot in char (mg)	mC total in raw Misc (mg)	Yield %C / g biomasse
Cellulose	250	63.6	0.64	0.99	4.18	428	0.98
	280	104.7	1.05	0.95	6.62	428	1.55
	300	173.5	1.74	0.95	10.97	428	2.56
	320	267.9	2.68	0.83	14.82	428	3.46
	330	264.5	2.65	0.61	10.76	428	2.51
Cellulose Imprégnée	300	100.75	1.01	0.61	4.09	417.50	0.98
	330	43.4	0.43	0.39	1.13	417.50	0.27
Miscanthus	250	131.5	1.32	0.94	8.25	450.7	1.83
	280	105.1	1.05	0.87	6.09	450.7	1.35
	300	73.3	0.73	0.69	3.37	450.7	0.75
	320	72.69	0.73	0.54	2.60	450.7	0.58
Miscanthus déminéralisé	280	96.2	0.96	0.90	5.77	471.20	1.22
	310	66.2	0.66	0.74	3.24	471.20	0.69
Miscanthus déminéralisé imprégné	280	152.85	1.53	0.82	8.30	458.50	1.81
	310	81.65	0.82	0.58	3.16	458.50	0.69

### Analyses Chromatographie d'exclusion stérique

Les analyses de caractérisation des sucres extraits des charbons de pyrolyse ont été réalisées par chromatographie HPLC (Shimadzu LC-MS 20) d'exclusion stérique équipée simultanément par un détecteur spectromètre de masse et un détecteur DEDL (Détecteur évaporatif à diffusion de lumière). Ce dispositif a permis de réaliser la séparation des différents sucres et de procéder à leur identification par spectrométrie de masse et leur quantification par détection DEDL. Deux colonnes SEC PL aquagel-OH 20 ont été utilisées pour réaliser la séparation. Un mélange méthanol/eau (50/50 v/v) a été utilisé comme phase mobile. 100µM d'ammonium acétate et 0.1% d'acide formique ont été ajoutés à l'éluant afin d'optimiser l'ionisation au niveau de l'électrospray. Le débit a été maintenu à 0.4 ml/min pour une pression de 50 bars. La température du four a été maintenue à 40°C. Un système de split placé en sortie de colonne a permis d'alimenter simultanément le spectromètre de masse et le détecteur DEDL. La longueur des tubes a été optimisée afin de pouvoir observer les produits simultanément.

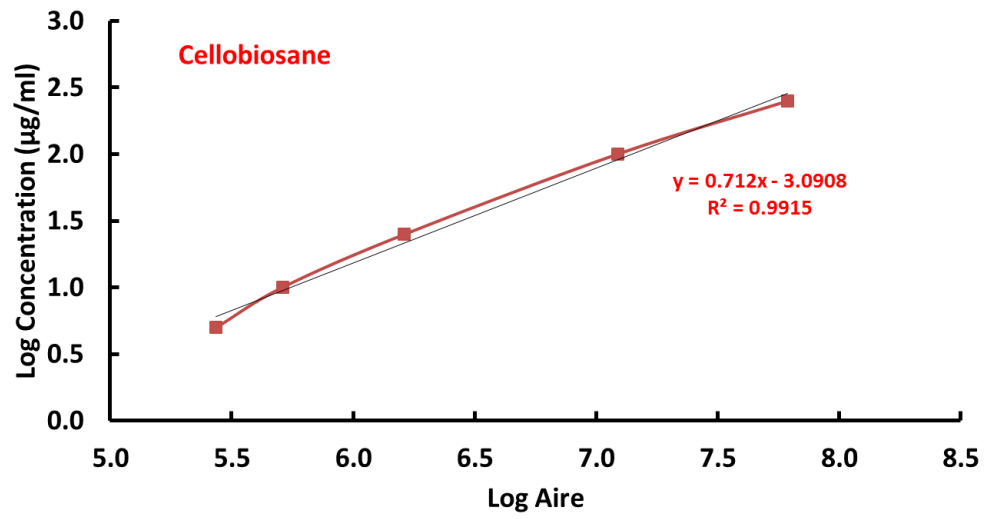
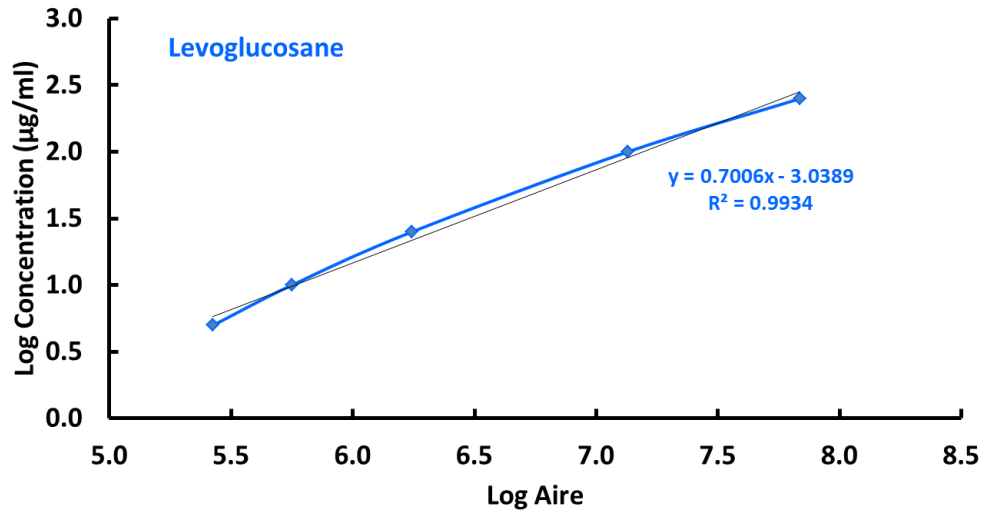


Figure A-2 : Calibration pour la quantification des sucres solubles

## Analyses par calorimétrie

Les expériences de calorimétrie ont été réalisées sur un appareil SETARAM® DSC 111. Concernant la mesure de la température, trois étalons (étain, plomb, indium) avec des points de fusion connus ont été chauffés à 5 °C/min au sein du calorimètre. Ces échantillons « standards » ont été choisis car leurs points de fusion s'étendent sur une gamme de température pertinente pour nos analyses calorimétrique de biomasses (150 à 350°C).

Tableau A-2 : Les standards utilisés pour la calibration de la température en calorimétrie

Echantillons	Masse (g)	Octobre-13	Juillet-14	Wikipédia
		T fusion mesurée (°C)	T fusion mesurée (°C)	T fusion (°C)
Etain	0.38	238.2	243	231.9
Plomb	0.32	331.2	337.4	327.4
Indium	0.31	163.2	165.7	156.2

La variation du signal détectée par la DSC correspondant à l'enthalpie de fusion de chacun des étalons nous a permis d'établir une droite de calibration entre la température donnée par le calorimètre et la température réelle de l'échantillon (Tableau A-2, Figure A-3). Deux calibrations ont été réalisées car les expériences de calorimétrie se sont déroulées en deux sessions. Une calibration a été effectuée pour les essais réalisés au mois d'Octobre 2013 (Calibration Oct 2013) et une autre pour les essais réalisés au mois de Juillet 2014 (Calibration Juillet 2014). Pour chaque standard, les mesures ont été répétées au moins deux fois et une troisième mesure a été effectuée si les deux premières mesures présentaient un écart trop significatif (plus de 3°C). Pour calibrer la sensibilité du signal, un coefficient correctif (1,086) a été déterminé à l'aide d'un échantillon standard de carbonate de zinc (ZnCO<sub>3</sub>).

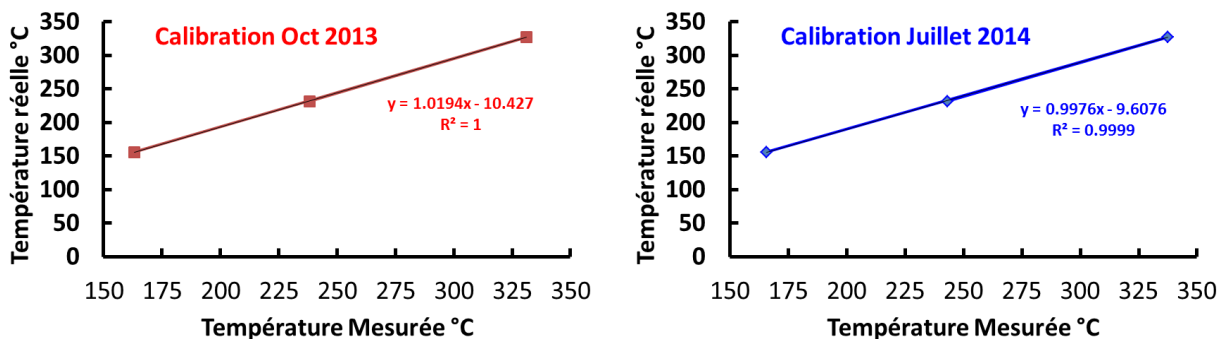


Figure A-3 : Les droites de calibration en température pour les analyses en calorimétrie

## Calibration de la température pour les mesures en $^1\text{H}$ RMN Haute Température

Le système de la sonde *Bruker* SEI ne permet pas d'avoir une mesure précise de la température au sein de la partie du tube présent dans la zone de détection. Le thermocouple de contrôle de la sonde étant placé 2 cm sous le tube dans le courant d'air chaud. Ce système est en effet optimal pour des chauffages isothermes ou avec des paliers importants. Cependant il ne convient pas à un mode de chauffage par rampe. Nous avons donc estimé la différence de température au sein de l'échantillon par rapport à la valeur donnée par le contrôleur. Pour cela deux mesures de montée en température à  $5^\circ\text{C}/\text{min}$  ont été effectuées et une correction de température a été déterminée (Figure A-4). Un thermocouple a été introduit dans un tube RMN avec 35mg de miscanthus afin de simuler une montée en température et ainsi établir la correction de température. La température donnée par la sonde RMN correspond parfaitement avec l'évolution de la température souhaitée ( $5^\circ\text{C}/\text{min}$  de  $25^\circ\text{C}$  à  $500^\circ\text{C}$ ), cependant la température mesurée au sein du tube est plus faible (Figure A-4). Cette correction a été prise en compte pour l'interprétation des résultats présentés dans ce rapport.

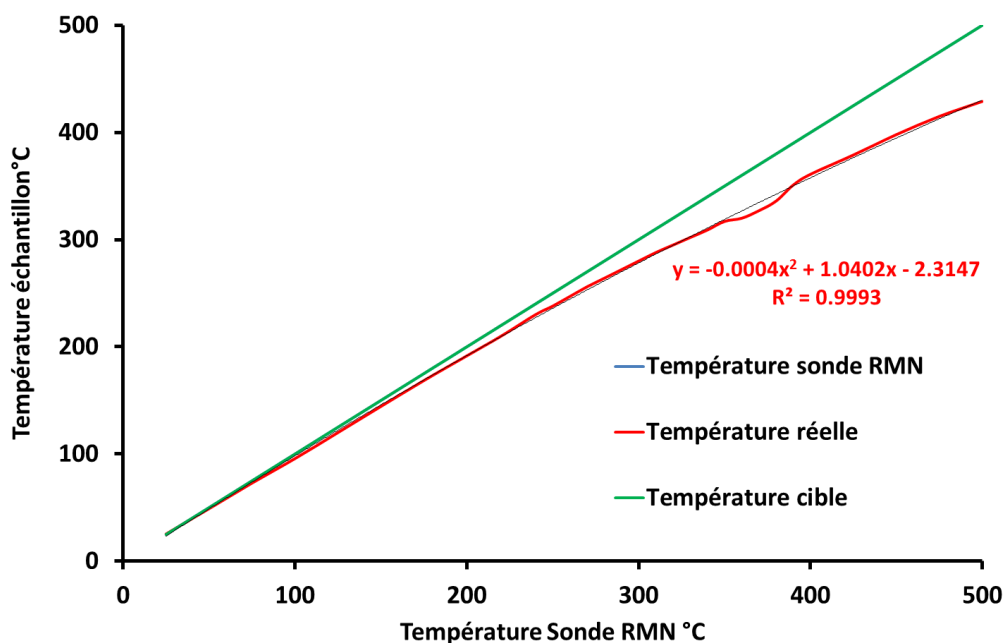


Figure A-4 : La droite de calibration en température pour les analyses  $^1\text{H}$  RMN

### **Analyse par chromatographie gazeuse et spectrométrie de masse et détecteur à ionisation de flamme avec « heartcutting » (GC\*GC/FID\*MS)**

La colonne HP-5MS (diphényl -5% - diméthylpolysiloxane -95%, apolaire, 30m × 250µm × 0,25µm) a été couplée avec une colonne DB-WAX (polyéthylenglycol, polaire, 30m × 320µm × 0.25µm). La complémentarité de ces deux colonnes permet une bonne caractérisation des systèmes complexes comme les huiles de pyrolyse primaire. La HP-5MS est connectée simultanément à un détecteur FID et MS afin de réaliser simultanément la quantification et l'identification des composés. La DBWAX est connectée à un détecteur FID. La méthode de quantification à l'aide de la méthode de St Laumer est décrite dans les informations supplémentaires du chapitre 4.

### **Analyse par µGC**

Les gaz formés lors des expériences de pyrolyse ont été collectés à l'aide de sac d'échantillonnage (ADTECH PVDF 10 L) par connexion directe avec le montage. Ils ont été analysés à l'aide d'un appareil µGC4900 Varian composés de quatre modules et de détecteur TCD.

A Nancy, le 24 août 2015

No étudiant : 31113419

LE BRECH YANN  
Appartement 108  
11 rue JEAN LAMOUR  
54000 NANCY

Monsieur,

Par décision en date du 24 août 2015, vous avez été autorisé à présenter en soutenance vos travaux en vue de l'obtention du diplôme :

**Doctorat de GENIE DES PROCEDES ET DES PRODUITS**

La soutenance aura lieu le 10 septembre 2015 à 9h00 à l'adresse suivante :

AMPHI DONZELOT ENSIC-LRGP 1 Rue Granville 54000 NANCY

La soutenance sera publique.

Je vous prie d'agréer, Monsieur, l'expression de mes salutations distinguées.

Le Vice-Président du Conseil Scientifique



Frédéric VILLIERAS

## **Résumé**

La biomasse est la ressource d'énergie renouvelable au plus fort potentiel. Les travaux de recherche actuels se concentrent principalement sur sa conversion, notamment thermochimique, en un autre vecteur énergétique plus facile à transporter et à valoriser (électricité, gaz ou liquide). La pyrolyse est le premier mécanisme intervenant dans tous les procédés de conversion thermochimique des solides (combustion, gazéification, pyrolyse). C'est également le plus important, car il contrôle la répartition et la composition des trois types de produits : gaz, charbon, goudrons. La prédiction des produits de pyrolyse et par conséquent la compréhension des mécanismes chimiques de pyrolyse sont primordiales pour le développement de procédés de conversion thermochimique. De nombreuses études analytiques ont été réalisées mais la grande hétérogénéité des biomasses étudiées et des conditions de pyrolyse utilisées rend actuellement difficile une approche globale des mécanismes. L'objectif de cette étude a été de réaliser des analyses complémentaires de produits de pyrolyse formés pour une large gamme de températures (200°C à 500°C) en pyrolyse lente (5 °C/min) pour différentes biomasses (miscanthus, chêne et douglas) à l'aide d'un lit fixe permettant un contrôle optimal des phénomènes de transfert de chaleur et de matière. De nombreuses méthodes physico-chimiques ont été utilisées pour caractériser les produits formés afin de réaliser un bilan global des mécanismes chimiques de dégradation : Résonance magnétique nucléaire (RMN) du proton  $^1\text{H}$  et du carbone  $^{13}\text{C}$  ; Calorimétrie (DSC) ; Thermogravimétrie ; GC/MS (*Gas Chromatography and Mass spectrometry*), LC/MS (*Liquid Chromatography and Mass Spectrometry*) et spectrométrie de masse à ionisation douce (*Single Photo Ionisation SPI*). Des techniques originales d'analyses dites *ex-situ* telles que l'analyse 2D RMN par la méthode HETCOR (*Heteronuclear correlation*)  $^1\text{H}$ - $^{13}\text{C}$  ainsi que des analyses *in-situ* en RMN  $^1\text{H}$  Haute Température ont été mises en place. Cette dernière a permis de caractériser de façon originale l'influence des interactions entre les minéraux et la biomasse lors des mécanismes de pyrolyse de la biomasse. Toutes ces analyses ont pour objectif final le développement d'un modèle cinétique détaillé pour prédire la composition des produits de pyrolyse et pour optimiser les réacteurs de transformation thermochimique notamment en orientant leur sélectivité vers des produits à forte valeur ajoutée.

**Mots clés** : Pyrolyse, Biomasse, Energie, Analyses, Bois

## **Summary**

Biomass is the renewable resource with the highest potential for energy production. Current research studies focus on biomass thermochemical conversion to produce other energetic vectors more appropriate to be conveyed, such as electricity, gas or liquid products. Pyrolysis is the first mechanism occurring in all thermochemical processes for solid fuels conversion (combustion, gasification, pyrolysis). It controls in a large extent products (gas, condensables and char) distribution and composition. The prediction of pyrolysis products and the understanding of the chemical mechanisms are thus pivotal for developing thermochemical reactors. Extensive work has been conducted for more than one century but the important heterogeneity of biomasses and pyrolysis conditions make it difficult to encompass a global chemical mechanism. The aim of this study is to develop complementary analyses of pyrolysis products. Pyrolysis is conducted in a fixed bed reactor under slow pyrolysis conditions (5 °C/min), for a wide range of final temperature (200°C and 500°C) and for different biomasses (miscanthus, douglas and oak). Various analytical methods have been used in order to characterise the pyrolysis products: nuclear magnetic resonance (carbon  $^{13}\text{C}$  and proton  $^1\text{H}$  NMR), Calorimetry, Thermogravimetry, GC/MS (*Gas Chromatography and Mass spectrometry*), LC/MS (*Liquid Chromatography and Mass Spectrometry*) and soft ionization mass spectrometry (Single Photo Ionisation SPI). Original analytical methods such as 2D NMR HETCOR  $^1\text{H}$ - $^{13}\text{C}$  (for the analysis of chemical moieties in char) and high temperature  $^1\text{H}$  NMR (for in-situ analysis of mobile protons) have been used. The latter allowed a novel characterization of the interaction between biomass and minerals during pyrolysis. These data will be used to develop a detailed kinetic mechanism (after this study) which will account for interactions between the polymers and the minerals.

**Keywords**: Pyrolysis, Biomass, Energy, Analysis, Wood